博士学位論文

翼竜類の解剖学・系統分類学・古病理学：中国産新標本に基づく洞察

周 炫宇

北海道大学大学院理学院

自然史科学専攻

令和 5 年 9 月

Doctoral Dissertation

Anatomy, Systematics and Paleopathology of Pterosaurs: insights based on new specimens from China

Xuanyu Zhou

Department of Natural History Sciences,

Graduate School of Science, Hokkaido University

September 2023

要旨

翼竜類は，ギリシャ語で「翼のあるトカゲ」を意味する *pterosauros* に由来し，Pterosauria (Diapsida, Archosauria) の飛行する爬虫類である。三畳紀末に出現し，白亜紀末に絶滅した。翼竜類は，非常に伸長した第四指（翼指），発達した前肢，貧弱な後肢，薄壁の中空骨といった，ユニークな骨格形状によって特徴づけられる。

中国には，世界で最も重要な翼竜発見地がいくつもある．2022 年までに，10 科に属するおよそ 62 属 66 種の翼竜類が発見されている．最も古い中国産翼竜類の化石記録は，中期〜後期ジュラ紀の Shaximiao 層で発見された．反対に，最も新しい中国産翼竜類の化石記録は，後期白亜紀の Tangshang 層から発見された．中国産翼竜類は *Angustinaripterus longicephalus* （四川省自貢市，中国西南部）と *Zhejiangopterus linhaiensis* （浙江省臨海市，中国東南部）を除けば，主に中国北部から産出している．特に，遼寧省西部とその周縁地域は最も代表的な発見地である．Tiaojishan 層 （オックスフォーディアン階-キンメリッジアン階）, Yixian 層 （バレミアン階〜アプチアン階）と Jiufotang 層 （アプチアン階）である．翼竜類の胚や軟組織，移行期の形態を示す *Darwinopterus modularis*，卵とともに保存されていたメスの *Kunpengopterus antipollicatus*，最古の拇指対向性を示す *Kunpengopterus antipollicatus* のホロタイプなど，最近の翼竜類における基盤的な発見研究のいくつかは，これらの地域からもたらされている．これらの発見により，この地域は，ジュラ紀の石灰岩層が広がるドイツ・Solnhofen や，白亜紀のブラジル・Santana 層群に匹敵する，世界で最も人気で興味をひく翼竜研究地の一つとなった．特に，原始型（短い首と長い尾をもつ），進化型（長い首と短い尾をもつ），遷移型（原始型と進化型の両方の特徴を併せもち，それらと区別される）の翼竜類が同時に発見された国は，世界で中国だけである．これらの発見は，翼竜類を理解する上でさらに重要な情報を提供する．本研究では，中国産の代表的なクレードを含む，3 つの型の翼竜類に関する見解を全て更新し，自身の翼竜研究フレームワークの全体像を構築する．解剖学，系統学，古病理学の手法を用いて，遼寧省西部とその周辺を含む地域から産出した 3 つの型全ての多様な標本を研究しており，それらを以下に示す：

1) 中国産原始型翼竜類の進展：この研究では，Tiaojishan 層から *Sinomacrops bondei* と名付けられた新しいアヌログナトゥス科翼竜を報告した．この新種は，ほぼ完全な骨格を表し，これまで発見されたアヌログナトゥス科標本の中でも，有名で最もよく知られた標本の一つである．重要なのは，この標本が，外側面観で保存された頭骨を示す，史上初のアヌログナトゥス科標本であることだ．この発見は，本グループの解剖学的特徴やその系統学的位置づけに新たな光をあてた．また，本グループについて見解を示した．

2) 中国産遷移型翼竜類の進展：この研究では，拇指対向性をもつダルウィノプテルス類翼竜である，*Kunpengopterus antipollicatus* を報告した．この Tiaojishan 層から発見された新種は，拇指対向性を示す初めての翼竜類であり，

化石記録上，その性質を示す最も古い例の一つである．また，新種と既知種との比較に基づくダルウィノプテルス類の分類学的改訂も提示されている．

3) 中国産進化型翼竜類の進展 1：新属 *Huaxiadraco* を含む，*Sinopterus* コンプレックスに基づく，中国産タペヤラ科の分類学的改訂も提示された．Jiufotang 層から新たに産出した 6 種のタペヤラ科標本は，*Sinopterus* コンプレックス（*Sinopterus* と *Huaxiapterus* に分類され，分類学的な議論の焦点となっている，7 種の名目上の種からなるタペヤラ科のコンプレックス）を詳細に再検討する機会を与えた．質的・量的解析を通して，*Sinopterus dongi* と“*Huaxiapterus*” *corollatus* の 2 種のみが有効であるものの，“*Huaxiapterus*”が無効であることから，*Huaxiadraco* という新属をたてる結論に至った．

4) 中国産進化型翼竜類の進展 2： Jiufotang 層から産出したの新たな Istiodactyliform の標本は，ほぼ完全な骨格に基づくもので，これまで発見された Istiodactyliform の中で最も知られた骨格標本であると言える。この新種は，翼竜類におけるエナメル上皮腫の最初の記録例となる。この病態について，組織学的分析を用いて詳細に調査された。

ABSTRACT

Pterosaurs, from the Greek, *pterosauros*, meaning “winged lizards”, were flying reptiles of the order Pterosauria (Diapsida, Archosauria). They originated in the late Triassic and went extinct at the end of the Cretaceous. Pterosaurs are characterized by unique skeletal features such as the extremely elongated fourth finger (the wing finger), a well-developed forelimb, a weak hindlimb, and pneumatic bones with thin walls.

China comprises some of the most important sites of pterosaurs discoveries in the world. There are about 62 genera 66 species belonging to ten families of pterosaurs discovered till 2022. The earliest Chinese pterosaur record was found in the Middle-Late Jurassic Shaximiao Formation. The latest Chinese pterosaur record was found in the Late Cretaceous Tangshang Formation. Chinese pterosaurs are mainly found in north China besides *Angustinaripterus longicephalus* (Zigong, Sichuan, Southwestern China) and *Zhejiangopterus linhaiensis* (Linhai, Zhejiang, Southeastern China). Especially, the western Liaoning and its surrounding areas are most representative location. Tiaojishan Formation (Oxdordian-Kimmeridgian), Yixian Formation (Barremian-Aptian) and Jiufotang Formation (Aptian) are the most representative stratum of this region. Some recent fundamental pterosaur discoveries researches have come from there, such as pterosaur embryos, soft tissues, the transitional form *Darwinopterus modularis*, the female *Kunpengopterus antipollicatus* preserved with her egg and the holotype of *Kunpengopterus antipollicatus* which exhibits the oldest record of opposed thumb. These discoveries make China one of the most productive regions in the world, that can outmatch Germany (Jurassic Solnhofen deposits) and Brazil (Cretaceous Santana Group). Especially, China is the only country which simultaneously found the primitive type (with a short neck and long tail), advanced type (with a long neck and short tail) and transitional type (bear a combination of characters and are distinguished from both) of pterosaurs in the world. All these discoveries provide further important information on our understanding of pterosaurs. In this study, the comment of Chinese representative clade from all three groups is periodically updated, and the holistic view of my pterosaur research framework is constructed. We use the methods of anatomy, systematic and paleopathology to study a varied sample of all three groups from the western Liaoning and surrounding areas, as follows:

1)Advances in Chinese primitive type pterosaur: Here we reported a new anurognathid pterosaur from the Tiaojishan Formation, named *Sinomacrops bondei*. This new species is represented by an almost complete skeleton, which is, notoriously, one of the best known anurognathid specimens found so far. Importantly, this is the first anurognathid specimen ever to exhibit a skull preserved in a lateral view. This discovery shed new light onto the anatomy of Anurognathids and their systematic position. We also commented on the group anurognathid.

2)Advances in Chinese transitional type pterosaur: Here we reported a new species of darwinopteran pterosaur revealing an oldest opposed thumb, named *Kunpengopterus antipollicatus*. A revision of Darwinopteran taxonomy, based on comparisons between the new material and the previously known species, is also presented.

3) Advances in Chinese advanced type pterosaur 1: A revision of Chinese Tapejarid taxonomy, based on the comparisons of *Sinopterus* complex with the new genus *Huaxiadraco*, is also presented. Six new tapejarid specimens from the Jiufotang Formation prompt here the opportunity to revise, in detail, the *Sinopterus* complex - a complex of seven nominal species that have been referred to *Sinopterus* and *Huaxiapterus* and that are the focus of taxonomic debate. Through qualitative and quantitative analyzes, we conclude that only two species are valid, *Sinopterus dongi* and "*Huaxiapterus*" *corollatus*, for which the new genus *Huaxiadraco* is erected given the fact that "*Huaxiapterus*" is found invalid.

4) Advances in Chinese advanced type pterosaur 2: A new istiodactyliform pterosaur from the Jiufotang Formation. This new species is based on an almost complete skeleton, which can be seen as the best known skeleton ever found of an istiodactyliform. It provides the first ever recorded case of ameloblastoma in a pterosaur. This pathological condition is explored in detail using histological analyses.

謝辞

私の博士学位論文が完成したのは，多くの方々の激励と支えがあったからこそである。

何よりも第一に，指導教官である小林快次教授の根気強いご指導や貴重なご指摘，絶え間ない激励により，この学位論文が無事に完成した。心から感謝申しあげる。小林教授の誠実な学問精神と自律した人格は，学術研究と日常生活の両面で私を鼓舞してくれた。小林教授は論文執筆における全ての過程において私に多くの協力と助言を与えてくださり，そのおかげで私の業績は達成された。

第二に，アカデミックな兄弟の大藪隼平に多大なる感謝の意を表することを忘れてはならない。私が博士課程在学中に過ごした札幌で，彼はいついかなる時も助けになってくれた。また，研究室の他のメンバーである久保孝太，清水洲平，高田健太郎，ここに名前を挙げていない方々にも感謝申し上げる。北海道大学 DX 博士人材フェローシップ（#JPMJSP2119）からの博士研究費と生活費の支援に心より感謝申し上げたい。さらに，日本国内での標本調査の際，国立科学博物館の坂田智佐子さんと真鍋真博士，東京都市大学の中島保寿准教授，東京大学の平沢達矢准教授，群馬県立自然史博物館の髙桒祐司博士は，コレクションを利用できるよう協力してくださったり，標本観察の機会を提供してくださったりした。大変感謝している。また，沢田健教授と伊庭靖弘准教授は博士論文の副査を快く引き受けてくださった。心から感謝申し上げる。お二方の尊敬すべき存在と学術的なご意見は，私の学問的探究におけるマイルストーンである博士論文の意義とインパクトをまちがいなく高めてくれるでしょう。

第三に，私の修士過程が始まった時から深く協力してくださった ABC 連邦大学（ブラジル）の Rodrigo V. Pêgas 博士と国立自然史博物館、スミソニアン協会（アメリカ）の Waisum Ma 博士に深謝申し上げる。中国北票翼竜博物館のリーダーである Cunyu Liu さんにも特別な感謝を捧げる。さらに，管理する標本の利用を許可してくださった，浙江自然博物院の Xingsheng Jin 教授，中国古动物館の Fengxia Zhao さん，中国地質博物館の Qiannan Zhang 博士，北京地質工学設計研究院の Shaowen Zhang さん，大連星海古生物博物館の Fangfang Teng さん，中国地質博物館本渓分館の Jun Zhang さんと Honggang Huo さん，錦州古生物博物館の Deyu Sun さん，中华恐竜園の Junjie Yao さん，そしてこのリストに含まれていない多くの人々に感謝申しあげる。彼らのコレクションがなければ，私の博士課程での研究は達成されなかっただろう。博士課程在学時に多大なる助力と激励をくださった，中国地質科学院地質研究所の Shu’an Ji 教授，Yongqing Liu 教授，Hongwei Kuang 教授，Zhanshen Ji 教授，Guichun Wu 教授と Suping Li 教授や，中国科学院古脊椎動物と古人類学研究所の Hailu You 教授，中国地質大学の Dangpeng Xi 教授，中国地質調査所成都センターの Xuefang Wei 博士，河北地質大学の Caizhi Shen 教授，モンゴル科学院地質古生物研究所 の Khishigjav Tsogtbaatar 博士，コペンハーゲン大学（デンマーク）の Maria E.C. Leal 教授と Niels Bonde 教授に感謝申し上げる。私の

学問の道標となった故 Junchang Lü教授（中国地質科学院地質研究所）は，私に真の研究者になることを教えてくださった。彼の教えを忘れることはないだろう。

末筆ながら，私が前へ進み，より良い人間になりたいと思う原動力となった，両親の愛情と支援に特別な感謝の意を表する。

ACKNOELEDGEMENTS

The completion of my thesis is attributed to many people's encouragement and support.

First and foremost, I want to extend my heartfelt gratitude to my supervisor, Prof. Yoshitsugu Kobayashi, whose patient guidance, valuable suggestions and constant encouragement make me successfully complete this thesis. His conscientious academic spirit and self-disciplined personality inspire me both in academic study and daily life. He gives me much help and advice during the whole process of writing, which has made my accomplishments possible.

Secondly, I would not forget to express my big thanks to my academic brother Shumpei Oyabu for his always helpful any time and supports in the Sapporo during my doctorate time. I am also gratitude to my other lab members, Kota Kubo, Shuhei Shimizu, Kentaro Takada, and other members whose names are not mentioned here. Special thanks should also go to the Hokkaido University DX Doctoral Fellowship (#JPMJSP2119). Moreover, I am greatly appreciated Chisako Sakata and Drs. Makoto Manabe of National Museum of Nature and Science, Prof. Yasuhisa Nakajima of Tokyo City University, Prof. Tatsuya Hirasawa of The University of Tokyo, Drs. Yuji Takakuwa of Gunma Museum of Natural History who helped me to access to the collection and provided me to observe specimens during my Japanese domestic visit. I would also like to extend my heartfelt appreciation for Prof. Ken Sawada and Prof. Yasuhiro Iba's gracious acceptance to participate as a committee member in my Ph.D. defense. Your esteemed presence and scholarly input will undoubtedly elevate the significance and impact of this milestone in my academic pursuit.

Thirdly, I express my deepest thanks to Drs. Rodrigo V. Pêgas from Federal University of ABC and Drs. Waisum Ma from National Museum of Natural History, Smithsonian Institution for their profound cooperation since my Master. Special thanks should also go to the leader of Beipiao Pterosaur Museum of China, Cunyu Liu. Moreover, I am grateful to Fengxia Zhao (Palaeozoological Museum of China), Prof. Xingsheng Jin (Zhejiang Museum of Natural History), Drs. Qiannan Zhang (Beijing Natural History Museum), Shaowen Zhang (Beijing Geological Engineering Design Research Institute), Fangfang Teng (Xinghai Museum of Prehistoric Life of Dalian), Jun Zhang (Benxi Geological Museum), Honggang Huo (Benxi Geological Museum), Deyu Sun (Jinzhou Museum of Paleontology), Junjie Yao (China Dinosaurs Park), and many others who are not included in this list for access to specimens under their care. Without their collections, my PhD researches would not be accomplished. I am greatly appreciated Prof. Shu'an Ji , Prof. Yongqing Liu, Prof. Hongwei Kuang, Prof. Zhanshen Ji, Prof. Guichun Wu and Prof. Suping Li from Institute of Geology, Chinese Academy of Geological Sciences, Prof. Hailu You from Institute of Vertebrate Paleontology and Paleoanthropology, Chinese Academy of Sciences, Prof. Dangpeng Xi from China University of Geosciences, Drs. Xuefang Wei from

Chengdu Center of China Geological Survey, Prof. Caizhi Shen from Hebei GEO University, Prof. Khishigjav Tsogtbaatar from Institute of Paleontology and Geology, Mongolian Academy of Sciences, and Prof. Maria E.C. Leal and Niels Bonde from Copenhagen University for their much help and encouragement during my doctorate time. Being the guide of my academic life, the late Prof. Junchang Lü teaches me to be a true researcher. I would not have forgotten his instruction ever.

Last but not least, I would like to express my special thanks to my parents, whose care and support motivate me to move on and make me want to be a better person.

目次

TABLE OF CONTENTS

LIST OF INSTITUTIONS

AMNH, American Museum of Natural History, New York, USA.
BMNH, BMNHC, BPV, Beijing Museum of Natural History, Beijing, China.
BPMC, Beipiao Pterosaur Museum of China, Beipiao, Liaoning, China.
BSP, Palaeontological Museum Munich, Munich, Germany.
BYU, Brigham Young University Museum of Paleontology, Provo, Utah, USA.
BXGM, Benxi Geological Museum, Benxi, Liaoning, China.
CAGS, IG-CAGS, Institute of Geology, Chinese Academy of Geological Sciences, Beijing, China.
CDM, China Dinosaur Park, Changzhou, Jiangsu, China.
CP, University of Contestado, Santa Catarina, Brazil.
D, DNHM, Dalian Natural History Museum, Dalian, Liaoning, China.
GMN, Geological Museum of Nanjing, Nanjing, Jiangsu, China.
HGM, Henan Geological Museum, Zhengzhou, Henan, China.
IVPP, Institute of Vertebrate Paleontology and Paleoanthropology, Beijing, China.
JPM, **JZMP**, Jinzhou Museum of Paleontology, Jinzhou, Liaoning, China.
PMC, Palaeozoological Museum of China, Beijing, China.
PMOL, LPM, Paleontological Museum of Liaoning, Shenyang, Liaoning, China.
MB, Museum für Naturkunde Berlin, Berlin, Germany.
MN/UFRJ, National Museum of Brazil/Federal University of Rio de Janeiro, Rio de Janeiro, Brazil.
NHM, NHM UK, National History Museum, London, UK.
NJU, Nanjing University, Nanjing, Jiangsu, China.
SDUST, Shandong University of Science and Technology,Qingdao, Shandong, China.
SMNH, Swedish Museum of Natural History, Stockholm, Sweden.
SMNK, State Museum of Natural History Karlsruhe, Baden-Württemberg, Germany.
UFABC, Federal University of ABC, São Paulo, Brazil.
USP, GP/2E, University of São Paulo, São Paulo, Brazil.
XHPM, Xinghai Paleontological Museum, Dalian, Liaoning, China.
ZMNH, Zhejiang Museum of Natural History, Hangzhou, Zhejiang, China.

CHAPTER I

PTEROSAUR RESEARCH IN CHINA: A REVIEW

China comprises some of the most important sites of pterosaur discoveries in the world. There are about 62 genera 66 species belonging to ten families of pterosaur discovered till 2022. The first one to study Chinese pterosaur is CC Young (Yang Zhongjian, 1897—1979) (Fig.1A), the father of Chinese Vertebrate Paleontology. He reported the first wing phalange from Mengyin of Shandong Province in 1935 (Fig.1B). He reported the first identified Chinese pterosaur *Dsungaripterus weii* from Urho of Xinjiang Uygur Autonomous Region in 1964 (Fig.1C).

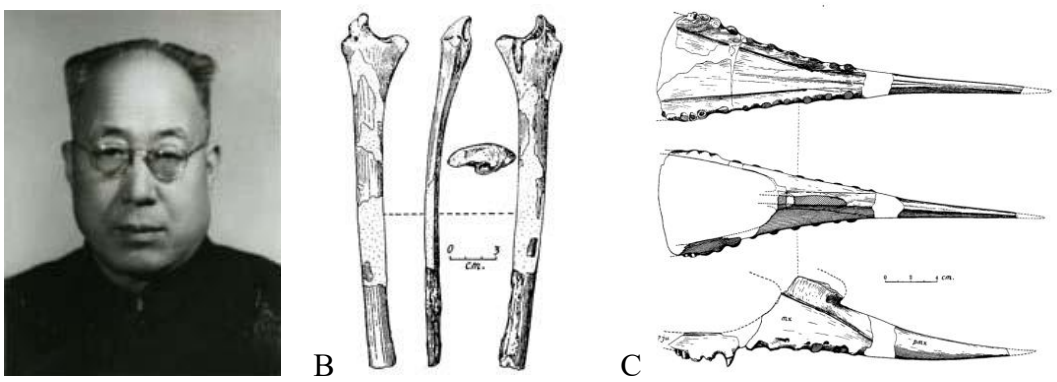

Figure.1 Yang Zhongjian. (A), The proximal portion of the first wing phalanx (Young, 1935). (B), *Dsungaripterus weii*, Anterior part of the skull ventral, dorsal and right side views (Young, 1964). (C)

Chinese pterosaur research can be divided two periods. During 1935-1997, a small amount of incomplete specimens have been discovered piecemeal in Shandong, Xinjiang, Sichuan and Zhejiang (Young 1935,1964; Dong, 1982; He *et al.*, 1983; Cai & Wei, 1994). After 1997, a large number of specimens have been found at the western Liaoning and its surrounding areas, and continue to be found until now. This area includes Western Liaoning (Jinzhou, Chaoyang and Huludao), Northern Hebei (Qinhuangdao) and Southeastern Inner Mongolia (Chifeng). Some recent fundamental discoveries researches have come from there, such as pterosaur embryo (Fig.2), soft tissue (Fig.3), the transitional form *Darwinopterus modularis* (Fig.4A), the female *Kunpengopterus antipollicatus* preserved with her egg (Fig.4B) and the holotype of *Kunpengopterus antipollicatus* which exhibits the oldest record of opposed thumb (Fig.4C) (Wang and Zhou, 2004; Yang *et al.*, 2018; Lü *et al.*, 2009; Lü *et al.*, 2011; Zhou *et al.*, 2021). In addition, a population of a new sexually dimorphic pterosaur species *Hamipterus tianshanensis* with exceptionally well-preserved three-dimensional eggs (Fig.5) was reported in Xinjiang (Wang *et al.*, 2014). Apart from that, *Ordosipterus planignathus* (Fig.6) and *Otogopterus haoae* (Fig.7) were reported at Ordos Region, southwestern Inner Mongolia. Beforehand, pterosaurs had never been found in this area (Ji, 2020; Ji & Zhang, 2020).These discoveries make

China one of the most productive regions in the world, that can outmatch Germany (Jurassic Solnhofen deposits) and Brazil (Cretaceous Santana Group). All these discoveries provide further important information on our understanding of pterosaurs.

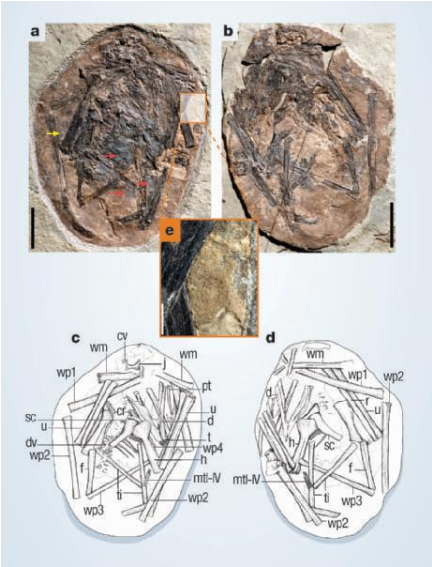

Figure 2. Pterosaur embryo inside an egg from the Early Cretaceous period from Liaoning, (IVPP V13758). Photographs of part (a) and counterpart (b) of the fossil and their correspon -ding line drawings (c, d), Close-up of the papilla-like ornamentation of the eggshell (e) (Wang and Zhou, 2004).

Figure 3. Pterosaur preserved soft tissues (CAGS-Z070. The Institute of Geology, Chinese Academy of Geological Sciences) from Daogugou locality, Ningcheng. Inner Mongolia (Yang *et al.*, 2018).

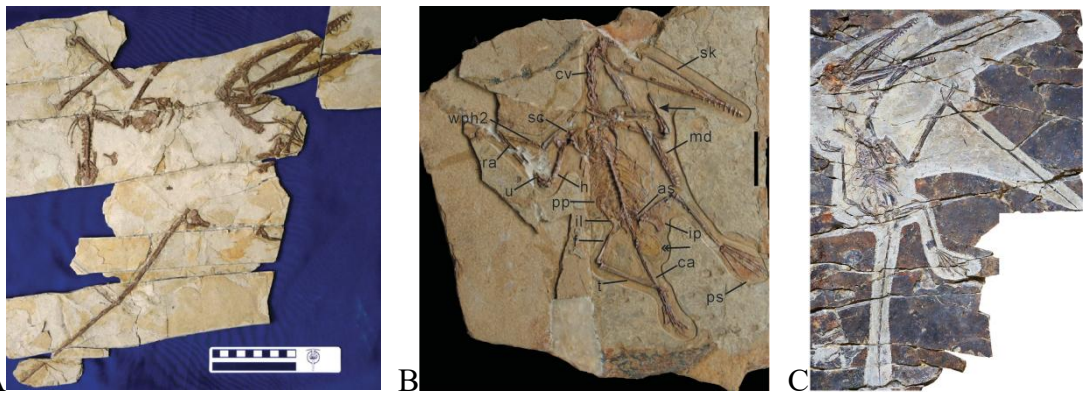

Figure 4. *Darwinopterus modularis* (ZMNH M8782, Lü *et al.*, 2009) (A), A female individual of *Kunpengopterus antipollicatus* associated with her egg (ZMNH M8802, Lü *et al.*, 2011) (B) , The holotype of *Kunpengopterus antipollicatus* exhibits the oldest record of opposed thumb (BPMC 0042, Zhou *et al.*, 2021) (C). All of them from Linglongta, Jianchang, Huludao, Liaoning, northeastern China.

Figure 5. *Hamipterus tianshanensis*, a block (IVPP V18932) with an incomplete skull (IVPP V18932.1) closely associated with an egg (IVPP V18932.2) and a right humerus from Hami, Xinjiang, northwestern China (Wang *et al.*, 2014).

Figure 6. *Ordosipterus planignathus* (IG V13-011), incomplete articulated Lower jaws. Dorsal view (A), left Lateral view (B), Ventral view (C) (Ji, 2020).

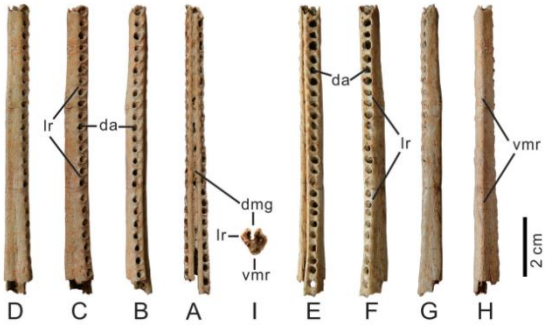

Figure 7. *Otogopterus haoae* (IG V14-001), partial mandibular symphysis. Dorsal view (A), left dorsolateral view (B), left lateral view (C), left ventrolateral view (D), right dorsolateral view (E), right lateral view (F), right ventrolateral view (G), ventral view (H), caudal view (I) (Ji and Zhang, 2020).

The earliest Chinese pterosaur *Angustinaripterus longicephalus* was found in the Middle-Late Jurassic Shaximiao Formation (Zigong, Sichuan, Southwestern China). The latest Chinese pterosaur *Zhejiangopterus linhaiensis* was found in the Late Cretaceous Tangshang Formation (Linhai, Zhejiang, Southeastern China). Chinese pterosaur are mainly found in north China besides *Angustinaripterus longicephalus* and *Zhejiangopterus linhaiensis* (He *et al.*, 1983; Cai & Wei, 1994). The late Early Cretaceous (Barremian-Aptian) is the extreme differentiation stage of Chinese pterosaur evolution, represented by deposits of Jehol Groups (mainly the Barremian-Aptian Yixian Formation and the Aptian Jiufotang Formation). During this time interval, most pterosaur families are found in China: Chaoyangopteridae,

Anurognathidae, Dsungaripteridae, Tapejaridae, Ctenochasmatidae, Istiodactylidae, Boreopteridae, Anhangueridae and Hamipteridae (Lü *et al.*, 2008; Wei *et al.*, 2021; Maisch *et al.*, 2004; Pêgas *et al.*, 2023; Zhou *et al.*, 2017; Zhou *et al.*, 2021; Lü & Ji, 2005; Wang & Zhou, 2003b; Wang *et al.*, 2014).

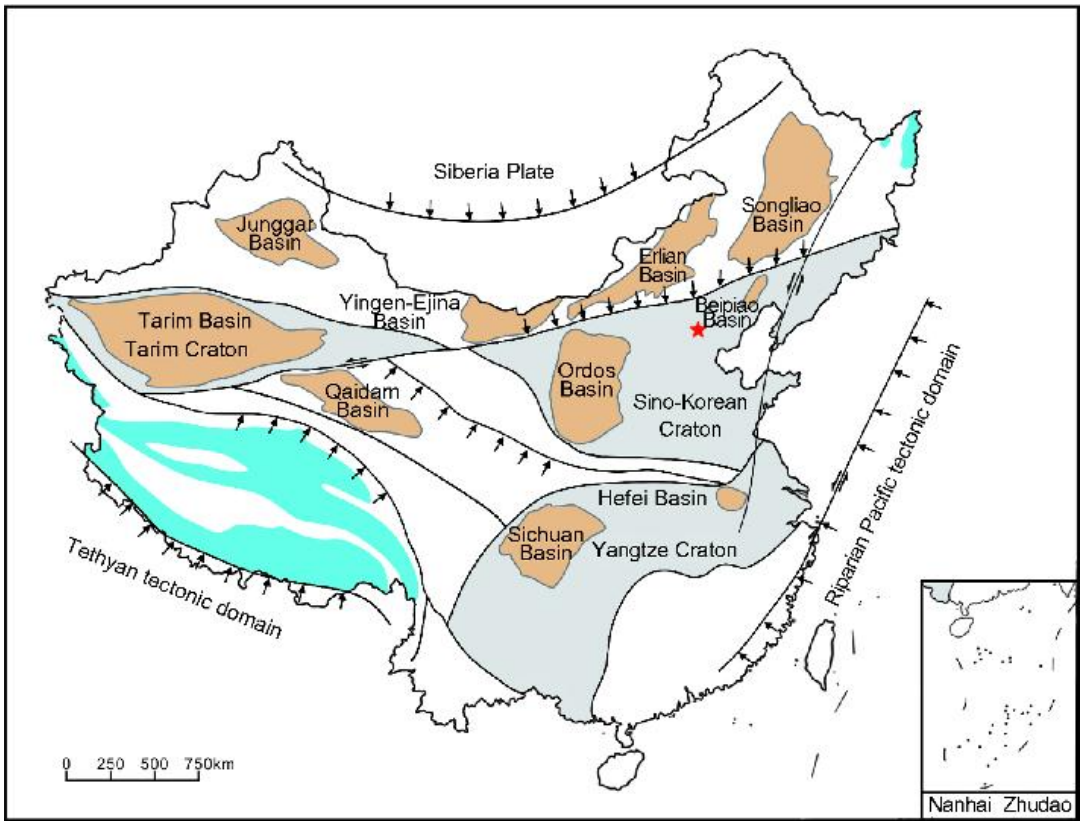

Figure 8. The general characters of the Jurassic deposition in China. Brown color represents the major terrestrial basins and the blue color represents the marine strata (Huang, 2019).

The Jurassic stratigraphy in China is dominated by continental sediments (Fig.8). Marine facies and marine-terrigenous facies sediment have developed locally in the Qinghai-Tibet area, southern South China, and northeast China (Huang, 2019). Tiaojishan Formation, Shaximiao Formation and Shishugou Formation are typical pterosaur horizons of Jurassic.Tiaojishan Formation is made up mainly of pyroclastic rock interspersed with basic volcanic and sedimentary rocks in Beijing, Hebei, Liaoning and Inner Mongolia, dating to the Middle-Late Jurassic period (Callovian-Kimmeridgian). The age of the Tiaojishan Formation is roughly 161-153 Ma (Liu *et al.*, 2006; Davis *et al.*, 2001; He *et al.*, 2004; Chang *et al.*, 2009; Liu *et al.*, 2012; Chu *et al.*, 2016; Huang, 2019). There are about 17 genera 21 species discovered till 2022: *Archaeoistiodactylus linglongtaensis*, *Cascocauda rong*, *Changchengopterus pani*, *Daohugoupterus delicatus*, *Darwinopterus modularis*, *D. linglongtaensis*, *D. robustodens*, *Dendrorhynchoides curvidentatus*, *D. mutoudengensis*, *Douzhanopterus zhengi*, *Fenghuangopterus lii*, *Jeholopterus ninchengensis*, *Jianchangnathus robustus*, *Jianchangopterus zhaoianus*, *Kunpengopterus sinensis*, *K. antipollicatus*, *Liaodactylus primus*, *Pterorhynchus*

wellnhoferi, *Qinglongopterus guoi*, *Sinomacrops bondei* , *Wukongopterus lii*. Shaximiao Formation includes two distinct subunits: the upper and lower Shaximiao Formations, also known as the Shangshaximiao Formation and Xiashaximiao Formation. It primarily consist of purple-red mudstones with variable sand inclusion and siltstones with interbedded sandstones in Chongqing and Sichuan, dating to Middle-Late Jurassic (Bajocian-Kimmeridgian). The age of the Shaximiao Formation is roughly 169-153 Ma (Li & Yang, 2009; Zhang *et al.*, 2020). *Angustinaripterus longicephalus* is a single skull with lower jaws, found in 1981 by researchers from the Zigong Historical Museum of the Salt Industry, in the Xiashaximiao Formation. It is the first skull specimen in Chinese pterosaur research history. Shishugou Group predominantly consist of conglomerate, with the majority of the formation consisting of red coloured mudstone with frequent channel/sheet sandstone lenses and occasional tuffaceous deposits in Xinjiang, dating to Middle-Late Jurassic (Callovian-Oxfordian). The Wucaiwan Member, once considered a separate, underlying formation, is now considered the lowest unit of the Shishugou Group (Weishampe *et al.*, 2004; Choiniere *et al.*, 2013). *Kryptodrakon progenitor* and *Sericipterus wucanwanensis* were found here.

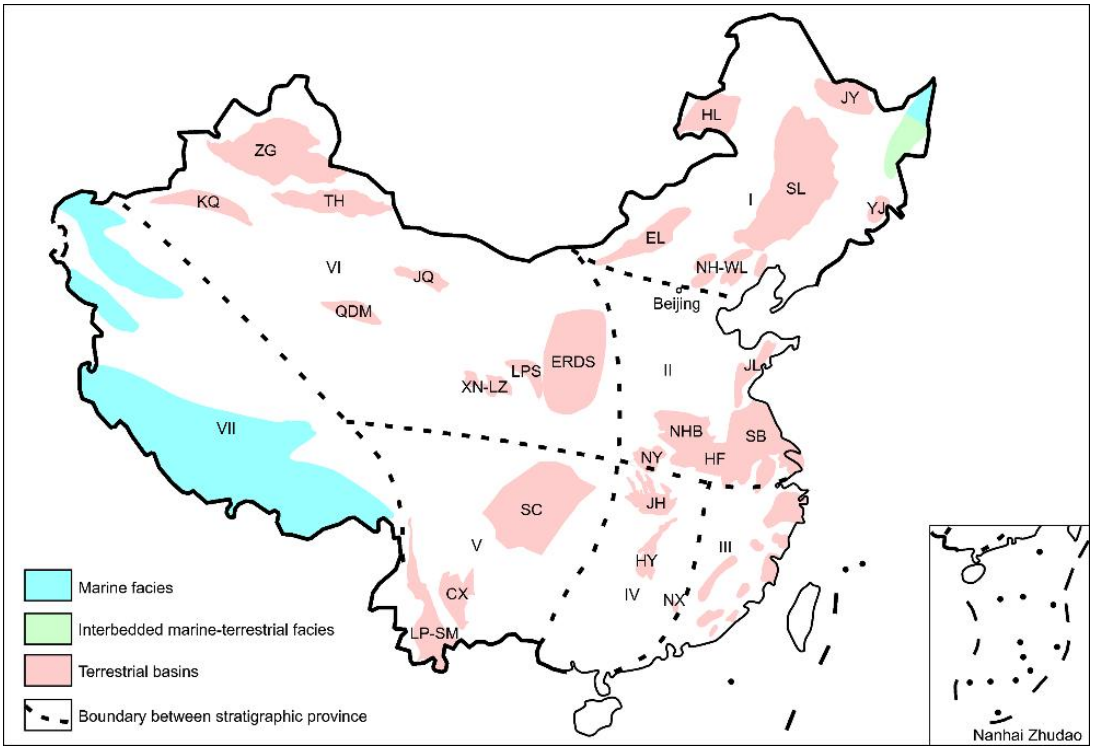

Figure 9. Distribution of Cretaceous sediments in China.. Stratigraphic provinces include I: northeast; II: north; III: southeast; IV: central-south; V: southwest; VI: northwest; VII: Xinjiang-Tibet Tethys. HL: Hailar Basin; JY: Jiayin Basin; SL: Songliao Basin; JL: Jiaolai Basin; NHB: South China Basin; HF: Hefei Basin; SB: Subei Basin; NY: Nanyang Basin; NX: Nanxiong Basin; SC: Sichuan Basin; JH: Jianghan Basin; CX: Chuxiong Basin; LPS: ERDS: Ordos Basin; Liupanshan Basin; XN-LZ: Xining-Lanzhou Basin; QDM: Qaidam Basin; JQ: Jiuquan Basin; ZG: Junggar Basin; TH: Tuha Basin; KQ: Kuqa Basin (Xi *et al.*, 2019).

Cretaceous strata are widely distributed across China and record a variety of depositional settings (Fig.9). The sedimentary facies consist primarily of terrestrial, marine and interbedded marine-terrestrial deposits, of which marine and interbedded facies are relatively limited (Xi *et al*., 2019). Yixian Formation, Jiufotang Formation, Zhidan Group, Lianmuqin Formation and Tangshang Formation are typical pterosaur horizons of the Chinese Cretaceous. Jehol Biota is distributed in western Liaoning and the adjacent northern Hebei and eastern Inner Mongolia, including the Yixian and Jiufotang Formations and equivalent strata. At present, although opinions differ to some extent, the most concentrated Jehol Biota deposit is thought to have a geological age of 131-120 Ma in the Early Cretaceous, reaching a maximum at 125 Ma (Zhou, 2006, 2014; Pan *et al*., 2013). There are about 35 genera 36 species discovered till 2022 for the Jehol Biota in the Jehol Group (Yixian and Jiufotang Fms): *Eosipterus yangi*, *Haopterus gracilis*, *Beipiaopterus chenianus*, *Feilongus youngi*, *Boreopterus cuiae*, *Eopteranodon lii*, *Cathayopterus grabaui*, *Yixianopterus jingangshanensis*, *Gegepterus changi*, *Elanodactylus prolatus*, *Ningchengopterus liuae*, *Zhenyuanopterus longirostris*, *Pterofiltrus qiui*, *Gladocephaloideus jingangshanensis*, *Moganopterus zhuiana*, *Boreopterus giganticus*, *Luchibang xinzhe*, *Sinopterus dongi*, *Chaoyangopterus zhangi*, *Liaoningopterus gui*, *Jidapterus edentus*, *Eoazhdarcho liaoxiensis*, *Huaxiadraco corollatus*, *Nurhachius ignaciobritoi*, *N. luei*, *Liaoxipterus brachyognathus*, *Istiodactylus sinensis*, *Shenzhoupterus chaoyangensis* , *Hongshanopterus lacustris*, *Nemicolopterus crypticus*, *Guidraco venator*, *Ikrandraco avatar*, *Linlongopterus jennyae*, *Forfexopterus jeholensis* , *Pangupterus liui*, *Lingyuanopterus camposi*. The Zhidan Group comprises a lower part of red, purplish to bluish mudstones and sandstones and an upper part of greyish-green to reddish-orange cross-bedded sandstones and siltstones in Ordos Basin (Gansu and Inner Mongolia), dating to Early Cretaceous. The Zhidan Group consists of five formations in ascending order: Yijun, Luohe, Huanhe, Luohandong and Jingchuan formations (Xi *et al*.,2019). *Huanhepterus qingyangensis* was found in Huanhe Formation. The new pterosaur locality of Ordos Basin is the Luohandong Formation in Xinzhao village of Otog Qi, Inner Mongolia. *Ordosipterus planignathus* and *Otogopterus haoae* were both found there in 2020. Lianmuqing Formation composed of interbedded red green and yellow variegated mudstones and siltstones in Junggar Basin (Xinjiang), dating to Early Cretaceous (Valanginian-Albian) (Lucas, 2001). The three pterosaurs found here are all members of Dsungaripteridae: *Dsungaripterus weii*, *Noripterus complicidens* and *Lonchognathosaurus acutirostris*. Tangshang Formation composed of light gray submerged tuff, tuff fine sandstone and siltstone, dating to Late Cretaceous (Turonian-Campanian) (Lu *et al*., 2006; Wang *et al*., 2014). *Zhejiangopterus linhaiensis*, the only Azhdarchidae in China, was found here.

CHAPTER II

ADVANCES IN CHINESE PRIMITIVE TYPE PTEROSAUR: A NEW ANUROGNATHID *SINOMACROPS BONDEI* AND COMMENTS ON THE GROUP

INTRODUCTION

The Anurognathidae is a very peculiar pterosaur group still poorly understood and rather obscure, characterized by a unique morphology and involved in a complex history of uncertainty about their phylogenetic affinities (Hone, 2020). Spanning from the Middle Jurassic (Callovian) to the Early Cretaceous (Aptian), anurognathids are small-sized (up to 900 mm in wingspan) and exhibit short skulls with a diminutive preorbital region, huge orbits and rounded jaws that are wider than long (Bennett, 2007; Hone, 2020). Due to their short wings with low aspect ratios and their peg-like teeth, these small pterosaurs have been interpreted as aerial insectivores (Bennett, 2007; Witton, 2008, 2013; Ősi, 2011; Habib, 2011; Hone, 2020), of possible arboreal habits (Ji & Ji, 1998; Bennett, 2007; Witton, 2013; Lü *et al.*, 2018; Hone, 2020).

The Anurognathidae have been defined as a node-based group, as the least inclusive clade containing *Anurognathus ammoni* and *Batrachognathus volans* (Kellner, 2003; Unwin, 2003). Recently, it has been redefined as a branch-based group, englobing all species closer to *Anurognathus* than to *Dimorphodon*, *Pterodactylus* or *Scaphognathus* (Hone, 2020). So far, this group comprises six nominal species, and is known by 12 specimens from Germany, Kazakhstan, Mongolia, China and North Korea (with a putative 13th one from the USA). The first described one was *Anurognathus ammoni*, coming from the Tithonian Solnhofen limestones of Bavaria (Döderlein, 1923) and being represented by two specimens (Bennett, 2007). It was not until the second specimen was described that several aspects of its morphology were clarified, such as the broad wings, the short preorbital region and extensive orbit, the jugal overlying the maxilla, the vertical (or slightly anteriorly inclined) quadrate, the reduced palatal elements, and the short tail lacking filiform processes of the zygapophyses and haemapophyses, convergent with pterodactyloids (Bennett, 2007).

The second nominal species was *Batrachognathus volans*, described from an incomplete skeleton including a partial skull from the Oxfordian-Kimmeridgian Karabastau Formation of Kazakhstan (Riabinin, 1948). A second specimen of *Batrachognathus volans* (Unwin, Lü & Bakhurina, 2000), still awaiting a full description, possesses a tail that bears well-developed rod-like processes of the haemapophyses and zygapophyses, and is longer than that of any other anurognathid (Costa *et al.*, 2013). With this discovery, *Batrachognathus volans* became the first known anurognathid to exhibit a long tail with developed rod-like processes as typical of most non-pterodactyloid pterosaurs (see Costa *et al.*, 2013).

The third anurognathid to be described was *Dendrorhynchoides curvidentatus*, the first recovered from a Cretaceous deposit, the early Aptian Jianshangou beds of the Yixian Formation (Ji & Ji, 1998). Originally thought of as Barremian, these beds are now viewed as early Aptian in age (see Chang *et al.*, 2009).

Jeholopterus ningchengensis, based on an almost complete skeleton with

extensive soft tissue preservation coming from the Daohugou beds near Daohugou (Ningcheng County, Inner Mongolia), was later described as another Cretaceous anurognathid (Wang *et al.*, 2002), on the basis of the now outdated view of the Daouhugou beds as part of the Yixian Formation (Barremian-Aptian). Subsequently, these beds were reinterpreted as part of the Middle-Late Jurassic Tiaojishan Formation. Presently, these rocks have been once more reinterpreted, and are now considered to belong to the Haifanggou/Jiulongshan Formation (Huang, 2015, 2016). The locality that has yielded *Jeholopterus ningchengensis* has been dated as Callovian-Oxfordian (Liu, Liu & Yang, 2006; Gao & Shubin, 2012). A second specimen from the same locality has been regarded as most likely conspecific with *Jeholopterus ningchengensis*, though a detailed description and a formal taxonomic assessment have not been provided yet (Ji & Yuan, 2002; Witton, 2013; Yang *et al.*, 2019).

Later, a second species for the genus *Dendrorhynchoides*, named *D. mutoudengensis*, was erected based on an almost complete skeleton from the Mutoudeng locality, Tiaojishan Formation (Lü & Hone, 2012). Recently, a new genus has been erected to accommodate this species: *Luopterus*, named after the late Prof. Junchang Lü (Hone, 2020). Moreover, a second Cretaceous anurognathid was also named recently, *Vesperopterylus lamadongensis*, known from an almost complete holotype from the late Aptian Jiufotang Formation (Lü *et al.*, 2018).

Indeterminate specimens include IVPP V16728, which stands out as the second specimen with a long tail and developed rod-like processes, similar to *Batrachognathus volans* (see Costa *et al.*, 2013) and unlike all remaining anurognathids. NJU–57003 is another long-tailed specimen from the Mutoudeng locality (Daohugou Beds, Tiaojishan Formation), only preliminarily described (Yang *et al.*, 2019). A relatively complete specimen from the Early Cretaceous of North Korea also awaits description (Gao *et al.*, 2009), as well as a fragmentary specimen comprised of wing elements from the Middle Jurassic (Aalenian/Bajocian) Bakhar deposits of Central Mongolia (Bakhurina & Unwin, 1995). Finally, the poorly-known *Mesadactylus ornithosphyos*, based on the holotype BYU 2024 (a synsacrum) from the Kimmeridgian-Tithonian Morrison Formation of the USA (Jensen & Padian, 1989), is a potential anurognathid (see Bennett, 2007).

Pterosaur phylogeny is intricated with controversies, but no other group compares to the Anurognathidae when it comes to uncertainty concerning its placement (Young, 1964; Unwin, 1992, 1995, 2003; Viscardi *et al.*, 1999; Kellner, 2003; Andres, Clark & Xu, 2010; Dalla Vecchia, 2014, 2019; Hone, 2020). Five cladistic hypotheses based on computed analyses have been presented for the Anurognathidae, wherein they are viewed as: the basalmost pterosaur group (Kellner, 2003); the sister-group of the Novialoidea (Unwin, 2003); the sister-group of the Breviquartossa (Dalla Vecchia, 2019); scaphognathids, whereby these are the sister-group of the Monofenestrata (Vidovic & Martill, 2017); or the sister-group of

the Pterodactyloidea (Andres, Clark & Xu, 2010, 2014). And even though the monophyly of the Anurognathidae has been strongly corroborated (Kellner, 2003; Unwin, 2003; Bennett, 2007; Andres, Clark & Xu, 2010; Dalla Vecchia, 2019), its intrarelationships have been poorly explored (Hone, 2020).

This work presents a new fossil coming from the Mutoudeng locality, JZMP-2012-001, representing a new genus and species of long-tailed anurognathid. Despite being crushed to the point of obliterating many details, the specimen is rather complete and provides new information for the group, including the first record of an anurognathid skull exposed in mostly lateral view. In other specimens, the skull is either exposed in mostly internal view, as in the holotype of *Anurognathus ammoni* (Döderlein, 1923; Wellnhofer, 1975; Bennett, 2007), or dorsoventrally crushed, as in all other specimens that preserve a skull (Riabinin, 1948; Ji & Ji, 1998; Bennett, 2007; Gao *et al.*, 2009; Lü & Hone, 2012; Lü *et al.*, 2018).

We further review the phylogenetic relationships of the group (both intra and inter), presenting an analysis including all proposed species and a resulting in a new hypothesis for the placement of the group as basal monofenestratans.

GEOLOGICAL SETTING

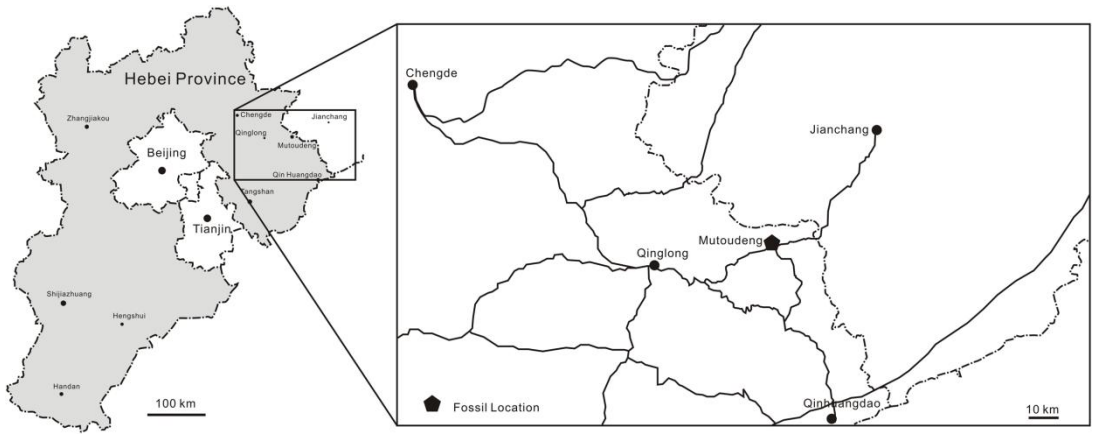

Figure 10. Fossil provenance. Maps indicating Hebei Province (China). JPM-2012-001 comes from the Mutoudeng locality.

The Tiaojishan Formation takes its name from the Tiaojishan Mountain (Mentougou District, Beijing), and was named by Ye (1920). This and the Haifanggou/Jiulongshan Formation have yielded the famous Yanliao Biota in western Liaoning and adjacent regions (Huang, 2015, 2016). This biota is well known for the beautiful preservation and abundancy of insects and vertebrate fossils, such as salamanders, feathered dinosaurs, pterosaurs and mammals (Sullivan *et al.*, 2014). The most important localities that yield the Yanliao Biota are Daohugou in Ningcheng County of southeast Inner Mongolia (Haifanggou Fm.), Linglongta of Jianchang County of western Liaoning Province (Tiaojishan Fm.), and Mutoudeng of Qinglong

County of northern Hebei Province (Tiaojishan Fm.; Lü *et al.*, 2013; Huang, 2015, 2016). From the Haifanggou Formation at Daohugou (Liu *et al.*, 2012), pterosaurs are relatively rare, with *Jeholopterus ningchengensis* (Wang *et al.*, 2002), *Pterorhynchus wellnhoferi* (Czerkas & Ji, 2002) and *Daohugoupterus delicatus* (Cheng *et al.*, 2015). From the slightly younger Tiaojishan Formation at the Linglongta locality, pterosaurs are abundant in number and in diversity (see Sullivan *et al.*, 2014 for a review), with wukongopterids (Wang *et al.*, 2009, 2010; Lü *et al.*, 2009; Cheng *et al.*, 2017a), *Jianchangopterus* (Lü & Bo, 2011), *Jianchangnathus* (Cheng *et al.*, 2012) and *Fenghuangopterus* (Lü, Fucha & Chen, 2010). From the Tiaojishan Formation at Mutoudeng come *Luopterus mutoudengensis* (Lü & Hone, 2012; Hone, 2020), *Qinglongpterus guoi* (Lü *et al.*, 2012) and *Changchengopterus pani* (Lü, 2009). It is from the Mutoudeng locality that comes the new specimen herein described (Fig. 10)

The Tiaojishan Formation is mainly distributed in the Chengde Basin (Maoniujiao–Xiaoguozhangzi–Jiyuqing Area) in northern Hebei Province. It is around 300 m thick (Zhang & Chen, 2015). It is mainly composed of neutral volcanic rock (Zhang & Chen, 2015). The lithology of the lower member includes dark grey, grey purple trachyandesites, quartz trachyandesites, small trachyandesitic agglomerate, small trachyandesitic ignimbrite (Zhang & Chen, 2015). The lithology of upper member includes dark grey, burgundy trachyandesites, trachyandesitic agglomerate, partially containing grayish purple, grayish green sedimentary tuff, tuffaceous conglomerate and tuffaceous sandstone (Zhang & Chen, 2015).

Zhang, Wang & Liu (2008) analyzed samples of volcanic rock from several typical localities (Luanping Basin, Chengde Basin, Sanshijiazi Basin and Jinlingsi-Yangshan Basin), utilizing LA-ICP-MS Zircon U-Pb. Their result suggest that the lower limit age of the Tiaojishan Formation should be around 165 Ma. Li *et al.* (2019) analyzed samples of volcanic rock from the bottom of the lower section and andesite from the top of the upper section, utilizing LA-ICP-MS Zircon U-Pb. Their result gave an age range of 170–153 Ma for the Formation as a whole, that is, from the Bajocian until the Kimmeridgian. A specific dating for the strata of the Linglongta locality has been provided by Liu *et al.* (2012), in order to provide a constrained age range for Linglongta wukongopterid pterosaurs. The bottom and the top of this locality were dated, resulting in an age range of 161–160 Ma (Liu *et al.*, 2012), falling within the Oxfordian (early Late Jurassic). Specific dating under geochemical approaches still lack for the Mutoudeng locality. However, biostratigraphic studies, based mainly on conchostracans, suggest that the Linglongta and Mutoudeng strata are chronocorrelate (Chu *et al.*, 2016).

MATERIALS AND METHODS

Computed tomography scanning

JPM-2012-001 was computed tomography (CT) scanned using a Nikon XTH225ST scanner at the Laboratory of Stratigraphy and Paleontology, Institute of

Geology, Chinese Academy of Geological Sciences (IG-CAGS), Beijing, China. The specimen was scanned at 160 kV and 131 mA. The data set includes 2,000 image slices (2,000 × 2,000 pixels) with a slice thickness of 0.121 mm. The data was imported into digital visualization software Avizo (version 9.1) for image processing and visualization.

Phylogenetic analysis

Concerning terminal taxa, our phylogenetic analysis is focused on non-pterodactyloid pterosaurs, following previous works that also focused on these forms (e.g. Dalla Vecchia, 2009, 2019; Andres, Clark & Xu, 2010; Lü *et al.*, 2012). Concerning our character list, we have gathered discrete characters from Vidovic & Martill (2017), Longrich, Martill & Andres (2018) and Dalla Vecchia (2019), all of which further encompass data from previous studies (e.g. Kellner, 2003; Unwin, 2003; Dalla Vecchia, 2009; Lü *et al.*, 2009; Wang *et al.*, 2012; Naish, Simpson & Dyke, 2013; Andres, Clark & Xu, 2014; Britt *et al.*, 2018). Following previous works, we did not employ composite coding (Colless, 1985). The character list is available in Supplemental File 1 (a nexus format file for the software Mesquite, containing the data matrix) and Supplemental File 2 (a TNT file ready for executing the analysis, that can also be opened as a txt file).

We did not employ the treatment of continuous data as such (for discussions on the subject see Goloboff, Mattoni & Quinteros, 2006; Bardin et al., 2014; Mongiardino Koch, Soto & Ramírez, 2015; Vidovic, 2018). The original discretized quantitative characters from previous analyses (see our character list) were not modified, except for morphometric characters 270 (humerus/femur length, modified from Kellner (2003)) and 368 Wei *et al.* (2021), PeerJ, DOI 10.7717/peerj.11161 5/37 (tibia/femur length). Discrete states for the morphometric characters 270 and 368 were categorized (discretized) by using the gap-weighting method (Thiele, 1993). In order to optimize the phylogenetic signal, following Bardin *et al.* (2014), state number was set at 3. The morphometric dataset subjected to gap-weighting is available as Supplemental File 3.

The resulting categorization is presented in Supplemental File 3 and the data matrix (Supplemental Files 1 and 2). Quantitative characters 1, 45, 106, 152, 191, 264, 265, 270, 285, 289, 290, 293, 304, 313, 320, 321, 323 and 362 were treated as ordered. Following other works, all characters were equally weighted (e.g. Fitzhugh, 2006).

The analysis was performed using TNT (Goloboff, Torres & Arias, 2018) and was divided in two steps. The first search was performed using New Technology Search (using Sectorial Search, Ratchet, Drift and Tree fusing, default parameters), with random seed = 0. Subsequently, using trees from RAM, we performed a Traditional Search swapping (using TBR, collapsing trees after search). The TNT file is available as Supplemental File 2.

Nomenclatural acts

The electronic version of this article in Portable Document Format will represent a published work according to the International Commission on Zoological Nomenclature (ICZN), and hence the new names contained in the electronic version are effectively published under that Code from the electronic edition alone. This published work and the nomenclatural acts it contains have been registered in ZooBank, the online registration system for the ICZN. The ZooBank Life Science Identifiers (LSIDs) can be resolved and the associated information viewed through any standard web browser by appending the LSID to the prefix http://zoobank.org/. The LSID for this publication is: urn:lsid:zoobank.org:pub:15997DEB-0EF7-40F6-80B0-2C40ED47D43B. LSID for the new genus: urn:lsid:zoobank.org:act:C1268C7D-80AA-4854-93E7-0E60220A05BC. LSID for the new species: urn:lsid:zoobank.org:act:048E9ADE-8C3A-47D4-B074-DCEFA40BDE9A. The online version of this work is archived and available from the following digital repositories: PeerJ, PubMed Central and CLOCKSS.

RESULTS

Systematic Paleontology

Pterosauria Owen, 1842
Novialoidea Kellner, 2003
Breviquartossa Unwin, 2003
Monofenestrata Lü *et al.*, 2009
Anurognathidae Kuhn, 1937
Batrachognathinae Kellner *et al.*, 2010

Definition. The most inclusive clade containing *Batrachognathus volans* but not *Anurognathus ammoni* (Kellner *et al.*, 2010).

Synapomorphies. Humeral deltopectoral crest reduced (less wide than humeral shaft; and less wide than proximodistally long), humeral deltopectoral crest subrectangular, ulnar crest of humerus rounded, humeral/femoral length ratio over 1.60, tibial/femoral length ratio over 1.70.

Included species. *Batrachognathus volans* and *Sinomacrops bondei* gen. et sp. nov.

Sinomacrops bondei gen. et sp. nov.

Etymology. The generic name is a combination of *Sino, macro* and *ops*; which are Ancient Greek for China, large, and eyes/face, respectively. This is in reference to both the large eyes and the broad faces that are typical of anurognathids, and to the Chinese origin of the new species. The specific epithet honors paleontologist Niels Bonde, for his many scientific contributions and being an inspiration for us.

Holotype. JPM-2012-001 (Figs. 11–15).

Locality and horizon. Mutoudeng, Qinglong County of Hebei Province. Daohugou Beds (Callovian-Oxfordian 164-158 Ma) of the Tiaojishan Formation (see Liu, Zhao & Liu 2006; Liu *et al.*, 2006; Gao & Shubin, 2012)

Diagnosis. The new taxon exhibits two autapomorphies: first three maxillary alveoli closely spaced, and tibiotarsus twice as long as the femur.

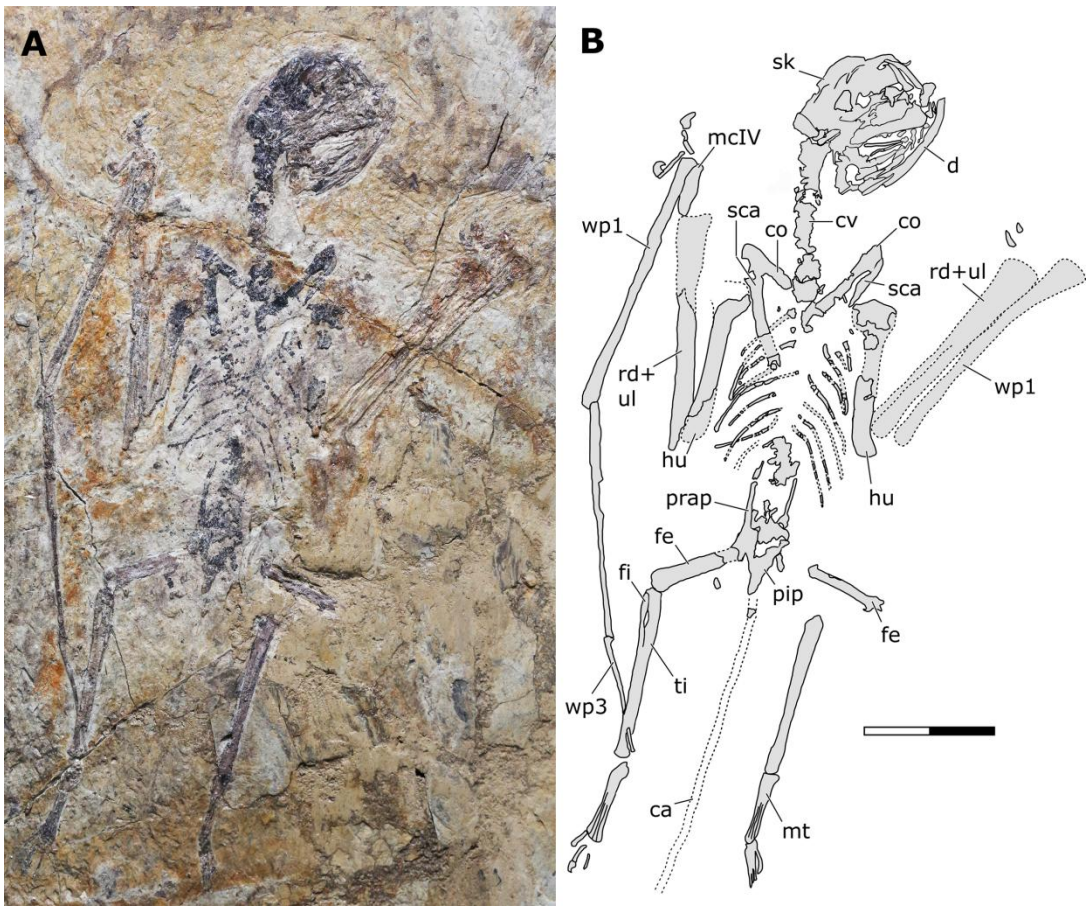

Figure 11. *Sinomacrops bondei* tax. nov., holotype (JPM-2012-001) overview. (A) Photograph; and (B) schematic drawing. Abbreviations: ca, caudal vertebrae; co, coracoid; cv, cervical vertebrae; d, dentary; fe, femur; fi, fibula; hu, humerus; mcIV, metacarpal IV; pip, puboischiadic plate; prap, preacetabular process of the illium; rd, radius; sca, scapula; sk, skull; ul, ulna; wp, wing phalanx. Scale bar equals 20 mm.

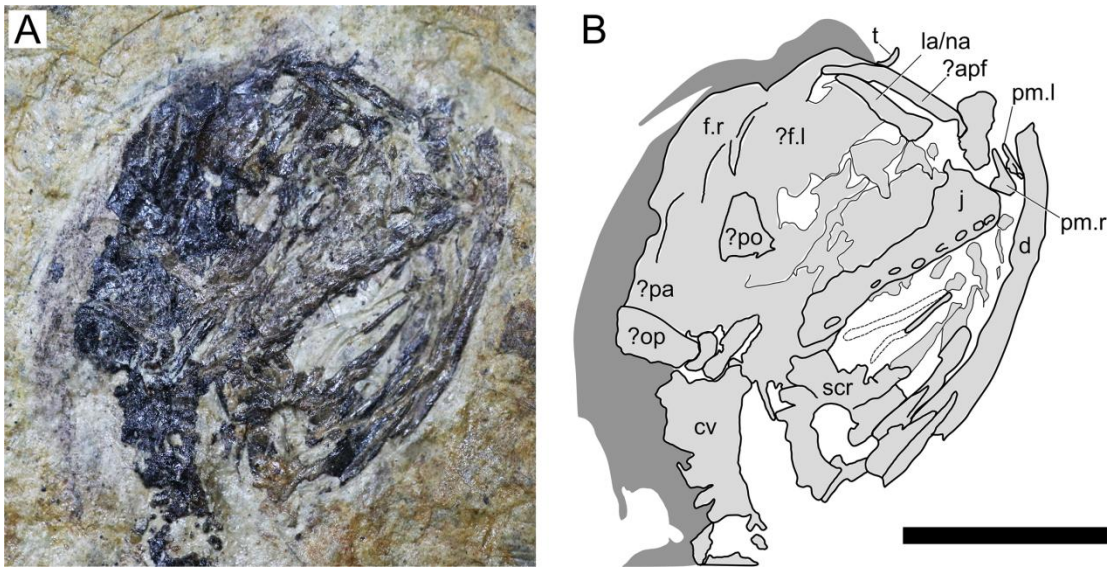

Figure 12. *Sinomacrops bondei* tax. nov., skull of JPM-2012-001. (A) Photograph; and (B) schematic drawing. Light grey represents bones; dark grey represents soft tissue. Abbreviations: apf, anterior process of the frontal; cv, cervical vertebrae; d, dentary; f, frontal; j, jugal; la, lacrimal; na, nasal; pa, parietal; po, postorbital; pm, premaxilla; op, opisthotic; scr, sclerotic ring. Scale bar equals 10 mm.

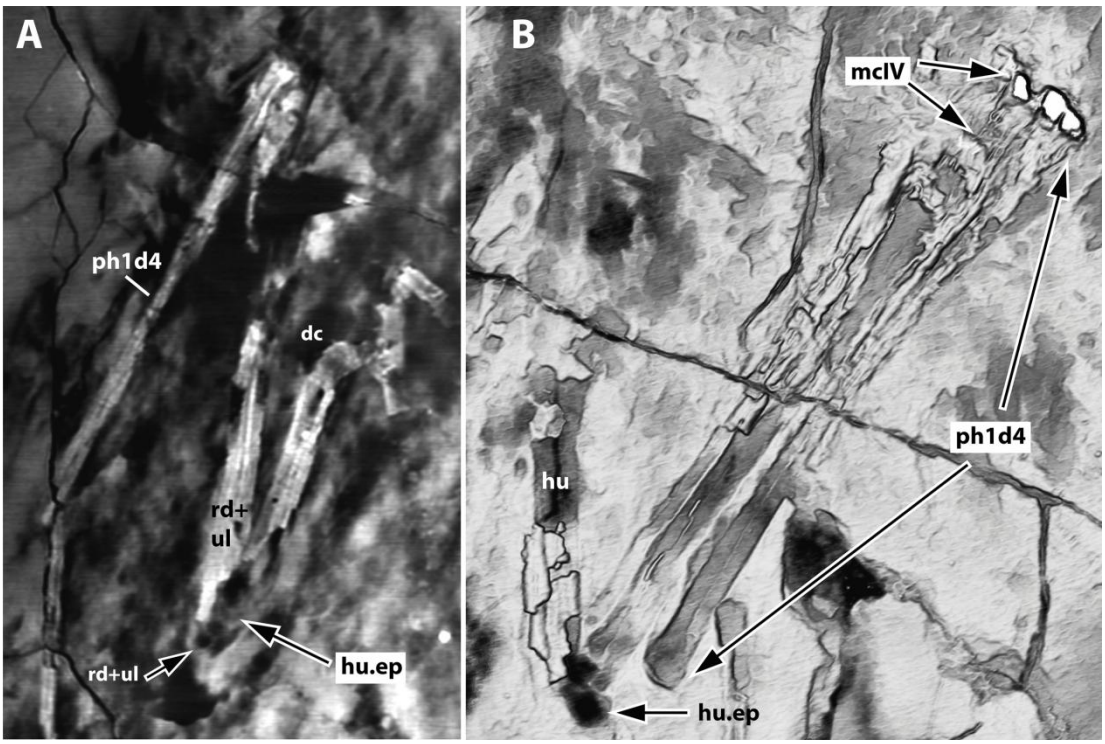

Figure 13. Computed-tomography images of the wings of JPM-2012-001. (A) Right wing; (B) left wing. Abbreviations: d, digit; dc, deltopectoral crest; hu.ep, humeral epiphysis; mc, metacarpal; ph, phalanx; rd, radius; ul, ulna.

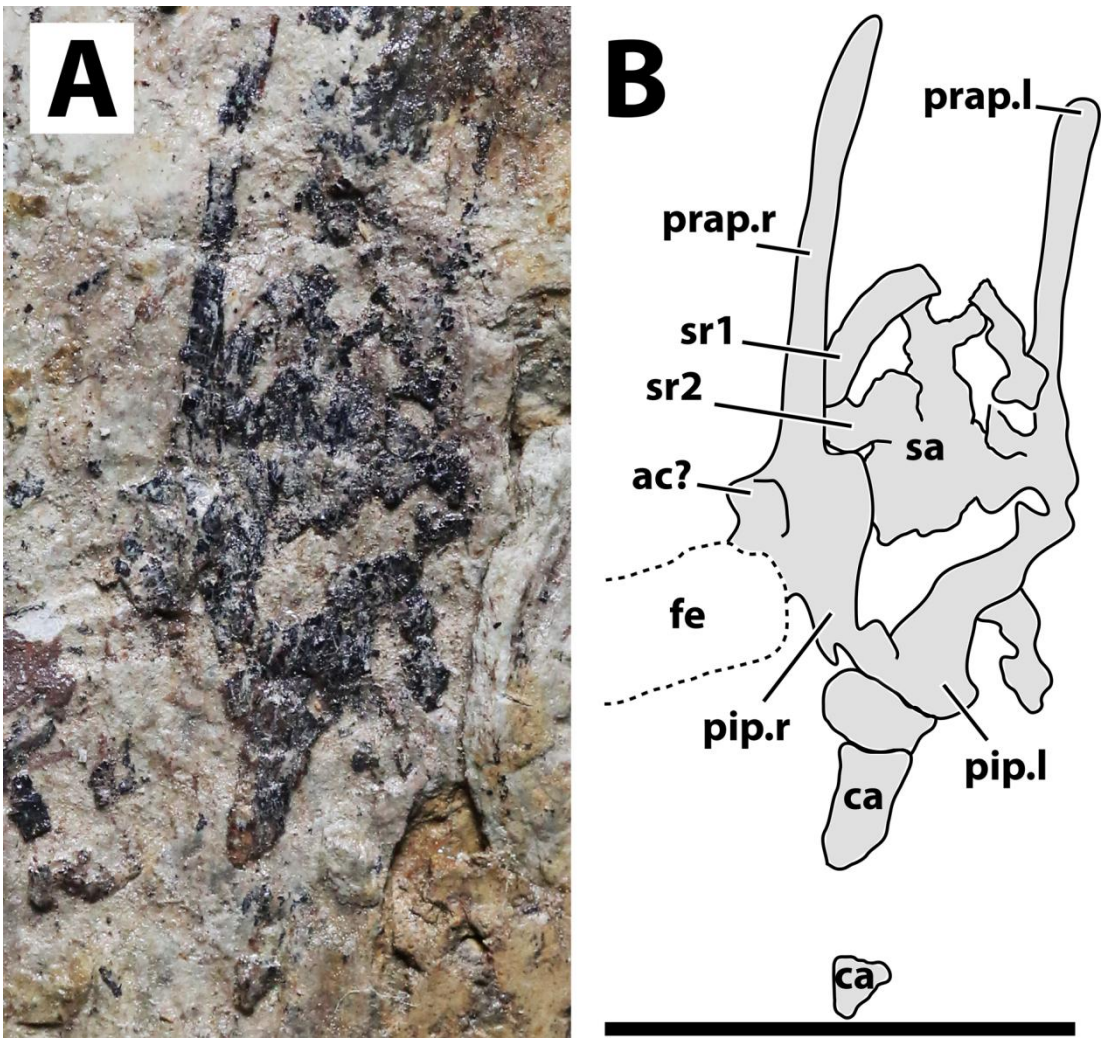

Figure 14. Sacral region of JPM-2012-001. (A) Photograph; (B) schematic drawing. Abbreviations: ac, acetabulum; ca, caudal vertebrae; fe, femur; pip, puboischiadic plate; prap, preacetabular process of the illium; sa, sacral vertebrae; sr, sacral rib. Scale bar equals 10 mm.

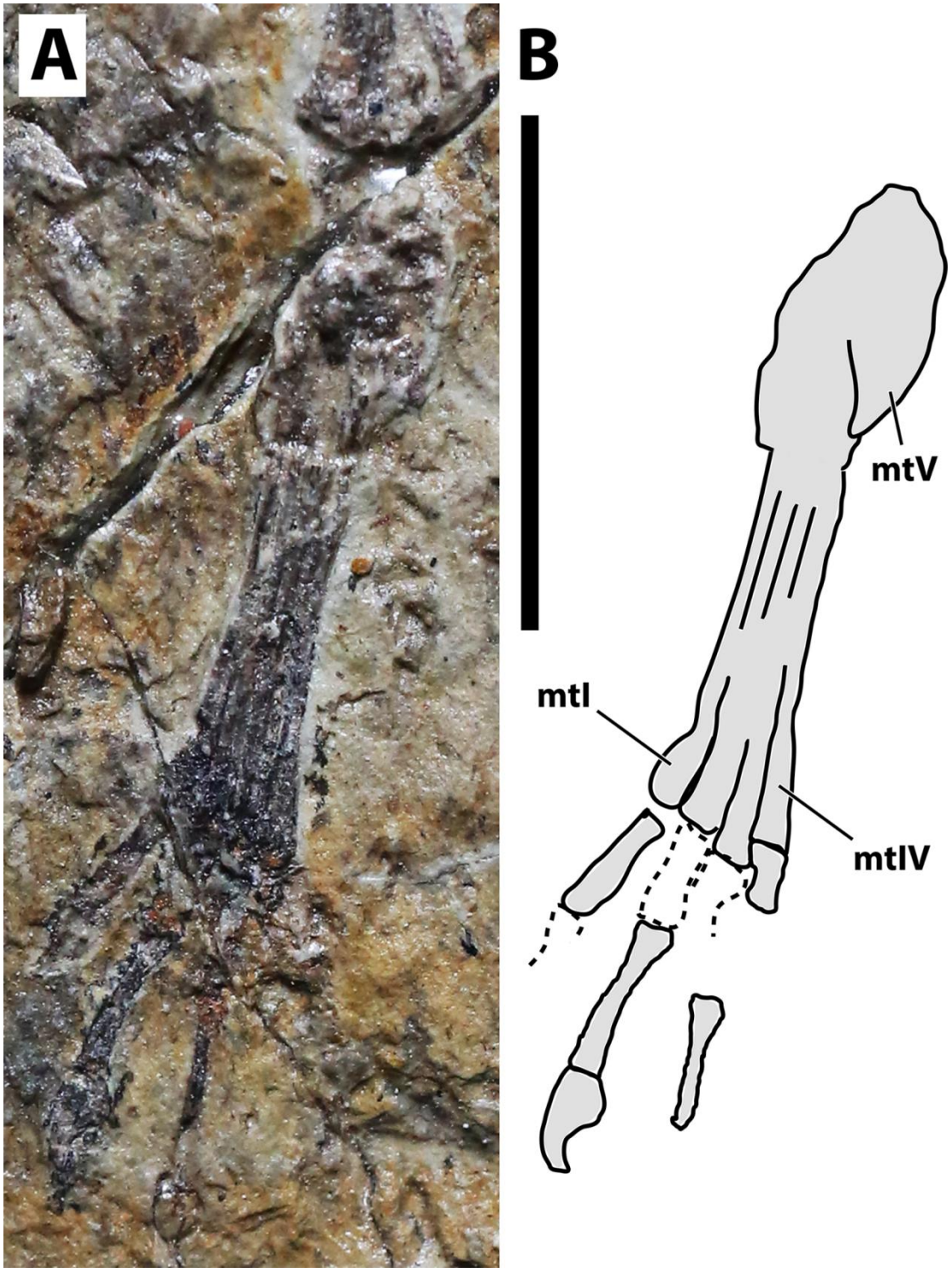

Figure 15. Right pes of JPM-2012-001. (A) Photograph; (B) schematic drawing. Abbreviations: mt, metatarsal. Scale bar equals 10 mm.

DESCRIPTION

Generalities.

JPM-2012-001 comprises a crushed skeleton (Fig. 11). While the cranium and some cervical vertebrae are exposed in right lateral aspect (Fig. 12), the remaining of the skeleton is exposed in ventral view. The preserved bone tissue exhibits a fragile, brittle condition. In consequence, in many regions of the skeleton, fragments of bone tissue have been lost posterior to collection of the specimen. These lost fragments left clear impressions on the matrix, indicating where they were originally present. Lost fragments include mainly the caudal vertebrae, sternum, distal epiphysis of right humerus, proximal epiphyses of right ulna and radius, parts of the left humerus, and most of the left manus.

Micro CT scan resulted in images with only limited resolution. Nonetheless, the images permitted better visualization of some impressions on the matrix (represented by empty spaces on the slices), helping in the identification of some bone limits and extensions. Such was the case of elements of the left wing (humerus epiphysis, radius and ulna, wing metacarpal and first wing phalanx), as well as the right humerus (Fig. 13). CT images did not provide enough resolution for additional data on other skeletal regions.

Soft tissue.

The skeleton includes preservation of soft tissue patches. The dorsal margin of the skull is covered by skin impressions that descends onto the neck region (Fig. 12). An irregular patch of soft tissue lateral to the left tibiotarsus suggests that the brachiopatagium extended posteriorly onto the distal region of the crus. A brachiopatagium extending distally on the crus is consistent with what is seen in *Jeholopterus ningchengensis* (see Kellner *et al.*, 2010) and pterosaurs in general (see Elgin, Hone & Frey, 2011). Another large patch of soft tissue is present medial to the right hindlimb, extending from the femoral region until the distal fifth of the tibiotarsus. This implies in an extensive cruropatagium, though it is not clear if the tail is integrated with it. An extensive cruropatagium can also be found in *Sordes pilosus* (Unwin & Bakhurina, 1994). Deeper investigation of the soft tissue remains of JPM-2012-001 is beyond the scope of the present contribution and shall be presented elsewhere.

Cranium.

The cranium of JPM-2012-001 is exposed in right lateral aspect (Fig. 12). A small pair of bones on the rostral tip of the skull seem to represent an unfused pair of premaxillae. Individually, they comprise basically two processes, one ascending and another one extending posteriorly. This indicates that the fused premaxillae would display a T-shape similar to other anurognathids, as seen in *Batrachognathus volans* (Riabinin, 1948) and *Anurognathus* (Bennett, 2007). The right premaxilla is exposed laterally, while the left one is slightly displaced and exposed in anteromedial aspect.

The dorsal process of the premaxilla seems to have extended for no further than half the height of the skull. It contacts an anterior process of the frontal, which is elongated and thin, as in *Anurognathus ammoni* (see Bennett, 2007). The posterior process of the premaxillae participates on the occlusal jaw margin, and presumably contacted the maxillae, though the bones are slightly displaced and not in natural contact.

The maxilla and jugal are fused, with not visible sutures, forming a large bony structure, posterior to the premaxillae. It forms most of the jaw as well as the ventral border of the orbit. The jugo-maxilla structure houses 9 alveoli. The lacrimal process of the jugal is present on the anterior region of this structure. It forms the anteroventral border of the orbit, and the posteroventral margin of the nasoantorbital fenestra. It is incomplete dorsally, but is clearly slender, much higher than long. The nasal and the lacrimal cannot be distinguished.

It appears that both frontals are visible: the right one in lateral aspect, and the left one in medial aspect. They are both positioned on the posterodorsal region of the orbit, and take part in the dorsal margin of the skull itself. Their limits are not clear, but the dorsal margin of the right frontal is convex, as is the dorsal margin of the skull in lateral view. Posterior to the right frontal, two bones are tentatively interpreted as the right parietal and a misplaced right opisthotic.

A large bone bearing 9 alveoli forms most of the right upper jaw margin, and is here interpreted as a jugomaxilla complex, similar to the one reported for *Anurognathus ammoni* where the jugal overlays the maxilla laterally, fusing with it (Bennett, 2007). The structure is seen in lateral view, and no sutures can be seen separating jugal from maxilla. The right jugomaxilla seems to be disarticulated from both the quadrate and the premaxilla.

A triangular bone located on the posterior margin of the orbit is tentatively interpreted as the postorbital. If this identification is correct, then the postorbital of *Sinomacrops* is quite different from that of *Anurognathus*, which is very slender (and dorsoventrally elongated). Thus, the postorbital of *Sinomacrops* would be more similar to that of some non-anurognathid pterosaurs such as *Dimorphodon* or rhamphorhynchids (e.g. Padian, 1983; Wellnhofer, 1991).

Ventral to the jugomaxilla, a rod-like bone is preserved, adjacent to the impression of another similar rod-like bone. These two rod-like bones are interpreted as either members of the hyoid apparatus, or members of the palate, which is composed of rod-like bones and bony processes (pterygoids, palatines, vomer, ectopterygoids) in *Anurognathus ammoni*, *Jeholopterus ningchengensis* and *Batrachognathus volans* (Riabinin, 1948; Bennett, 2007; Yang *et al.*, 2019).

A partial sclerotic ring is preserved, displaced from its natural position and

located ventral to the posterior region of the skull. Though partially preserved, it is complete enough to allow for an estimation of its diameter. It is estimated as ~7 mm, what is close to the estimated diameter of the orbit (7.5 mm).

Mandible.

An hemimandible is exposed beneath the skull (Fig. 12). No alveoli can be observed, suggesting that it is the left hemimandible in ventral view. We infer that this hemimandible is complete because its length equals that of the upper jaw. It is only slightly bowed, as in *Batrachognathus volans*, instead of strongly semicircular as in the jaws of *Dendrorhynchoides* (Ji & Ji, 1998), *Luopterus* (Lü & Hone, 2012; Hone, 2020), *Jeholopterus* (Wang *et al.*, 2002), *Anurognathus* (Bennett, 2007) or *Vesperopterylus* (Lü *et al.*, 2018).

Dentition.

A single preserved tooth crown is visible, displaced from the jaws and located near the anterodorsal region of the skull (Fig. 12). This tooth is slender and slightly recurved. At least 9 alveoli are present on the right maxilla. The alveoli on the right premaxilla are unclear. The first three maxillary alveoli are closely spaced, with the spacing between them being shorter than their diameter. Posteriorly, the spacing between the subsequent alveoli is subequal to their diameter.

Axial postcranium.

Throughout the whole specimen, the vertebrae are highly damaged and details of their anatomy cannot be retrieved (Fig. 11). Still, as the skeleton is almost complete, the lengths of each segment can be estimated, with 23 mm for the cervical series; 30 mm for the dorsal series; 11 mm for the sacral series; and >36 mm for the caudal series. The sacral series thus seems to have been elongated, similarly to the condition seen in the possible anurognathid *Mesadactylus* (see Jensen & Padian, 1989). The rib of the first sacral is strongly inclined posteriorly, while the rib of the second sacral is less inclined (Fig. 14). This configuration is very similar to that of *Mesadactylus* (see Jensen & Padian, 1989). At least 9 pairs of ribs anterior to the sacral region can be seen (Fig. 11), all of which are long and slender, and interpreted as dorsal ribs. This is the same number of dorsal ribs seen in *Dendrorhynchoides* (Ji & Ji, 1998), *Anurognathus* (Bennett, 2007) and *Jeholopterus* (Wang *et al.*, 2002). Concerning caudal vertebrae, only three incomplete remains of proximal caudal centra are present, near the sacral region. They are simple, lacking lateral processes.

Forelimb.

The scapulae and coracoids of JPM-2012-001 are elongate and slender, as in other anurognathids (e.g. Bennett, 2007; Lü *et al.*, 2018). Although fragments of the bone tissue have been lost post-collection due to the brittle nature of the fossil, the remaining impression of the right humerus is quite clear upon close inspection. The deltopectoral crest is subrectangular, as can be better seen on the left side (Fig. 11). As in *Batrachognathus volans*, the deltopectoral crest of the humerus in JPM-2012-001

was reduced (less wide than proximodistally long, and less wide than humeral shaft) and rectangular in shape. The shape of the ulnar crest is rounded, but it is proximodistally shorter than the deltopectoral crest, as in other anurognathids (Döderlein, 1923; Riabinin, 1948; Ji & Ji, 1998, Wang *et al.*, 2002; Bennett, 2007; Lü & Hone, 2012; Lü *et al.*, 2018; Yang *et al.*, 2019).

Incomplete preservation prevents the observation of any details of ulna and radius, although their lengths can be assessed due to their clear impressions on both sides. The right wing-finger preserves complete first, second and third wing phalanges (Fig. 11). The distal region of the third wing phalanx underlies the tibia on the matrix, but the distal end can be seen due to damage on the tibia, revealing the phalanx beneath. The distal end of the third wing phalanx seems to be slightly expanded, indicating a probable articular region for a fourth phalanx, which is not preserved. A free digit with a long, slender proximal phalanx and a robust, strongly recurved ungual is preserved.

Table 1. Measurements of JPM-2012-001.

Element	Right	Left
Scapula	~1.95	?
Coracoid	?	~1.37
Humerus	2.36	2.39
Radius/ulna	3.63	3.47
Metacarpal IV	~0.67	-
Wing phalanx 1	4.12	~3.84
Wing phalanx 2	3.60	-
Wing phalanx 3	1.81	-
Femur	1.36	1.31
Tibiotarsus	2.66	2.53*
Metatarsus	~1.1	~1

Note:
Measurements are given in centimeters. Values for long bones correspond to their lengths. Interrogations mean the element is too incomplete for an informative value. Dashes mean the element is not preserved. Asterisk means the element is slightly incomplete.

Hindlimb.

Neither femora are fully preserved in terms of bone tissue, though impressions of the lost regions remain on both sides so that their total lengths can be confidently measured (Fig. 11). The right femur is preserved in an approximately natural position relative to the pelvic region, and only part of the proximal region was lost, though an impression remains, showing that it was preserved in articulation with the pelvis. The left femur is displaced, but the proximal region is preserved. The distal region is lost, but an impression also remains. The tibia is quite elongate relative to the femur (Fig.

11), more so than in any other anurognathid (Table. 1). On the right crus, tibia and fibula are incompletely ossified, and a gap can be seen between the two (Fig. 11). Despite damage on the proximal region of the right metatarsus, the distal region is well-preserved. It can be clearly seen that the metatarsal IV is shorter than metatarsals II and III (Fig. 14). A single ungual can be identified on the right pes, which is slightly less robust than the manual unguals (Fig. 15).

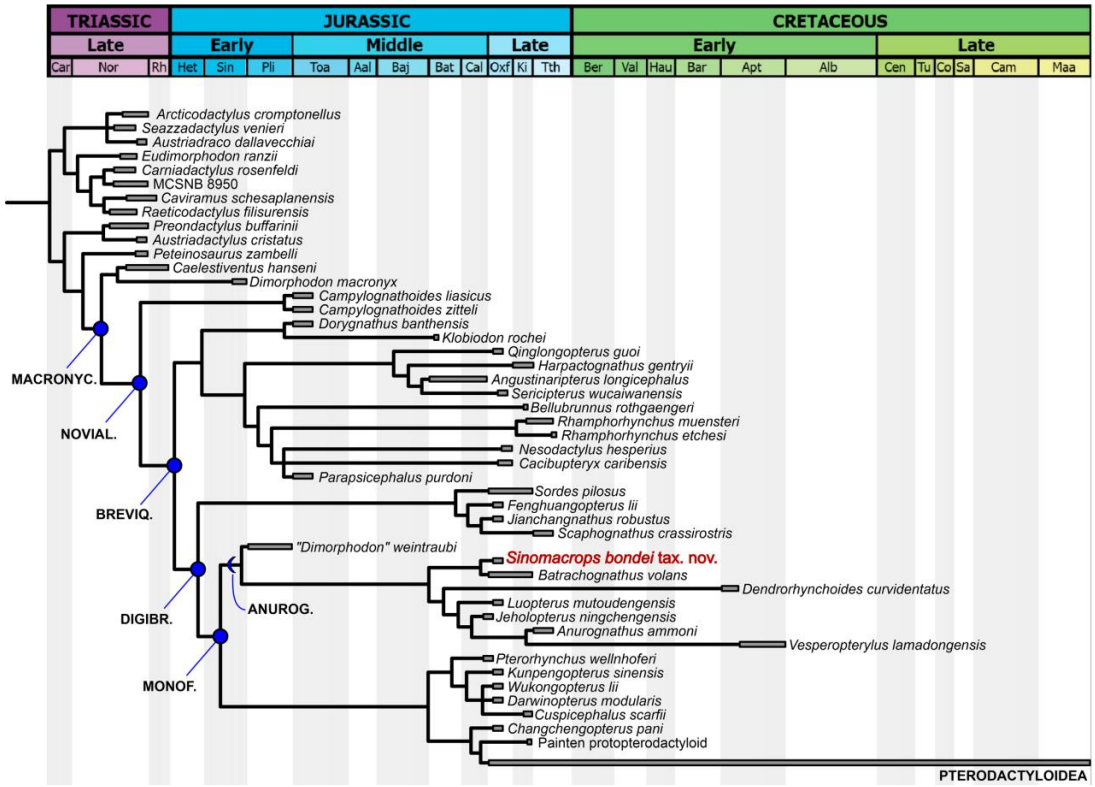

Figure 16. Phylogenetic analysis results. Strict consensus tree showing the phylogenetic relationships of *Sinomacrops bondei* and anurognathids. Dashed line indicates result exclusive to the semi-strict consensus tree.

PHYLOGENETIC ANALYSIS RESULTS

Our analysis produced two most parsimonious trees, with 1,115 steps, CI of 0.456 and RI of 0.668. In the strict consensus tree (Fig. 16), the new species is the sister-group of *Batrachognathus volans*. The Anurognathinae were recovered with *Dendrorhynchoides* at the base, plus the newly recognized clade *Luopterus* + (*Jeholopterus* + (*Anurognathus* + *Vesperopterylus*)).

Our phylogenetic analysis places *Sinomacrops bondei* alongside *Batrachognathus volans* forming the Batrachognathinae, separately from the clade containing all other Chinese anurognathids plus *Anurognathus ammoni* (the Anurognathinae as herein defined). Five synapomorphies support Batrachognathinae in our analysis: char. 269 (2), humeral/ femoral length proportion (over 1.6); char. 271

(0) the width of the humeral deltopectoral crest (reduced, less wide than proximodistally long), char 272 (3), the shape of the deltopectoral crest (subrectangular); char. 280 (2), the shape of the ulnar crest of the humerus (rounded); and char. 367 (2), the tibia/femur length proportion (over 1.7).

The Anurognathinae would be composed of, according to our results, *Dendrorhynchoides curvidentatus*, *Luopterus mutoudengensis*, *Jeholopterus ningchengensis*, *Anurognathus ammnoni* and *Vesperopterylus lamadongensis*. These taxa share the following synapomorphies: char. 30 (2) the semicircular arching of the jaws, distinct from the elliptical one seen in batrachognathines, char. 244 (1) caudal series shorter than the dorsal series, char. 275 (1) deltopectoral crest subequal to humeral head in size and char. 310 (5) pteroid curved and subparallel-sided (Andres, Clark & Xu, 2014).

The non-monophyly of the genus *Dendrorhynchoides* encompassing *D. curvidentatus* plus *D. mutoudengensis* (Lü & Hone, 2012) is corroborated here, which is consistent with Wu, Zhou & Andres (2017) and Hone (2020). *Luopterus mutoudengensis* is recovered as the sister-group of the *Jeholopterus* – *Anurognathus* – *Vesperopterylus* clade, with which it shares char. 378 (0), a straight last phalanx of pedal digit V (whereas this phalanx is curved in *Dendrorhynchoides curvidentatus*). The straight condition is a synapomorphy joining these taxa, while the curved condition is plesiomorphic for anurognathids and present at the base of the Novialoidea, as seen in *Campylognathoides*, "*Dimorphodon weintraubi*", *Changchengopterus pani* and wukongopterids (Clark *et al.*, 1998; Lü, 2009; Padian, 2008a, 2008b; Wang *et al.*, 2009, 2010).

The clade composed of *Jeholopterus ningchengensis*, *Anurognathus ammoni* and *Vesperopterylus lamadongensis* is supported by three synapomorphies: char. 272 (1) deltopectoral crest of the humerus trapezoidal and broad, char 241 (0) caudal vertebrae lacking filiform zygapophyses, and char. 242 (0) caudal vertebrae lacking filiform haemapophyses. The sister-group relationship between *Anurognathus ammoni* and *Vesperopterylus lamadongensis* is supported by one synapomorphy: char. 271 (2), the complete loss of mid-cervical ribs.

Our dataset combines discrete characters coming from previous contributions (Kellner, 2003; Unwin, 2003; Dalla Vecchia, 2009, 2019; Andres, Clark & Xu, 2010, 2014; Vidovic & Martill, 2017). According to the present results, anurognathids are basal monofenestratans, and thus are also members of the Novialoidea and of the Breviquartossa. As our results have produced a novel topology, this warrants some discussion.

According to our results, anurognathids exhibit the following synapomorphies of the Novialoidea:

Character 192 (0). Dentition, variation in crown shape along the upper jaw: absent; and char. 193 (0) for the lower jaw (Unwin, 2003, char. 19; Dalla Vecchia, 2019 char. 37 and char. 38 for the lower jaw). Remarks: the secondary loss of heterodonty (which is present in basal pterosaurs) had already been recovered previously as a synapomorphy of the Novialoidea (Andres, Clark & Xu, 2014; Dalla Vecchia, 2014, 2019).

Character 340 (1). Postacetabular process of the illium length: shorter than preacetabular process (Vidovic & Martill, 2017, char. 212). This feature had already been recovered as a synapomorphy of the Novialoidea (Vidovic & Martill, 2017). It can be seen in *Dendrorhynchoides* (Ji & Ji, 1998), *Jeholopterus* (Wang *et al.*, 2002) and *Anurognathus* (Bennett, 2007).

Character 380 (2). Pedal digit V, phalanx 2, length: shorter than preceding phalanx (Vidovic & Martill, 2017, char. 195). This feature is primitive for novialoids as seen in *Campylognathoides* (Padian, 2008b), *Sordes* (Unwin & Bakhurina, 1994), *Scaphognathus* (Bennett, 2014), darwinopterans (Wang *et al.*, 2010) and pterodactyloids (see Vidovic & Martill, 2017). It is present in *Jeholopterus* and *Luopterus* (Wang *et al.*, 2002; Lü & Hone, 2012), although it is reversed in *Dendrorhynchoides* and *Anurognathus* (Ji & Ji, 1998; Bennett, 2007).

Anurognathids further share with the Breviquartossa the following synapomorphies:

Character 48 (1). Premaxilla extending to orbit, but no further. This feature had already been recovered as a synapomorphy of the Breviquartossa by Unwin (2003). This feature can be seen in *Anurognathus* (Bennett, 2007).

Character 147 (1). Mandible, surangular eminence: absent (Unwin, 2003, char. 16). Remarks: the secondary loss of this feature had already been considered a synapomorphy of the Breviquartossa (Unwin, 2003). The feature is absent in *Anurognathus ammoni* (Bennett, 2007) and cannot be assessed in other species.

Character 179 (2). Dentition, distal teeth, spacing relative to successive teeth: more than diameter of teeth (Andres, Clark & Xu, 2014). This character had already been recovered as a synapomorphy of the Breviquartossa (anurognathids included) by Andres, Clark & Xu (2014).

Character 284 (1). Humerus, shaft, cross-section: tapered (Andres, Clark & Xu, 2014). Remarks: this feature, as opposed to a subcircular cross-section of the humeral shaft, has already been recovered as a synapomorphy of the Breviquartossa, anurognathids included (Andres, Clark & Xu, 2014).

Character 368 (1). Fibula, relative length: shorter than tibia (Dalla Vecchia, 2009

char. 68, modified from Unwin, 2003 char. 8). Remarks: this feature has already been recovered as a synapomorphy of the Breviquartossa, including anurognathids, by Dalla Vecchia (2009).

Character 373 (2). Metatarsals, relative length of metatarsal IV: shorter than metatarsals I–III (Unwin, 2003, char. 21). This feature has already been recovered as a synapomorphy of the Breviquartossa, and the clade name actually derives from this feature (Unwin, 2003). In anurognathids, this feature can be seen in *Vesperopterylus* and *Jeholopterus*, although metatarsal IV is only slightly shorter than metatarsal III (by, approximately, the width of their diaphyses; Fig. 17). The length difference is thus less conspicuous than in *Rhamphorhynchus* or *Scaphognathus* (Wellnhofer, 1975, 1978), but similar to that seen in *Sordes* (Wellnhofer, 1978), *Darwinopterus* (Lü *et al.*, 2009), *Pterodactylus antiquus* or *Diopecephalus kochi* (Wellnhofer, 1970, 1978). The feature is lost in *Anurognathus*, in which metatarsals I–IV are subequal in length (Bennett, 2007).

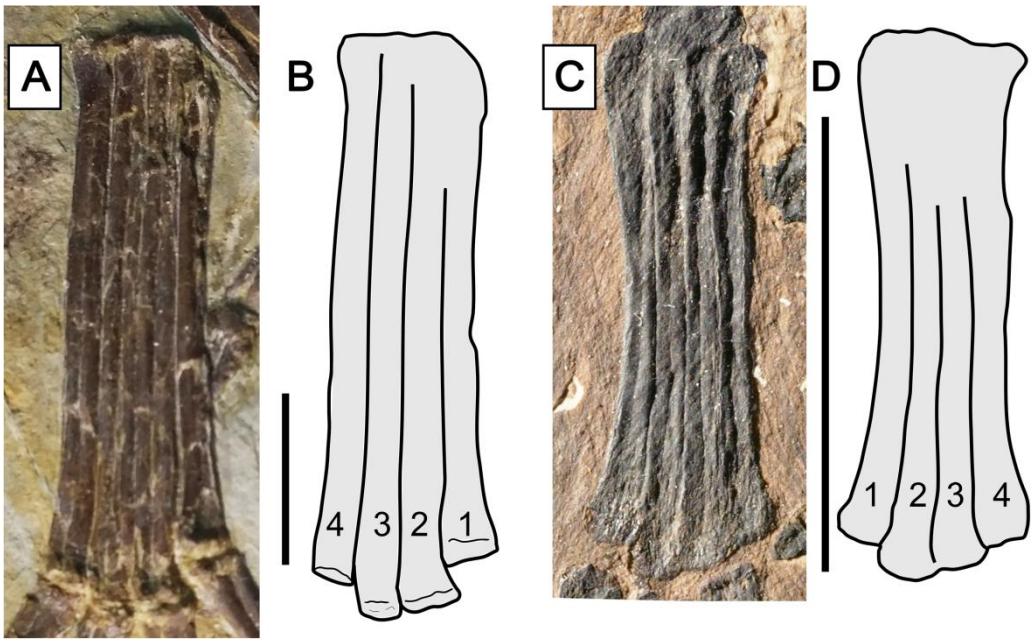

Figure 17. Metatarsus in anurognathids. (A) *Vesperopterylus lamadongensis* holotype BMNHC-PH-001311. (B) Schematic drawing. (C) *Jeholopterus ningchengensis* specimen CAGS IG 02-81. (D) Schematic drawing. Numbers refer to metatarsals. Scale bar equals 10 mm.

Character 378 (1). Pedal digit V, phalanx 2, shape: curved (Kellner, 2003, char. 74). Remarks: primitively, this phalanx is straight, as seen in non-breviquartossans such as *Campylognathoides* (Wellnhofer, 1978; Padian, 2008b), *Dimorphodon* (Padian, 1983), and Triassic forms (Dalla Vecchia, 2014). The phalanx is curved in rhamphorhynchids (Wellnhofer, 1975, 1978; Lü *et al.*, 2012; Hone *et al.*, 2012), *Dendrorhynchoides* (Ji & Ji, 1998) and *Kunpengopterus* (Wang *et al.*, 2010; Cheng *et al.*, 2017), and changes to "bent, angled" (state 2 of same character) in some taxa such as *Dorygnathus*, *Scaphognathus* and *Darwinopterus* (Andres, Clark & Xu, 2014;

Vidovic & Martill, 2017; Dalla Vecchia, 2019), and reverses to "straight" (state 0) in the *Luopterus–Jeholopterus–Anurognathus* clade, in which this phalanx is straight (Wang *et al.*, 2002; Lü & Hone, 2012; Bennett, 2007; Andres, Clark & Xu, 2014).

Our analysis has also recovered the Digibrevisauria, coined by Vidovic & Martill (2017) for a clade that comprises the Scaphognathidae and the Monofenestrata, to the exclusion of rhamphorhynchids. Anurognathids show the following features that were recovered as synapomorphies of the Digibrevisauria: 236 (1) proximal caudal vertebrae lack distinct lateral processes; 275 (2) humerus deltopectoral crest not as long as the humeral head is wide (seen in *Sinomacrops* and *Batrachognathus*, reversed to state 1 in the clade containing the remaining anurognathids); 313 (1) metacarpal IV lacks a crista metacarpi; 375 (1) phalanges of pedal digit IV unequal in length with the distal phalanx larger than all those preceding it, and 376 (1) phalanges 2 and 3 of pedal digit IV are squared or shorter than they are wide (Vidovic & Martill, 2017).

Within digibrevisaurians, anurognathids were recovered as basal monofenestratans. The Monofenestrata have been phylogenetically defined by Andres, Clark & Xu (2014) as a synapomorphy-based clade, defined by the presence of a confluent nasoantorbital fenestra synapomorphic with the one seen in *Pterodactylus antiquus*. In summary, considering the interpretation put forward by Andres, Clark & Xu (2010) that anurognathids possess a nasoantorbital fenestra (corroborated here), this would mean that the clade Anurognathidae + (Darwinoptera + Pterodactyloidea) corresponds to the Monofenestrata. According to our results, thus, anurognathids are basal monofenestratans. The Monofenestrata were recovered based on the following four features:

Character 15 (1): Confluent nasoantorbital fenestra. Remarks: most workers have coded a confluent nasoantorbital fenestra as absent for anurognathids (Kellner, 2003; Unwin, 2003; Bennett, 2007; Lü *et al.*, 2018; Vidovic & Martill, 2017), except for Andres, Clark & Xu (2010, 2014) and Dalla Vecchia (2019). Due to the extremely reduced preorbital region and the small absolute size of anurognathids, investigation of their preorbital fenestration is indeed difficult. In most specimens, the situation cannot be confirmed, such as the holotypes of *Jeholopterus ningchengensis*, *Dendrorhynchoides curvidentatus*, *Luopterus mutoudengensis* and *Vesperopterylus lamadongensis*, and also the specimen NJU–57003. The only specimen for which a skull element was tentatively interpreted as an ascending process of the maxilla (and thus a bony bar effectively separating naris and antorbital fenestra, as two distinct openings) is the second specimen of *Anurognathus ammoni* (Bennett, 2007). The identification of this process has been reviewed and challenged by Andres, Clark & Xu (2010), who argued that the purported process could not be unequivocally identified as an ascending maxillary process separating the nares from the antorbital fenestra, as it could only be seen on the right side, was a faint impression, and was displaced, so that even its natural orientation cannot be unambiguously assessed.

Based on its rough location and shape, we offer a tentative interpretation for it as a palatal element. Andres, Clark & Xu (2010) further noted that there are two previously described anurognathid specimens in which the preorbital region is well preserved and the ascending processes of the maxilla is absent on both sides: the holotype of *Batrachognathus* and CAGS IG 02-81 (see Riabinin, 1948; Ji & Yuan, 2002; Andres, Clark & Xu, 2010; Yang *et al.*, 2019 and also Fig. 18). In accordance, in the small preorbital region of *Sinomacrops*, only a single opening is present. We thus favor the interpretation of Andres, Clark & Xu (2010) that a nasoantorbital fenestra is present in anurognathids (Fig. 18).

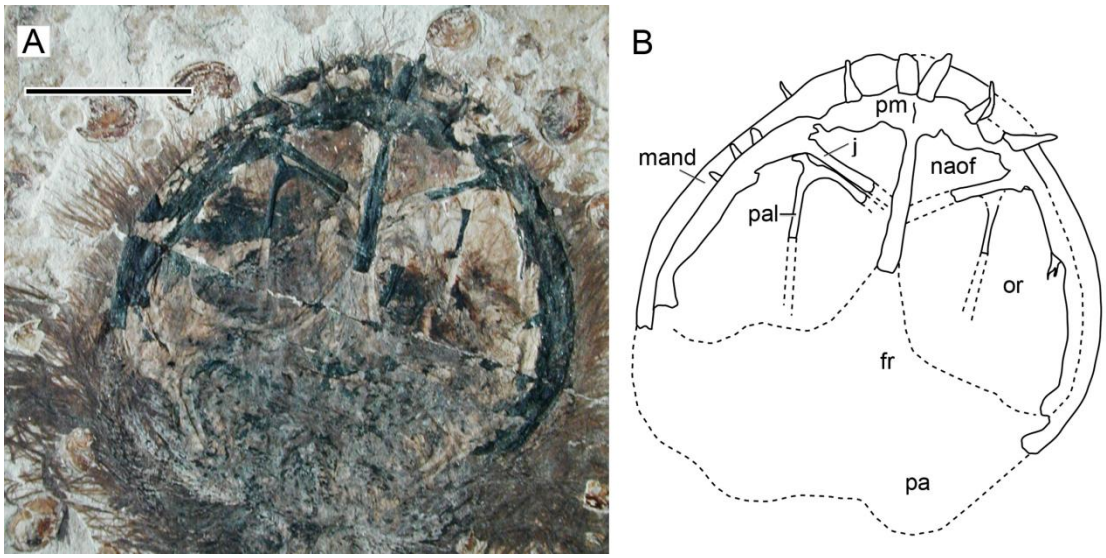

Figure 18. Nasoantorbital fenestra in *Jeholopterus* CAGS IG 02-81. (A) Skull exposed in dorsal view, and (B) schematic drawing. Abbreviations: fr, frontal; mand, mandible; max, maxilla; naof, nasoantorbital fenestra; or, orbit; pa, parietal; pal, palatine; pm, premaxilla. Scale bar equals 10 mm.

Character 95 (1). Jugal, lacrimal process, subvertical. Remarks: this feature has already been recovered as a synapomorphy of a clade containing Monofenestrata + *Sordes* (Andres, Clark & Xu, 2014). In the present analysis, we coded this character as "anteriorly inclined" (state 0) for *Sordes* (as in the dataset from Vidovic & Martill (2017)), so that the feature is restricted to the Monofenestrata.

Character 216 (1) Atlantoaxis fusion. Remarks: this feature has already been recovered as a synapomorphy of the Monofenestrata, including anurognathids (Andres, Clark & Xu, 2014). This feature is present in *Anurognathus* (Wellnhofer, 1975; Bennett, 2007).

Character 221 (1). Mid-cervical vertebrae, ribs: short. Remarks: as already noticed before (Unwin, 2003), the reduction of mid-cervical ribs can be seen in anurognathids and pterodactyloids. Short mid-cervical ribs have been reported for *Jeholopterus* (see Wang *et al.*, 2002) and are absent (state 2 of this same character) in

Anurognathus and *Vesperopterylus* (see Bennett, 2007; Lü *et al.*, 2018). The mid-cervical ribs are also short (and quite slender) in the Darwinoptera (Wang *et al.*, 2009, 2010; Cheng *et al.*, 2017).

Finally, Darwinoptera + Pterodactyloidea is supported by the following features that are absent in anurognathids: char 1 (1) elongated skull, over four times skull height (Dalla Vecchia, 2019, char. 1), char. 112 (1), the craniomandibular joint is located under the orbit (and not posterior to it), char. 230 (0) first dorsal rib larger than others (Vidovic & Martill, 2017, char. 236; homoplastic with *Eudimorphodon*), char. 311 (2) pteroid over 2/5 ulnar length (Dalla Vecchia, 2019 char. 70), char. 317(0) metacarpal IV posterior crest absent (Vidovic & Martill, 2017 char. 164; present in *Dendrorhynchoides*, see Ji & Ji, 1998), char. 366 (1) femur less than twice the length of metacarpal IV (Kellner, 2003 char. 71; homoplastic with Rhamphorhynchini, *Eudimorphodon*, *Fenghuangopterus* and *Sinomacrops*), 370 (1) splayed metatarsals (Dalla Vecchia, 2009, char.70; homoplastic with rhamphorhynchids, *Sordes* and *Scaphognathus*), and char. 375 (3) distal and proximal phalanges of pedal digit IV longer than those between (reversing to state 1, proximal phalanx is the largest, in the Pterodactyloidea).

In summary, these results provide support for the inclusion of the Anurognathidae within the Breviquartossa and, more specifically, within the Monofenestrata (as in Andres, Clark & Xu (2010, 2014)), though not closer to pterodactyloids than darwinopterans. In this way, these results represent a new hypothesis for the position of the group, being somewhat intermediate between the results of Andres, Clark & Xu (2010) and of Dalla Vecchia (2009, 2019). Still, as well-put by a reviewer (N. Jagieslka), pterosaur phylogeny is a "fluid, ever-expanding field", and as noted by Vidovic & Martill (2017, p.9), studies of anurognathid phylogeny are hampered by their "aberrant morphology". Thus, much work will be needed before the phylogenetic position of anurognathids stabilizes (hopefully with the discovery of "transitional-morphs"), although the present results do lend support for their interpretation as monofenestratans.

DISCUSSION

As detailed above, JPM-2012-001 exhibits a particular feature regarding its dentition: the first three maxillary alveoli are closely spaced, with the spacing between them being shorter than their diameter; while the spacing between the subsequent alveoli is subequal to their diameter. This pattern is unprecedented for anurognathids. In *Batrachognathus volans*, *Dendrorhynchoides curvidentatus*, *Jeholopterus ningchengensis* and *Anurognathus ammoni*, tooth spacing is constant and larger than tooth diameter (Riabinin, 1948; Ji & Ji, 1998; Ji & Yuan, 2002; Bennett, 2007). In *Vesperopterylus lamadongensis*, tooth spacing is also constant, and subequal to (only fractionally larger than) tooth diameter (Lü *et al.*, 2018). The pattern of tooth spacing in *Luopterus mutoudengensis* is so far unclear (Lü & Hone, 2012;

Hone, 2020).

Another particular feature is its tibiotarsus/femur length ratio, which is unique within anurognathids (and pterosaurs overall) in that the tibiotarsus is about twice as long as the femur (Table 2; Supplemental File 3). In *Batrachognathus volans*, this same ratio is 1.75, while it ranges from 1.22 to 1.47 in other anurognathids (Table 2).

Apart from the unique features mentioned above, Sinomacrops bondei further differs from *Batrachognathus volans* in exhibiting a relatively larger ulnar crest of the humerus (Riabinin, 1948; Hone, 2020). The new species further differs from *Anurognathus*, *Jeholopterus* and *Vesperopterylus* in humerus deltopectoral crest shape (trapezoidal in the latter three taxa) and in exhibiting an elongate tail, longer than the dorsal series (Hone, 2020). The new species also differs from *Luopterus mutoudengensis* and *Dendrorhynchoides curvidentatus* in the morphology of the deltopectoral crest of the humerus, which is relatively larger and triangular in shape in the latter two (Ji & Ji, 1998; Lü & Hone, 2012; Hone, 2020).

CONCLUSIONS

JZMP-2012-001 represents a new anurognathid, here named *Sinomacrops bondei* (Fig. 19). It is the second anurognathid from the Tiaojishan Formation, and the first anurognathid specimen to exhibit a skull exposed in lateral view. In our new phylogenetic analysis, it is recovered as the sister-group of *Batrachognathus volans*, with which it comprises the Batrachognathinae. All other taxa were recovered as closer to *Anurognathus*. The exclusion of *Luopterus mutoudengensis* from the genus *Dendrorhynchoides* is corroborated. *Vesperopterylus lamadongensis* is recovered as the sister-group of *Anurognathus ammoni*, with *Jeholopterus ningchengensis* as their successive sister-group.

Some previous interpretations of anurognathid morphology and systematics have relied on limited available information. With time and new specimens being discovered, new data have been provided and new interpretations were presented. For this reason, each new specimen is crucial for the understanding of the group. The present information available leads us to interpret anurognathids as basal members of the Monofenestrata, as the sister-group of Darwinoptera + Pterodactyloidea.

Table 2. Comparative table showing skeletal element ratios among anurognathids.

Anurognathiade	hu/mcIV	hu/fe	hu/ul	hu+ul/ fe+ti	ul/ mcIV	ul/ fe	sc/ co	ph1d4/ ul+mcIV	ph1d4 /ti	ph2d4/ ph1d4	ph3d4/ ph1d4	ph3d4/ ph2d4	ph4d4/ ph1d4	fe/ mcV	ti/fe	mtIII /ti	caS/fe
Anurognathus ammoni (holotype)	2.91	1.19	0.70	1.16	4.18	1.70	?	1.01	1.49	?	?	?	?	2.45	1.44	0.46	0.50
Anurognathus ammoni (referred)	3.64	1.25	0.70	1.26	5.10	1.76	?	0.95	1.44	0.77	0.44	0.56	?	2.90	1.39	0.42	?
Vesperopterylus lamadongensis	2.75	1.35	0.74	1.34	3.73	1.83	0.97	0.96	1.64	0.81	0.60	0.74	0.12	2.04	1.37	0.47	0.59
Jeholopterus ningchengensis (holotype)	3.26	1.55	0.70	1.67	4.68	2.22	1.96	0.86	1.86	0.88	0.65	0.73	0.17	2.10	1.25	0.44	?
Jeholopterus ningchengensis (CAGS IG 02-81)	3.39	1.52	0.78	1.59	4.03	1.99	1.28	0.88	1.88	0.89	?	?	?	2.02	1.22	0.47	?
Dendrorhynchoides curvidentatus	2.99	1.43	0.78	1.37	3.82	1.82	1.15	0.99	1.66	0.80	?	?	?	2.40	1.37	0.45	?
Luopterus mutoudengensis (holotype)	2.45	1.28	0.64	1.44	3.81	2.00	1.88	0.94	1.85	0.82	0.50	0.61	0.10	1.91	1.29	0.44	>0.86
NJU-57003	2.60	1.34	0.60	1.42	4.31	2.15	1.27	0.90	1.63	0.86	0.40	0.46	0.10	1.97	1.47	0.45	1.78
IVPP V16728	?	1.43	?	?	?	?	?	?	?	?	?	?	?	?	~1.40	0.38	>1.49
Sinomacrops bondei	3.55	1.77	0.66	1.51	5.29	2.70	1.42	0.97	1.59	0.87	0.44	0.50	?	~2	1.99	0.48	>1.69
Batrachognathus volans	?	1.93	?	?	?	?	?	?	?	?	?	?	?	?	1.75	?	1.47*

Note:

The asterisk indicates a value taken from the referred specimen of *Batrachognathus volans* (Costa *et al.*, 2013). The other values for this species were taken from the holotype (Riabinin, 1948)

Figure 19. Life reconstruction of *Sinomacrops bondei*. Paleoart courtesy of Zhao Chuang, reproduced with permission.

CHAPTER III

ADVANCES IN CHINESE TRANSITIONAL TYPE PTEROSAUR: A NEW DARWINOPTERAN *KUNPENGOPTERUS ANTIPOLLICATUS* AND COMMENTS ON THE GROUP

INTRODUCTION

The clade Monofenestrata defined as the group consisting of *Pterodactylus* and all species sharing with *Pterodactylus* the synapomorphy of an external nostril confluent with the antorbital fenestra, the major skull opening on the side of the snout (Lü *et al.*, 2010). The Darwinoptera, a primitive subgroup of monofenestratans showing this transitional anatomy, was also named for *Darwinopterus* and defined as all descendants of its common ancestor with *Pterorhynchus* (Andres, Clark & Xu, 2014).

The first nominal species was *Darwinopterus modularis*, described from an incomplete skeleton including a partial skull. It provides the first insights into a prominent, but poorly understood transition between basal, predominantly long-tailed pterosaurs and the more derived, exclusively short-tailed pterodactyloids. (Lü *et al.*, 2010). The second *Darwinopterus* specimen provides direct evidence of gender in pterosaurs and insights into the reproductive biology of these extinct fliers. This new find and several other examples of *Darwinopterus* demonstrate that males of this pterosaur had a relatively small pelvis and a large cranial crest, whereas females had a relatively large pelvis and no crest (Lü *et al.*, 2011a). Both from the Tiaojishan Formation at the Linglongta locality of Jianchang, Huludao, Liaoning (northeastern China), dating to the Middle-Late Jurassic period (Callovian-Kimmeridgian). From the Tiaojishan Formation at the Linglongta locality, pterosaurs are abundant in number and in diversity (see Sullivan *et al.*, 2014 for a review), with wukongopterids (Wang *et al.*, 2009, 2010; Lü *et al.*, 2009; Cheng *et al.*, 2017a), *Jianchangopterus* (Lü & Bo, 2011), *Jianchangnathus* (Cheng *et al.*, 2012) and *Fenghuangopterus* (Lü, Fucha & Chen, 2010).

This work presents a new fossil coming from the Linglongta locality, BPMC-0042, representing a new species of *Kunpengopterus*. We further review the phylogenetic relationships of the group (both intra and inter), presenting an analysis including all proposed species.The new species exhibits the oldest record of palmar (or true) opposition of the pollex, which is unprecedented for pterosaurs and represents a sophisticated adaptation related to arboreal locomotion.

GEOLOGICAL SETTING

The Tiaojishan Formation takes its name from the Tiaojishan Mountain (Mentougou District, Beijing), and was named by Ye (1920). This and the Haifanggou/Jiulongshan Formation have yielded the famous Yanliao Biota in western Liaoning and adjacent regions (Huang, 2015, 2016). This biota is well known for the beautiful preservation and abundancy of insects and vertebrate fossils, such as salamanders, feathered dinosaurs, pterosaurs and mammals (Sullivan *et al.*, 2014). The most important localities that yield the Yanliao Biota are Daohugou in Ningcheng County of southeast Inner Mongolia (Haifanggou Fm.), Linglongta of Jianchang

County of western Liaoning Province (Tiaojishan Fm.), and Mutoudeng of Qinglong County of northern Hebei Province (Tiaojishan Fm.; Lü *et al.*, 2013; Huang, 2015, 2016).

Zheng et al. (2009) and Xu et al. (2009) reported feathered dinosaurs at Linglongta and Yaolugou, Jianchang, Western Liaoning in early 2009, their interpretations of the strata in which the specimens were found are questionable. Based on the above-mentioned fossil assemblages, lithological associations, stratigraphic succession and a regional correlation, Jiang et al. (2010) suggests that the fossil-bearing lithological succession at Linglongta is equivalent to the Tiaojishan Formation in northern Hebei and western Liaoning, China, and dates to the Middle Jurassic.

MATERIALS AND METHODS

UV-light and computed tomography scanning

Observation of BPMC 0042 under UV-light (Vansky 51 LEDs UV lantern , 395 nm wavelength). BPMC 0042 was also computed tomography (CT) scanned at Institute of Geology, Chinese Academy of Geological Sciences, Beijing, China, using a Nikon XTH225ST scanner. The region of interest (left forearm) was scanned at 160 kV and 131 µA. The final dataset contains 1988 image slices (2000 x 2000 pixels, slice thickness 0.121 mm). The CT data was imported into digital visualization software Avizo (version 9.1) for image processing and segmentation of skeletal elements. The segmented surface models were optimized using Blender (version 2.81a).

Phylogenetic analyses

We have performed three distinct analyses, modified from distinct datasets from previous works. TXT files for each analysis (including the complete lists of characters, coding, and analysis commands) are available.

Dataset 1. To this dataset, we have included as operational taxonomic units: *Changchengopterus*, *Pterorhynchus*, *Kunpengopterus antipollicatus* sp. nov., ZMNH M8802, *Kunpengopterus sinensis*, *Wukongopterus lii*, IVPP V 17959, *Darwinopterus modularis*, HGM 41HIII0309A, IVPP V 16049 and *Cuspicephalus*. We have not included *Archaeoistiodactylus* in the present analyses, as it is herein regarded as undiagnostic. This analysis was performed under TNT, using default New Technology Search followed by a TBR swapping using trees from RAM (Dalla Vecchia, 2019; Goloboff & Catalano, 2016).

Dataset 2. To this dataset, we have included *Changchengopterus*, *Pterorhynchus*, *K. antipollicatus*, ZMNH M8802, *Wukongopterus*, IVPP V 17959, *Darwinopterus modularis* and *Cuspicephalus*. The analysis was performed under TNT, using default New Technology Search followed by a TBR swapping using trees from RAM (Pêgas

et al., 2019; Goloboff & Catalano, 2016).

Dataset 3. This dataset is comprehensive regarding both non-pterodactyloids and pterodactyloids. Concerning darwinopterans, this dataset already included *Pterorhynchus*, *Kunpengopterus sinensis*, *Wukongopterus*, *Darwinopterus modularis* and *Cuspicephalus*. We have thus added IVPP V 17959, ZMNH M8802 and *K. antipollicatus* holotype. For the present dataset, 6 characters were modified for *Cuspicephalus* (characters 84, 97, 107, 110, 111 and 174). We have also corrected character 110 for *Kunpengopterus sinensis*. We followed the original protocol (Wu *et al.*, 2017).

Nomenclatural acts

This publication and the nomenclatural acts it contains have been registered in ZooBank under the following LSIDs: urn:lsid:zoobank.?tjl]org:pub:022AA16E-6952-4102-A139-72C9816F24E5 (publication); urn:lsid:zoobank.org:act:53B54A80-2431-4112-B96A-B5606EEBEF3F (*K. antipollicatus* sp. nov.); and urn:lsid:zoobank.org:act:94C25C23-DF41-4024-8E0A-40FC5DF090F3 (Wukongopterinae subfam. nov.).

RESULTS

Systematic Paleontology

Pterosauria Owen, 1842
Monofenestrata Lü *et al.*, 2009
Darwinoptera Andres *et al.*, 2014
Wukongopteridae Wang *et al.*, 2010

Content

Wukongopterus, *Darwinopterus* and *Cuspicephalus*.

Stem-based definition

The most inclusive clade containing *Wukongopterus lii* but not *Kunpengopterus sinensis*.

Synapomorphies

Orbit piriform; nasoantorbital fenestra posteroventral margin (lacrimal) convex; fourth wing phalanx larger than first wing phalanx; and pedal digit V second phalanx strongly angled.

***Wukongopterus lii* Wang *et al.*, 2009**

Holotype

IVPP V 15113.

Referred specimens
IVPP V 17959.

Diagnosis
Conspicuous protrusion of the upper jaw rostral tip; ossified premaxillary crest restricted to the rostrum; ossified premaxillary crest bearing posterodorsally directed parallel ridges; large nasoantorbital fenestra (~60% of total skull length); piriform lacrimal foramen; nasal process elongated; an angle of 90° between nasal process and main body of the nasal; distal end of pteroid expanded; preacetabular portion of the ilium reduced; strongly curved second pedal phalanx of the fifth toe with an angle between the proximal and distal segment about 70°.

Remarks
Prior to this paper, *Wukongopterus lii* has been restricted to its holotype and diagnosed by: first two pairs of premaxillary teeth protruding beyond the dentary almost vertical; dentition formed by short cone-shaped and very pointed teeth; preacetabular portion of the ilium reduced; strongly curved second pedal phalanx of the fifth toe with an angle between the proximal and distal segment about 70°; proximal segment of the second pedal phalanx of the fifth toe elongated. We note that the extent of the nasoantorbital fenestra can also be considered as diagnostic for *W. lii*. The skull of the holotypic specimen is incomplete, but the anterior margin of the nasoantorbital fenestra is preserved. Even though the posterior margin is not preserved, its position can be inferred. In darwinopterans, the posterior margin of the nasoantorbital fenestra is consistently level with 8% – 11% of the distance from craniomandibular joint and rostral tip. In this way, the extent of the nasoantorbital fenestra in the holotype of *W. lii* can be estimated to be around 60% of skull length. This is the largest value for all darwinopterans, seen only in the holotype of *W. lii* as well as specimen IVPP V 17959. This specimen was described as an unnamed new species. A single remarkable difference could be found between IVPP V17959 and the holotype of *W. lii*: in the former, the adductor fossa is relatively twice as long. However, in *W. lii* the medial surface of the left ramus is worn and the exact extent of the adductor fossa cannot be assessed with certainty (R.V.P., unpublished data). IVPP V17959 is thus indistinguishable from *Wukongopterus lii* and shares with it at least one autapomorphy (an extended nasoantorbital fenestra, accounting for ~60% of skull length). We thus refer IVPP V17959 to this species (Wang *et al.*, 2009, 2010; Cheng *et al.*, 2016).

***Darwinopterus modularis* Lü *et al.*, 2010**

Holotype
ZMNH M8782.

Referred specimens

IVPP V 16049 and HGM 41HIII0309A.

Revised diagnosis

Premaxillary crest anterodorsally expanded; premaxillary crest anterior region showing concentric ridges; posterior region of the skull elongated (~9% of skull length).

Remarks

Presently, three species have been attributed to *Darwinopterus*: *D. modularis* (type), *D. linglongtaensis*, and *D. robustodens*. While the type species is represented by an incomplete skeleton (including the skull but lacking the pedes, for example), the other two species were erected on the basis of virtually complete specimens. A single difference was found between *D. modularis* and D. robustodens: the dentition pattern, with *D. robustodens* bearing purportedly more robust, sharper teeth, swollen at the crown base (Lü *et al.*, 2011b). However, later on, it was stated that their dentition patterns were consistent with each other, and not disparate (Sullivan *et al.*, 2014). This latter notion is supported here. We note that, at a first glance, the holotype of *D. modularis* seems to exhibit spike-like, elongated teeth; but this is because most teeth (crown plus root) are dislodged from the natural position, with their roots partially exposed. The crowns consistently match the morphology seen in *D. robustodens* (short, cone-shaped, slightly compressed, slightly swollen at the crown base; see Lü *et al.*, 2010, 2011b). No further differences could be found and they are thus regarded as conspecific. Concerning *Darwinopterus linglongtaensis*, this species was erected on the basis of the following diagnosis: “posterior region of the skull less elongated than in *Darwinopterus modularis*; dentition formed by short cone-shaped; lacrimal process of the jugal comparatively thin*; foramen on nasal process rounded*; curved second pedal phalanx of the fifth toe with an angle between the proximal and distal segment about 115° ” (Wang *et al.*, 2010). The posterior region of the skull of *D. linglongtaensis* accounts for ~8% of the squamosal-premaxilla distance. This same value is 9% for the holotype of *D. modularis*, and 8% for HGM 41HIII0309A; and thus cannot be considered as diagnostic for *D. linglongtaensis*. Concerning dentition, as explored above, short cone-shaped teeth are also present in *D. modularis*. A conspicuously thin lacrimal process of the jugal present in HGM 41HIII0309A, and also in the holotype of *D. modularis* (despite unclearly due to an overlap of the two processes from both sides) (Lü *et al.*, 2011b). The distal and proximal segments of the second phalanx of pedal digit 5 are angled at 124° , what is not so distant from the 136° of HGM 41HIII0309A, especially considering that some variation in this angle can be seen in *Rhamphorhynchus* (Cheng *et al.*, 2017a; Sullivan *et al.*, 2014). A round foramen on the nasal process, despite unreported, is also present in the holotype of *D. modularis*. Furthermore, some features seen in the holotype of *D. linglongtaensis* seem to indicate that it represents a younger ontogenetic stage relative to the holotypes of *D. modularis* and *D. robustodens*: the degree of skeletal fusion, the relative size of the orbit and rostrum, and crest morphology. Also, skull length in the holotype of *D. linglongtaensis* is about 33% smaller than in the holotypes of *D.*

modularis and *D. robustodens*. In this way, we attribute their differences to ontogeny (Witton, 2013).

***Kunpengopterus* Wang *et al.*, 2010**

Type species
Kunpengopterus sinensis Wang *et al.*, 2010

Included species
Kunpengopterus antipollicatus sp. nov. and *Kunpengopterus sinensis*.

Revised diagnosis
Orbit shape subcircular; nasoantorbital fenestra around 40% the skull length; rostrum slightly downturned, with ventral margin concave; premaxillary ossified crest smooth; maxillary process of the jugal thin and relatively short; quadrate inclination about 150° ; skull posterior region (squamosal) rounded; dentary symphysis tip forming an odontoid process; prepubis anterodorsal margin (in lateral view) approximately straight; prepubis posteroventral flange reduced and rounded.

***Kunpengopterus sinensis* Wang *et al.*, 2010**

Holotype
IVPP V 16047.

Referred specimens
IVPP V 23674, IVPP V 17957.

Diagnosis
Dorsal margin of skull straight; lacrimal process of the jugal thick; posterodorsal margin of ischium rising dorsally; first pedal phalanx of digit V short, less than 70% of metatarsal IV; proximal segment of the second pedal phalanx of the fifth toe about 30% length of the distal segment, shorter than in other wukongopterids.

Remarks
Specimen IVPP V 17957 was only briefly described and identified as an indeterminate wukongopterid (Cheng *et al.*, 2017b). A complete description is necessary before any interpretations can be confidently drawn. However, some features are worthy of note: nasoantorbital fenestra accounting for 40% of total skull length; anterior rostrum slightly downturned, with the ventral margin concave; dentary tip presenting an odontoid process; straight/slightly concave skull dorsal margin. We therefore attribute this specimen to *Kunpengopterus sinensis*. Its tooth count and spacing also matches closely that of *K. sinensis* (Cheng *et al.*, 2017a; Wang *et al.*, 2010). It bears a premaxillary crest, which differs from those of *Pterorhynchus*, *Wukongopterus* and *Darwinopterus* in being smooth rather than striated (Cheng *et al.*,

2017b). Although a bony crest is absent in the holotype of *K. sinensis*, this variation can easily be attributed to ontogeny and/or sexual dimorphism (Witton, 2013). We offer the following preliminary hypothesis: the cranial crest of *Kunpengopterus sinensis* started its development as soft-tissue and then ossified gradually at a late ontogenetic stage. We acknowledge that bony-crestless specimens of *K. sinensis* (holotype and IVPP V 23674) are quite close to osteological maturity (Cheng *et al.*, 2017a; Wang *et al.*, 2010). Nonetheless, it remains possible that the ossification of the crest occurred only late in ontogeny and rather Fast (Witton, 2013). Distinguishing species solely on the basis of cranial crest absence/presence/expression is dangerous, even though certain morphological features of cranial crests might be diagnostic (Witton, 2013; Cheng *et al.*, 2017b).

***Kunpengopterus antipollicatus* sp. nov.**

Holotype
BPMC 0042 (Fig. 20, 21, and 22), an almost complete skeleton lacking the posterior region of the skull. The specimen is permanently deposited and available for researchers at a public repository, the Beipiao Pterosaur Museum of China, Beipiao, Liaoning Province, China.

Paratype
Zhejiang Museum of Natural History (ZMNH) M8802 (Fig.23), an incomplete skeleton including two eggs.

Locality and horizon
Linglongta Town, Jianchang County, Huludao City, Liaoning Province, China. Linglongta strata (Oxfordian, 161–158 Ma) of the Tiaojishan Formation (Bajocian-Oxfordian).

Diagnosis
Dorsal margin of the skull convex; first dentary tooth pair procumbent; relatively small metacarpus (half of humerus length); wing phalanx 3 shorter than wing phalanx 2; proximal segment of phalanx 2 of pedal digit V subequal in length to the distal segment length (autapomorphies).

Remarks
A reversed pollex is potentially diagnostic for the genus, being possibly present in *K. sinensis*, pending further discoveries (Fig.24). *Kunpengopterus antipollicatus* can be distinguished from *K. sinensis* on the basis of the following features: the dorsal margin of the skull is convex, whereas it is mostly straight/slightly concave in the rostrum in *K. sinensis*; wing phalanx 3 is shorter than wing phalanx 2, whereas wing phalanx 3 is subequal to/slightly longer than wing phalanx 2 in *K. sinensis*; the posterodorsal margin of the ischium projects posteroventrally, whereas it rises dorsally in *K. sinensis*; the first phalanx of pedal digit V is subequal in length to

metatarsal IV, whereas it is less than 70% of metatarsal IV in *K. sinensis* (autapomorphy).In our phylogenetic analyses, we have included all darwinopteran species into three different datasets (Wu *et al.*, 2017; Dalla Vecchia, 2019; Pêgas *et al.*, 2019). Our results corroborate the placement of *K. antipollic* as the sister species of *K. sinensis* (Fig. 20C).

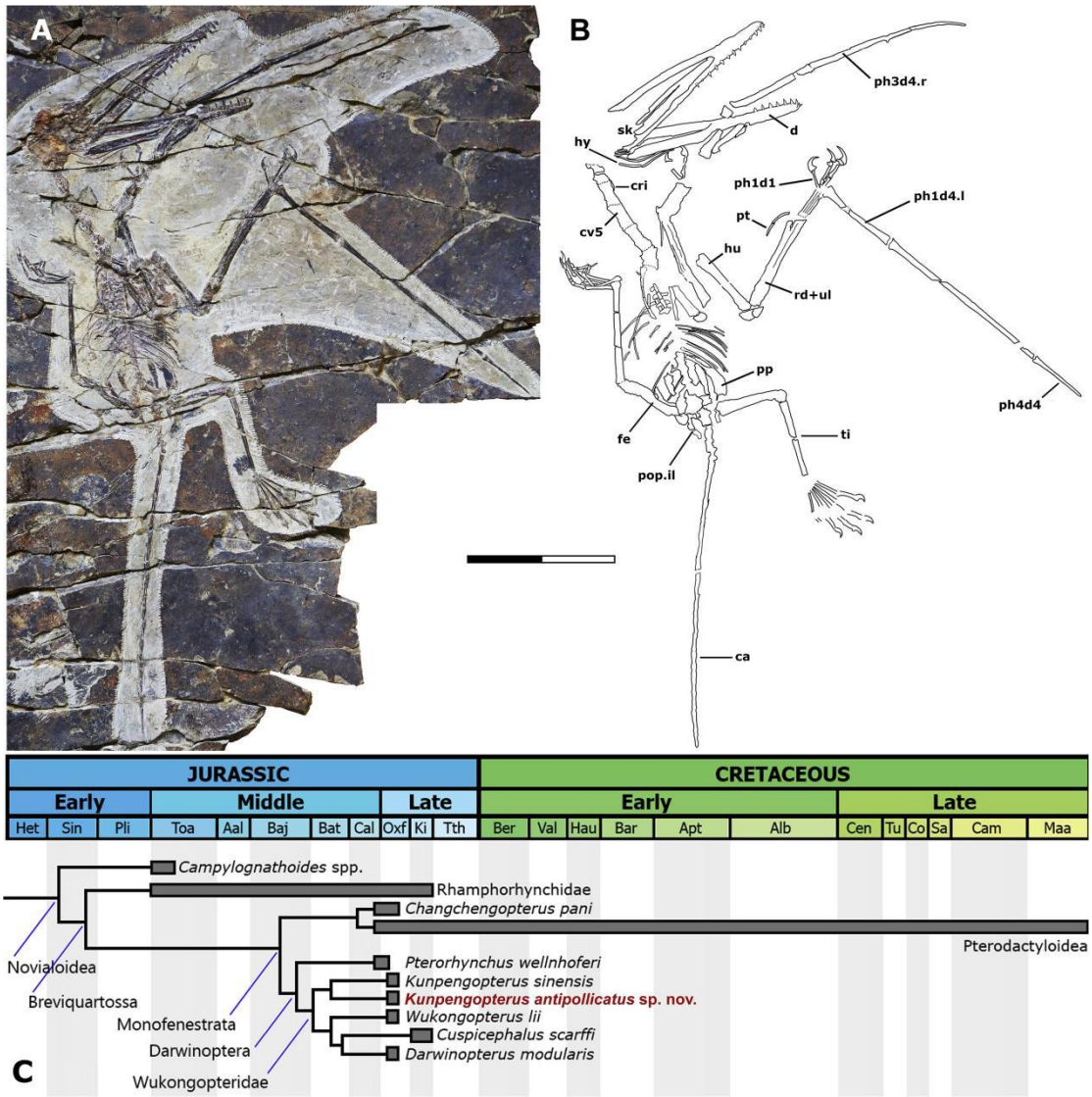

Figure 20. *K. antipollicatus* and its phylogenetic position (A and B) Holotype specimen BPMC 0042 (A) and a schematic skeletal drawing (B). Scale bars, 50 mm. (C) Phylogenetic relationships of the new species. Abbreviations: ca, caudal series; cri, cervical rib; cv, cervical vertebra; d, digit; de, dentary; fe, femur; hu, humerus; hy, hyoid apparatus; mc, metacarpal; ph, phalanx; pop.il, postacetabular process of the illium; pp, prepubis; pt, pteroid; rd, radius; sk, skull; ti, tibia; ul, ulna.

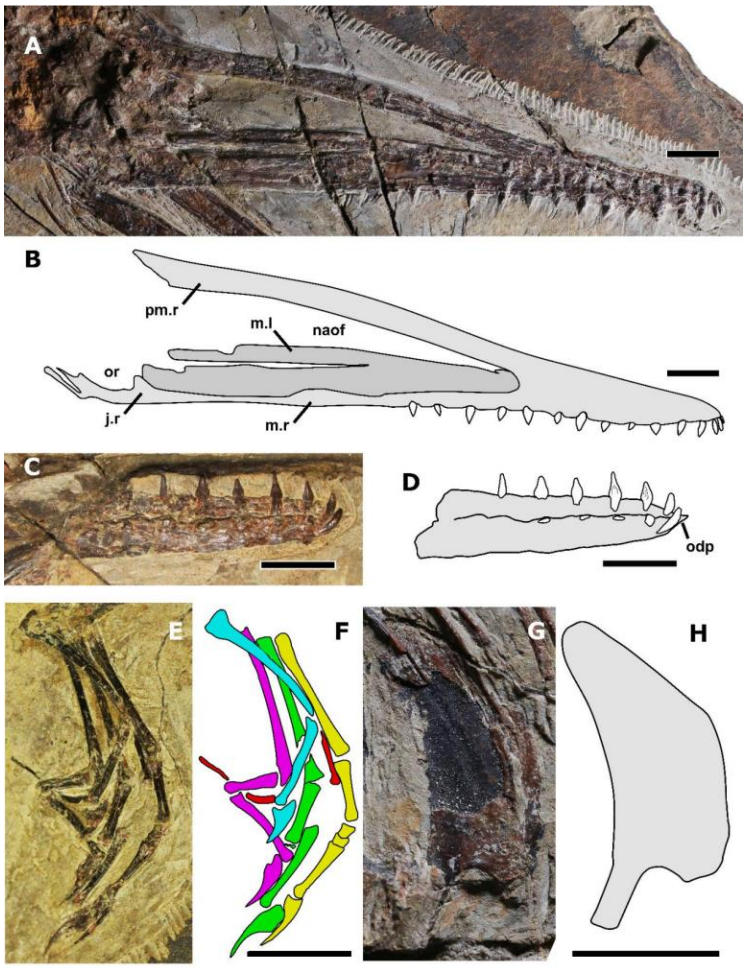

Figure 21. Details of BPMC 0042. (A, B) Skull. (C, D) Dentary symphysis. (E, F) Right foot. (G, H) Left prepubis. Abbreviations: j, jugal; l, left; m, maxilla; naof, nasoantorbital fenestra; odp, odontoid process; or, orbit; pm, premaxilla; r, right. Scale bars, 10 mm. Colors represent each pedal digit: blue, I; magenta, II; green, III; yellow, IV; red, V.

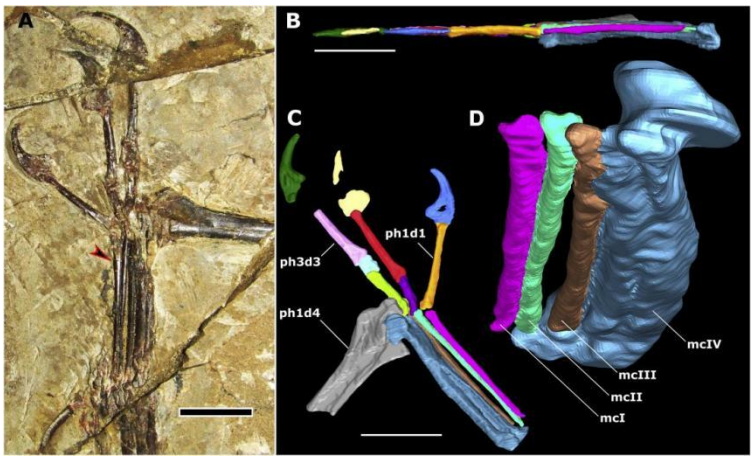

Figure 22. Left manus. (A) Detail of the left manus, exposed in ventral view. (B) 3D reconstruction of the left manus based on mCT data, anterior view. (C) Dorsal view. (D) Oblique distal view of the metacarpus, showing torsion of metacarpal I. Scale bars, 10 mm. The arrowhead indicates the twist on metacarpal I. d, digit; mc, metacarpal; ph, phalanx.

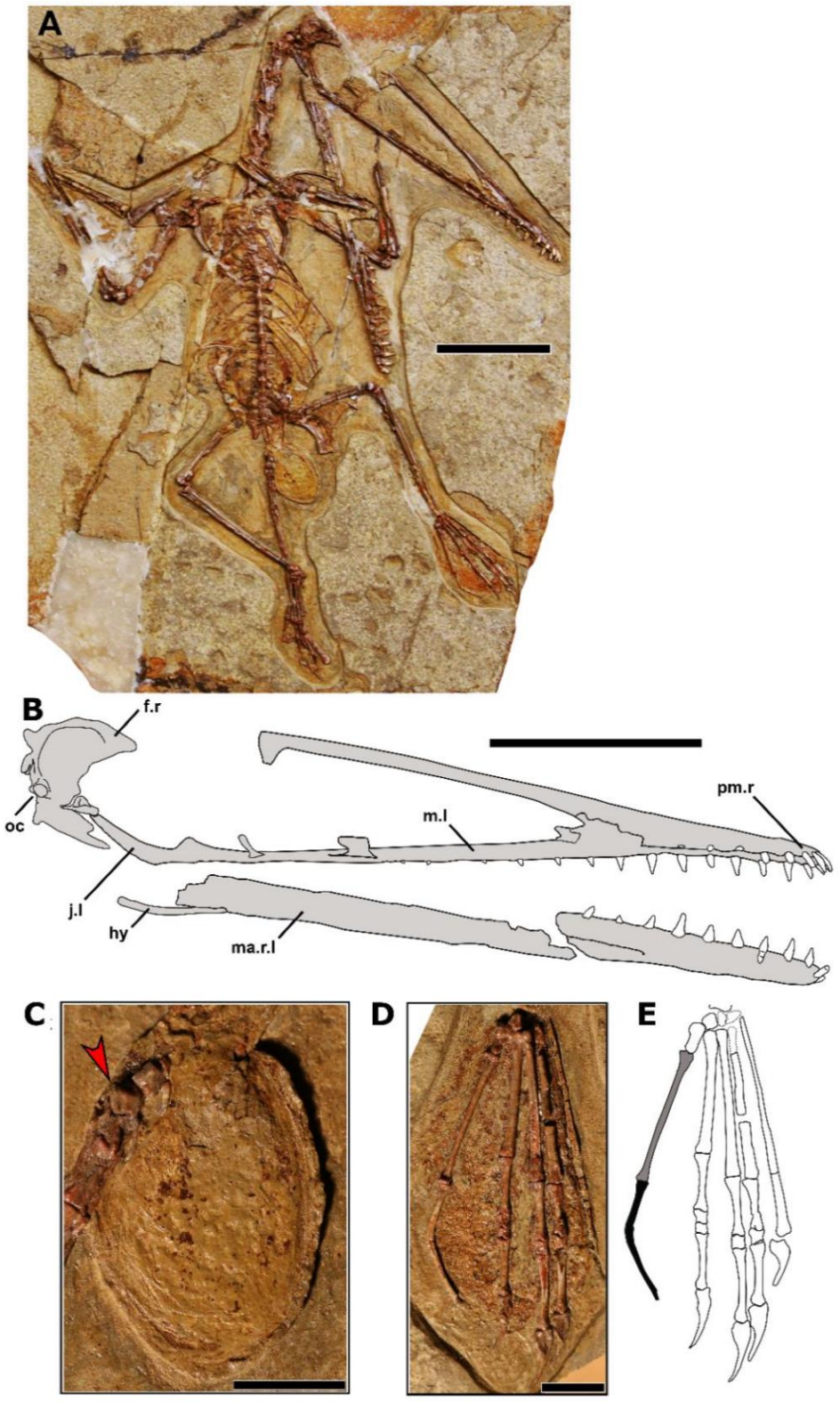

Figure 23. Morphology of *Kunpengopterus antipollexus*, paratype ZMNH M8802. (A) Main-slab. (B) Schematic drawing of the skull. Scale bars, 50 mm. (C) Associated egg. (D, E) Left foot, with proximal and distal phalanges of digit V in grey and black, respectively. Scale bars, 10 mm. Red arrow indicates a proximal caudal vertebra lacking filiform processes. Abbreviations: f, frontal; hy, hyoid (ceratobranchial I); j, jugal; l, left; mand.r, mandibular ramus; m, maxilla; pm, premaxilla; r, right; o, occipital.

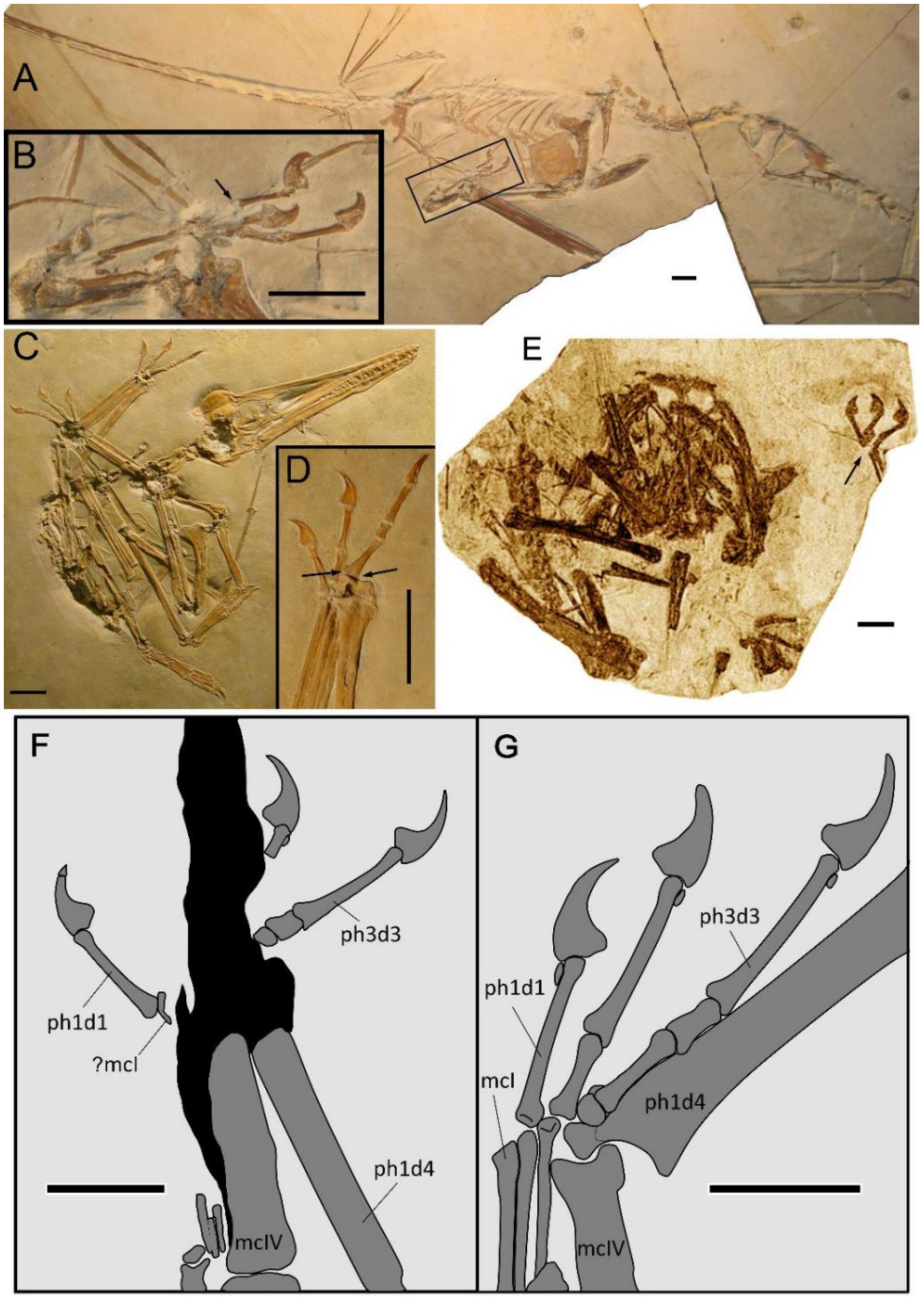

Figure 24. Cases of taphonomic digit flipping in pterosaurs, and the indeterminate situation in *Kunpengopterus sinensis*. (A) Taphonomic digit flipping in *Rhamphorhynchus* MB R. 3633. (B) Close-up of flipped digit. (C) Taphonomic digit flipping in *Diopecephalus* BSP 1878 VI 1. (D) Close-up of flipped digit. (E) Possible taphonomic digit flipping in holotype of *Batrachognathus*. Photo modified from S1 and colorized. (F) Left manus of *Kunpengopterus sinensis* holotype specimen, drawn fromS2. (G) Referred specimen IVPP V 23674 of *K. sinensis*, right manus. Scale bars, 10 mm. Black arrows indicate flipped digits. Light grey, matrix; dark grey, bone; black: crack. Notice that the elements were likely in natural articulation prior to cracking in the holotype; and that the elements are close to their natural positions in the referred specimen.

DESCRIPTION

Specimen BPMC 0042 (Fig. 20, 21, and 22) is almost complete, except for the posterior region of the skull, which was damaged during collection. The skull is exposed in right lateral view, while the trunk is exposed in ventral view. The left wing is also preserved in ventral view, while the right wing is folded over the trunk and exposed approximately in dorsal view. The skeleton is almost completely articulated; except for the prepubes and the lost posterior region of the skull.

ZMNH M8802 has been previously reported in a work that revolved around the preserved egg and its implications for pterosaur reproduction (Lü *et al.*, 2011a). ZMNH M8802 comprises the main slab of a single specimen that further includes the material IVPP V 18043, the counter-slab (Wang *et al.*, 2015). Originally regarded as a specimen of *Darwinopterus*, this specimen was later referred to as *Kunpengopterus* sp (Lü *et al.*, 2011a; Wang *et al.*, 2015). We designate it as the paratype of *Kunpengopterus antipollicatus*. A further detailed account on its osteology will be presented elsewhere. The description below is focused on BPMC 0042.

Skull

The cranium of BPMC 0042 is exposed in right lateral view. The long axis of the anterior half of the prenarial rostrum is slightly bent downward, with the ventral margin being concave, similarly to *K. sinensis* but unlike other darwinopterans (Lü *et al.*, 2010, 2011b; Wang *et al.*, 2009, 2010). The dorsal margin of the skull is gently convex, as in ZMNH M8802 (with no indications of deformation), while it is straight in *K. sinensis* and concave/sinusoidal in other darwinopterans. A fragment of the lacrimal process of the jugal can be seen, allowing for estimation of the location of the orbit and the posterior margin of the nasoantorbital fenestra. From this, we can calculate the nasoantorbital fenestra must have occupied about 42% of total skull length. The quadrate is visible, inclined backward at 149 relative to the jaw line. The mandible is exposed in an oblique, right dorsolateral view, so that the left mandibular ramus is exposed in medial view, except for its posterior region which is obscured by the skull (presumably articulated to it, as is the right ramus). At the anterior tip of the dentary symphysis, a small odontoid process is present, as in *K. sinensis* (Cheng *et al.*, 2017a). It is anterodorsally oriented, and about half the length of the adjacent teeth. The exact extent of the mandibular symphysis cannot be assessed. The mandibular fossa cannot be observed, most likely obscured by the skull, implying that it must have been relatively short. The retroarticular process is short and slender in lateral view. Both ceratobranchials I are visible ventral to the posterior region of the mandible. They are rod-like and elongated. The preserved portions extend for about the posterior fourth of the mandibular length. They are sigmoidal, similar to *Pterorynchus wellnhoferi*, *Darwinopterus robustodens* and *D. modularis*.

Dentition

There are 14 teeth preserved in the right upper jaw. It is unclear if any empty

alveoli are preserved posterior to the fourteenth upper tooth. On the lower jaw, 6 teeth are preserved on the left side (exposed in lingual view), and once again the total count is unclear. On the upper jaw, the first and second teeth are closely packed. Their interalveolar distance is under their alveolar diameters, while all remaining tooth positions are wide apart from the subsequent ones by interalveolar distances longer than their diameters. The first and second teeth are also smaller than the subsequent ones, and they are slightly anteroventrally oriented, while subsequent ones are ventrally oriented. This particular configuration is a wukongopterid feature that can be seen in *Wukongopterus*, *Kunpengopterus sinesis*, and *Darwinopterus* (Lü *et al.*, 2010, 2011b; Wang *et al.*, 2009, 2010). Spacing is approximately constant, being only slightly larger by the posterior third of the dentition. On the lower jaw, as in the upper, the teeth are approximately equally spaced. In shape, the teeth are slightly labiolingually compressed, with an elliptical cross-section – not as compressed as in istiodactylids (Zhou *et al.*, 2019). Their long axis is recurved lingually.

Vertebral series

The mid-cervical vertebrae are moderately elongate. Slender cervical ribs are present, but are no longer than the centra. The dorsal centra are longer than wide, and they exhibit transverse processes that are subequal in mediolateral extension to centrum length. The caudal series bears at least 25 vertebrae. In the anterior region of the caudal series, a number (5 or 6) of caudal vertebrae are relatively short and lack any rod-like processes of the haemapophyses and zygapophyses. All subsequent caudals are elongate and completely enclosed by long filiform processes. This is typical of most non-pterodactyloid pterosaurs (Lü *et al.*, 2010). In total, the caudal series of BPMC 0042 is quite elongated, extending for about 1.18 times the length of the trunk. This is similar to other darwinopterans, and longer than *Douzhanopterus* and *Changchengopterus* (Lü *et al.*, 2010, 2011b; Wang *et al.*, 2009, 2010).

Appendicular skeleton

The humeral entepicondyle is large and robust. The distal epiphysis is fused. Radius and ulna are of subequal diameters. The left pteroid is well recurved, similarly to *K. sinensis* and *Wukongopterus*; but unlike *Darwinopterus* whose pteroid is less recurved (Lü *et al.*, 2010, 2011b). Metacarpals I-III are about the same size and reach the carpus. The first metacarpal twists medially along its axis, so that its distal articulation is inverted. Its distal end is slightly expanded. The distal end of metacarpal II is slightly chipped (what presumably occurred during collection or preparation), and metacarpals III-IV are slightly compressed against one another. The fourth metacarpal is surprisingly short, accounting for half the length of the humerus. This value is about 0.6, or even higher, in other wukongopterids (Table. 4). The free digits bear robust, well-recurved unguals that bear a lateral groove. The manual unguals are about as large and as recurved as the pedal unguals, similarly to *K. sinensis* and differently from *Wukongopterus* and *Darwinopterus* (Lü *et al.*, 2010, 2011b; Wang *et al.*, 2009, 2010). The first phalanx exhibits a completely fused extensor tendon process. The longest wing phalanx is the second, followed by the

third and then the first (Table 3). The preacetabular processes are elongate and dorsoventrally flattened. The left prepubis is exposed in ventral view. Its anterodorsal flange exhibits an approximately straight dorsal margin, and the posteroventral flange is reduced and oriented posteriorly. This can also be seen in *K. sinensis* (Cheng *et al.*, 2017a; Wang *et al.*, 2010). In Darwinopterus, the prepubis is distinctively hatchet-shaped: the proximal process is elongate, the anterodorsal flange is strongly recurved, and the posteroventral process is elongate (Wang *et al.*, 2010; Lü *et al.*, 2011b). In IVPP V 17959 (most likely *Wukongopterus*, see above), the proximal process is elongate, the anterodorsal flange is strongly recurved, and the posteroventral process is ventrally expanded (Cheng *et al.*, 2016). The right femur exhibits a potential pathology. Its long axis is sigmoidal, apparently a result of a healed fracture. The fibula is not completely fused to the tibia, with an open suture on the proximal half of the tibia. The first phalanx of the fifth pedal digit is elongate, as in *Darwinopterus* and *Wukongopterus*, but unlike *K. sinensis* (Cheng *et al.*, 2017a; Wang *et al.*, 2010). The second phalanx of the fifth pedal digit bears an elongate proximal segment, differently from other darwinopterans. The angle between proximal and distal segments of this phalanx is 134°, very close to ZMNH M8802 (137°). The same angle is 145° - 147° for *Kunpengopterus sinensis*, 124° - 136° for *Darwinopterus* and 71° for *Wukongopterus* (Cheng *et al.*, 2017a).

Table 3. Measurements of BPMC 0042.

Element	Length(mm)
Skull	~156
Nasoantorbital fenestra	66
Mandible	134
Humerus	55
Ulna/radius	~80
Metacarpal IV (l)	28
Phalanx 1 digit 4 (l)	62
Phalanx 1 digit 4 (r)	~59
Phalanx 2 digit 4 (l)	69
Phalanx 2 digit 4 (r)	64
Phalanx 3 digit 4 (l)	59
Phalanx 3 digit 4 (r)	59
Phalanx 4 digit 4 (l)	44
Phalanx 4 digit 4 (r)	58
Femur (l)	52
Femur (r)	55
Tibia (l)	72
Tibia (r)	73

Table 4. Data of Wukongopterids.

Taxon /specimen	Naof/skull	hu/mcIV	hu/fe	hu/ul	hu+ul/fe+ti	ul/mcIV	ul/fe	ul/ti	sc/co	ph1d4/mcIV	ph1d4/ul+mcIV	ph1d4/ti	ph2d4/ph1d4	ph3d4/ph1d4	ph3d4/ph2d4	ph4d4/ph1d4	fe/meV	ti/fe	mtIII/ti
Darwinopterus modulars holotype	0.43	1.64	?	0.68	?	2.42	?	?	?	2.08	0.61	?	?	?	?	?	?	?	?
YH-2000	?	1.69	1.1	0.69	1.15	2.46	1.60	1.19	1.04	1.84	0.53	0.88	1.15	1.23	1.07	1.10	1.54	1.35	0.31
Darwinopterus robustodens	0.44	1.67	1.16	0.63	1.26	2.67	1.86	1.33	1.13	2.17	0.59	1.08	1.15	1.15	1.00	1.03	1.43	1.40	0.35
Darwinopterus linglongtaensis	0.43	1.69 1.69	1.03 1.00	0.70 0.65	1.10 1.13	2.58 2.59	1.47 1.53	1.16 1.23	1.25	1.88 2.05	0.57 0.52	0.93	1.10 1.17	1.15 1.21	1.05 1.03	1.16 1.21	1.75 1.70	1.26 1.24	0.34
Kunpengopterus sinensis holotype	0.35	1.57	0.92 0.88	0.61	1.02 1.00	2.57	1.44 1.50	1.09	1.21	2.35	0.66	0.99	1.07	1.09	1.02	0.90	1.70 1.79	1.32 1.39	0.38 0.40
Kunpengopterus sinensis referred	0.40	1.55 1.59	?	0.65	?	2.34 2.46	?	1.18	1.14	1.96 1.91	0.57	0.94	1.11	1.02	1.01	1.02	?	?	0.39
ZMNH M8802/ IVPP V18403	0.41	?	1.27	0.74	1.20	?	1.71	1.15	?	~2.32	0.50	0.84	1.15	?	?	?	?	1.49	0.33
BPMC 0042	0.45	1.96	1.06	0.71	1.09	2.85	1.34	1.14	?	2.22	0.58	0.87	1.20	1.03	0.85	0.66	1.72	1.59	0.33
Archaeoistiodactylus linglongtaensis	?	1.68	1.07	0.67	1.10	2.50	1.59	1.13	?	?	?	?	?	?	1.00	?	1.57	1.40	?
Wukongopterus lii	? 0.55	1.69	1.09 1.16	0.63	1.14	2.71	1.74 1.86	1.18	1.35	2.00	0.54	0.87	1.24	1.28	1.03	1.13	1.45 1.55	1.48 1.58	0.32 0.33
IVPP V17959	0.55	1.49	?	0.61	?	2.44	?	?	?	2.09	0.58	?	1.08	?	?	?	?	?	?
Changchengopterus pani	?	1.66	1.23	0.70	1.36	2.35	1.75	1.47	1.22	1.92	0.57	1.20	1.07	1.00	0.94	?	1.35	1.19	?
Pterorhynchus wellnhoferi		1.82	1.24	0.57	?	3.19	?		?			?	1.25	?	?	?	1.47	?	?

DISCUSSION

K. antipollicatus sp. nov. exhibits the typical darwinopteran modular morphology, with an advanced monofenestratan skull (shared with pterodactyloids) and a primitive, elongate tail (reduced in pterodactyloids, typical of basal pterosaurs) (Lü *et al.*, 2010, 2011b; Wang *et al.*, 2009, 2010; Martill & Etches, 2012). Based on the holotype, its estimated wingspan is ~850mm, which falls well within the drawinopteran rang (~600 to 1200 mm) (Lü *et al.*, 2010, 2011b; Wang *et al.*, 2009, 2010; Martill & Etches, 2012; Bestwick *et al.*, 2018). Darwinopterans, particularly wukongopterids, have been the focus of significant findings in the last decade, mostly due to their complex morphology that has revealed a modular evolutionary history for pterosaurs, as well as discussions on pterosaur reproduction, through a female specimen gravid with two eggs (Lü *et al.*, 2010, 2011b; Wang *et al.*, 2015). Concerning the new species, the most striking feature of the holotype is that, on both sides, the pollex is preserved in an opposed position, with its palmar side facing the palmar side of the other digits (Fig. 21 and 23).

Varying degrees of pollex orientation exist in tetrapods, which has led to the proposition of classification systems (Napier, 1961, 1980; Christel & Fragaszy, 2000). ‘‘Nonopposable pollices’’ are those where the orientation of the pollex is similar to that of other digits. “True opposed pollices” are those where the opposition is palmar, with the palmar side of the thumb facing the palmar side of the other digits (Napier, 1961, 1980). In contrast, a pollex that is medially offset but not fully opposed (and thus it faces the lateral side of the other digits, rather than the palmar side) has been termed “pseudo-opposed” or “laterally opposed” or, alternatively, an “offset thumb” in contrast to an “opposed thumb” (Napier, 1961, 1980; Christel & Fragaszy, 2000; Padian, 1989). Offset (but not truly opposed) thumbs can be found in the anomodont synapsid Suminia and in the base of the Dinosauria, as seen in many early species and several theropods (Fröbisch & Reisz, 2009; Bakker & Galton, 1974; Gauthier, 1986; Burch, 2014). On the other hand, true (or palmar) opposition of the pollex is a sophisticated adaptation unusual for reptiles, and is typically associated with arborealism (Sustatia *et al.*, 2013). It is mostly restricted to mammals (such as primates) other than some tree frogs, being absent in reptiles, although something similar occurs in chameleons and drepanosaurs due to their zygodactyl-like condition (see Sustatia *et al.*, 2013). In primates, opposition of the pollex is achieved by movement, through rotation at the first carpometacarpal joint. In *K. antipollicatus*, however, there is no indication of this mobility. Instead, its osteological configuration is similar to that observed in the avian reversed hallux. In birds, the opposition of the hallux is due to the distal torsion of the long axis of metatarsal I, reminiscent of the torsioned metacarpal I of *K. antipollicatus* (Middleton, 2001). As in the avian hallux, we interpret the pollex of *K. antipollicatus* as permanently opposed in a natural position (anisodactyl-like).

Microcomputed tomography (mCT) scanning of the left hand reveals a complex

morphology (Fig. 23) that indicates adaptation toward grasping. The distal half of metacarpal I torsions on its long axis, with the palmar surface suffering a dorsomedial deflection (or supination) of 150° . The distal articulation of metacarpal I is thus torsioned, affecting the orientation of the pollex. This indicates that the tendon of musculus flexor digitorum longus (mFDL), the muscle responsible for digit flexion and that runs along the metacarpals, would also torsion its orientation, thus causing the pollex to flex toward the other free digits (Burch, 2014). This unique morphology would grant a grasping ability. In the unguals, the flexor tubercle (insertion site for mFDL) is well developed (Fig. 23), whereas the extensor tubercle (insertion site for musculus extensor digitorum brevis, responsible for ungual extension) is reduced, as in other wukongopterids. This suggests that ungual flexion, and thus grasping, played a more important role in manual function (Burch, 2014). Antungual sesamoids, which may be related to hypertension of the unguals, could not be found in BPMC 0042, despite being widespread in wukongopterids (Cheng *et al.*, 2017a; Witton, 2015). Still, their absence in BPMC 0042 could be due to ontogeny and incomplete ossification. Despite this, the distal articular surface of metacarpal I is expanded, what possibly favored pollex extension (Middleton, 2001).

CONCLUSION

BPMC-0042 represents a new darwinopteran, here named *Kunpengopterus. antipollicatus* (Fig. 25). It is the second *kunpengopterus* from the Tiaojishan Formation, and the oldest evidence for a true opposed pollex in the fossil record . In our new phylogenetic analysis, *Kunpengopterus siensis* and *K. antipollicatus* are recovered as the sister-group of them ((*Darwinopterus modularis* + *Cuspicephalus scarffi*) + *Wukongopterus lii*). All Wukongopteridae (((*Darwinopterus modularis* + *Cuspicephalus scarffi*) + *Kunpengopterus*) were recovered as close to *Pterorhynchus wellnhoferi*, with which it comprises the Darwinoptera.

With the oldest evidence for a true opposed pollex in the fossil record, darwinopterans keep providing unexpected and invaluable information on the evolutionary history of pterosaurs. This unique clade seems to have experienced an evolutionary trajectory richer than initially thought, having been much more than an evolutionary step toward advanced pterodactyloids.

Figure 25. Life reconstruction of *Kunpengopterus. antipollicatus* (from Zhao Chuang).

CHAPTER IV

ADVANCES IN CHINESE ADVANCED TYPE PTEROSAUR 1: A TAXONOMIC REVISON OF THE TAPEJARIDAE *SINOPTERUS* COMPLEX WITH NEW GENUS *HUAXIADRACO*

INTRODUCTION

The Tapejaridae (sensu Andres, 2021) are a clade of Cretaceous edentulous pterosaurs of the group Azhdarchoidea (Pterodactyloidea, Eupterodactyloidea), characterized by their short, downturned rostra and peculiar premaxillary crests (Kellner & Campos, 2007; Pêgas, Leal & Kellner, 2016). They comprise over 10 species (up to 14 valid species following Zhang *et al.*, 2019), spanning from the Barremian to the Santonian; with records from Brazil, Morocco, Europe, and China (Kellner & Campos, 2007; Vullo *et al.*, 2012; Andres, Clark & Xu, 2014; Pêgas, Leal & Kellner, 2016).

Tapejarids are a relatively common element of the famous Jehol Biota of China. From the Yixian Formation, a single species has been described: *Eopteranodon lii*, represented by two specimens (Lü & Zhang, 2005; Lü *et al.*, 2006c). Originally regarded as an undetermined pterodactyloid (Lü & Zhang, 2005) or a pteranodontid (Lü *et al.*, 2006c), it was later reinterpreted as a tapejarid (Andres & Ji, 2008; Vullo *et al.*, 2012). In contrast with the Yixian Fm. (late Barremianearly Aptian), a great abundance of tapejarids is found in the Jiufotang Formation (Aptian). In total, 15 specimens of Jehol tapejarids have been formally described in the literature (Wang & Zhou, 2003a; Li, Lü & Zhang, 2003; Lü & Zhang, 2005; Lü & Yuan, 2005; Lü *et al.*, 2006a, 2006b, 2006c, 2007, 2016; Liu *et al.*, 2014; Zhang *et al.*, 2019; Shen *et al.*, 2021; Zhou, Niu & Yu, 2022; Zhou *et al.*, 2022). Under the accounts of Shen *et al.* (2021), the total number of recovered specimens, scattered around Chinese institutions, must be close to a hundred.

The first tapejarid to be recovered from China was *Sinopterus dongi*, from the Jiufotang Formation (see Wang & Zhou, 2003a). Further six Jiufotang tapejarid species have been named posteriorly: *Sinopterus gui*, *Sinopterus lingyuanensis*, *Huaxiapterus jii*, *Huaxiapterus corollatus*, *Huaxiapterus benxiensis*, and *Huaxiapterus atavismus* (see Wang & Zhou, 2003a; Li, Lü & Zhang, 2003; Lü & Yuan, 2005; Lü *et al.*, 2006a, 2007, 2016). These proposed speices of Jiufotang tapejarids are involved in a series of complex taxonomic disputes, with the genera *Huaxiapterus* and *Sinopterus* having been synonymized (Wang & Zhou, 2006; Wang *et al.*, 2008; Witton, 2013; Zhang *et al.*, 2019). Thus, the Jiufotang tapejarids will heretofore be referred to as the *Sinopterus* complex.

The type species *Sinopterus dongi* was described by Wang & Zhou (2003a) and its validity has never been contested. A second species, *Sinopterus gui*, was proposed by Li, Lü & Zhang (2003), but its holotype was later reinterpreted as an undiagnostic juvenile specimen, indistinct from *S. dongi* (Kellner & Campos, 2007; Kellner, 2010).

Following the description of these two species, the genus *Huaxiapterus* was erected for the type-species *Huaxiapterus jii* by Lü & Yuan (2005). Afterwards, Wang & Zhou (2006) synonymized *Huaxiapterus jii* with *Sinopterus dongi*, regarding that

the two holotypic specimens were indistinguishable. Kellner & Campos (2007) accepted the validity of *H. jii* at the species level, but referred it to the genus *Sinopterus*, as *Sinopterus jii.* Later, however, Kellner (2010) and Zhang *et al.* (2019) regarded *S. jii* as a synonym of *S. dongi*, following the proposition by Wang & Zhou (2006). A consequence of this species-level synonymy is that the genus *Huaxiapterus* would become invalid.

Later, Lü *et al.* (2006a) attributed a second species to the genus *Huaxiapterus*, *H. corollatus*. Kellner & Campos (2007) accepted the species-level validity of *H. corollatus* and suggested that it required a new genus name (recognizing the proposed synonymy between *H. jii* and *S. dongi*, and considering that *H. corollatus* was sufficiently distinct from *S. dongi* to warrant another genus name). Later, another species was proposed for the genus *Huaxiapterus* by Lü *et al.* (2007): *Huaxiapterus benxiensis*.

Subsequently, Witton (2013) proposed that the majority of the previously described Jiufotang tapejarids could possibly represent a single ontogenetic continuum. Witton (2013) noticed that the diagnoses of the proposed species relied heavily on crest size and shape, what is problematic since this is most likely strongly influenced by sexual and ontogenetic variation (e.g., Bennett, 1993; Wang *et al.*, 2014; Manzig *et al.*, 2014; Pinheiro & Rodrigues, 2017). Though Witton (2013) made a case for this possibility, it has never been investigated in detail so far. Andres, Clark & Xu (2014) did not contest the validity of any of the previously proposed species, having coded all the then-described species in their phylogenetic analysis: *Sinopterus dongi*, *Huaxiapterus jii*, *Sinopterus gui*, *Huaxiapterus corollatus* and *Huaxiapterus benxiensis*.

More recently, Lü *et al.* (2016) rejected all proposed synonymies and further proposed two new species, *Sinopterus lingyuanensis* and *Huaxiapterus atavismus*. Subsequently, Zhang *et al.* (2019) sank all species ever attributed to *Huaxipterus* onto *Sinopterus*, and recognized five species as valid: *Sinopterus dongi*, *Sinopterus corollatus*, *Sinopterus benxiensis*, *Sinopterus lyngyuanensis* and *Sinopterus atavismus*. Zhang *et al.* (2019) regarded *Sinopterus gui* and *Sinopterus jii* as junior synonyms of *Sinopterus dongi*. Still, Zhang *et al.* (2019) did not present detailed discussions concerning this taxonomic proposal.

Subsequently, Naish, Witton & Martin-Silverstone (2021) preliminarily corroborated the proposition of Witton (2013) that all Jiufotang tapejarids represent an ontogenetic continuum of a single species. Still, Naish, Witton & Martin-Silverstone (2021) noted that at least *Huaxiapterus corollatus* was an apparent outlier regarding limb proportions, thus suggesting that it "may represent a second taxon", pending further testing. More recently, Shen *et al.* (2021) supported the proposition by Naish, Witton & Martin-Silverstone (2021).

In summary, a total of seven tapejarid species have been proposed for the Jiufotang Formation, all eventually attributed to the genus *Sinopterus* and intricated in a series of complex disputes based on preliminary considerations. A detailed review of the *Sinopterus* complex is still lacking, and a critical survey of anatomical variation is thus of the uttermost importance.

We hope to reinterpret the *Sinopterus* complex and provide a taxonomic reassessment, based on which new specimens can be identified. Pivotal to the taxonomic history of the *Sinopterus* complex is the role of cranial crests in pterosaur taxonomy. It is clear that cranial crest features used alone make for problematic taxonomic decisions (Witton, 2013), as they could rather reflect ontogenetic or sexual variations (Bennett, 1993; Wang *et al.*, 2014; Manzig *et al.*, 2014; Pinheiro & Rodrigues, 2017). However, it is also clear that some closely related species may exhibit disparate cranial crest morphologies (at least when inferred mature males are considered), which can thus contain taxonomic signal (e.g., *Pteranodon longiceps* and *Pteranodon sternbergi*; see Bennett, 1994). It is for this reason that, in this work, we aim at revising the taxonomy of the *Sinopterus* complex with extra caution regarding cranial crest variation, by making a primary taxonomic assessment without input from cranial crest data first, and then assessing and interpreting cranial crest variation subsequently; instead of using cranial crest variation as an a priori source of taxonomic signal.

GEOLOGICAKL SETTING

The Jiufotang Formation is widely distributed in the terrestrial volcanic sedimentary basins of northern Hebei and western Liaoning, which have yielded the diverse Jehol Biota (Xi *et al.*, 2019). It represented a lacustrine environment surrounded by temperate forests (Zhou, Barrett & Hilton, 2003; Benton *et al.*, 2008). Although specimens are typically crushed, preservation is nonetheless exceptional and soft tissue is often found (Benton *et al.*, 2008; Zhou & Wang, 2010).

The Jiufotang Formation of western Liaoning is distributed within six continental faulted basins, trending northeast: Fuxin-Yixian Basin, Beipiao-Chaoyang Basin, Dapingfang-Meileyingzi Basin, Dachengzi-Siguanyingzi Basin, Jianchang Basin, Lingyuan-Sanshijiazi Basin (Su *et al.*, 2008; Wu *et al.*, 2018; Xi *et al.*, 2019; Fig. 26).

The rock layers are mainly grey to greyish green in color, interbedded with greyish yellow, greyish white, greyish black and occasionally purple rocks (Wu *et al.*, 2018). They consist of calcareous silty shales, shales, and siltstones, interbedded with oil shales, tuffs, bentonites, coal seams, marlstones, sandstones, and conglomerates (Wu *et al.*, 2018). This sedimentary association is dominated by lake sediments and includes abundant macrofossils of animals and plants. The thickness of Jiufotang Formation varies from ~200–3,000 m depending on locality, contacting the underlying Yixian Formation through a parallel unconformity (Wu *et al.*, 2018). It is

overlaid by formations as among which Binggou Formation and Fuxin Formation.

Unique fossil-bearing bed (UFBB) refers to a set of Chinese national key protected fossils (classified as level three or above, by National Standard for classification of Paleontological Fossils, China), such as reptiles and birds, which is known from a regionally stable and significant geological formation. A number of unique fossil-bearing beds have been named (e.g., Duan *et al.*, 2006, 2010; Wu *et al.*, 2018, Gao *et al.*, 2018; Fig.27).

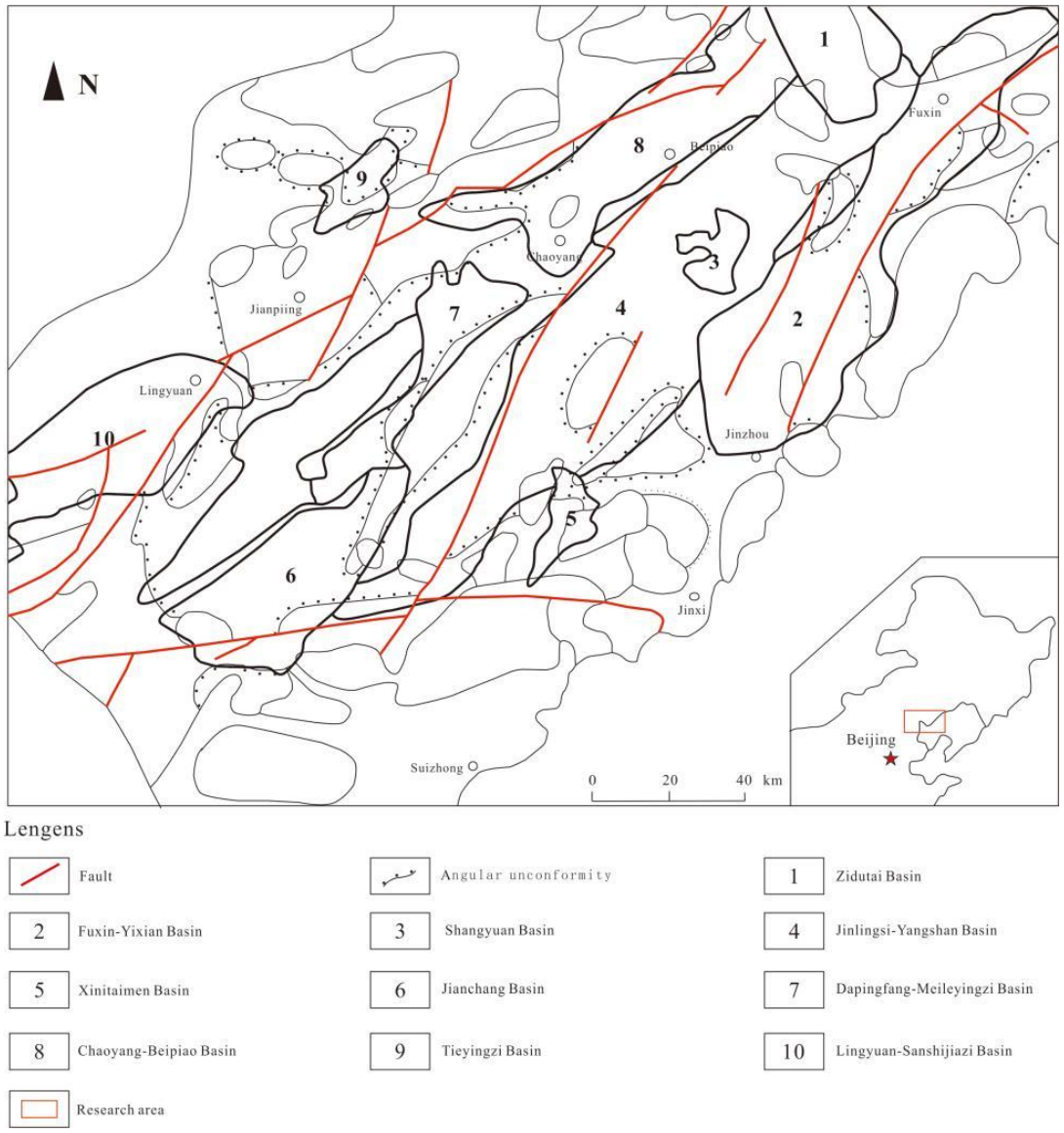

Figure 26. Distribution map of Mesozoic basins in western Liaoning, northeastern China.

Wu *et al.* (2018) divided the Jiufotang Formation into three sections from bottom to top, based on lithology, depositional cycle, basic sequence, and fossil assemblage. In general, the base of every section consists of yellowish brown-yellowish green, thick-bedded medium to coarse conglomerate. The top layer is made up of yellowish green thin to very thin tuffaceous siltstone and thin silty mudstone. A short-term cycle

is formed by conglomerate (containing glutenite), sandstone, siltstone and shale. About seven to nine short-term cycles form a mid-term cycle (three sections of Jiufotang Formation) that exhibits finer grain sizes and thinner beds progressively upward, as shown in a schematic division and correlation diagram of the Jiufotang Formation and the UFBB in western Liaoning (including five basins: Fuxin-Yixian Basin, Beipiao-Chaoyang Basin, DapingfangMeileyingzi Basin, Dachengzi-Siguanyingzi Basin and Jianchang Basin; Wu *et al.*, 2018). Detailed paleoenvironmental reconsctructions for each bed are still needed.

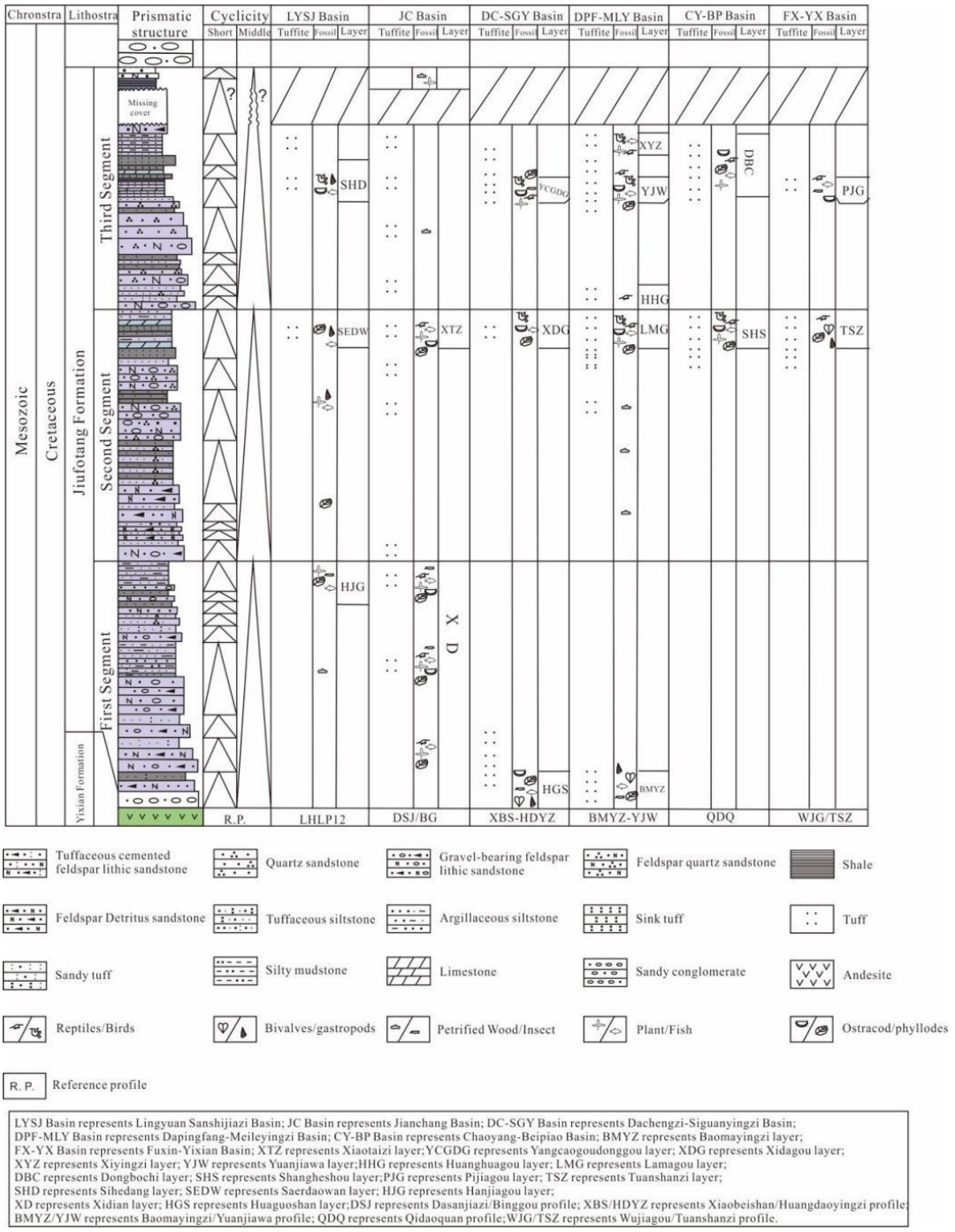

Figure 27. Unique fossil-bearing bed (UFBB) in western Liaoning, northeastern China.

Due to the highly fossiliferous nature of the Jehol Group, several fossils are commonly found by local collectors, although without a precise control over their stratigraphic provenance (e.g., Kellner, 2010; Lü *et al.*, 2016). A notable exception is the holotype of *Sinopterus dongi*, known to come from the Lamagou UFBB, of the Second Member of the Jiufotang Formation (Zhang *et al.*, 2007). The holotypes of *Sinopterus gui* and *Huaxiapterus jii* come from the mudstone/shale layers of Nanlu, Shengli Town, which correspond to the Yuanjiawa UFBB of the Third Member of the Jiufotang Formation (Zhang *et al.*, 2007). Specimens PMOL-AP00030 and D3072 are known to have come from the Dapingfang locality (Liu *et al.* 2014; Shen *et al.*, 2021), where the Third Member of the Jiufotang Fm. outcrops (see Wu *et al.*, 2018).

The holotype of Sinopterus lingyuanensus and specimen IVPP V 23388 are known to come from Sihedang, Lingyuan, and they are preserved in shales (Lü *et al.*, 2016; Zhang *et al.*, 2019), what indicates they likely come from the Third Member Sihedang beds (see Wu *et al.*, 2018).

The holotype of Huaxiapterus benxiensis is reported to come from Lianhe Town (Lü *et al.*, 2007), and thus from the Dapingfang Basin, meaning it comes from either the Second or Third Member (Zhang *et al.*, 2007; Wu *et al.*, 2018).

For specimens D2525 and the holotype of *H. corollatus*, the only information available is that they come from Chaoyang City (Lü *et al.*, 2006b, 2007). The same applies to the new specimens reported here (D4019, BPMC 103, BPMC 104, BPMC 105, BPMC 106, and BPMC 107). Within Chaoyang City, two fossiliferous beds of the Jiufotang Formation occur: the Dongpochi Bed of the Second Member, and the Shangheshou Bed of the Third Member (Zhang *et al.*, 2007). Unfortunately, it is hard to define from which bed came each of the remaining Jiufotang tapejarid specimens, but it can be said that they come from either the Second or the Third Member.

MATERIALS AND METHODS

Phylogenetic analysis

Subsequent to our reassessment of the species-level taxonomy of the *Sinopterus* complex, we proceeded to perform a phylogenetic analysis, which is the last step of the present work. After obtaining the results from our taxonomic reassessments (see below for our taxonomic proposals and species circumscriptions), we included and coded all Chinese tapejarid species (those that were considered as valid here) in an updated version of the data matrix from Pêgas *et al.* (2021). For this reason, in the present article, a separate Phylogenetic Analysis section is presented only after the main Discussion section.

We performed a cladistic analysis using the software TNT 1.5 (Goloboff, Farris & Nixon, 2008), which was divided in two steps, following the same protocol as

previously described by Wei *et al.* (2021). New Technology Search was used for the first search (using Sectorial Search, Ratchet, Drift and Tree fusing, default parameters), with random seed = 0. In sequence, using trees from RAM, a traditional search swapping was performed (using TBR, 10,000 replications, collapsing trees after search). All characters were treated with equal weights. A Mesquite file (Nexus format) containing the data matrix is available as Supplemental File 5. A TNT file, ready for analysis execution in TNT, is available as Supplemental File 6.

Coding for *Bakonydraco galaczi* is restricted to jaw elements (Ősi, Weishampel & Jianu, 2005; Ősi, Buffetaut & Prondvai, 2011). Coding for *Afrotapejara zouhri* is based on the holotype and the three referred specimens (Martill *et al.*, 2020a). Coding for *Aerotitan sudamericanus* follows the interpretation of the holotype as a lower jaw (Pêgas *et al.*, 2021; contra Andres, 2021). The holotype of *Alanqa saharica* is also coded here as a lower jaw (Pêgas *et al.*, 2021; contra Ibrahim *et al.*, 2020); however, its coding is corrected here based on an anatomical reinterpretation, with a dentary occlusal eminence being absent and instead a pair of dentary raised ridges being present (R. Smith & D. Martill, 2022, personal communication; see also Ibrahim *et al.*, 2020), similar to that seen in specimen FSAC KK 4000 (Martill & Ibrahim, 2015; Ibrahim *et al.*, 2020).

Nomenclatural acts

The electronic version of this article in Portable Document Format (PDF) will represent a published work according to the International Commission on Zoological Nomenclature (ICZN), and hence the new names contained in the electronic version are effectively published under that Code from the electronic edition alone. This published work and the nomenclatural acts it contains have been registered in ZooBank, the online registration system for the ICZN. The ZooBank LSIDs (Life Science Identifiers) can be resolved and the associated information viewed through any standard web browser by appending the LSID to the prefix http://zoobank.org/. The LSID for this publication is: urn:lsid:zoobank.org:pub:E836D564-B986-497A-9E3C-8277EF8EF50E. LSID for the new genus: urn:lsid:zoobank.org:act:39AA06E5-6882-4041-9585-8F2106424C81.

Phylogenetic nomenclature

The present work favors the recent propositions of the PhyloCode (de Queiroz, Cantino & Gauthier, 2020) as a means of standardizing and stabilizing phylogenetic nomenclature. We thus primarily follow the phylogenetic definitions given and registered by Andres (2021) and Pêgas *et al.* (2021) concerning azhdarchoids, though with a few unrestricted emendations. The phylogenetic nomenclatural scheme employed here, following recommendations of the PhyloCode, is presented in Table 5.

Of particular note concerning phylogenetic nomenclature in azhdarchoids is the conflicting usages of the terms Tapejaridae, Tapejarinae, and Thalassodrominae.

Originally, the family Tapejaridae was erected in order to encompass *Tapejara wellnhoferi* and *Tupuxuara longicristatus* (Kellner, 1989), and later defined as the least inclusive clade containing these two taxa (*Kellner, 2003*). Tapejaridae was later divided into Tapejarinae and Thalassodrominae, which can be roughly described, respectively, as a "Tapejara-Sinopterus group" and a "Thalassodromeus-Tupuxuara group" (Kellner & Campos, 2007). Disagreement over the sister-group relationship between the "Tapejara-Sinopterus group" and the "Thalassodromeus-Tupuxuara group" led to a restrictive redefinition of the Tapejaridae by some workers, as the least inclusive clade containing *Tapejara wellnhoferi* and *Sinopterus dongi*, with the "Thalassodromeus-Tupuxuara group" thus elevated to a family-level Thalassodromidae (Lü *et al.*, 2006a; Andres, 2021). A consequence of this problem is: even though the existence of both a "Tapejara-Sinopterus group" and of a "Thalassodromeus-Tupuxuara group" has been remarkably consensual, the same clades have received different names according to preferred phylogeny. Albeit valid under the ICZN, this situation is conflictive with the principles of phylogenetic nomenclature.

Under the light of phylogenetic nomenclature, it is undesirable that two equivalent clades should bear inconsistent names across distinct phylogenies. If distinct phylogenies agree on recovering a given clade (which is a great feat in pterosaur systematics), then this clade should have a consistent name, for the sake of stability. Different clade names should only exist when de facto distinct clade proposals exist. For example, a clade that includes Thalassodromeus and Azhdarcho but excludes *Tapejara* does not exist in certain propositions (e.g., Kellner, 2003). However, this clade exists in others (Unwin, 2003; Andres, 2021), under which such a proposed clade does need a name ("Neoazhdarchia"). Thus, Neoazhdarchia is a name that only exists (or is valid) within the context of a certain phylogenetic proposal (Unwin, 2003; Andres, 2021). In contrast, a clade that includes *Sinopterus* and *Tapejara* and excludes *Thalassodromeus* and *Azhdarcho* is universally accepted among pterosaur researchers. It is unfortunate that such welcome phylogenetic consensus is not accompanied by nomenclatural stability, as it should. It is for this reason that we adopt here the restrictive usage of Tapejaridae sensu Andres (2021), which has already been proposed and registered under the PhyloCode. This definition can be utilized in any phylogenetic proposal, and its adoption will prevent different workers from referring to different clades by, confoundingly, using the same names—as well as from referring to a same clade by different names.

Arguments for the restrictive usage of Tapejaridae sensu Andres (2021) need not come exclusively from the point of view of the PhyloCode, but could also be argued for under the ICZN. In the same way that the expansive Pteranodontidae sensu Bennett (1989, 1994) was elevated to the Pteranodontoidea of Kellner (2003), turning Pteranodontidae more restricted, then one might also regard that the original Tapejaridae sensu Kellner (1989, 2003) should be elevated to the Tapejaromorpha, with Tapejaridae becoming more restricted. We emphasize that the usage of these

definitions as explored here do not imply, in any way, which phylogeny is preferred, and can stably be employed onto any presently existent phylogenetic proposal. In fact, the preferred proposal employed here is based on Pêgas *et al.* (2021), which is ultimately derived from Kellner (2003)—we corroborate the sister-group relationship between Tapejaridae and Thalassodromidae.

Table 5. Systematic nomenclature.

Clade	Nominal author	Definition	Composition and remarks	ICPN conversion and Regnum code
Tapejaroidea	Kellner (2003)	The least inclusive clade containing *Tapejara wellnhoferi* Kellner, 1989, *Quetzalcoatlus northropi* Lawson 1975, and *Dsungaripterus weii* Young 1964.	Includes the sister-taxa Dsungaripteridae and Azhdarchoidea.	This work, [820].
Azhdarchoidea	Unwin (1995)	The least inclusive clade containing *Tapejara wellnhoferi* Kellner, 1989 and *Quetzalcoatlus northropi* Lawson 1975.	Includes the sister-taxa Tapejaromorpha and Azhdarchomorpha.	Andres (2021),[355].
Tapejaromorpha	Andres, Clark & Xu (2014)	The most inclusive clade containing *Tapejara wellnhoferi* Kellner, 1989 but not *Azhdarcho lancicollis* Nessov 1984.	Includes the sister-taxa Tapejaridae and Thalassodromidae.	Andres (2021), [356].
Thalassodromidae	Witton (2009)	The least inclusive clade containing *Thalassodromeus sethi* Kellner & Campos 2002 and *Tupuxuara longicristatus* Kellner & Campos 1988.	Includes *Thalassodromeus*, *Tupuxuara*, and *Kariridraco*.	Andres (2021), [770].
Tapejaridae	Kellner (1989)	The least inclusive clade containing *Tapejara wellnhoferi* Kellner, 1989, Sinopterus dongi Wang & Zhou, 2003, and *Caupedactylus ybaka* Kellner, 2013.	The first registered definition (Andres, 2021) is (unrestrictedly) emended here in order to stabilize the clade's diagnosis, usage, and content, under the context of the present reference phylogeny. Characterized mainly by downturned rostra and tall rostral crests, it contains Caupedactylia and Eutapejaria.	Andres (2021), [357], unrestrictedly Emended here.
Caupedactylia	This work.	The most inclusive clade containing *Caupedactylus ybaka* Kellner, 2013 but not *Tapejara wellnhoferi* Kellner, 1989.	Includes *Caupedactylus* and *Aymberedactylus*. This clade contains tapejarids which share a symphyseal shelf dorsoventrally steep and	This work, [821].

			deep, and a flat dentary fossa.	
Eutapejaria	This work	The most inclusive clade containing *Tapejara wellnhoferi* Kellner, 1989 but not *Caupedactylus ybaka* Kellner, 2013.	This clade contains tapejarids which share a dorsal dentary eminence, encompassing Tapejarinae and Sinopterinae (sensu Andres, 2021).	This work, [822].
Azhdarchomorpha	Pêgas *et al.* (2021)	The most inclusive clade containing *Azhdarcho lancicollis* Nessov 1984 but not *Thalassodromeus sethi* Kellner & Campos 2002 or *Tapejara wellnhoferi* Kellner, 1989.	Includes *Keresdrakon*, Chaoyangopteridae, Alanqidae, and Azhdarchidae.	Pêgas *et al.* (2021), [574].
Chaoyangopteridae	Lü *et al.* (2008)	The most inclusive clade containing *Chaoyangopterus zhangi* Wang & Zhou, 2003 but not *Quetzalcoatlus northropi* Lawson 1975.	Includes *Chaoyangopterus*, *Jidapterus*, *Shenzhoupterus*, and *Lacusovagus.*	Andres (2021), [368].
Azhdarchiformes	Andres (2021)	The most inclusive clade containing *Quetzalcoatlus northropi* Lawson 1975 but not *Chaoyangopterus zhangi* Wang & Zhou, 2003.	Under the present reference phylogeny, the Azhdarchiformes include Alanqidae and Azhdarchidae.	Andres (2021), [771].
Alanqidae	Pêgas *et al.* (2021)	The most inclusive clade containing *Alanqa saharica* Ibrahim *et al.* 2010 but not *Chaoyangopterus zhangi* Wang & Zhou, 2003 or *Azhdarcho lancicollis* Nessov 1984.	Includes *Alanqa*, *Argentinadraco*, *Xericeps*, *Leptostomia*, and *Montanazhdarcho*. Characterized by bowed-out lateral jaw margins in cross-section, and possibly by a pair of dentary occlusal ridges.	Pêgas *et al*. (2021), [576]
Azhdarchidae	Padian (1986)	The least inclusive clade containing *Azhdarcho lancicollis* Nessov 1984, *Phosphatodraco mauritanicus* Pereda-Suberbiola *et al.* 2003, and *Quetzalcoatlus northropi* Lawson 1975.	Includes *Eurazhdarcho*, *Aralazhdarcho*, *Phosphatodraco*, *Wellnhopterus*, *Zhejiangopterus*, *Azhdarcho*, and Quetzalcoatlinae. Characterized by a vestigial cervical neural spine.	Andres (2021), [371]. Emended by Pêgas *et al.* (2021).

DISCUSSION

Specimen-level variation survey

The generalized osteological pattern of *Sinopterus* complex specimens has already been described elsewhere (Zhang *et al.*, 2019; Shen et al., 2021; Zhou, Niu & Yu, 2022). This section is not intended as a monographical account of the morphology of each specimen, but as a report of their most striking features, with particular focus on the anatomical variations we surveyed. Monographical descriptions are beyond the scope of the present paper and will be provided elsewhere. Specimens PMOL-AP00030 (Liu *et al.*, 2015), SDUST-V1012 (Zhou, Niu & Yu, 2022) and SDUST-V1014 (Zhou *et al.*, 2022) are not included in the present reassessment due to their rather incomplete nature. The holotype of *Nemicolopterus crypticus*, which may be a hatchling tapejarid (Witton, 2013; Naish, Witton & Martin-Silverstone, 2021), is also not included due to its very immature nature and disputed identification, and is thus discussed separately further below in the Discussion section.

Despite the relative completeness of several specimens, observation of anatomical details is rather limited due to preservational issues. As all specimens are crushed, bones are usually visible from a single side, sometimes obscured by overlaying bones, and sometimes too damaged, thus highly limiting comparisons. Osteological details are given below as possible. However, in most circumstances, details do not go further than gross shape seen from a single view (as demonstrated in our plates) and measurements. All specimens were measured first-hand, and raw measurements are presented in Supplemental File 4 (Sheet 1). Specimens are presented below in chronological order of publication, from the oldest reported one to the most recently reported ones, and then finally with the ones reported here for the first time (D4019, BPMC 103, BPMC 104, BPMC 105, BPMC 106, and BPMC 107).

IVPP V 13363 (holotype of *Sinopterus dongi*)

This specimen (Fig. 28) was originally described by Wang & Zhou (2003a). It exhibits a relatively slender rostrum (~36% of jaw length), with a very low, incipien premaxillary crest and a low dentary crest. The rostrum is gently downturned at about 14° relative to the posterior occlusal line. The premaxillary crest is parabolical in outline. The nasoantorbital fenestra length/height ratio is not readily clear due to a slight anteroventral displacement of the orbitotemporal region. Still, it can be restored as somewhere between 2.8 and 3.2 (by restoring the position of the orbitotemporal region based on the inferred location of the quadratomandibular joint as indicated by the proportions of the mandible). The orbit has been described as subcircular (e.g., Andres, Clark & Xu, 2014), since its height and length are subequal. However, it may be described as subquadrangular due to the angular corners. This differs from the typical elongated piriform condition (higher than long, with a round dorsal margin and tapered ventral margin) of tapejarids and azhdarchoids in general (e.g., Kellner & Campos, 2007). Still, a tapered shape of the lower orbital margin is still present (in the

jugal). The lacrimal process of the jugal is subvertical (only slightly anterodorsally oriented). A pair of slender, anteroventrally directed, and medially placed descending nasal processes is present. The posterior cranial crest processes (the posterior process of the premaxillae, and the frontoparietal crests) curve upwards. The quadrate is posteriorly reclined at ~160°relative to the palatal plane. The observable cervical formula is III < IV > V > VI > VII. The scapula is about 1.30 the length of the coracoid. The coracoid exhibits a clear ventral flange. The humeral deltopectoral crest is tongue-like and its long axis is sub-perpendicular relative to the long axis of the humeral shaft. The pteroid accounts for 43% of ulnar length. Metacarpal I is elongate, reaching the carpal region, while metacarpals II and III are reduced and restricted distally. Metatarsal I is the longest of the metatarsals (Wang & Zhou, 2003a; Zhang *et al.*, 2019).

Remarks

This specimen is the holotype of *Sinopterus dongi*—the first genus and species of tapejarid to be described for the Jiufotang Fm. and Jehol Group as a whole. The validity of this genus and species has never been questioned.

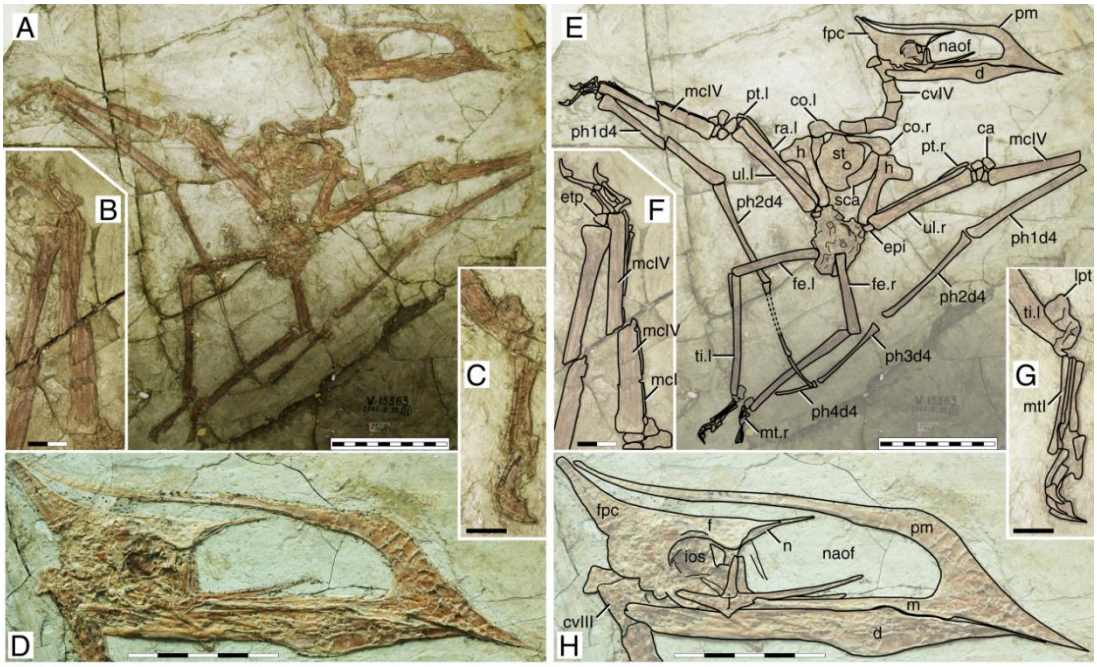

Figure 28. *Sinopterus dongi* holotype (IVPP V 13363). (A) Skeleton overview; (B) left metacarpus; (C) left foot; (D) skull (right lateral view). (E–H) Respective schematic drawings. Abbreviations: ca, carpus; co, coracoid; cv, cervical vertebra; d, dentary; d1–d4, digits 1–4; epi, epiphysis; etp, extensor tendon process; f, frontal; fe, femur; fpc, frontoparietal crest; h, humerus; ios, interorbital septum; l, left; lpt, lateral proximal tarsal; m, maxilla; mc, metacarpal; mt, metatarsal; n, nasal; naof, nasoantorbital fenestra; pm, premaxilla; ph, phalanx; pt, pteroid; ti, tibia; ul, ulna; r, right; rad, radius; sca, scapula; st, sternum. Scale bars: A, 50 mm; E, 50 mm; F, 20 mm; G, 10 mm; H, 20 mm.

BPV-077 (holotype of *Sinopterus gui*)

The specimen (Fig. 29) is unfortunately badly preserved, with quite damaged and crushed bone surfaces (Li, Lü & Zhang, 2003). Still, general outlines of some of the skull and appendicular bones can be discerned. The skull is exposed mostly in left lateral view, except for the posterior region which seems to be broken and exposed in a slightly dorsolateral view. The rostrum accounts for ~39% of total jaw length. It is very slender (RI = 0.33) and crestless, while the dentary symphysis bears a very shallow crest. The nasoantorbital fenestra is very elongate (length/height ratio ~3.2). Quadrate inclination is unclear due to the bad preservation of the posterior region of the skull. Details of the cervical series are unclear due to bad preservation. The coracoid ventral margin bears a flange, similar to other *Sinopterus* complex specimens (see below). The deltopectoral crest of the humerus is rectangular, proximally placed, and bears a long axis roughly perpendicular relative to the main humeral shaft. The relative length of metacarpals I – III cannot be assessed. Of the wing fingers, only a first phalanx is preserved, thus obscuring wing phalanges proportions. Unfortunately, not much further details can be assessed due to the very limited preservational quality of the specimen.

Remarks

This specimen is the holotype of *Sinopterus gui*—the second species of tapejarid to be described for the Jiufotang Fm. and Jehol Group as a whole (Li, Lü & Zhang, 2003). It was subsequently recognized as a very young juvenile (Kellner & Campos, 2007). The validity of this species has been questioned several times, in all such cases being regarded as a junior synonym of *S. dongi* even when multiple Jiufotang tapejarid species were accepted, on the basis that it could not be distinguished from *S. dongi* (Kellner & Campos, 2007; Kellner, 2010; Zhang *et al.*, 2019). This is problematic because recent publications have simply repeated the interpretation of *S. gui* being indistinguishable from *S. dongi* while not comparing *S. gui* to other more recently named species considered as valid, thus not justifying why it is indistinguishable from *S. dongi* only and not from any further species (e.g., Zhang *et al.*, 2019). First described by Li, Lü & Zhang (2003), these authors recognized it as distinct from *Sinopterus dongi* at a species-level, yet sufficiently similar to be placed in the same genus. Originally, Li, Lü & Zhang (2003) proposed the following diagnosis for the new species: “[e]leven dorsal vertebrae fused into notarium, and they are nearly equal in length. At least four sacral vertebrae, humerus longer than scapula, wing metacarpal slightly shorter than the first wing phalange, the distal end of the deltopectoral process not expanded, ratio of the femur to the tibia is approximately 0.49” (Li, Lü & Zhang, 2003: p. 445). Later, Kellner & Campos (2007) observed that this specimen does not present a notarium (which is an advanced ontogenetic feature). Instead, it represents a very young, juvenile specimen (Kellner & Campos, 2007; Kellner, 2010). Most authors have, since then, been unable to distinguish *S. gui* from *S. dongi*, and thus interpreted the holotype of *Sinopterus gui* as

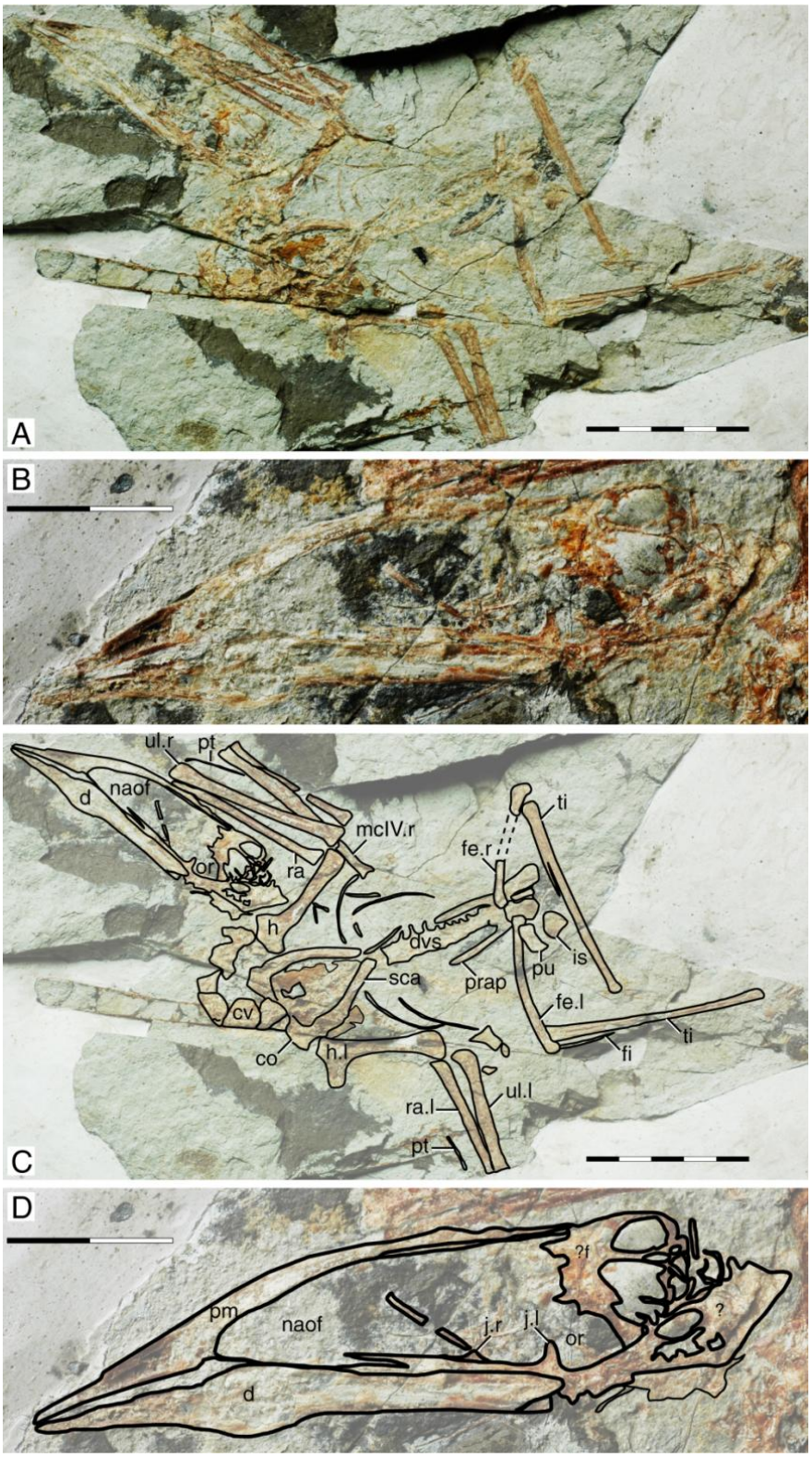

Figure 29. *Sinopterus gui holotype* (BPV-077). (A) Skeleton overview; (B) skull (left lateral view). (C and D) Respective schematic drawings. Abbreviations: co, coracoid; cv, cervical vertebra; d, dentary; dvs, dorsal vertebral series; f, frontal; fe, femur; fi, fibula; fpc, frontoparietal crest; h, humerus; is, ischium; j, jugal; l, left; mc, metacarpal; mt, metatarsal; n, nasal; naof, nasoantorbital fenestra; or, orbit; pt, pteroid; pu, pubis; prap, preacetabular process; ti, tibia; ul, ulna; r, right; rad, radius; sca, scapula. Scale bars: C, 50 mm; D, 50 mm.

a juvenile specimen of *Sinopterus dongi* (e.g., Kellner & Campos, 2007; Zhang *et al.*, 2019), although Kellner (2010) noticed that it could represent a juvenile of some other Jiufotang tapejarid instead, such as *Huaxiapterus corollatus* (therein referred to as *Sinopterus corollatus*). The interpretation of the holotype of *S. gui* as a juvenile of *S. dongi* (and not any other Jiufotang tapejarid species) has been maintained by Zhang *et al.* (2019) without further justifications, even though these authors accept the validity of several other *Sinopterus* species (*S. lingyuanensis, S. corollatus, S. benxiensis,* and *S. atavismus*). We maintain here that *S. gui* is indeed indistinguishable from *S. dongi* except for the complete absence of a premaxillary crest in the former, which is easily attributed to ontogeny (Witton, 2013; Zhang *et al.*, 2019).

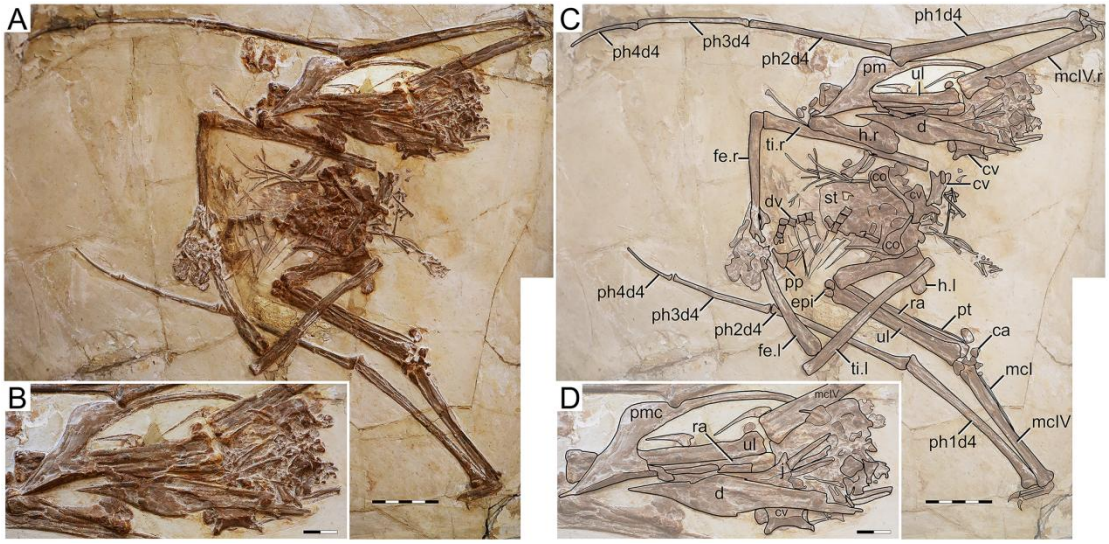

Figure 30. *Huaxiapterus jii holotype* (GMN-03-11-001). (A) Skeleton overview; (B) skull (left lateral view, slightly ventrolateral). (C and D) Respective schematic drawings. Abbreviations: ca, carpus; co, coracoid; cv, cervical vertebra; d, dentary; d1–d4, digits 1–4; dv, dorsal vertebra; epi, epiphysis; fe, femur; h, humerus; j, jugal; l, left; mc, metacarpal; pm, premaxilla; ph, phalanx; pp, prepubis; pt, pteroid; ti, tibia; ul, ulna; r, right; rad, radius; sca, scapula; st, sternum. Scale bars: C, 50 mm; D, 20 mm.

GMN-03-11-001 (holotype of *Huaxiapterus jii*)

This almost complete specimen includes a partial skull, although the posterior region is disarticulated and damaged (Fig. 30). The rostrum is ventrally deflected at 14° relative to the posterior palatal plane. The rostrum exhibits a premaxillary crest. It is similar in shape to that of *S. dongi* (parabolical in outline), despite being larger. It is distinct from the premaxillary crest condition of other proposed species, such as the pointed premaxillary crests of *Huaxiapterus atavismus* (both specimens, the holotype XHPM 1009 and the referred specimen IVPP V 22338) or the trapezoidal crests of *Huaxiapterus corollatus* and *Huaxiapterus benxiensis*, or the crestless conditions seen in *Sinopterus gui* and *Sinopterus lingyuanensis*. Most of the posterior region of the skull is badly damaged, except for the left jugal which is partially preserved. The

jugal is triradiate, unlike the tetraradiate condition seen in *Tapejara wellnhoferi* (Wellnhofer & Kellner, 1991), *Caiuajara dobruskii* (Manzig *et al.*, 2014) and *Tupandactylus navigans* (Beccari *et al.*, 2021). The lacrimal and postorbital processes of the jugal describe a roughly perpendicular angle. The proportions of the nasoantorbital fenestra cannot be readily measured due to the damaged nature of the posterior region of the skull, but an estimate can still be given based on the location of the lacrimal process of the jugal (about three times as long as high). As with the premaxillary crest, the dentary crest is also larger than in *S. dongi.* Only two disarticulated cervical vertebrae can be seen, so that the cervical formula cannot be assessed. Pteroid length is equivalent to about 44% of the ulna length. Metacarpal I is elongate, extending for at least 90% the length of metacarpal IV. Wing proportions are closest to the holotype of *S. dongi* (Fig. 30; Supplemental File 4, Sheets 1, 3). Pedal elements are entirely disarticulated, so that the metatarsal formula cannot be assessed.

Remarks

This specimen was originally described as representing a new genus and species, *Huaxiapterus jii* (Lü & Yuan, 2005). Subsequent publications have considered it either as a species of *Sinopterus*, as *S. jii* (Kellner & Campos, 2007; Pinheiro *et al.*, 2011; Kellner, 2013), or as a junior synonym of *Sinopterus dongi* (Wang & Zhou, 2006; Witton, 2013; Zhang *et al.*, 2019), thus invalidating the genus *Huaxiapterus*. Still, other researchers still considered *H. jii* as valid and as a distinct taxon, with the genus *Huaxiapterus* being valid (Andres, Clark & Xu, 2014; Lü *et al.*, 2016).

This taxon was originally diagnosed based on cranial crest development: premaxillary and dentary crests deeper than in *Sinopterus dongi* and shallower than in *Tapejara wellnhoferi* (see Lü & Yuan, 2005), though without precise quantitative comparisons. Later, this species has been regarded as a junior synonym of *Sinopterus dongi*: Wang & Zhou (2006) were unable to find differences between the holotypes of the two species, and thus synonymized them. At the time, these two species (together with *Sinopterus gui*) were the only named species within the *Sinopterus* complex. We maintain that the holotypes of *S. gui* and *S. jii* are indistinguishable from *S. dongi*, and further add that *S. jii* shares with *S. dongi* the following features: metacarpal I articulating with the carpus, and wing phalanx 4/phalanx 1 length ratio about ~0.30, which distinguish these proposed taxa from other proposed taxa such as *H. corollatus* and *H. benxiensis* (see below). Sadly, these features are uncertain in the holotype of *S. gui.*

ZMNH M813 (holotype of *Huaxiapterus corollatus*)

This specimen is almost complete, although some skeletal regions are badly damaged and anatomical details are obliterated, particularly the posterior region of the skull, post-cervical vertebrae, and the pedes (Fig. 31). The skull exhibits a trapezoidal premaxillary crest and a shallow dentary crest. The rostrum is relatively robust, akin to that of the holotype of *Huaxiapterus ji*i and unlike the holotypes of *S. dongi* or

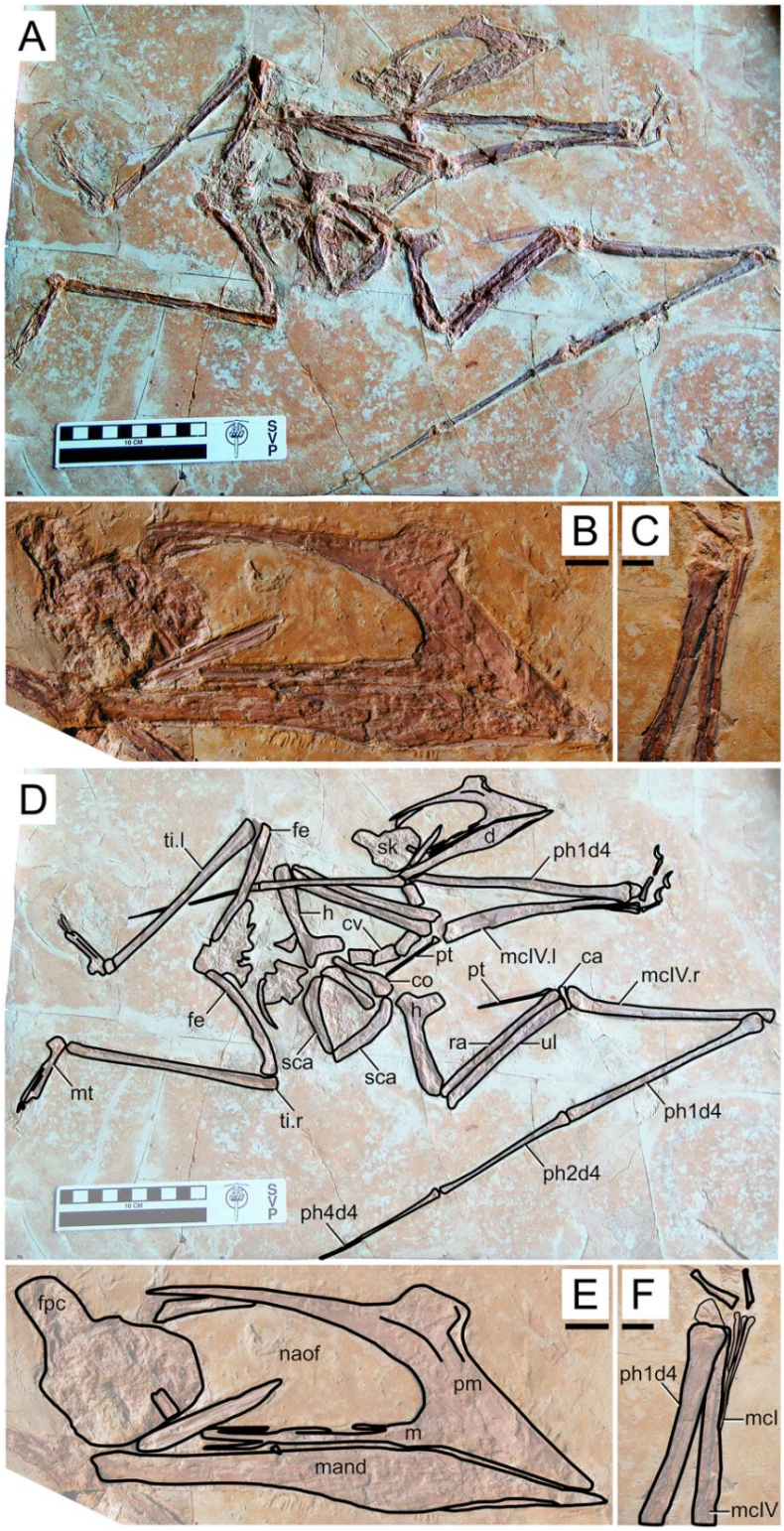

Figure 31. *Huaxiapterus corollatus* holotype (ZMNH M813). (A) Skeleton overview; (B) skull (right lateral view); (C) left metacarpus. (D–F) Respective schematic drawings. Abbreviations: ca, carpus; co, coracoid; cv, cervical vertebra; d, dentary; d1 – d4, digits 1 – 4; fe, femur; fpc, frontoparietal crest; h, humerus; l, left; m, maxilla; mand, mandible; mc, metacarpal; mt, metatarsal; n, nasal; naof, nasoantorbital fenestra; pm, premaxilla; ph, phalanx; pt, pteroid; ti, tibia; ul, ulna; r, right; rad, radius; sca, scapula; sk, skull. Scale bars: A, D, 100 mm; E, F, 10 mm.

S. gui. The rostrum is ventrally deflected by 21° (contra 14° in the holotypes of *S. dongi* and *H. jii*). The nasoantorbital fenestra is relatively short, with an estimated length/height ratio of about 2.2 (based on its length as inferred from the location of the quadratomandibular joint, as indicated by the preserved mandible, as it roughly correlated to the posterior margin of the nasoantorbital fenestra in sinopterines and tapejarids overall; e.g., Kellner & Campos, 2007; Kellner, 2013; Lü *et al.*, 2016). A clear occlusal gap is present between the dentary and the rostrum (as originally indicated, see Lü *et al.*, 2006a), unlike what has been represented in some reconstructions (e.g., Witton, 2013). The cervical series is partially obscured by the radius and ulna, which lay over cervicals IV–V, hindering assessment of their relative lengths. Metacarpals I–III are reduced, and it can be seen that metacarpals I and II do not contact the carpus, reaching only about a third of the length of metacarpal IV. Wing proportions deviate from previously reported specimens in that the fourth wing phalanx is relatively shorter, accounting for only ~20% of the first phalanx (contra ~30% in the holotypes of *S. dongi* and *S. jii*).

Remarks

This specimen was designated as the holotype of *Huaxiapterus corollatus* by Lü *et al.* (2006a). The species-level validity of this species (irrespective of its generic status) has been mostly accepted (Pêgas, Leal & Kellner, 2016; Lü *et al.*, 2016; Zhang *et al.*, 2019; Andres, 2021), except for Witton (2013) who preliminarily proposed that all Jiufotang tapejarids were synonymous with *S. dongi*. It is interesting to note that, although Naish, Witton & Martin-Silverstone (2021) preliminarily corroborated Witton (2013) view, they highlighted that at least the holotype of *H. corollatus* could potentially represent a new taxon (based on its limb proportions), pending further study.

The taxon *Huaxiapterus corollatus* was originally diagnosed on the basis of cranial crest features, namely crest shape (“hatchet-shaped”), position (level with the anterior margin of the nasoantorbital fenestra), and orientation (“short axis perpendicular to the anterodorsal margin of the nasoantorbital fenestra”; see Lü *et al.*, 2006b). Martin-Silverstone (2021), cranial crest features used alone make for dangerous taxonomic decisions, as they could rather reflect ontogenetic or sexual variations. Still, the holotype of *H. corollatus* also differs from the holotypes of *S. dongi* and *S. jii* in exhibiting a reduced metacarpal I, and in wing proportions (Supplemental File 4, Sheet 1). *H. corollatus* exhibits a reduced wing phalanx 4, which accounts for ~20% of the length of the first wing phalanx, contra ~30% in the previously named *S. dongi* and *H. jii*. Naish, Witton & Martin-Silverstone (2021) noticed that the holotype of *H. corollatus* was an apparent outlier within the *Sinopterus* complex regarding limb proportions, leading them to propose that it could be a potentially valid taxon pending further study.

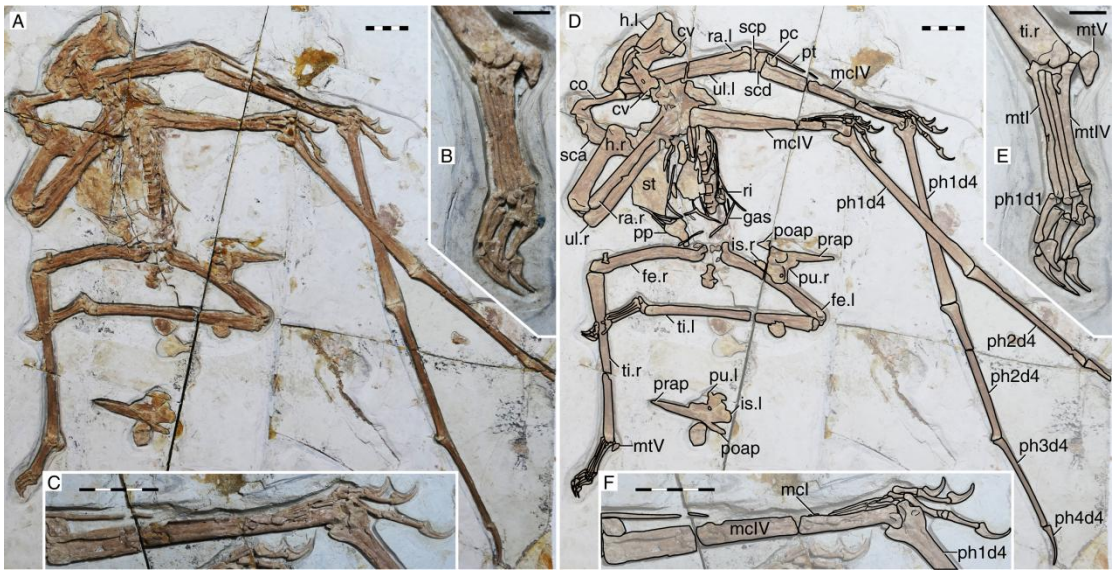

Figure 32. Specimen D2525. (A) Skeleton overview; (B) right foot; (C) right metacarpus. (D–F) Respective schematic drawings. Abbreviations: co, coracoid; cv, cervical vertebra; d, dentary; d1–d4, digits 1–4; dsc, distal synpcarpal; etp, extensor tendon process; f, frontal; fe, femur; fpc, frontoparietal crest; gas, gastralia; h, humerus; ios, interorbital septum; is, ischium; l, left; lpt, lateral proximal tarsal; mc, metacarpal; mt, metatarsal; pc, preaxial carpal; ph, phalanx; poap, postacetabular process; pp, prepubis; prap, preacetabular process; psc, proximal syncarpal; pt, pteroid; pu, pubis; ti, tibia; ul, ulna; r, right; rad, radius; ri, rib; sca, scapula; st, sternum. Scale bars: D, 50 mm; E, 10 mm; F, 50 mm.

D2525

D2525 is an almost complete postcranial skeleton, lacking the skull, part of the anterior cervical series, part of the posterior dorsal series, and the sacral and caudal series (Fig. 32). The preserved cervical vertebrae, as well as shoulder girdle and right humerus, are badly damaged. Although previously unreported, the ?fourth cervical (exposed in ventral view, retaining some tridimensionality) clearly exhibits a pneumatic foramen piercing its lateral surface. The sternum is approximately square, with the posterior margin convex. The left coracoid bears a well-developed ventral flange. The left humerus is exposed in dorsal view, and no dorsal proximal pneumatic foramen can be seen in this specimen, as in IVPP V 23388 (Zhang *et al.*, 2019). The ulnar crest is rounded. The humeral shaft is mostly straight, except for the distal portion which is slightly anteriorly recurved. Metacarpals I – III are tightly appressed to metacarpal IV on the distal metacarpal region on both sides. Metacarpal I extends for only about 40% of the length of metacarpal IV (Fig. 32). Wing proportions are very similar to the holotypes of *H. corollatus* and *H. benxiensis*, with the fourth wing phalanx corresponding to ~20% the length of the first wing phalanx (contra ~30% in *S. dongi* and *S. jii*). Wing phalanges are exposed in ventral view, and a longitudinal ridge can be seen in phalanges 2 and 3, similarly to *H. atavismus* (Lü *et al.*, 2016) and IVPP V 23388 (Zhang *et al.*, 2019). In the pedes, metatarsal I is distinctively shorter than metatarsal II, which is the longest.

Remarks

This specimen was originally described as a new specimen of *Sinopterus dongi*, based on the assertion that the limb proportions of D2525 were most similar to *S. dongi* than to *S. gui*, *H. jii* or *H. corollatus*, which were the four existing nominal species at the time (Lü *et al.*, 2006b). Such referral has never been contested in the literature. Contrary to previous reports (Lü *et al.*, 2006b), the limb proportions of D2525 are most similar to the holotype of *H. corollatus*, and not *S. dongi* (see Supplemental File 4, Sheets 1, 3). In fact, D2525 is herein considered as indistinguishable from H. corollatus, with which it shares a shortened metacarpal I (about 40% the length of metacarpal IV, contra >90% in *S. dongi* and *S. jii*) and a shortened fourth wing phalanx (~20% of first phalanx length, contra ~30% in *S. dongi* and *S. jii*). It differs from the holotypes of *S. dongi* and *H. jii* in wing proportions and in metatarsals I–II relative length (metatarsal II is the longest one in D2525, instead of metatarsal I as in *S. dongi*).

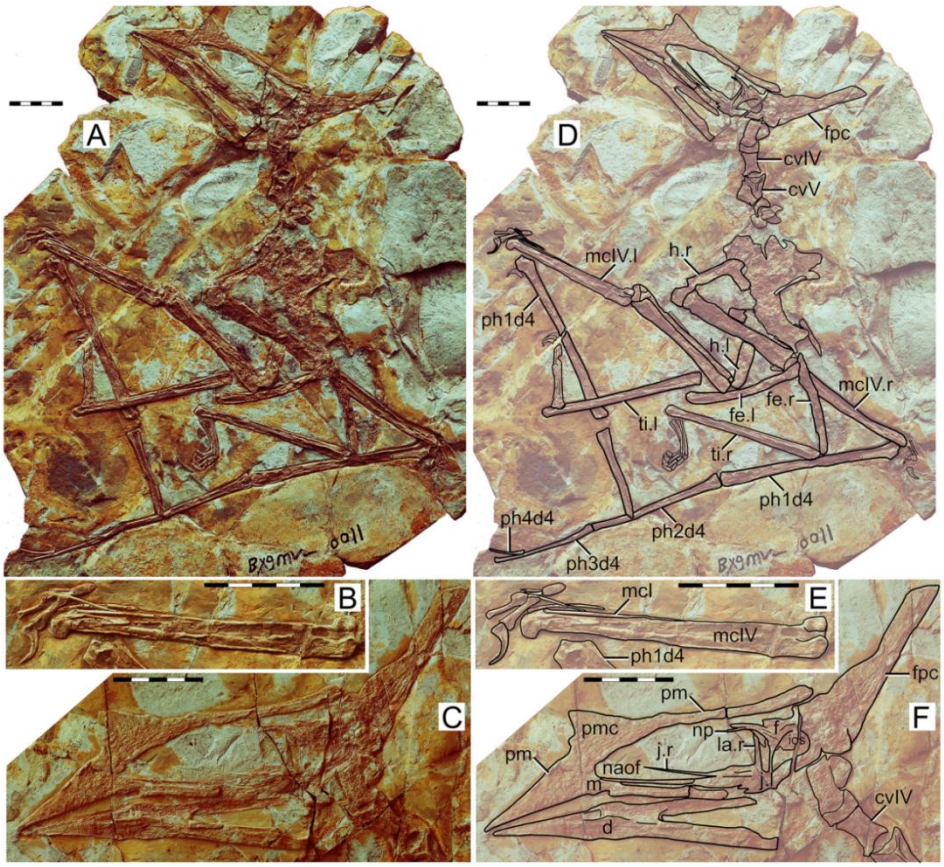

Figure 33. *Huaxiapterus benxiensis* holotype (BXGM V0011). (A) Skeleton overview; (B) left metacarpus; (C) skull (left lateral view). (D–F) Respective schematic drawings. Abbreviations: cv, cervical vertebra; d, dentary; d1–d4, digits 1–4; f, frontal; fe, femur; fpc, frontoparietal crest; h, humerus; ios, interorbital septum; j, jugal; l, left; m, maxilla; la, lacrimal; mc, metacarpal; mt, metatarsal; naof, nasoantorbital fenestra; np, nasal process; pm, premaxilla; ph, phalanx; pt, pteroid; ti, tibia; ul, ulna; r, right; rad, radius. Scale bars: 50 mm.

BXGM V0011 (holotype of *Huaxiapterus benxiensis*)

This specimen consists on a virtually complete specimen (Fig. 33). However, some anatomical regions are damaged and/or partially obscured, mainly the torso region (with the post-cervical vertebral series, sternum, ribs, and scapulocoracoid). The rostrum is built similarly to the holotype of *H. corollatus*, with a downward deflection of 20° . The premaxillary crest is slightly larger than in the holotype of *H. corollatus*, but it is similar in being distinctively anterodorsally protrusive with abrupt limits, unlike the smoothly-transitioning borders of the parabolical crests of the holotypes of *S. dongi* and *S. jii*. Despite broken, the premaxillary crests seems to have been trapezoidal in shape, as in the holotype of *H. corollatus*. The posterior process of the premaxillae is steeply dorsally recurved. An elongate posterior spine (posterior process of the premaxillae + frontoparietal crest) is present, much larger than in the holotype of *S. dongi*. The nasoantorbital fenestra is approximately as elongate as in *S. dongi*, with a length/ height ratio of about 2.4. The long axis of the nasal process is very deflected anteriorly, unlike the almost verticalized nasal process seen in the holotype of *S. dongi*. The shape of the jugal (as seen from the lacrimal and postorbital processes) demonstrates that the orbit was piriform, with a tapered ventral margin, and quite higher than wide, unlike the subquadrangular orbit of *S. dongi*. The quadrate is posteriorly inclined at about 153°. Not much further detail can be seen due to extensive superficial damage. The observable cervical formula is III < IV < V > VI. Both humeri are badly damaged, with only a section being exposed. The original description reported on an oddly short humerus only 55% the length of the femur (Lü *et al.*, 2007), but this seems to have been based on the fairly incomplete right humerus. We reidentify here the damaged proximal and distal limits of the left humerus, which indicate it was comparable to that of other Jiufotang tapejarids (about 80% of femur length) instead of oddly short (Figs. 33A and 33D). The extension of the pteroid is unclear. Metacarpal I confidently extends for only ~40% the length of metacarpal IV. The proximal extension of metacarpals II and III is unfortunately obscure, since it is unclear if the proximal tips are broken or not. Wing proportions closely match *H. corollatus*, with relatively short fourth wing phalanges (20% the length of the first phalanx). The relative length of metatarsals I – III overall cannot be assessed due to poor preservation.

Remarks

The species *H. benxiensis* was erected on the basis of BXGM V0011 and attributed to the genus *Huaxiapterus*, following *H. jii* and *H. corollatus*. The validity of this species has been mostly accepted without further comments (Pinheiro *et al.*, 2011; Kellner, 2013; Pêgas, Leal & Kellner, 2016; Zhang *et al.*, 2019; Andres, 2021), except for works that argued for the "restrictive taxonomic scheme" of the *Sinopterus* complex, which regarded it as most likely a junior synonym of *S. dongi* along with all other nominal species of Jiufotang tapejarids (Witton, 2013; Naish, Witton & Martin-Silverstone, 2021).

Huaxiapterus benxiensis has been regarded as distinct from *H. corollatus* on the basis of an "elongate parietal spine", "well-developed premaxillary crest", and a shallow groove on the occlusal surface of the dentary symphysis (Lü *et al.*, 2007). Witton (2013) noticed that crest-related features could be influenced by ontogeny rather than interspecific variation. We further note that the "shallow groove" on the anterior end of the symphysis corresponds to the anterior occlusal depression (ubiquitous to tapejarids), interrupted posteriorly by a transverse ridge (similar to the condition seen in *Bakonydraco galaczi*; see Ősi, Weishampel & Jianu, 2005). This condition can also not set *H. benxiensis* apart from any other proposed Jehol tapejarid species, since preservation precludes the verification of this feature in other type specimens. *H. benxiensis* is here considered as indistinguishable from *H. corollatus*, with which it shares a rostrum deflection of ~20 °, a reduced metacarpal I, and a reduced fourth wing phalanx (~20% of first wing phalanx length). Both *H. benxiensis* and *H. corollatus* further differ from *S. dongi* and *S. gui* in exhibiting a relatively shorter nasoantorbital fenestra (only 2.2–2.4 in height/length ration, contra ~3 in *S. dongi* and *S. gui*).

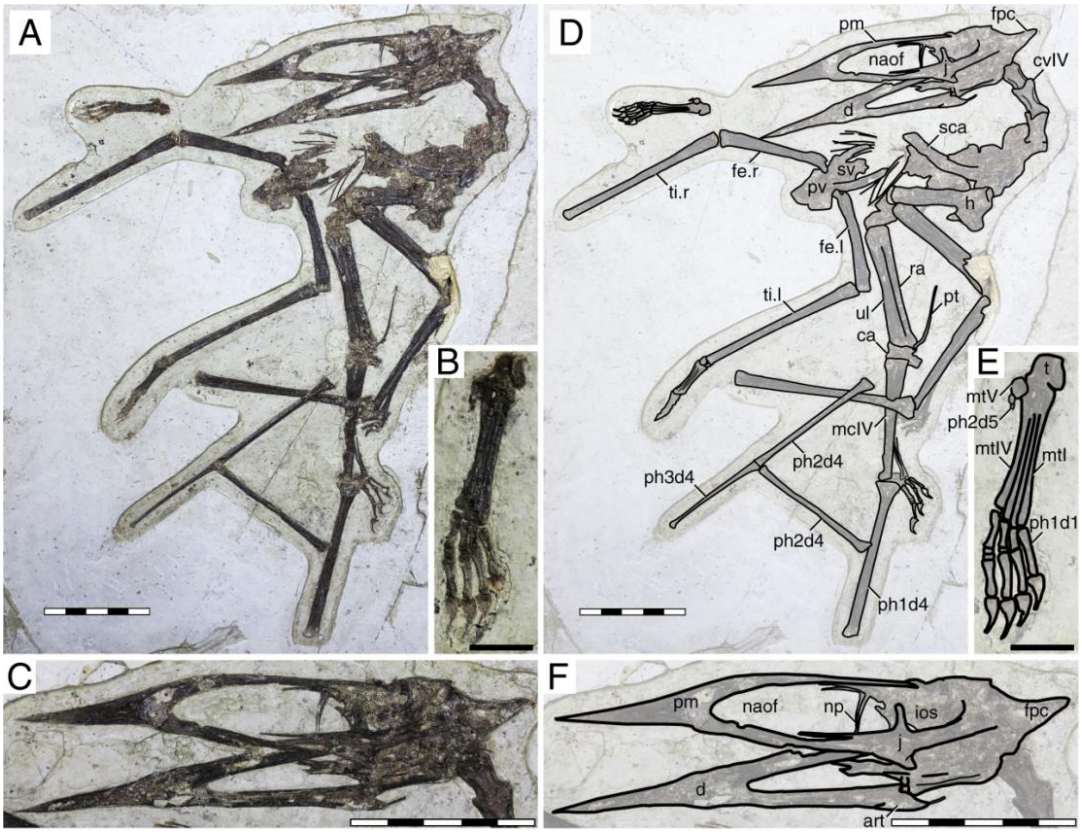

Figure 34. *Sinopterus lingyuanensis* holotype (JPM-2014-005). (A) Skeleton overview; (B) right foot; (C) skull (left lateral view). (D–F) Respective schematic drawings. Abbreviations: art, articular; ca, carpus; cv, cervical vertebra; d, dentary; d1–d4, digits 1–4; fe, femur; fpc, frontoparietal crest; h, humerus; ios, interorbital septum; j, jugal; l, left; lpt, lateral proximal tarsal; mc, metacarpal; mt, metatarsal; naof, nasoantorbital fenestra; np, nasal process; pm, premaxilla; ph, phalanx; pt, pteroid; pv, pelvis; t, tarsus; ti, tibia; ul, ulna; r, right; rad, radius; sca, scapula; sv, sacral vertebrae. Scale bars: D, 50 mm; E, 10 mm; F, 50 mm.

JPM-2014-005 (holotype of *Sinopterus lingyuanensis*)

The holotype of *S. lingyuanensis* exhibits a relatively fine preservation, comprising an almost complete skeleton lacking only some distal wing phalanges and the tail. Some anterior trunk and appendicular elements, such as posterior cervical vertebrae, some dorsal vertebrae, ribs, sternum, and pectoral girdle, are severely crushed against each other and cannot be discerned (Fig. 34). Other than that, most other skeletal elements are discernible, with decent surface preservation despite crushing. The skull is exposed mainly in left lateral view, and the occipital region is laterally displaced towards the left, thus being visible in a somewhat posterolateral view. The rostrum is entirely crestless and slender, accounting for 44% of total jaw length. The rostrum is gently deflected at 12°relative to the palatal plane. Beneath the anterior level of the nasoantorbital fenestra, a bulge is present on the jaw margin, indicating the presence of a slight lateral palatal expansion similar to what is seen in *Tapejara* and *Caiuajara* (Wellnhofer & Kellner, 1991; Manzig *et al.*, 2014). The nasoantorbital fenestra is quite elongate, being 3.25 times longer than high. The nasals exhibit a pair of descending nasal processes, which are subvertical and elongate, similar to *S. dongi* and unlike the anteriorly directed, short condition seen in *H. benxiensis*. The orbit is roughly subquadrangular, about as wide as high, similarly to *S. dongi*. The divergence angle between the lacrimal and postorbital processes of the jugal is about ~90°, similar to *S. dongi* and *H. jii* but unlike *H. benxiensis* (~68°), which exhibits a piriform orbit. The quadrate is reclined at about 160°. A small, short frontoparietal crest is present, extending beyond the occiput. The mandible is exposed in dorsal view. Sadly, the occlusal surface is not well-preserved. Still, it can be seen that a slight lateral expansion occurs at the posterior region of the symphysis, as in *Tapejara* and *Caiuajara* (Wellnhofer & Kellner, 1991; Manzig *et al.*, 2014), matching the slight lateral palatal expansion beneath the anterior margin of the nasoantorbital fenestra. The dentary symphysis and the retroarticular process account for, respectively, 53% and 4% of total mandibular length. Atlas and axis cannot be observed. The observable cervical formula is III < IV > V > VI, similar to S. dongi and unlike H. benxiensis in which the fifth cervical is the longest. The mid-cervicals clearly exhibit at least one pneumatic foramen piercing their lateral sides. The pteroid accounts for 47% of ulnar length. Sadly, the distal extensions of metacarpals I – III are obscured by metacarpal IV. The relative length of the fourth wing phalanx is also unknown. In the pedes, the metatarsal formula is I < II > III > IV, similar to D2525 but unlike *S. dongi*.

Remarks

This specimen was originally designated as the holotype of a new species, *S. lingyuanensis*, by Lü *et al.* (2016). This was subsequent to Witton (2013) proposition that all Jiufotang tapejarids formed an ontogenetic continuum of *S. dongi*, which was not accepted by Lü *et al.* (2016). Later, Zhang *et al.* (2019) expressed their approval over the validity of *S. lingyuanensis*, without further comments. Later, Naish, Witton & Martin-Silverstone (2021) echoed the proposition of Witton (2013) that all

proposed Jiufotang tapejarids most likely represented a single species (to the potential exclusion of *H. corollatus*), including *S. lingyuanensis*.

The species *Sinopterus lingyuanensis* was proposed based on the following features: nasoantorbital fenestra length/height ratio 3.2, rostral index 3.03, femur/tibia length ratio 0.66, and wing phalanx 2/wing phalanx 1 length ratio 0.85 (Lü *et al.*, 2016). However, all of these values fit well within the spectrum seen in the *Sinopterus* complex (Supplemental File 4, Sheet 1) and cannot set *S. lingyuanensis* apart from other species, particularly from *S. dongi*, *S. gui* and *H. jii* which also exhibit nasoantorbital fenestra about three times as long as high (distinct in this regard from the holotypes of H. corollatus and H. benxiensis). Still, *S. lingyuanensis* does differ from *S. dongi* in metatarsal configuration (I ≈ II, rather than I > II), and also differs from *H. benxiensis* in orbit shape (subcircular rather than piriform), nasal descending process configuration (subvertical and elongate, rather than anteriorly directed and short), and cervical formula (IV > V, rather than IV < V). It also differs from both *H. corollatus* and *H. benxiensis* in exhibiting a gentler rostrum deflection (12° rather than 20°). The significance of these variations will be discussed further below, in the Discussion section.

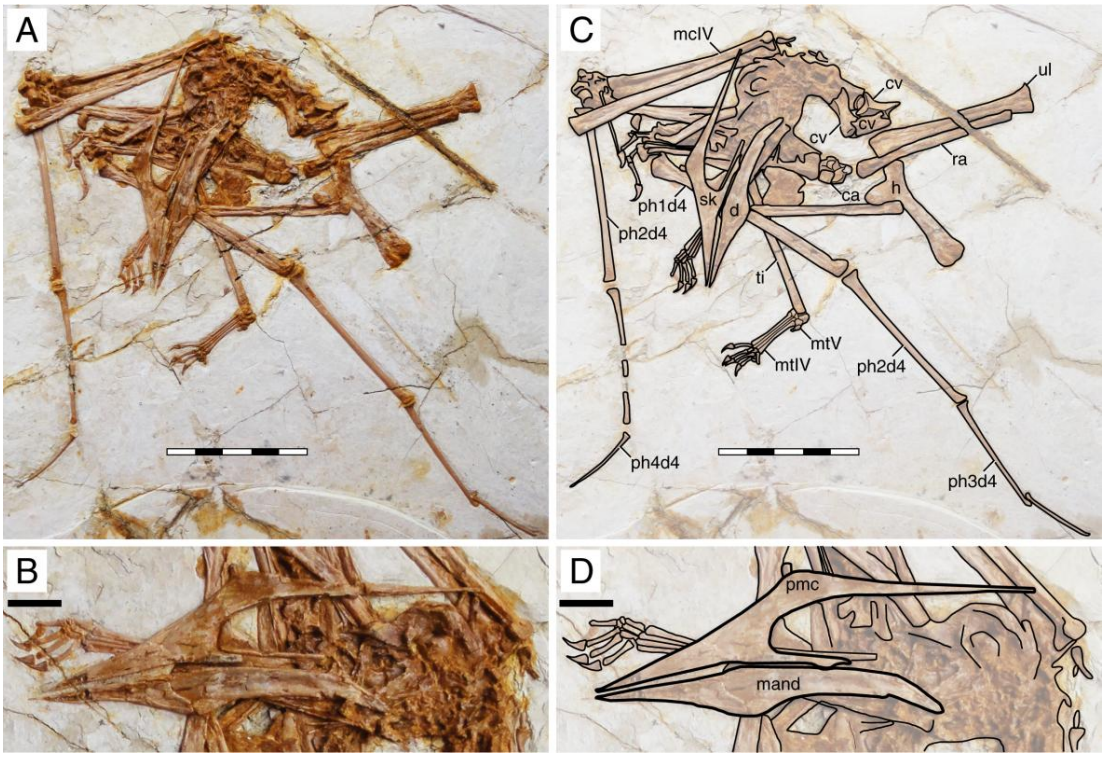

Figure 35. *Huaxiapterus atavismus* holotype (XHPM 1009). (A) Skeleton overview; (B) skull (left lateral view). (C and D) Respective schematic drawings. Abbreviations: ca, carpus; cv, cervical vertebra; co, coracoid; d, dentary; d1–d4, digits 1–4; fe, femur; fpc, h, humerus; mand, mandible; mc, metacarpal; mt, metatarsal; pmc, premaxillary crest; ph, phalanx; ti, tibia; ul, ulna; r, right; rad, radius; sk, skull. Scale bars: 50 mm.

XHPM 1009 (holotype of *Huaxiapterus atavismus*)

Despite virtually complete, many skeletal remains of this specimen are quite jumbled together, preventing the observation of much anatomical data (Fig. 35). The rostrum exhibits a very small, triangular-shaped premaxillary crest, whose apex is anterodorsally oriented and located posterior to the anterior margin of the nasoantorbital fenestra (this configuration is distinct from any other tapejarid specimen previously published, but similar to specimens IVPP V 23388 and D4019). The rostrum is slender, ventrally deflected by 14 °, and with a deflection point anteriorly located, similarly to *S. lingyuanensis*. A small, yet clearly perceivable, occlusal gap is present. The dentary bears a slight dorsal eminence, as well as a low dentary crest. The observable cervical formula is III < IV > V ≅ VI > VII > VIII. Not much can be discerned from the remaining of the axial skeleton, and the same is true for the pectoral girdle. The pteroid accounts for 40% of ulnar length. Unfortunately, the relative lengths of the metacarpals cannot be assessed. Wing phalanx proportions are a close match for *S. dongi* and *S. jii* (Supplemental File 4, Sheet 1), and distinct from *H. corollatus*, *H. benxiensis* and D2525 which exhibit a comparatively reduced fourth wing phalanx about 20% the length of the first wing phalanx (Supplemental File 4, Sheet 1). Metatarsal I is shorter than metatarsal II, which is the longest, unlike *S. dongi*.

Remarks

This specimen was originally designated as the holotype of a new species, *H. atavismus*, by Lü *et al.* (2016). This was subsequent to Witton (2013) proposition that all Jiufotang tapejarids formed an ontogenetic continuum of *S. dongi*. Still, Zhang *et al.* (2019) accepted the validity of this species, which they assigned to the genus *Sinopterus*, as *Sinopterus atavismus*. Later, Naish, Witton & Martin-Silverstone (2021) echoed the proposition of Witton (2013) in interpreting all Jiufotang tapejarids as probable synonyms, to the inclusion of *S. atavismus*.

The species *H. atavismus* was originally diagnosed based on the presence of a squared premaxillary crest and of a ventral groove on the second wing phalanx. As noticed by Zhang *et al*. (2019), the crest is actually not squared (Fig. 35), and cranial crest morphology should be viewed with caution when discussing pterosaur diagnoses; while the ventral groove on the second wing phalanx is probably common within tapejarids (see Kellner, 2004; Zhang *et al.*, 2019), although admittedly hard to ascertain in other *Sinopterus* complex specimens due to heavy crushing. *H. atavismus* shares with *S. dongi* and *S. lingyuanensis* a fourth cervical vertebra longer than the fifth, distinct from *H. benxiensis* and other tapejarids. *H. atavismus* differs from the holotype of *S. dongi* in pedal morphology, showing the typical condition (metatarsal II the longest), and not the unique condition seen in *S. dongi* (metatarsal I the longest). *H. atavismus* differs from *H. corollatus* and *H. benxiensis* in exhibiting a gentler rostrum deflection and a more elongate fourth wing phalanx (Supplemental File 4, Sheet 1), and from D2525 in the latter aspect as well.

IVPP V 23388

This specimen has been described and figured in detail by Zhang *et al.* (2019). The rostrum is elongate and slender, with a gentle ventral deflection of 14 °. The rostrum deflection point lies anterior to the anterior margin of the nasoantorbital fenestra, as in *S. lingyuanensis* and *H. atavismus*. The premaxilla produces a small, subtriangular crest, as noted by Zhang *et al.* (2019), similar to that seen in the holotype of *H. atavismus*. Despite the incomplete, disarticulated nature of the skull remains, the nasoantorbital fenestra is notoriously elongate, and was confidently over three times as elongate as high (Zhang *et al.*, 2019). The jugal is triradiate, and the angle formed between the lacrimal and postorbital processes is very wide (~90 °, similar to *S. dongi* and *S. lingyuanensi*s), indicating the orbit was probably subquadrangular in shape, and not ventrally tapered (piriform) as in *H. benxiensis*. The postoccipital extension of the premaxillae is elongate and curved posterodorsally. The observable cervical formula is IV > V ≅ VI > VII > VIII > IX (contra Zhang *et al.*, 2019). The coracoid exhibits a deep ventral flange proximally. Metacarpals II and III are reduced, while the preserved metacarpal I extends for about 85% the length of metacarpal IV. The proximalmost tip of metacarpal I is missing due to a crack in the slab. Sadly, pteroid and wing phalanges 4 are missing. Metatarsal I is shorter than metatarsal II, which is the longest.

Remarks

This specimen has been attributed to *Sinopterus atavismus* (=*Huaxiapterus atavismus*) by Zhang *et al.* (2019). No alternative attributions have been given by any other workers, except for Naish, Witton & Martin-Silverstone (2021) who preliminarily considered that all Jiufotang tapejarids were most likely conspecific with *S. dongi* (to the potential exception of *H. corollatus* only).

This fairly complete specimen was described recently by Zhang *et al.* (2019), who were unable to distinguish it from *Huaxiapterus atavismus* and thus referred the new specimen to this species (using the combination *Sinopterus atavismus*). Zhang *et al.* (2019) considered that three features allowed IVPP V 23388 to be identified as *H. atavismus*: the shape of the premaxillary crest, the shape of the anterodorsal margin of the premaxilla, and the proportions between metatarsals I and II (Zhang *et al.*, 2019). However, the first two features are influenced by the development of the premaxillary crest, which, as discussed above, is prone to sexual and ontogenetic variation, and should be viewed with caution before being utilized in diagnoses, as will be discussed further below in this work.

Furthermore, proportions between metatarsals I and II in IVPP V 23388 (metatarsals I/II = ~0.90) and the holotype of *H. atavismus* are rather close to those of other specimens such as *S. lingyuanensis* (Supplemental File 4, Sheets 1, 3), and thus this condition should be seen with caution. These three specimens also match well in the configuration of the nasoantorbital fenestra (over three times as long and high)

and rostrum deflection angle (12 ° –14 °), also matching *S. dongi* and *H. jii* in these regards, being all distinct from *H. corollatus* and *H. benxiensis* (with nasoantorbital fenestrae about 2.3 times as long as high, and rostrum deflections of 20 °–21 °). We regard that IVPP V 23388, along with the holotype of *H. atavismus*, are both indistinguishable from *S. lingyuanensis*. They are all also undistinguishable from *S. dongi* except for the metatarsi proportions.

D3072

This specimen has been recently described and figured in detail by Shen *et al.* (2021). It consists of a partial postcranial skeleton, comprising most of the cervical and dorsal series, the forelimbs, and partial hindlimbs. The observable cervical formula is III < IV > V > VI > VII > VIII > IX. Single pneumatic foramina can be seen piercing the lateral sides of some cervical vertebrae (at least III, IV and V; unclear in others). Metacarpal I is elongate, with a preserved portion accounting for about 90% of metacarpal IV length; the proximal tip is missing and it may have been longer. The first wing phalanx exhibits two pneumatic foramina piercing the ventral side of the proximal region, similar to Keresdrakon vilsoni (see Kellner *et al.*, 2019). The fourth phalanx is relatively large, accounting for 36% the length of the first wing phalanx, approaching more closely the value seen in the holotype of *S. dongi* and in IVPP V 23388 (30%). In the pedes, metatarsal I is the longest one.

Remarks

This specimen has been referred to *S. dongi* by Shen *et al.* (2021), as accepted by Zhou *et al.* (2022) and not commented on the literature any further so far. Shen *et al.* (2021) noticed that D3072 shares with the holotype of *S. dongi* similar limb proportions as well as a reduced metatarsal I (shorter than metatarsals II and III), which has been considered a diagnostic apomorphy for *S. dongi* within the expansive taxonomic scheme of the *Sinopterus* complex (Zhang *et al.*, 2019).

D4019 (new specimen)

This specimen comprises an almost complete skeleton, although not very well preserved. Many of the elements are articulated, except for most skull and manual elements (Fig. 36). The rostrum is slender and gently decurved (by 13 °) and bears a well-developed, heaped crest. The dorsal margin of the premaxilla is slightly jagged. The jugal-quadratojugalquadrate complex indicates the quadrate was strongly reclined (by 162 °). Unfortunately, the jugal is incompletely preserved and lacks a lacrimal process. A well-developed and posterodorsally inclined frontoparietal crest is present. The cervical vertebrae not very well-preserved and not much can be observed beyond their lengths. The fourth cervical is the longest. The trunk region is very crushed and not much can be observed. Limb elements bear slightly abraded surfaces, precluding observation of much detail. Scapulocoracoid, humeral epiphyses, and carpal elements are unfused. As preserved, metacarpal I reaches 82% the length of metacarpal IV, but

its proximal end is unclear and it may have been longer. Both pedes are badly preserved and not much can be discerned.

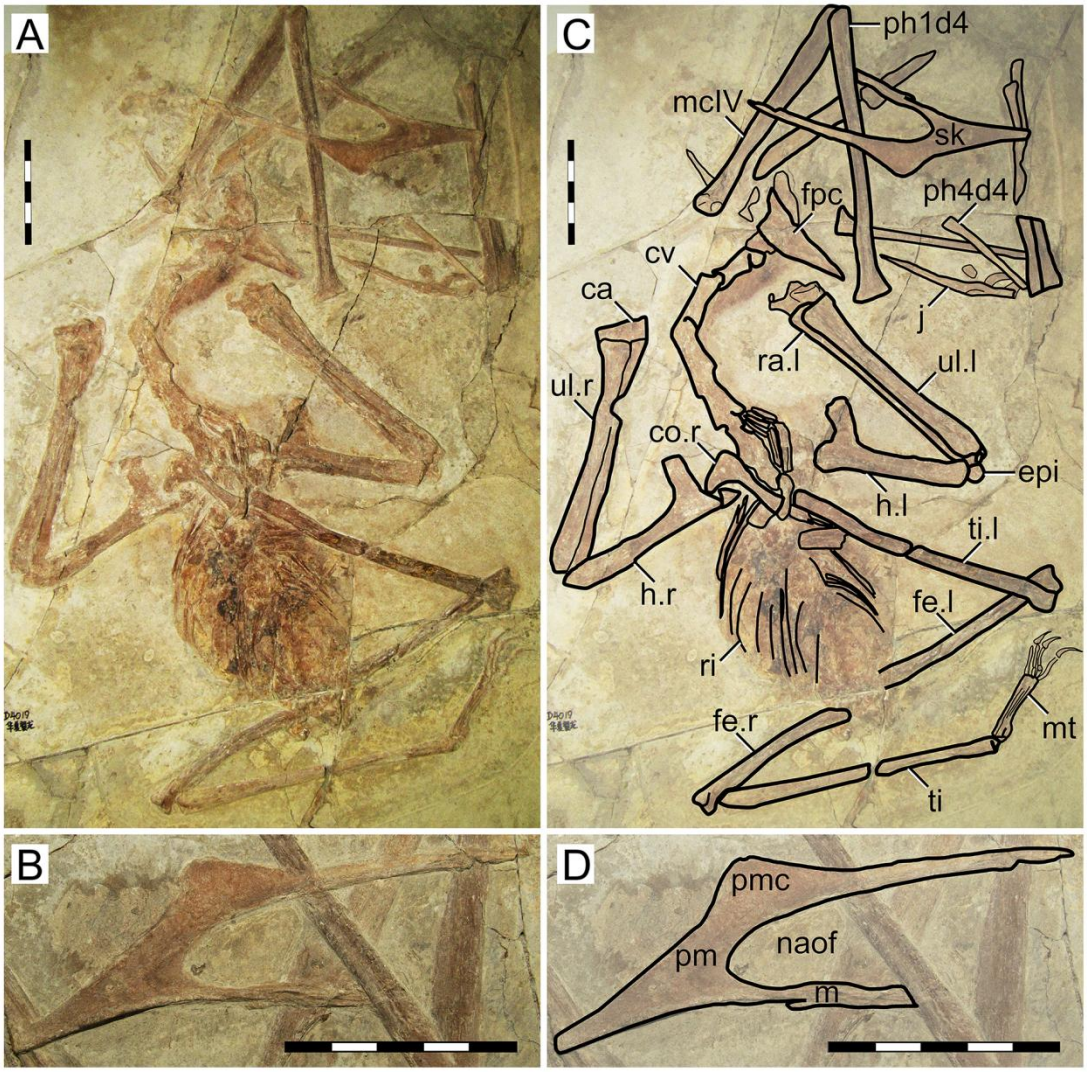

Figure 36. New specimen D4019. (A) Skeleton overview; (B) skull (left lateral view). (C and D) Respective schematic drawings. Abbreviations: ca, carpus; cv, cervical vertebra; d, dentary; d1–d4, digits 1–4; fpc, frontoparietala crest; h, humerus; j, jugal; m, maxilla; mc, metacarpal; mt, metatarsal; naof, nasoantorbital fenestra; pm, premaxilla; pmc, premaxillary crest; ph, phalanx; ti, tibia; ul, ulna; r, right; rad, radius; ri, rib; sk, skull. Scale bars: 50 mm.

BPMC 103 (new specimen)

This specimen includes an almost complete skull (exposed in left lateral view), incomplete cervical series (exposed in dorsal view), incomplete forelimbs, and incomplete hindlimbs (Fig. 37). The rostrum is slender and deflected ventrally at an angle of 20° . A slight ventrolateral tilt of the plane of exposure of the rostrum reveals that the occlusal surface is sulcate, sporting thick tomial edges that emarginate an elongate sagittal excavation. Slit-like neurovascular foramina pierce the lateral surface of the rostrum close to the tomial edge (unclear in the occlusal surface). The

premaxillary crest is large and protrusive. The anterior margin is roughly perpendicular to the main dorsal margin of the rostrum, anterodorsally oriented, similar to *H. benxiensis* and *H. corollatus*, and thus seems to have been originally trapezoidal in shape. The posterodorsal edge of the premaxillary crest is damaged, but it seems to have been anteroposteriorly longer than dorsoventrally high. The proportions of the nasoantorbital fenestra are not directly clear due to the disarticulation of the posterodorsal margin (nasal and lacrimal), but can be estimated at around 2.5 based on its length and mid-height. The dentary symphysis accounts for roughly 55% of total mandibular length, and sports a dorsal eminence as well as a low ventral crest. The anterior symphyseal region is pierced by slit-like foramina close to the occlusal line. Although the forelimbs are incompletely preserved, a partial humerus and both wing fingers are completely preserved. Metacarpal I preserves a clear proximal end and extends for only about 40% the length of metacarpal IV. The fourth wing phalanx accounts only for 20% of the first wing phalanx length. Metatarsal II is the longest one.

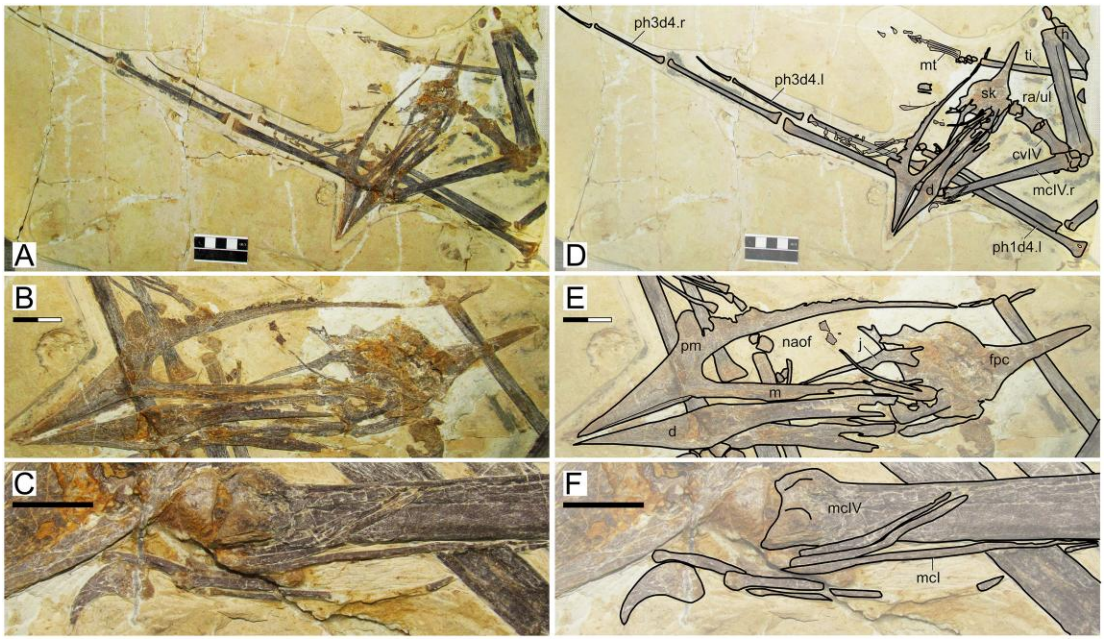

Figure 37. New specimen BPMC 103. (A) Skeleton overview; (B) skull (left lateral view); (C) metacarpus, distal region. (D–F) Respective schematic drawings. Abbreviations: cv, cervical vertebra; d, dentary; d1–d4, digits 1–4; fpc, frontoparietala crest; h, humerus; j, jugal; m, maxilla; mc, metacarpal; mt, metatarsal; naof, nasoantorbital fenestra; pm, premaxilla; pmc, premaxillary crest; ph, phalanx; ti, tibia; ul, ulna; r, right; rad, radius; ri, rib; sk, skull. Scale bars: D, 50 mm; E, 20 mm; F, 10 mm.

BPMC 104 (new specimen)

This specimen includes most of the skeleton, including a premaxillomaxilla, an almost complete mandible, incomplete cervical and dorsal series, and almost complete

fore and hindlimb elements (Fig. 38). The rostrum is relatively robustly built and ventrally deflected at an angle of 20°. The rostrum deflection point is located roughly beneath the anterior margin of the nasoantorbital fenestra, where a bulge also seems to indicate the presence of a slight lateral palatal expansion. The premaxillary crest is unfortunately incompletely preserved, but it extends anterior to the anterior margin of the nasoantorbital fenestra and its broad base suggests it was relatively large. Despite the incompleteness of the skull, the length of the nasoantorbital fenestra can be assessed based on the location of the remains of the base of the lacrimal process of the jugal. The height of the nasoantorbital fenestra was measured at its mid-length, to account for the typical position of its maximum height limit as seen in more complete specimens. In this way, the length/height ratio of the nasoantorbital fenestra of BPMC 104 can be estimated at roughly 2.3. The lacrimal process of the jugal is not preserved. The jagged dorsal skull margin is reminiscent of the conditions seen in *Tupandactylus* (Campos & Kellner, 1997; Frey, Martill & Buchy, 2003), suggesting it sported a soft tissue crest. The dentary exhibits a dorsal eminence as well as a low ventral crest. Cervical formula cannot be assessed. The sacral vertebrae (number unclear) are partially fused and bear intersacral fenestrae. The coracoid bears a large ventral flange. The extension of metacarpal I can be assessed due to the good preservation of its proximal tip, despite the loss of some of the diaphysis (Fig. 38G). It extends for 41% the length of metacarpal IV, similar to *H. benxiensis*. The first wing phalanx exhibits a single pneumatic foramen on its ventral surface. The fourth wing phalanx is relatively reduced, corresponding to 20% of first wing phalanx length. In the pelvic girdle, the medial margin of the postacetabular process is excavated by a fossa, similar to *Tapejara wellnhoferi* and *Vectidraco daisymorrisae* (Eck, Elgin & Frey, 2011; Naish, Simpson & Dyke, 2013). The neck of the postacetabular process is relatively thick and elongate, similar to *Vectidraco daisymorrisae* (Naish, Simpson & Dyke, 2013) and unlike the rather constricted condition seen in *Tapejara wellnhoferi* (Eck, Elgin & Frey, 2011) or short condition seen in *Tupandactylus navigans* (Beccari *et al.*, 2021). The femoral head exhibits a thick neck, with no visible constriction in posterior view. The greater trochanter is well-developed, and a large pneumatic foramen is present near its base. The distal end of the femur is expanded. In lateral view, the femur bows posteriorly. Two (?femoral) unfused epiphyses are present near the proximal end of the tibia. In the pedes, metatarsal II is the longest one.

BPMC 105 (new specimen)

Despite being relatively complete, this specimen is badly preserved—most bones are jumbled together, and most bone surfaces are badly weathered or cracked beyond the point of bearing relevant anatomical details (Fig. 39). Notwithstanding, the outlines of some bones and structures still reveal some interesting data. The skull, exposed in left lateral view, exhibits a trapezoidal premaxillary crest that is conspicuously protrusive, higher than anteroposteriorly long. The shape of the rostrum and the configuration of its ventral deflection are unclear. The nasoantorbital fenestra is about 2.2 times as long as high. The orbit seems to have been piriform. The

dentary symphysis bears a dorsal eminence and a low ventral crest. Measurements for visible limb bones are given in Supplemental File 4 (Sheet 1), but not much further comparative information can be retrieved. Wing proportions closely match those of *H. corollatus* and *H. benxiensis*, with the fourth wing phalanx accounting for roughly 20% the length of the first wing phalanx. The second metatarsal is the longest. Not much further information can be assessed.

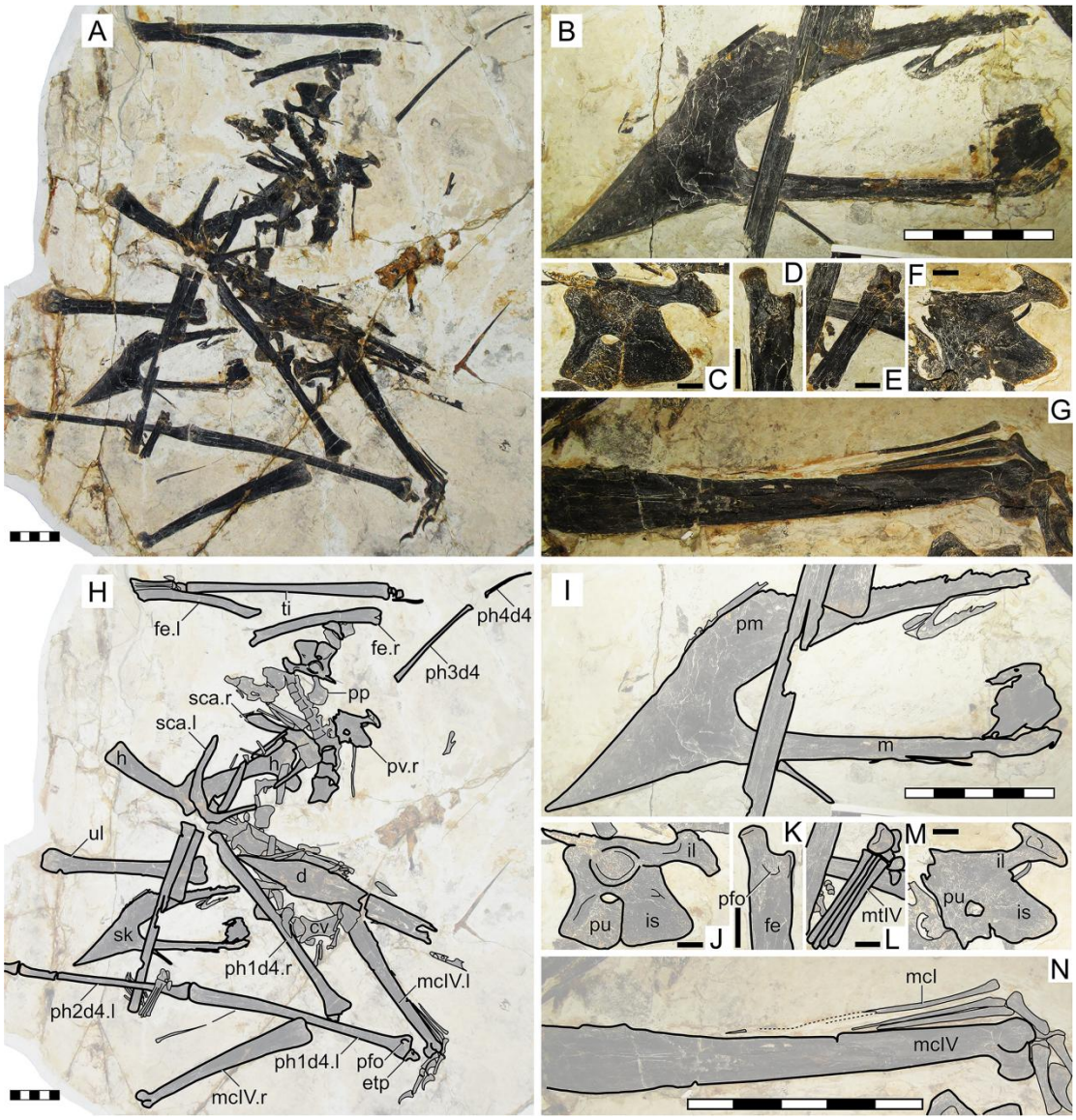

Figure 38. New specimen BPMC 104. (A) Skeleton overview; (B) skull (left lateral view); (C) left pelvis; (D) right femur; (E) right metatarsus; (F) right pelvis; (G) left metacarpus. (H–N) Respective schematic drawings. Abbreviations: cv, cervical vertebra; d, dentary; d1–d4, digits 1–4; etp, extensor tendon process; fe, femur; h, humerus; il, illium; is, ischium; m, maxilla; mc, metacarpal; mt, metatarsal; naof, nasoantorbital fenestra; pfo, pneumatic foramen; pm, premaxilla; ph, phalanx; pp, prepubis; pu, pubis; pv, pelvis; ti, tibia; ul, ulna; r, right; sca, scapula; sk, skull; ti, tibia. Scale bars: H, 50 mm; I, 50 mm; J–N, 10 mm; G, 50 mm.

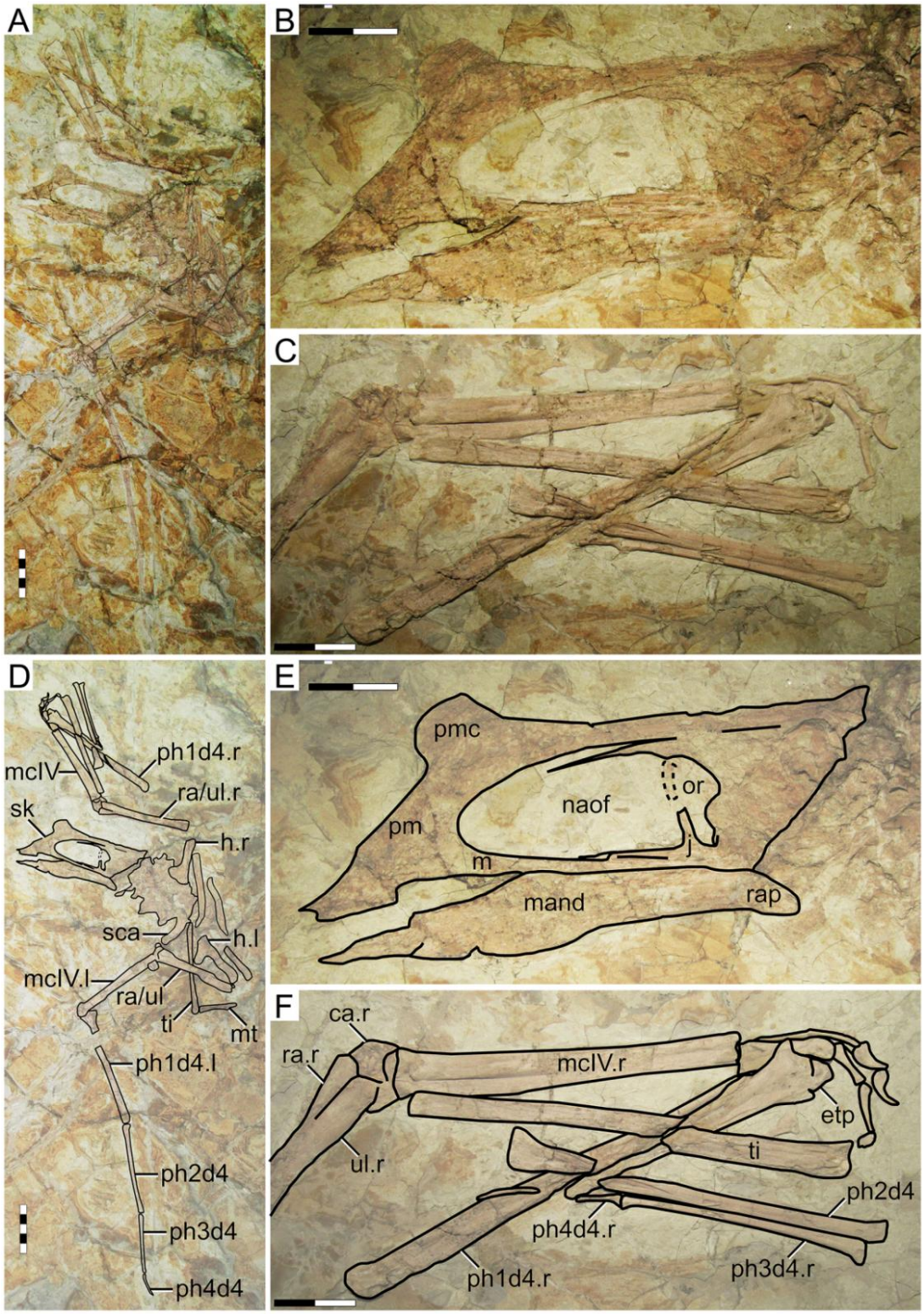

Figure 39. New specimen BPMC 105. (A) Skeleton overview; (B) skull (left lateral view); (C) detail of right manus. (D–F) Respective schematic drawings. Abbreviations: ca, carpal; etp, extensor tendon process; h, humerus; j, jugal; l, left; mand, mandible; mc, metacarpal; naof, nasoantorbital fenestra; or, orbit; pm, premaxilla; pmc, premaxillary crest; ul, ulna; r, right; ra, radius; rap, retroarticular process; sca, scapula; sk, skull; ti, tibia. Scale bars: A, D, 50 mm; B, C, E, F, 20 mm.

BPMC 106 (new specimen)

This small specimen preserves mainly a partial skull (missing the rostrum) and partial forelimbs other than partial cervical and dorsal series, although not much can be observed (Fig. 40). A triangular, dorsally oriented premaxillary crest is present, located anterior to the inferred anterior limit of the nasoantorbital fenestra, similarly to the holotype of *H. atavismus* and specimens IVPP V 23388 and D4019. The dorsal edge of the premaxillary crest, and of the posterior process of the premaxilla as well, is jagged (as in *Tupandactylus* spp.; see Frey, Martill & Buchy, 2003), indicating the potential presence of soft tissue extension. The proportions of the nasoantorbital fenestra are unclear due to the incompleteness of the rostrum and disarticulation between the premaxillomaxilla and the posterior skull region. The shape of the jugal indicates the base of the orbit was broad, implying the orbit was probably subquadrangular/subcircular in shape. The first metacarpal is quite elongate, reaching at least 95% the length of the wing metacarpal.

BPMC 107 (new specimen)

This specimen comprises an almost complete skeleton, despite exhibiting badly preserved bone surfaces (Fig. 41). The rostrum is relatively slender and exhibits only a faint, incipient premaxillary crest, very similar to the holotype of *S. dongi.* The nasoantorbital fenestra is very elongate, with an estimated length/height ratio of about 3. The orbital region is not preserved. The posterodorsal region of the skull exhibits a short frontoparietal crest. The dentary symphysis is exposed in ventral view. It exhibits a dentary crest, which is dorsoventrally crushed and thus appears as a crushed keel. The dentary symphysis accounts for about half of mandibular length. The posterior region of the symphysis is damaged. The left mandibular ramus is complete, including the articular region and the retroarticular process, allowing for estimation of the location of the quadratomandibular articulation in the skull despite the absence of a preserved quadrate (and hence allowing for a rough estimation of the proportions of the nasoantorbital fenestra). The cervical series is incompletely preserved, and the longest cervical vertebra cannot be assessed. The preserved wings exhibit morphology and proportions comparable to the holotype of Sinopterus dongi, although metacarpals I – III cannot be assessed (Supplemental File 4, Sheet 3). The sternum exhibits a rounded posterior margin. Metatarsal I is slightly longer than metatarsal II.

Short comments on the usage of cranial crests in pterosaur taxonomy

In summary, we interpret here that, within Jiufotang tapejarids, (1) variation in crest presence/development is linked to ontogeny, (2) variation in crest size can be also linked to individual/sexual variation, and (3) crest shape is linked to interspecific variation. As an example of a similar case, we can mention the *Pteranodon* complex. By following the most restrictive taxonomic interpretation of this species complex (Bennett, 1994; Martin-Silverstone *et al.*, 2017), it can be said that crest shape (as seen in proposed mature males) is diagnostic for the two valid *Pteranodon* species:

elongate and posteriorly oriented in *Pteranodon longiceps*, and “bulbous” and upright in *Pteranodon sternbergi* (Bennett, 1994). In contrast to that, juveniles and females of these two *Pteranodon* species cannot be set apart by cranial crest morphology, since these morphs would bear underdeveloped crest morphologies (Bennett, 1994; Martin-Silverstone *et al.*, 2017). We regard that we should expect for pterosaurs the same amount of complexity we see in extant birds: species with and without sexual dimorphism in ornaments; closely related species with distinct (and diagnostic) ornaments; and closely related species with similar ornaments. We regard here that each case will need its own assessment, and that no general pattern should be expected for pterosaurs as a whole—a very diverse group that radiated for over 165 million years.

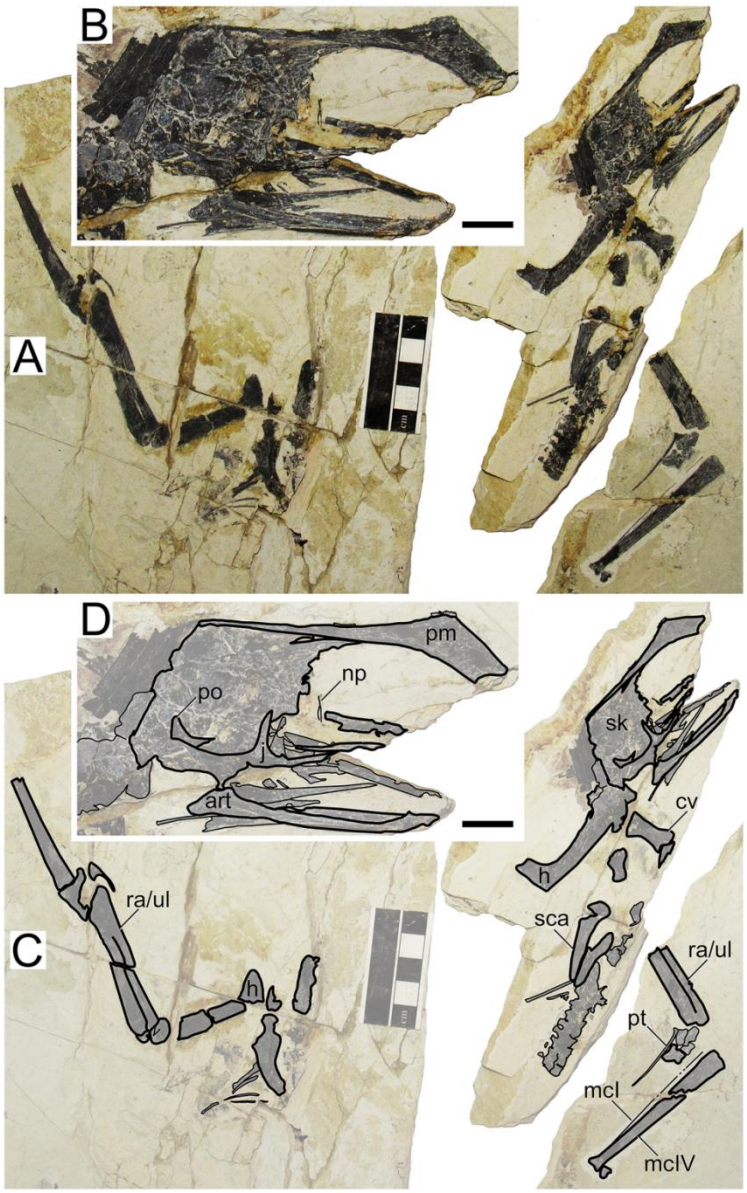

Figure 40. New specimen BPMC 106. (A) Skeleton overview; (B) skull (right lateral view). (C and D) Respective schematic drawings. Abbreviations: art, articular; cv, cervical vertebra; h, humerus; j, jugal; mc, metacarpal; np, nasal process; pm, premaxilla; po, postorbital; pt, pteroid; ul, ulna; rad, radius; sca, scapula; sk, skull. Scale bars: A, C, 50 mm; B, D, 10 mm.

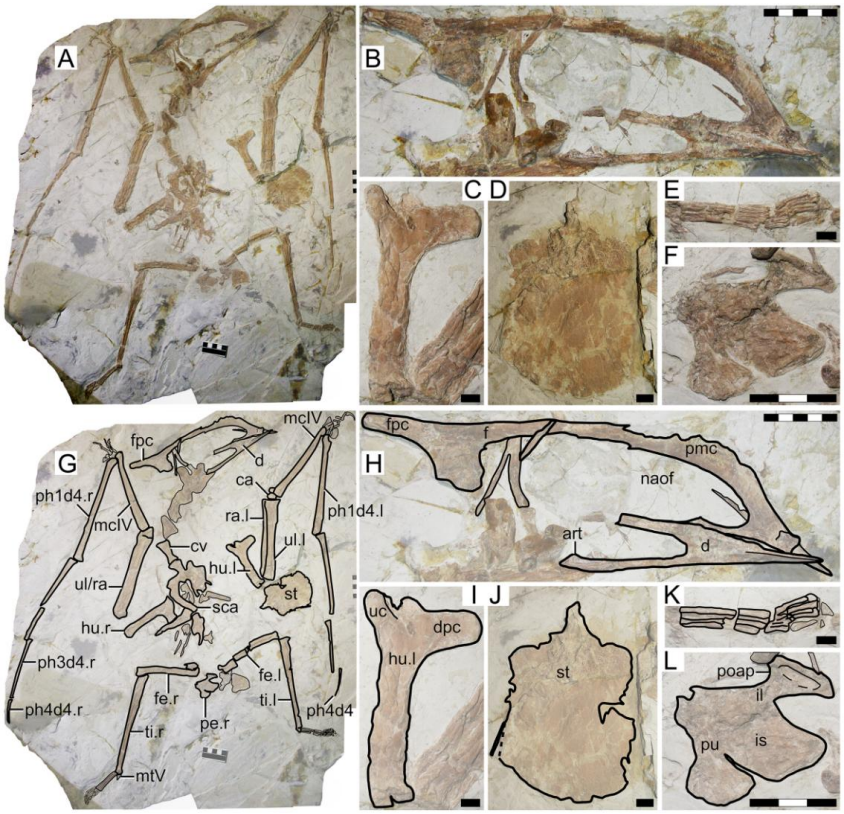

Figure 41. New specimen BPMC 107. (A) Skeleton overview; (B) skull (right lateral view); (C) left humerus; (D) sternum; (E) left foot; (F) right pelvis. (G–L) Respective schematic drawings. Abbreviations: art, articular; ca, carpus; cv, cervical vertebra; d, dentary; d1–d4, digits 1–4; dpc, deltopectoral crest; f, frontal; fe, femur; fpc, frontoparietal crest; h, humerus; il, illium; is, ischium; l, left; mc, metacarpal; mt, metatarsal; naof, nasoantorbital fenestra; pmc, premaxillary crest; ph, phalanx; poap, postacetabular process; pt, pteroid; pu, pubis; ti, tibia; ul, ulna; r, right; rad, radius; sca, scapula; st, sternum; uc, ulnar crest. Scale bars: A, B, G, H, 50 mm; I–K, 10 mm; L, 30 mm.

Short comments on *Nemicolopterus crypticus* ((IVPP V-14377)

As observed by Witton (2013) and Naish, Witton & Martin-Silverstone (2021), the holotype specimen of *Nemicolopterus crypticus* (Fig. 42) clearly represents a young juvenile, as indicated by its "small size, proportionally enormous orbit, rounded and unfused pelvic bones, poorly defined limb articulations with unfused epiphyses, unfused skull bones, unfused scapulocoracoid, and lack of fusion between the tibia and tarsus" (Naish, Witton & Martin-Silverstone, 2021). Furthermore, it resembles tapejarids due to a combination of several features, most importantly edentulousness, a downturned rostrum, a slender and subvertical lacrimal process of the jugal, a jaw joint ventral to the anterior half of the orbit, and relatively elongate hindlimbs (Naish, Witton & Martin-Silverstone, 2021). We further note that one of the proposed diagnostic features of *Nemicolopterus crypticus*, a penultimate phalanx of pedal digit 4 longer than the first (Wang *et al.*, 2008), is a feature it shares with Jiufotang tapejarids (e.g., Shen *et al.*, 2021; Zhou *et al.*, 2022).

Here, we highlight that *Nemicolopterus crypticus* exhibits a morphology that is far distinct from any other Jiufotang tapejarid specimen, what can be attributed to its very young stage—this is expressed by the entire lack of cranial crests, a relatively large orbit, a relatively diminutive nasoantorbital fenestra, a not much reclined quadrate, and a "knifeshaped" humeral deltopectoral crest (Wang *et al.*, 2008). Absence of cranial crests and large orbits are well-known indicators of young ontogenetic stages (e.g., Bennett, 1993). It is interesting to note that the distinctive shape of the humeral deltopectoral crest of the holotype of *N. crypticus* could easily be explained by an incipient ossification of the structure—in fact, neonate specimens of *Hamipterus tianshanensis* seem to be characterized by incipiently ossified humeral deltopectoral crests (Wang *et al.*, 2017).

Concerning the holotype of *N. crypticus*, we regard that its very early juvenile status (near-hatchling; Naish, Witton & Martin-Silverstone, 2021) is insufficient for a satisfactory diagnosis and prevents a confident identification as conspecific with either *S. dongi* or *'H.' corollatus* (or yet a distinct species). Thus, we consider that the holotype of *Nemicolopterus crypticus* should be regarded as an indeterminate Sinopterinae.

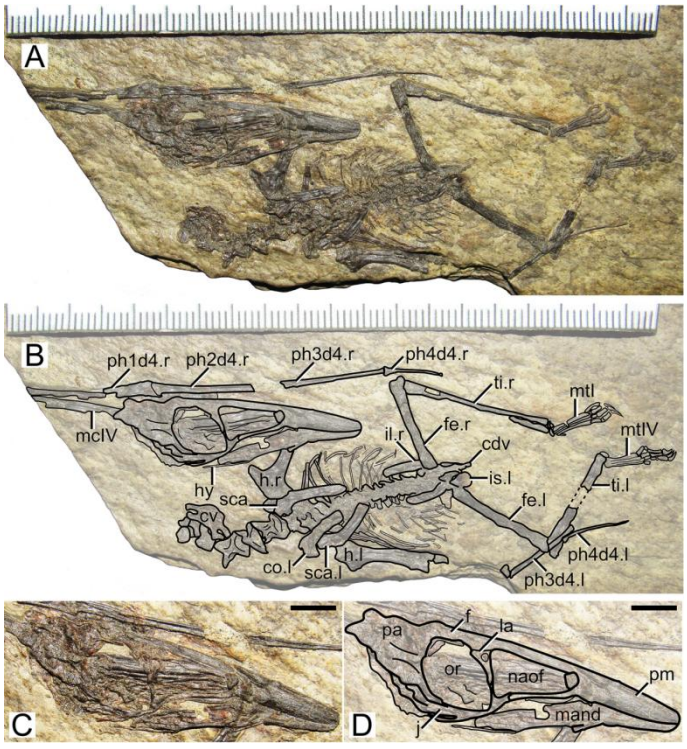

Figure 42. *Nemicolopterus crypticus* holotype (IVPP V-14377). (A) Skeleton overview, and (B) schematic drawing. (C) Skull (right lateral view), and (D) schematic drawing. Abbreviations: cdv, caudal vertebrae; co, coracoid; cv, cervical vertebra; d1–d4, digits 1–4; f, frontal; fe, femur; h, humerus; hy, hyoid; il, illium; is, ischium; j, jugal; l, left; la, lacrimal; mand, mandible; mc, metacarpal; mt, metatarsal; naof, nasoantorbital fenestra; or, orbit; pa, parietal; pm, premaxilla; ph, phalanx; ti, tibia; r, right; sca, scapula. Scale bars: A–B, 100 mm; C–D, 5 mm

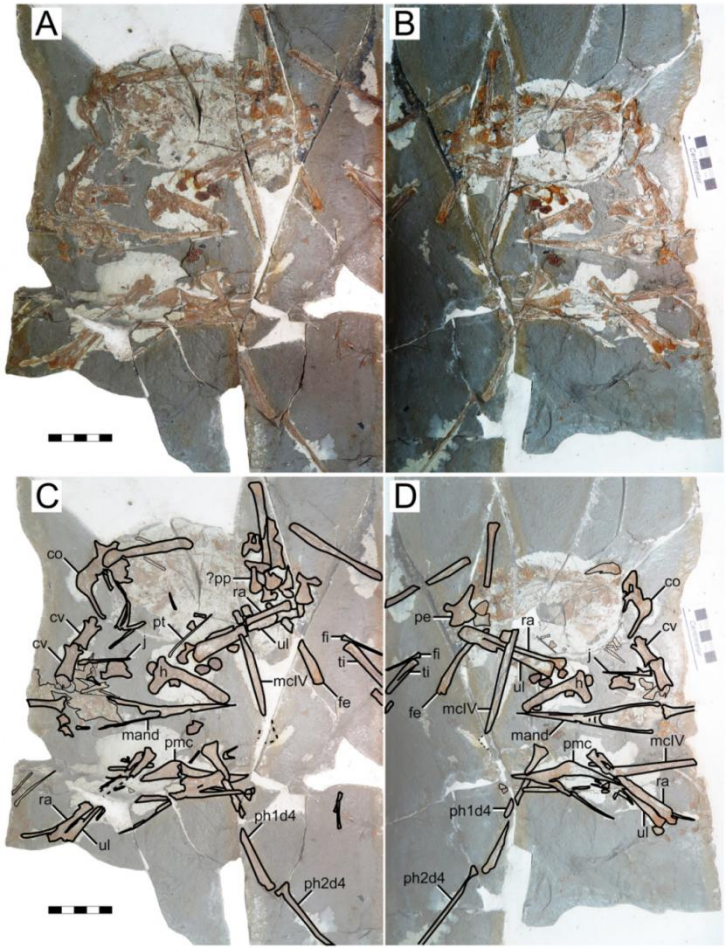

Figure 43. *Eopteranodon lii* holotype (BPV 078). (A) Counterpart; (B) main part. (C and D) Respective schematic drawings. Abbreviations: cv, cervical vertebra; co, coracoid; d1–d4, digits 1–4; fe, femur; fi, fibula; h, humerus; j, jugal; mand, mandible; mc, metacarpal; pmc, premaxillary crest; pe, pelvis; ph, phalanx; ti, tibia; ul, ulna; rad, radius. Scale bars: C, 50 mm; D, 10 mm.

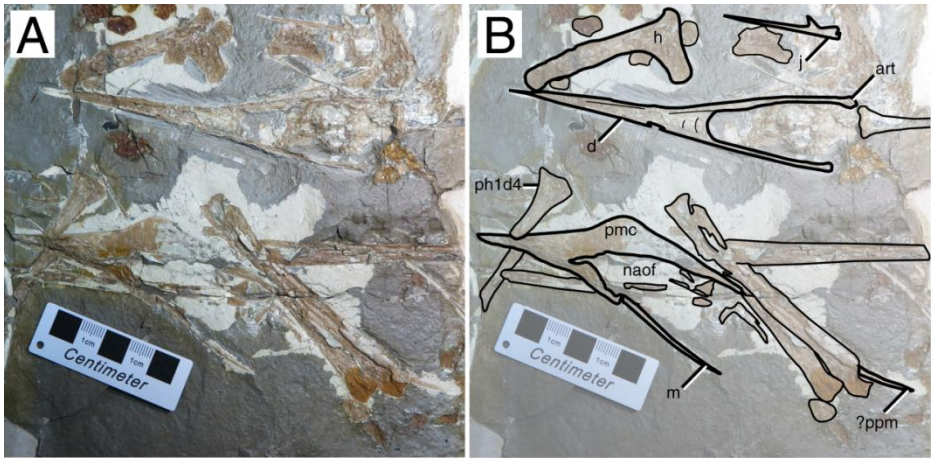

Figure 44. *Eopteranodon lii* holotype (BPV 078) details. (A) Close-up of the specimen's main part, and (B) schematic drawing. Abbreviations: art, articular; d, dentary; h, humerus; m, maxilla; naof, nasoantorbital fenestra; pmc, premaxillary crest; ppm, posterior premaxillary process. Scale bars: 50 mm.

Short comments on *Eopteranodon lii* (BPV 078)

As discussed above, *Eopteranodon lii* is a tapejarid species that comes from the Yixian Formation, which is slightly older than and underlies the Jiufotang Formation (from which the *Sinopterus* complex comes from). *Eopteranodon lii* has been regarded as a close relative of the genus *Sinopterus* in several phylogenetic analyses (Vullo *et al.*, 2012; Andres, Clark & Xu, 2014; Pêgas *et al.*, 2021), a result that is corroborated here (see below). However, the tapejarid nature of *Eopteranodon lii* has not been consensual. This taxon has been, at times, interpreted as a chaoyangopterid (e.g., Lü *et al.*, 2008). Furthermore, Martill *et al.* (2020b) noted that a tapejarid-like downturned rostrum could not be verified in the holotype of *Eopteranodon lii* due to the lack of detailed illustrations, and that a re-study of the holotype would be desirable. Close analysis of the type specimen reveals clear tapejarid features (Figs. 43 and 44), including a downturned rostrum with a premaxillary crest (note that the original identifications of skull and mandibular remains were mistakenly switched).

Eopteranodon lii exhibits striking similarities to *Sinopterus dongi*, especially in orbit shape (subquadrangular), quadrate reclination (about 160°), and in cervical IV being the longest one. Still, *Eopteranodon lii* differs from *Sinopterus dongi* in exhibiting a stouter nasoantorbital fenestra (about 2.5 times as long as high), a fairly elongate pteroid (pteroid/ulna length ratio about 0.56), an elongate wing phalanx 4 (wing phalanx 4/phalanx 1 length ratio about 0.45), and a metatarsal I shorter than metatarsal II. Thus, we corroborate the distinction between *Eopteranodon lii* and *Sinopterus dongi*, as well as *'H.' corollatus*.

We further note that, due to the close proximity between *Eopteranodon lii* and *Sinopterus dongi*, and to the fact that the former is chronologically older than the latter, it is possible that *Eopteranodon lii* and *Sinopterus dongi* could be linked in an anagenetic continuum and thus represent chronospecies. This is similar to what has been proposed for other closely related pterosaur species that are stratigraphically successive: *Pteranodon sternbergi* and *P. longiceps* (Bennett, 1994), and *Nurhachius luei* and *N. ignaciobritoi* (Zhou *et al.*, 2019).

PHYLOGENETIC ANALYSIS RESULTS

Our search produced three minimum-length trees, with 551 steps, ensemble consistency index of 0.593 and ensemble retention index of 0.860. In our strict consensus tree, we recovered a clade of Jehol tapejarids, in which the clade *Eopteranodon lii* + *Sinopterus dongi* is the sister-group of *'H.' corollatus*. This Jehol clade (comprising *Eopteranodon lii*, *Sinopterus dongi*, and *'H.' corollatus*) is supported by the following unambiguous synapomorphies: char. 109(1) posteriorly shifted apex of the dentary dorsal eminence (located posterior to the anterior third of mandibular length); char. 127(2) concave dorsal margin of the mandibular ramus; and

char. 131(2), elongate retroarticular process (char. 161 of Wu, Zhou & Andres, 2017).

The node joining *Eopteranodon lii* and *Sinopterus dongi* was supported by the following four synapomorphies: char. 8(1), subquadrangular orbit; char. 30(0), skull height (from squamosal to premaxilla, exclusive of cranial crests) relative to jaw length under 25% of jaw length (modified from Witton, 2012; Andres, Clark & Xu, 2014); char. 70(4) quadrate reclination about 160° (ambiguous synapomorphy); and char. 178(1) fourth mid-cervical longer than the fifth.

Based on the compelling anatomical differences between *S. dongi* and *'Huaxiapterus' corollatus*, along with the fact that *S. dongi* is recovered here as closer to *E. lii* than to *'Huaxiapterus' corollatus*, we regard that *'Huaxiapterus' corollatus* requires a new generic name—agreeing with previous suggestions (Kellner & Campos, 2007) and phylogenetic analyses (Andres, Clark & Xu, 2014). We thus erect *Huaxiadraco* gen. nov. to accommodate *Huaxiadraco corollatus* comb. nov.

It is interesting to note that the relationships between the Jehol tapejarid (Fig. 45) species as recovered by our phylogenetic analysis is different from the distance-based relationships between the morphotypes in our morphometric analysis. Particularly, *Tupandactylus navigans* is recovered closer to Morphotype II than to *Tapejara wellnhoferi* and *Caiuajara dobruskii*. It is important to bear in mind that the cluster analysis is based on similarity (which are measured by distance, and can reflect homoplasy), and not shared traits (as is the case of the phylogenetic analysis). This kind of analysis may produce useful information on a species-level taxonomy (granted the analyzed traits are not sexual or ontogenetic in nature, as discussed here), but it has no bearing on the phylogenetic relationships between the analyzed species. While our species circumscriptions are based on morphological and morphometric variation (thus the utility of a specimen-level phenogram in order to cluster specimens), our generic attributions must be guided by our phylogenetic results.

Figure 45. Life reconstruction of the Jiufotang tapejarids. The coexistence between *Sinopterus dongi* and *Huaxiadraco corollatus* comb. nov. in the Jiufotang paleoenvironment. Art: courtesy of Zhao Chuang.

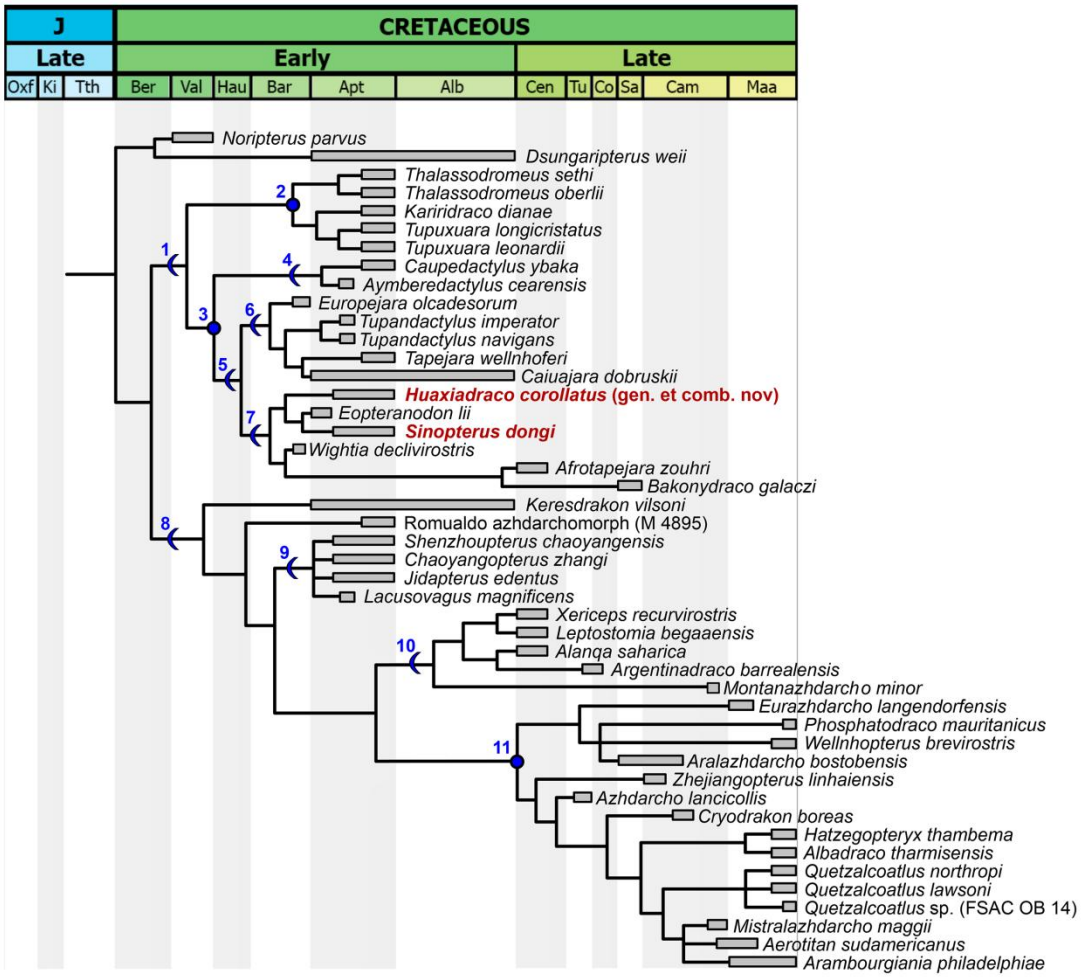

Figure 46. Time-calibrated strict consensus tree. The two species of the *Sinopterus* complex here regarded as valid are indicated in dark red. 1: Tapejaromorpha. 2: Thalassodromidae. 3: Tapejaridae. 4: Caupedactylia. 5: Tapejarinae. 6: Sinopterinae. 7: Azhdarchomorpha. 8: Chaoyangopteridae. 9: Alanqidae. 10: Azhdarchidae.

Systematic Paleontology
Pterosauria Owen, 1842
Pterodactyloidea Plieninger, 1901
Azhdarchoidea Unwin, 1995 (sensu Kellner, 2003)
Tapejaromorpha Andres, Clark & Xu, 2014 (sensu Andres, 2021)

Tapejaridae Kellner, 1989

Node-based definition. The least inclusive clade containing *Tapejara wellnhoferi* Kellner, 1989, *Sinopterus dongi* Wang & Zhou, 2003a, and *Caupedactylus ybaka* Kellner, 2013 (unrestricted emendation). Reference phylogeny: Fig. 46.

Composition. Caupedactylia clad. nov. and Eutapejaria clad. nov. (see Table 5). Caupedactylia contains *Caupedactylus ybaka* and *Aymberedactylus cearensis*. Eutapejaria contains Tapejarinae and Sinopterinae (see below).

Diagnostic apomorphies. Lateral expansion of the jaws (both) level with anterior margin of the nasoantorbital fenestra; main part of dorsal skull margin (excluding cranial crests) convex in lateral view; prenarial rostrum and dentary symphysis ventrally deflected; lacrimal bearing extensive fenestration; dentary symphysis bearing a ventral sagittal crest.

Remarks. The original PhyloCode-compliant phylogenetic definition (Andres, 2021) is unrestrictedly emended here by the simple addition of *Caupedactylus ybaka* as a third internal specifier. Although this taxon was not included in the reference phylogeny from Andres (2021), it is recovered here as closely related to tapejarines and sinopterines (sensu Andres, 2021) as in previous studies (e.g., Vidovic & Martill, 2014; Pêgas *et al.*, 2021), due to exhibiting a series of well-established diagnostic features of Tapejaridae (sensu Lü *et al.*, 2006a; Andres, 2021), as listed above. The present unrestricted emendation is thus done to preserve the stability of Tapejaridae in terms of diagnosis, usage, and content, under the context of the present reference phylogeny (Fig. 46). Tapejaridae (sensu this work) thus includes Caupedactylia and Eutapejaria (see Table 5).

Eutapejaria new clade name

Branch-based definition. The most inclusive clade containing *Tapejara wellnhoferi* Kellner, 1989 but not *Caupedactylus ybaka* Kellner, 2013. Reference phylogeny: Fig. 46.

Composition. Tapejarinae (sensu Andres, 2021) and Sinopterinae (sensu Andres, 2021). Tapejarinae contains *Tapejara wellnhoferi*, *Caiuajara dobruskii*, *Tupandactylus imperator*, *Tupandactylus navigans*, and *Europejara olcadesorum*. Sinopterinae contains *Sinopterus dongi*, *Eopteranodon lii*, *Huaxiadraco corollatus* gen. et comb. nov., *Bakonydraco galaczi*, *Afrotapejara zouhri*, and *Wightia declivirostris*.

Diagnostic apomorphies. Marked gap between jaws during occlusion; premaxillary crest anteriorly tall and forming a low, rod-like process extending posteriorly; dorsal dentary eminence present on the dentary symphysis; dentary symphysis anterior surface sulcate with thick, well-marked tomial edges; humeral ulnar crest rounded in shape and posterodorsally flared.

Sinopterinae Lü *et al.*, 2016 (sensu Andres, 2021)

***Sinopterus dongi* Wang & Zhou, 2003**

Holotype. IVPP V 13363.

Referred material. BPV-077, GMN-03-11-001, JPM-2014-005, XHPM 1009, IVPP V 23388, D3072, D4019, BPMC 106, BPMC 107.

Synonymy. *Sinopterus gui* Li, Lü & Zhang (2003), *Huaxiapterus jii* Lü & Yuan (2005), *Sinopterus lingyuanensis* Lü *et al.* (2016), and *Huaxiapterus atavismus* Lü *et al.* (2016).

Type locality and horizon. Chaoyang City of Liaoning Province. Jiufotang Formation.

Diagnostic apomorphies. Sinopterinae with the following unique features (autapomorphies): nasoantorbital fenestra relatively elongate (over three times as long as high); pteroid shorter than half of ulna length; metatarsal I subequal to or longer than metatarsal II (longer than metatarsal III).

Differential diagnosis. Sinopterinae species with the following combination of features: premaxillary crest heaped in outline, in the crested morph (=*Eopteranodon*, ≠*Huaxiadraco*); rostrum deflection of 12–15° (=*Eopteranodon*, ≠*Huaxiadraco*); nasoantorbital fenestra relatively elongate, over three times as long as high (autapomorphy); nasal process subvertical and elongate (=*Eopteranodon*, ≠*Huaxiadraco*); subquadrangular orbit (=*Eopteranodon*, ≠*Huaxiadraco*); quadrate reclination of ~160°(=*Eopteranodon*, ≠*Huaxiadraco*); fourth cervical vertebrae the longest (=*Eopteranodon*, ≠*Huaxiadraco*); pteroid shorter than half of ulna length (autapomorphy); metacarpal I subequal to metacarpal IV (=*Eopteranodon*, ≠*Huaxiadraco*); wing phalanx 4/phalanx 1 length ratio about 0.30 (≠*Eopteranodon*, ≠*Huaxiadraco*); metatarsal I subequal to or longer than metatarsal II, and longer than metatarsal III (autapomorphy).

***Eopteranodon lii* Lü & Zhang, 2005**
Holotype. BPV-078.

Referred material. D2526.

Type locality and horizon. Beipiao, Liaoning Provice. Yixian Formation.

Diagnostic apomorphies. Tapejarid with the following autapomorphies: elongate pteroid (pteroid/ulna length ratio about 0.56); elongate wing phalanx 4 (subequal to phalanx 3 and about 45% the length of phalanx 1).

Differential diagnosis. Sinopterinae with following combination of features: premaxillary crest heaped in outline, in the crested morph (=*Sinopterus*, *Huaxiadraco*); rostrum deflection of 15° (=*Sinopterus*, ≠*Huaxiadraco*); nasoantorbital fenestra relatively stout, about 2.5 times as long as high (≠*Sinopterus*, =*Huaxiadraco*); nasal process subvertical and elongate (=*Sinopterus*, ≠

Huaxiadraco); subquadrangular orbit (=*Sinopterus*, ≠*Huaxiadraco*); quadrate reclination of ~160° (=*Sinopterus*, ≠*Huaxiadraco*); fourth cervical vertebrae the longest (=*Sinopterus*, ≠*Huaxiadraco*); pteroid over half of ulna length (autapomorphy); metacarpal I subequal to metacarpal IV (=*Sinopterus*, ≠ *Huaxiadraco*); elongate wing phalanx 4, subequal to phalanx 3 and about 45% the length of phalanx 1 (autapomorphy); metatarsal I shorter than metatarsal II (≠ *Sinopterus*, =*Huaxiadraco*).

***Huaxiadraco* gen. nov.**

Etymology. After *Huaxia*, an ancient, pre-imperial name for the Chinese civilization (literal meaning: beautiful grandeur), and draco, Latin for dragon.

Type species. *Huaxiadraco corollatus* (Lü *et al.*, 2006a), new combination.

Diagnosis. As for type and only species.

***Huaxiadraco corollatus* (Lü *et al.*, 2006a) comb. nov.**

Holotype. ZMNH M813.

Referred material. BXGM V0011, D2525, BPMC 103, BPMC 104, BPMC 105.

Synonymy. *Huaxiapterus benxiensis* Lü *et al.*, 2005.

Type locality and horizon. Chaoyang City of Liaoning Province. Jiufotang Formation.

Diagnostic apomorphies. Sinopterinae with the following unique features (autapomorphies): premaxillary crest trapezoidal in shape and slanting anterodorsally (in the crested morph); nasal descending process anteriorly oriented; short metacarpal I (30–40% the length of metacarpal IV); and short wing phalanx 4 (~20% the length of wing phalanx 1)

Differential diagnosis. Sinopterinae species with premaxillary crest trapezoidal in shape and slanting anterodorsally, in the crested morph (autapomorphy); orbit piriform in shape (≠*Sinopterus*, ≠*Eopteranodon*); rostrum deflection of ~20° (≠*Sinopterus*, ≠*Eopteranodon*); nasoantorbital fenestra relatively stout, 2.2–2.5 times as long as high (≠*Sinopterus*, =*Eopteranodon*); quadrate reclination of ~150° (≠*Sinopterus*, ≠*Eopteranodon*); fifth cervical vertebrae the longest (≠*Sinopterus*, ≠*Eopteranodon*); short metacarpal I, 30–40% the length of metacarpal IV (autapomorphy); short wing phalanx 4, ~20% the length of wing phalanx 1 (autapomorphy); and metatarsal I shorter than metatarsal II (≠*Sinopterus*, =*Eopteranodon*).

CHAPTER V

ADVANCES IN CHINESE ADVANCED TYPE PTEROSAUR 2: A CASE OF MAXILLARYAMELOBLASTOMA IN NEW ISTIODACTYLIFORM PTEROSAUR

Ameloblastoma is a rare tumor related to odontogenic epithelium. The worldwide incidence was determined to be 0.92 cases per million people per year in humans (Hendra *et al.*, 2020). The peak age incidence is the third decade of life among humans, and the most common type of ameloblastoma was multicystic, predominantly occurring in mandibles (Petrovic *et al.*, 2018). Although most ameloblastomas are benign more severe cases can destruct dentition (Petrovic *et al.*, 2018). Some cases of maxillary ameloblastoma can invade the nasal, orbit, and even braincase (Petrovic *et al.*, 2018). To date, the pathogenesis and evolutionary history of odontogenic tumor remains elusive, thus limiting further guidance for molecular targeted therapies.

Pathological diagnosis of tumors in fossil animals is challenging due to the absence of soft tissue and irreproducibility and uniqueness of fossilised bones. Cases of reported tumors in extinct vertebrates were diagnosed based on gross morphological examination, histological analysis, and/or computerized tomography of hard tissues (Ekhtiari *et al.*, 2020; Haridy *et al.*, 2019). In amniotes, fossil evidence of several neoplasms have been presented in dinosaurs , turtles, marine reptiles, ground sloths, and hominids, most of which occur in the postcranial skeleton (Haridy *et al.*, 2019; Rehemtulla, 2010; Barbosa *et al.*, 2021; Odes *et al.*, 2016). To date, to our knowledge, no cases of tumor have been reported in the cranium of fossil amniotes.

Figure 47. Unnamed new istiodactyliform pterosaur (BPMC-0101).

Here we report a maxillary ameloblastoma in a 120-million-year-old pterosaur, which represents the oldest reported case of cranial bone tumor in amniote evolutionary history so far. The gross examination and histological evidence

demonstrates features consistent with multicystic ameloblastoma in both humans and dogs (Tjepkema, Bell & Soukup, 2020).

The pterosaur specimen (BPMC 0101) comes from the Early Cretaceous Jiufotang Formation in Northeastern China, accessioned at the Beipiao Pterosaur Museum of China (Fig. 47). Preliminary analysis suggests it represents a new species of istiodactyliform pterosaur, which will be described in detail elsewhere. We have conducted gross examination and histological analysis of the specimen. Samples for histological section were extracted from tissue of the lesion site in the maxilla (Fig. 48). Radiological approach was not used due to compressed, two-dimensional nature of the preserved fossil and size and resolution limitations of CT scanning.

Figure 48. Sample location in the maxilla of BPMC-0101.

Gross examination reveals a 3 x 7 cm lesion in the lateral surface of the maxilla, close to the toothline (Fig. 47). The lesion is pyriform in shape, with its base on the palate, two sides on posterior nasal wall and anterior nasoantorbital fenestra. Damaged area of bone seems to have resulted from an expansile mass. The lytic lesion originally contained a mass of soft tissue or other non-osseous structure, and penetrated by minimally remodeled trabeculae (Rothschild, Witzke & Hershkovitz, 1999). In this case, irregularly shaped trabeculae filled the involved segment of the medullary cavity. Surrounding cortical bone is invaded leaving no residual cortical shell at the buccal maxillary margins. Besides, the mass has transgressed the cortex of alveolar bone extended into the soft tissues, and thus results from pathological root resorption of teeth surrounded the mass and alveolar bone loss (Fig. 49a). And maxillary molars showed significant shift, which indicating that is a tumor-like space

occupying lesion instead of inflammation (Fig. 49b).

Figure 49. Details of pathological damaged area .

To further confirmed the histological structure, we observed ground section of trabeculae-like tissues in the lesion of the medullary cavity. Results showed mineralized matrix such as lamellae and osteocytes lacunae at the borders of adjacent lamellae (Fig. 50). The microscopic structural unit of this sample is composed of

lamellae arranged in parallel or concentric rings. The central canal surrounded by concentric layers of mineralized matrix represent Haversian canals (Fig. 50 arrows). Therefore, the trabeculae-like structures in the mass were highly calcified bone structures.

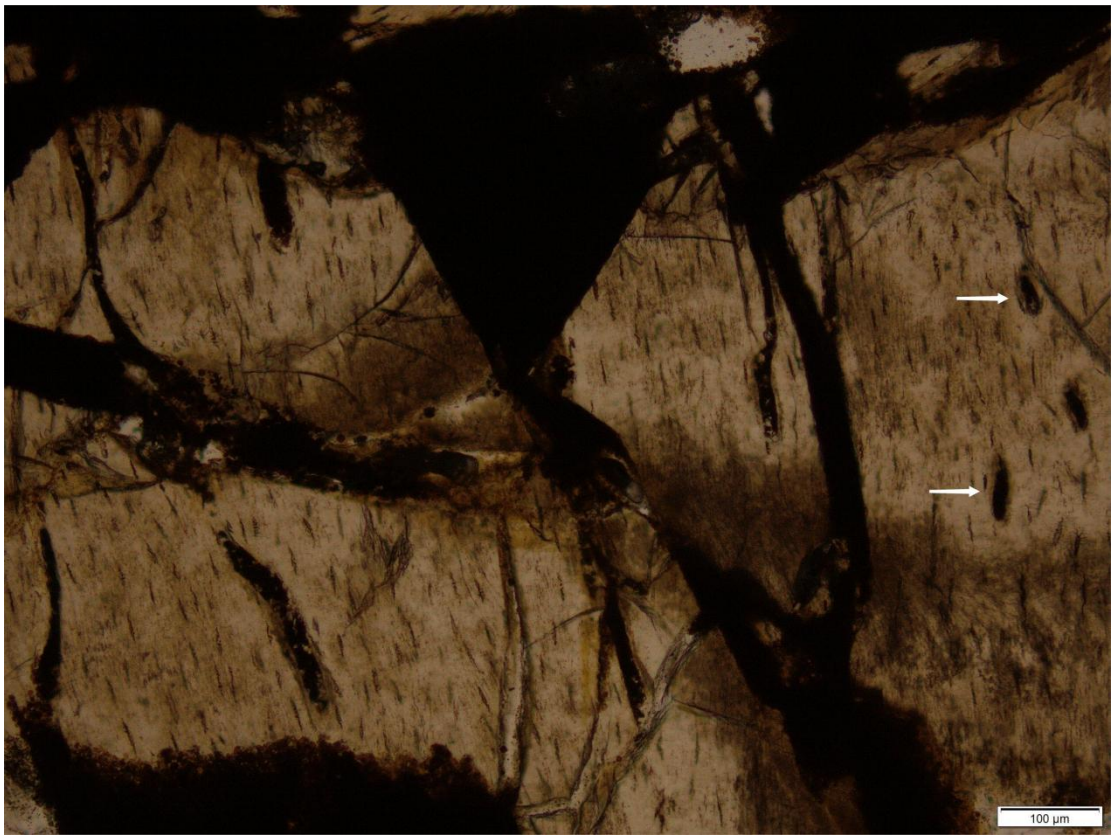

Figure 50. Micro Photo of maxilla sample (cellular level).

Ameloblastoma is the most common benign odontogenic tumor and occurs in all tooth forming locations of jaws in humans. Ameloblastoma typically shows a painless swelling and expansion of the buccal cortical plate (Effiom *et al.*, 2018; Kreppel & Zöller, 2018). The roots of adjacent teeth could be displaced or resorpted by the expanding tumor. In macroscopic features, the ameloblastoma appears well demarcated from surrounding bone. The gross appearance of the pterosaur maxilla we describe are similar to the human ameloblastoma, although we did not confirm the diagnosis pathologically and radiographically. Since histopathological analysis is not possible, we can only identify subtypes based on the location and general view of the tumor. In this case, images showed malocclusion, loose teeth, tumor infiltrated into the adjacent tissue and resorbed the cortical plate. In addition, irregularly shaped trabeculae filled the involved segment of the medullary cavity. These suggested the case might belong to multicystic ameloblastoma.

Differential diagnosis of ameloblastoma includes osteomyelitis, ossifying fibroma, osteosarcoma, and metastatic tumors of jaws. Osteomyelitis is characteristic with pockmarking and the bone-forming nature in the lesion, which is not consistent

with our sample (Ekhtiari *et al.*, 2020). Ossifying fibroma is characteristic with trabeculae formed by immature bone arranged in a network, was rejected because of the highly disorganised bone structure in our sample. Osteosarcoma and metastatic tumors of jaws are malignant with no well-defined zone of transition between normal and abnormal bone. In this case, the lesion of the medullary cavity has a very sharp zone of transition. Furthermore, osteosarcoma was rejected because of the lack of neocortex formation surrounding tumor.

The pterosaur specimen presented herein is the oldest case of ameloblastoma in the maxilla of a reptile. Although the sample size is very limited in reptiles, previous cases of mandibular ameloblastoma in a modern snake and an extinct dinosaur have no sign of invasion to dentition, indicating a less severe condition (Comolli *et al.*, 2015; Dumbravă *et al.*, 2016). This is similar to patterns observed in human and veterinary species, where maxillary ameloblastoma is usually more aggressive than mandibular ameloblastoma (Petrovic *et al.*, 2018; Tjepkema, Bell & Soukup, 2020). The difference was postulated to be due to the lower cortical composition in maxilla than in mandible (Tjepkema, Bell & Soukup, 2020).

In conclusion, we provide the first occurrence of maxillary tumor in a fossil amniote, revealing that tumor formation is not limited to mandible and postcranial elements. This case is of particular interest because of the presence of ameloblastoma in a maxilla, a phenomenon not previously reported in pterosaur and reptiles more broadly. The condition is more severe compared to reported cases of mandibular ameloblastoma in other reptiles. A similar pattern is also observed in human and non-human mammalian ameloblastoma, suggesting an onset pattern that is deeply rooted in the amniote tree of life.

CHAPTER VI

CONCLUSION AND PROSPECT

The western Liaoning and its surrounding areas (northeastern China) are the one of most productive pterosaur research regions in the world. Based on a varied sample of pterosaur group (Anurognathidae, Darwinoptera, Tapejaridae and Istiodactylidae), the following results and enlightenments are gained:

1.JPM-2012-001 represents a new anurognathid, named *Sinomacrops bondei*. It is the second anurognathid from the Tiaojishan Formation, and the first anurognathid specimen to exhibit a skull exposed in lateral view. In our new phylogenetic analysis, it is recovered as the sister-group of *Batrachognathus volans*, with which it comprises the *Batrachognathinae*. All other taxa were recovered as closer to *Anurognathus*. The exclusion of *Luopterus mutoudengensis* from the genus *Dendrorhynchoides* is corroborated. *Vesperopterylus lamadongensis* is recovered as the sister-group of *Anurognathus ammoni*, with *Jeholopterus ningchengensis* as their successive sister-group. With time and new specimens being discovered, new data have been provided and new interpretations were presented. For this reason, each new specimen is crucial for the understanding of the group. The present information available leads us to interpret anurognathids as the sister-group of Darwinoptera + Pterodactyloidea.

2.BPMC-0042 represents a new darwinopteran, here named *Kunpengopterus. antipollicatus*. It is the second *kunpengopterus* from the Tiaojishan Formation, and the oldest evidence for a true opposed pollex in the fossil record . In our new phylogenetic analysis, *Kunpengopterus siensis* and *K. antipollicatus* are recovered as the sister-group of them ((*Darwinopterus modularis* + *Cuspicephalus scarffi*) + *Wukongopterus lii*). All Wukongopteridae (((*Darwinopterus modularis* + *Cuspicephalus scarffi*) + *Kunpengopterus*) were recovered as close to *Pterorhynchus wellnhoferi*, with which it comprises the Darwinoptera. With the oldest evidence for a true opposed pollex in the fossil record, darwinopterans keep providing unexpected and invaluable information on the evolutionary history of pterosaur.

3.Jiufotang tapejarids were originally divided into seven nominal species, all entangled in a series of disputed interpretations. We diagnose each species by compelling and unique combinations of features (including autapomorphies) that are unlikely to be explained by intraspecific variation. In our new phylogenetic analysis, we corroborate the view of *Sinopterus dongi* (*Sinopterus gui*, *Huaxiapterus jii*, *Sinopterus lingyuanensis*, and *Huaxiapterus atavismus* as synonymy) as being more closely related to the Yixian tapejarid *Eopteranodon lii* than to *Huaxiadraco corollatus* (*Huaxiapterus benxiensis* as synonymy), and regard *Nemicolopterus crypticus* as a very young, undiagnostic, indeterminate sinopterine.

4.BPMC 0101 provides the first occurrence of maxillary tumor in a fossil

amniote, revealing that tumor formation is not limited to mandible and postcranial elements. This case is of particular interest because of the presence of ameloblastoma in a maxilla, a phenomenon not previously reported in pterosaur and reptiles more broadly. The condition is more severe compared to reported cases of mandibular ameloblastoma in other reptiles. A similar pattern is also observed in human and non-human mammalian ameloblastoma, suggesting an onset pattern that is deeply rooted in the amniote tree of life.

Apart from Chinese pterosaurs in Asia, pterosaur specimens have also been discovered in Japan, Mongolia, Thailand, South Korea, North Korea, Uzbekistan, Kyrgystan, Kazakhstan, Siberia and Lebanon. However, these other Asian pterosaur remains are rather incomplete and scarce if compared to the Chinese record. Based on Chinese pterosaur research, I will pay more attention to the other Asian specimens in the future. Organizing an international collaborative research team focusing in Asian pterosaurs promote the proceeding of the research of pterosaur geographic distribution, migration and evolution in the Asian context. Based on some newfound Asian pterosaur specimens, I have already established the new academic cooperation with Prof. Yasuhisa Nakajima (Tokyo City University, Japan), Prof. Khishigjav Tsogtbaatar (Institute of Paleontology and Geology, Mongolian Academy of Sciences) and Prof. Sita Manitkoon (Mahasarakham University, Thailand). Collaborative description of newfound fossils are ongoing.

REFERENCES

Arnold EN. 1998. Structural niche, limb morphology and locomotion in lacertid lizards (Squamata, Lacertilia); a preliminary survey. Bull. Br. Mus. Nat. Hist. Zool., 64:63–89.

Andres B. 2021. Phylogenetic systematics of *Quetzalcoatlus* Lawson 1975 (Pterodactyloidea: Azhdarchoidea). Journal of Vertebrate Paleontology，41(sup1):203–217.

Andres B, Clark JM, Xu X. 2010. A new rhamphorhynchid pterosaur from the Upper Jurassic of Xinjiang, China, and the phylogenetic relationships of basal pterosaurs. Journal of Vertebrate Paleontology, 30(1):163–187.

Andres B, Clark JM, Xu X. 2014. The earliest pterodactyloid and the origin of the group. Current Biology, 24(9):1011–1016.

Andres B, Ji Q. 2008. A new pterosaur from the Liaoning Province of China, the phylogeny of the Pterodactyloidea, and the convergence in their cervical vertebrae. Palaeontology, 51:453–469.

Andres B, Langston W Jr. 2021. Morphology and taxonomy of *Quetzalcoatlus* Lawson 1975 (Pterodactyloidea: Azhdarchoidea). Journal of Vertebrate Paleontology, 41(sup1):46–202.

Angst D, Barnoud J, Cornette R, Chinsamy A. 2020. Sex and ontogenetic variation in the crest of Numida meleagris: implications for crested vertebrates. The Anatomical Record.

Bakhurina NN, Unwin DM. 1995. A survey of pterosaurs from the Jurassic and Cretaceous of the former Soviet Union and Mongolia. Historical Biology, 10(3):197–245.

Bakker RT, Galton PM. 1974. Dinosaur monophyly and a new class of vertebrates. Nature, 248:168-172.

Barbosa FHS, Porpino KO, Rothschild BM, Silva RC, Domenico Capone D. 2021. First cancer in an extinct Quaternary non-human mammal, Historical Biology, 33(11):2878-2882.

Bardin J, Rouget I, Yacobucci MM, Cecca F. 2014. Increasing the number of discrete character states for continuous characters generates well-resolved trees that do not reflect phylogeny. Integrative Zoology, 9(4):531–541.

Beard KC. 1990. Gliding behavior and paleoecology of the alleged primate family Paromomyidae (Mammalia, Dermoptera). Nature, 345:340-341.

Beccari V, Pinheiro FL, Nunes I, Anelli LE, Mateus O, Costa FR. 2021. Osteology of an exceptionally well-preserved tapejarid skeleton from Brazil: revealing the anatomy of a curious pterodactyloid clade. PLOS ONE, 16(8):e0254789.

Bennett SC. 1989. A pteranodontid pterosaur from the Early Cretaceous of Peru, with comments on the relationships of Cretaceous pterosaurs. Journal of Paleontology, 63:669677.

Bennett SC. 1993. The ontogeny of *Pteranodon* and other pterosaurs. Paleobiology, 19(1):92-106.

Bennett SC. 1994. Taxonomy and systematics of the Late Cretaceous pterosaur *Pteranodon* (Pterosauria, Pterodactyloidea). Occasional Papers of the History Museum/The University of Kansas, 169:1–70.

Bennett SC. 1997. The arboreal leaping theory of the origin of pterosaur flight. Hist. Biol. 12:265-290.

Bennett SC. 2007. A second specimen of the pterosaur *Anurognathus ammoni*. Paläontologische Zeitschrift, 81(4):376.

Bennett SC. 2013. The phylogenetic position of the Pterosauria within the Archosauromorpha re-examined. Historical Biology, 25(5–6):545–563.

Bennett SC. 2014. A new specimen of the pterosaur *Scaphognathus crassirostris*, with comments on constraint of cervical vertebrae number in pterosaurs. Neues Jahrbuch für Geologie und Paläontologie—Abhandlungen, 271(3):327–348.

Benton MJ, Zhonghe Z, Orr PJ, Fucheng Z, Kearns SL. 2008. The remarkable fossils from the Early Cretaceous Jehol Biota of China and how they have changed our knowledge of Mesozoic life. Proceedings of the Geologists’ Association, 119(3-4):209-228.

Bestwick J, Unwin DM, Butler RJ, Henderson DM, Purnell MA. 2018. Pterosaur dietary hypotheses: a review of ideas and approaches. Biol. Rev. Camb. Philos. Soc., 93:2021-2048.

Billerman SM, Keeney BK, Rodewald PG, Schulenberg TS. 2022. Birds of the World. Ithaca, NY, USA: Cornell Laboratory of Ornithology.

Birn-Jeffery AV, Miller CE, Naish D, Rayfield EJ, Hone DW. 2012. Pedal claw

curvature in birds, lizards and mesozoic dinosaurs—complicated categories and compensating for mass-specific and phylogenetic control. PLoS ONE, 7:e50555.

Britt BB, Dalla Vecchia FM, Chure DJ, Engelmann GF, Whiting MF, Scheetz RD. 2018. *Caelestiventus hanseni* gen. et sp. nov. extends the desert-dwelling pterosaur record back 65 million years. Nature Ecology and Evolution, 2(9):1386–1392.

Brown MA, Sagebiel JC, Andres B. 2021. The discovery, local distribution, and curation of the giant azhdarchid pterosaurs from Big Bend National Park. Journal of Vertebrate Paleontology, 41(sup1):2-20.

Burch SH. 2014. Complete forelimb myology of the basal theropod dinosaur *Tawa hallae* based on a novel robust muscle reconstruction method. J. Anat., 225:271-297.

Cai ZQ, Wei F. 1994. A new Late Cretaceous pterosaur from Linhai, Zhejiang (in Chinese). Vertebrata PalAsiatica, 32(3): 181-194 .

Campos D, Kellner AWA. 1997. Short note on the first occurrence of Tapejaridae in the Crato Member (Aptian), Santana Formation, Araripe Basin, Northeast Brazil. Anais da Academia Brasileira de Ciências, 69:83–87.

Chang SC, Zhang H, Renne PR, Fang Y. 2009. High-precision 40Ar/39Ar age for the Jehol Biota. Palaeogeography, Palaeoclimatology, Palaeoecology, 280(1–2):94–104.

Cheng X, Jiang S, Wang X, Kellner AWA. 2016. New information on the Wukongopteridae (Pterosauria) revealed by a new specimen from the Jurassic of China. PeerJ, 4:e2177.

Cheng X, Jiang S, Wang X, Kellner AWA. 2017a. New anatomical information of the wukongopterid *Kunpengopterus sinensis* Wang *et al.*, 2010 based on a new specimen. PeerJ, 5:e4102.

Cheng X, Jiang S, Wang X, Kellner AWA. 2017b. Premaxillary crest variation within the Wukongopteridae (Reptilia, Pterosauria) and comments on cranial structures in pterosaurs. An. Acad. Bras. Cienc, 89:119-130.

Cheng X, Wang X, Jiang S, Kellner AWA. 2012. A new scaphognathid pterosaur from western Liaoning, China. Historical Biology, 24(1):101–111.

Cheng X, Wang X, Jiang S, Kellner AWA. 2015. Short note on a non-pterodactyloid pterosaur from Upper Jurassic deposits of Inner Mongolia, China. Historical Biology, 27(6):749–754.

Choiniere JN, Clark JM, Forster CM, Norell MA, Eberth DA, Erickson GM, Chu H, Xu X. 2013. A juvenile specimen of a new coelurosaur (Dinosauria: Theropoda) from the Middle–Late Jurassic Shishugou Formation of Xinjiang, People's Republic of China. Journal of Systematic Palaeontology, 12(2):177–215.

Chu Z, He H, Ramezani J, Bowring SA, Hu D, Zhang L, Zheng S, Wang X, Zhou Z, Deng C, Guo J. 2016. High-precision U-Pb geochronology of the Jurassic Yanliao Biota from Jianchang (western Liaoning Province, China): age constraints on the rise of feathered dinosaurs and eutherian mammals. Geochemistry, Geophysics, Geosystems, 17(10):3983–3992.

Clark JM, Hopson JA, Fastovsky DE, Montellano M. 1998. Foot posture in a primitive pterosaur. Nature, 391(6670):886–889.

Cobb SE, Sellers WI. 2020. Inferring lifestyle for Aves and Theropoda: a model based on curvatures of extant avian ungual bones. PLoS ONE, 15:e0211173.

Codorniú L, Carabajal AP, Pol D, Unwin DM, Rauhut OW. 2016. A Jurassic pterosaur from Patagonia and the origin of the pterodactyloid neurocranium. PeerJ, 4(1):e2311.

Colless DH. 1985. On “character” and related terms. Systematic Zoology, 34(2):229–233.

Comolli JR, Olsen HM, Seguel M, Schnellbacher RW, Fox AJ, Divers SJ, Sakamoto K. 2015. Ameloblastoma in a wild black rat snake (Pantherophis alleghaniensis). J Vet Diagn Invest., 27(4):536-539.

Costa FR, Alifanov V, Dalla Vecchia FM, Kellner AWA. 2013. On the presence of an elongated tail in an undescribed specimen of Batrachognathus volans (Pterosauria: Anurognathidae: Batrachognathinae). In: Sayão JM, Costa FR, Bantim RAM, Kellner AWA, eds. Short Communications, Rio Ptero 2013—International Symposium on Pterosaurs. Rio de Janeiro: Universidade Federal do Rio de Janeiro, Museu Nacional, 54–56.

Czerkas SA, Ji Q. 2002. A new rhamphorhynchoid with a headcrest and complex integumentary structures. Feathered Dinosaurs and the Origin of Flight, 1:15–41.

Dalla Vecchia FM. 2009. Anatomy and systematics of the pterosaur *Carniadactylus* gen. n. *rosenfeldi* (Dalla Vecchia, 1995). Rivista Italiana di Paleontologia e Stratigrafia, 115(2):159–188.

Dalla Vecchia FM. 2014. Triassic pterosaurs. Geological Society, London, Special Publications, 379(1):119–155.

Dalla Vecchia FM. 2018. Comments on Triassic pterosaurs with a commentary on the "ontogenetic stages" of Kellner (2015) and the validity of Bergamodactylus wildi. Rivista Italiana di Paleontologia e Stratigrafia, 124(2):317-341.

Dalla Vecchia FM. 2019. *Seazzadactylus venieri* gen. et sp. nov., a new pterosaur (Diapsida: Pterosauria) from the Upper Triassic (Norian) of northeastern Italy. PeerJ, 7:e7363.

Davis G A, Zheng Y, Wang C, Darby B J, Zhang C, Gehrels G. 2001. Mesozoic tectonic evolution of the Yanshan fold and thrust belt, with emphasis on Hebei and Liaoning provinces, northern China. Geol Soc Am Mem, 194:171-197.

de Queiroz K, Cantino PD, Gauthier JA. 2020. Phylonyms: A Companion to the PhyloCode. Boca Raton: CRC Press.

Dececchi TA, Larsson HC. 2011. Assessing arboreal adaptations of bird antecedents: testing the ecological setting of the origin of the avian flight stroke. PLoS ONE, 6:e22292.

Döderlein L. 1923. *Anurognathus ammoni* ein neuer Flugsaurier. Sitzungsberichte der Bayerischen Akademie der Wissenschaften, Mathematisch-Naturwissenschaftlichen, 1923:117–164.

Dong ZM. 1982. On a new Pterosauria (*Huanhepterus quingyangensis* gen. et sp. nov.) from Ordos, China (in Chinese with English abstract). Vertebrata PalAsiatica, 20(2): 115-121 .

Duan Y, Zhang LJ, Li L, Cheng SL. 2006. Division and correlation of unique fossil-bearing beds of Jiufotang Formation in Dapingfang-Meileyingzi Basin of western Liaoning (in Chinese with English abstract). Global Geology 25(2):113–119.

Duan Y, Zhang LJ, Zhang LJ, Hu DY. 2010. Division and correlation of unique fossil-bearing beds of Jiufotang Formation in Jianchang Basin of western Liaoning (in Chinese). Chinese Journal of Geology 45(2):606–613.

Dumbravă M, Rothschild B, Weishampel D, Csiki-Sava Z, Andrei RA, Acheson KA, Codrea VA. 2016. A dinosaurian facial deformity and the first occurrence of ameloblastoma in the fossil record. Sci Rep, 6:29271.

Eck K, Elgin RA, Frey E. 2011. On the osteology of *Tapejara wellnhoferi* Kellner 1989 and the first occurrence of a multiple specimen assemblage from the Santana Formation, Araripe Basin, NEBrazil. Swiss Journal of Palaeontology, 130(2):277.

Effiom OA, Ogundana OM, Akinshipo AO, Akintoye SO. 2018. Ameloblastoma: current etiopathological concepts and management. Oral Dis., 24(3):307-316

Ekhtiari S, Chiba K, Popovic S, Crowther R, Wohl, Kin On Wong A, Tanke DH, Dufault DM, Geen OD, Parasu N, Crowther MA, Evans DC. 2020. First case of osteosarcoma in a dinosaur: a multimodal diagnosis. The Lancet Oncology, 21(8):1021-1022.

Elgin RA, Hone DW, Frey E. 2011. The extent of the pterosaur flight membrane. Acta Palaeontologica Polonica, 56(1):99–111.

Ezcurra MD, Nesbitt SJ, Bronzati M, Dalla Vecchia FM, Agnolin FL, Benson RB, Egli FB, Cabreira SF, Evers SW, Gentil AR, Irmis RB, Martinelli AG, Novas FE, da Silva LR, Smith ND, Stocker MR, Turner AH, Langer MC. 2020. Enigmatic dinosaur precursors bridge the gap to the origin of Pterosauria. Nature, 2020:1–5.

Fitzhugh K. 2006. The philosophical basis of character coding for the inference of phylogenetic hypotheses. Zoologica Scripta, 35(3):261–286.

Frey E, Martill DM, Buchy MC. 2003. A new species of tapejarid pterosaur with soft-tissue head crest. Geological Society, London, Special Publications, 217(1):65-72.

Fröbisch J, Reisz RR. 2009. The Late Permian herbivore Suminia and the early evolution of arboreality in terrestrial vertebrate ecosystems. Proc. Biol. Sci., 276:3611-3618.

Gao FL, Jiang Y, Pan YQ, Wang X, Wu ZJ, Fan S, Dai DY. 2018. Division and significance of the precious fossil-bearing beds of Jiufotang Formation in Sihedang area, Liaoning Province. Geology and Resource (in Chinese with English abstract). Geology and Resources, 27(6):503–507.

Gao KQ, Li Q, Wei M, Pak H, Pak I. 2009. Early Cretaceous birds and pterosaurs from the Sinuiju Series, and geographic extension of the Jehol Biota into the Korean Peninsula. Journal of the Paleontological Society of Korea, 25(1):57–61.

Gao KQ, Shubin NH. 2012. Late Jurassic salamandroid from western Liaoning, China. Proceedings of the National Academy of Sciences of the United States of America, 109(15):5767–5772.

Gauthier J. 1986. Saurischian monophyly and the origin of birds. Mem. Calif. Acad. Sci., 8:1–55.

Christel MI, Fragaszy D. 2000. Manual function in *Cebus apella*. Digital mobility,

preshaping, and endurance in repetitive grasping. Int. J. Primatol., 21:697–719.

Goloboff PA, Catalano SA. 2016. TNT version 1.5, including a full implementation of phylogenetic morphometrics. Cladistics, 32:221–238.

Goloboff PA, Farris JS, Nixon KC. 2008. TNT, a free program for phylogenetic analysis. Cladistics, 24(5):774–786.

Goloboff PA, Mattoni CI, Quinteros AS. 2006. Continuous characters analyzed as such. Cladistics, 22(6):589–601.

Goloboff PA, Torres A, Arias JS. 2018. Weighted parsimony outperforms other methods of phylogenetic inference under models appropriate for morphology. Cladistics, 34(4):407–437.

Green TL, Kay DI, Gignac PM. 2022. Intraspecific variation and directional casque asymmetry in adult southern cassowaries (Casuarius casuarius). Journal of Anatomy, 241(4):951-965.

Griffin TM, Main RP, Farley CT. 2004. Biomechanics of quadrupedal walking: how do four-legged animals achieve inverted pendulumlike movements? J. Exp. Biol., 207:3545-3558.

Habib MB. 2011. Functional morphology of anurognathid pterosaurs. Geological Society of America Abstracts with Programs, 43(1):118.

Hamrick MW. 2001. Primate origins: evolutionary change in digital ray patterning and segmentation. J. Hum. Evol, 40:339-351.

Hammer Ø, Harper DA, Ryan PD. 2001. PAST: paleontological statistics software package for education and data analysis. Palaeontol. Electronica 4, 4.

Haridy Y, Witzmann F, Asbach P, Schoch RR, Fröbisch N, Rothschild BM. 2019. Triassic Cancer-Osteosarcoma in a 240-Million-Year-Old Stem-Turtle. JAMA Oncol., 5(3):425-426.

He H, Wang X, Zhou Z, Zhu R, Jin F, Wang F, Ding X, Boven A. 2004. 40Ar/39Ar dating of ignimbrite from Inner Mongolia, northeastern China, indicates a post-Middle Jurassic age for the overlying Daohugou Bed. Geophys Res Lett, 31: L20609.

He XL, Yang DH, Shu CK. 1983. A new middle Jurassic pterosaur from Dashanpu, Zigong, Sichuan (in Chinese). ACTA CHENGDU GEOLOGICAL COLLEGE, S1:27-32.

Hendra FN, Van Cann EM, Helder MN, Ruslin M, de Visscher JG, Forouzanfar T, de Vet HCW. 2020. Global incidence and profile of ameloblastoma: A systematic review and meta-analysis. Oral Dis., 26(1):12-21.

Holgado B, Pêgas RV, Canudo JI, Fortuny J, Rodrigues T, Company J, Kellner AWA. 2019. On a new crested pterodactyloid from the Early Cretaceous of the Iberian Peninsula and the radiation of the clade Anhangueria. Scientific Reports, 9(1):1–10.

Hone DW. 2020. A review of the taxonomy and palaeoecology of the Anurognathidae (Reptilia, Pterosauria). Acta Geologica Sinica-English Edition, 94(5):1676–1692.

Hone DW, Benton MJ. 2007. An evaluation of the phylogenetic relationships of the pterosaurs among archosauromorph reptiles. Journal of Systematic Palaeontology, 5(4):465–469.

Hone DW, Fitch AJ, Ma F, Xu X. 2020. An unusual new genus of istiodactylid pterosaur from China based on a near complete specimen. Palaeontol. Electronica, 23:a09.

Hone DW, Jiang S, Xu X. 2018. A taxonomic revision of *Noripterus complicidens* (Young, 1973) and Asian members of the Dsungaripteridae. Geological Society, London, Special Publications, 455(1):149–157.

Hone DW, Ratcliffe JM, Riskin DK, Hermanson JW, Reisz RR. 2021. Unique near isometric ontogeny in the pterosaur *Rhamphorhynchus* suggests hatchlings could fly. Lethaia, 54(1):106–112.

Hone DW, Tischlinger H, Frey E, Röper M. 2012. A new non-pterodactyloid pterosaur from the Late Jurassic of Southern Germany. PLOS ONE, 7(7):e39312.

Huang D. 2015. Yangliao biota and Yanshan movement. Acta Palaeontologica Sinica, 54:501–546.

Huang D. 2016. The Daohugou biota. Shanghai: Shanghai Scientific & Technical Publishers, 332.

Huang D. 2019. Jurassic integrative stratigraphy and timescale of China. Science China Earth Sciences, 62: 223–255.

Ibrahim N, Sereno PC, Varricchio DJ, Martill DM, Dutheil DB, Unwin DM, Baidder L, Larsson HCE, Zouhri S, Kaoukaya A. 2020. Geology and paleontology of the upper cretaceous Kem Kem group of eastern Morocco. ZooKeys, 928:1–126.

Ibrahim N, Unwin DM, Martill DM, Baidder L, Zouhri S. 2010. A new pterosaur (Pterodactyloidea: Azhdarchidae) from the Upper Cretaceous of Morocco. PLOS ONE, 5(5):e10875.

Jensen JA, Padian K. 1989. Small pterosaurs and dinosaurs from the Uncompahgre fauna (Brushy Basin member, Morrison formation: ?Tithonian), late Jurassic, western Colorado. Journal of Paleontology, (3):364–373.

Ji S, Ji Q. 1998. Discovery of a new pterosaur in Western Liaoning. China Acta Geologica Sinica, 71:115.

Ji S. 2020. First record of Early Cretaceous pterosaur from the Ordos Region, Inner Mongolia, China. China Geological, 1:1-7.

Ji S, Zhang L. 2020. A new Early Cretaceous pterosaur from the Ordos region, Inner Mongolia. Earth Science Frontiers, 27(6):365-370.

Ji Q, Yuan CX. 2002. Discovery of two kinds of protofeathered pterosaurs in the Mesozoic Daohugou Biota in the Ningcheng region and its stratigraphic and biologic significances. Geological Review, 48(2):221–224.

Jiang S, Wang X, Cheng X, Costa FR, Huang J, Kellner AWA. 2014. Short note on an anurognathid pterosaur with a long tail from the Upper Jurassic of China. Historical Biology, 27(6):718–722.

Kellner AWA. 1989. A new edentate pterosaur of the Lower Cretaceous from the Araripe Basin, Northeast Brazil. Anais da Academia Brasileira de Ciências, 61:439–446.

Kellner AWA. 2003. Pterosaur phylogeny and comments on the evolutionary history of the group. Geological Society, London, Special Publications, 217(1):105–137.

Kellner AWA. 2004. New information on the Tapejaridae (Pterosauria, Pterodactyloidea) and discussion of the relationships of this clade. Ameghiniana, 41(4):521–534.

Kellner AWA. 2010. Comments on the Pteranodontidae (Pterosauria, Pterodactyloidea) with the description of two new species. Anais da Academia Brasileira de Ciências, 82(4):1063–1084.

Kellner AWA. 2013. A new unusual tapejarid (Pterosauria, Pterodactyloidea) from the Early Cretaceous Romualdo Formation, Araripe Basin, Brazil. Earth and Environmental Science Transactions of the Royal Society of Edinburgh, 103(3–4):409–421.

Kellner AWA. 2015. Comments on Triassic pterosaurs with discussion about ontogeny and description of new taxa. Anais da Academia Brasileira de Ciências, 87(2):669–689.

Kellner AWA, Campos DA. 2007. Short note on the ingroup relationships of the Tapejaridae (Pterosauria, Pterodactyloidea). Boletim do Museu Nacional, Nova Série, Rio de Janeiro-Brasil. Geologia, 75:1–14.

Kellner AWA, Campos DA, Sayão JM, Saraiva AA, Rodrigues T, Oliveira G, Cruz LA, Costa FR, Silva HP, Ferreira JS. 2013. The largest flying reptile from Gondwana: a new specimen of *Tropeognathus* cf. *T. mesembrinus* Wellnhofer, 1987 (Pterodactyloidea, Anhangueridae) and other large pterosaurs from the Romualdo Formation, Lower Cretaceous, Brazil. Anais da Academia Brasileira de Ciências, 85:113–135.

Kellner AWA, Tomida Y. 2000. Description of a new species of Anhangueridae (Pterodactyloidea) with comments on the pterosaur fauna from the Santana Formation (Aptian-Albian), Northeastern Brazil. National Science Museum, Tokyo, Monographs, 17:1–135.

Kellner AWA, Wang X, Tischlinger H, Campos DA, Hone DW, Meng X. 2010. The soft tissue of *Jeholopterus* (Pterosauria, Anurognathidae, Batrachognathinae) and the structure of the pterosaur wing membrane. Proceedings of the Royal Society B: Biological Sciences, 277(1679):321–329.

Kellner AWA, Weinschütz LC, Holgado B, Bantim RA, Sayao JM. 2019. A new toothless pterosaur (Pterodactyloidea) from Southern Brazil with insights into the paleoecology of a Cretaceous desert. Anais da Academia Brasileira de Ciências, 91:e20190768

Kreppel M, Zöller J. 2018. Ameloblastoma-Clinical, radiological, and therapeutic findings. Oral Dis., 24(1-2):63-66.

Kuhn O. 1967. Die fossile wirbeltierklasse pterosauria. Oeben: Krailing bei München.

Leal MEC, Pêgas RV, Bonde N, Kellner AWA. 2018. Cervical vertebrae of an enigmatic pterosaur from the Crato Formation (Lower Cretaceous, Araripe Basin, NE Brazil). Geological Society, London, Special Publications, 455(1):195–208.

Lehman TM. 2021. Habitat of the giant pterosaur *Quetzalcoatlus* Lawson 1975 (Pterodactyloidea: Azhdarchoidea): a paleoenvironmental reconstruction of the Javelina Formation (Upper Cretaceous), Big Bend National Park. Texas Journal of

Vertebrate Paleontology, 41(sup1):21–45.

Li B, Cheng J, Liu M, Yang F, Wu Z, Du J. 2019. Formation age and geochemical characteristics of the Tiaojishan Formation in the Western Liaoning Province. Geological Review, 65:63–64.

Li JJ, Lü JC, Zhang BK. 2003. A new lower Cretaceous sinopterid pterosaur from Western Liaoning, China. Acta Palaeontologica Sinica 42:442 – 447.

Li Y, Yang C. 2010. Vertebrate fossils from the Shaximiao Formation in Sichuan Basin and their chronology (in Chinese). Proceedings of the 25th Annual Congress of Palaeontological Society of China, 177-178.

Liu Y, Kuang H, Jiang X, Peng N, Xu H, Sun H. 2012. Timing of the earliest known feathered dinosaurs and transitional pterosaurs older than the Jehol Biota. Palaeogeography, Palaeoclimatology, Palaeoecology, 323:1–12.

Liu Y, Liu Y, Ji SA, Yang Z. 2006. U-Pb zircon age for the Daohugou Biota at Ningcheng of Inner Mongolia and comments on related issues. Chinese Science Bulletin, 51(21):2634–2644.

Liu J, Zhao Y, Liu X. 2006. Age of the Tiaojishan Formation volcanics in the Chengde Basin, northern Hebei province (in Chinese). Acta Petrologica Sinica, 22:26172630.

Liu DX, Zhou CF, Wang JQ, Li WG, Wei QW. 2014. New data on the cervical morphology of the Chinese tapejarine. Historical Biology, 27(6):638–645.

Longrich NR, Martill DM, Andres B. 2018. Late Maastrichtian pterosaurs from North Africa and mass extinction of Pterosauria at the Cretaceous-Paleogene boundary. PLOS Biology, 16(3):e2001663.

Lu CZ, Gu MG, Yu YW, Liang H. 2006. Age of the Tangshang Formation in Different Basins of Eastern Zhejiang. Journal of Stratigraphy, 30(1):81−86.

Lucas SG. 2001. Chinese Fossil Vertebrates. Columbia University Press. p.158.

Lü JC. 2009. A new non-pterodactyloid pterosaur from Qinglong County, Hebei Province of China. Acta Geologica Sinica-English Edition, 83(2):189–199.

Lü JC, Bo X. 2011. A new rhamphorhynchid pterosaur (Pterosauria) from the Middle Jurassic Tiaojishan Formation of Western Liaoning, China. Acta Geologica Sinica-English Edition, 85(5):977–983.

Lü JC, Fucha XH, Chen JM. 2010. A new scaphognathine pterosaur from the Middle Jurassic of western Liaoning, China. Acta Geoscientica Sinica, 31(2):263–266.

Lü JC, Gao CL, Liu JY, Meng QJ, Ji Q. 2006c. New material of the pterosaur *Eopteranodon* from the Early Cretaceous Yixian Formation, western Liaoning, China. Geological Bulletin of China, 25:555–571.

Lü JC, Gao YB, Xing LD, Li ZX, Sun ZY. 2007. A new species of *Huaxiapterus* from the Early Cretaceous of western Liaoning, China. Acta Geologica Sinica, 81(5):683–687.

Lü JC, Hone DW. 2012. A new Chinese anurognathid pterosaur and the evolution of pterosaurian tail lengths. Acta Geologica Sinica—English Edition, 86(6):1317–1325.

Lü JC, Ji Q. 2005. A New Ornithocheirid from the Early Cretaceous of Liaoning province, China. ACTA GEOLOGICA SINICA, 79(2):157-163.

Lü JC, Jin X, Gao C, Du T, Ding M, Sheng Y, Wei X. 2013. Dragons of the skies (recent advances on the study of pterosaurs from China). Zhejiang: Zhejiang Science & Technology Press, 127.

Lü JC, Jin XS, Unwin DM, Zhao LJ, Azuma Y, Ji Q. 2006a. A new species of *Huaxiapterus* (Pterosauria: Pterodactyloidea) from the Lower Cretaceous of western Liaoning, China with comments on the systematics of tapejarid pterosaurs. Acta Geologica Sinica, 80(3):315–326.

Lü JC, Liu JY, Wang XR, Gao CL, Meng QJ, Ji Q. 2006b. New material of the pterosaur *Sinopterus* (Reptilia: Pterosauria) from the Early Cretaceous Jiufotang Formation, Western Liaoning, China. Acta Geologica Sinica, 80:783–789.

Lü JC, Meng Q, Wang B, Liu D, Shen C, Zhang Y. 2018. Short note on a new anurognathid pterosaur with evidence of perching behaviour from Jianchang of Liaoning Province, China. Geological Society, London, Special Publications, 455(1):95–104.

Lü JC, Teng FF, Sun DY, Shen CZ, Li GQ, Gao X, Liu HF. 2016. The toothless pterosaurs from China. Acta Geologica Sinica, 90(9):2513-2525.

Lü JC, Unwin DM, Deeming DC, Jin XS, Liu YQ, and Ji Q. 2011a. An Egg-Adult Association, Gender, and Reproduction in Pterosaurs. Science, 331:321-324.

Lü JC, Unwin DM, Jin XS, Liu YQ, Ji Q. 2009. Evidence for modular evolution in a long-tailed pterosaur with a pterodactyloid skull. Proceedings of the Royal Society

B: Biological Sciences, 277(1680):383–389.

Lü JC, Unwin DM, Jin X, Liu Y, Ji Q. 2010. Evidence for modular evolution in a long-tailed pterosaur with a pterodactyloid skull. Proc. Biol. Sci., 277:383–389.

Lü JC, Unwin DM, Xu L, Zhang X. 2008. A new azhdarchoid pterosaur from the Lower Cretaceous of China and its implications for pterosaur phylogeny and evolution. Naturwissenschaften, 95:891-897.

Lü JC, Unwin DM, Zhao B, Gao C, Shen C. 2012. A new rhamphorhynchid (Pterosauria: Rhamphorhynchidae) from the Middle/Upper Jurassic of Qinglong, Hebei Province, China. Zootaxa, 3158(1):1–19.

Lü JC, Xu L, Chang H, Zhang X. 2011b. A new darwinopterid pterosaur from the Middle Jurassic of western Liaoning, northeastern China and its ecological implications. Acta Geol. Sin.-Engl., 85:507-514.

Lü JC, Yuan CX. 2005. New tapejarid pterosaur from western Liaoning, China. Acta Geologica Sinica, 79(4):453-458.

Lü JC, Zhang BK. 2005. New pterodactyloid pterosaur from the Yixian Formation of western Liaoning. Geological Review, 51:458-462.

Manzig PC, Kellner AWA, Weinschütz LC, Fragoso CE, Vega CS, Guimarães GB, Godoy LC, Liccardo A, Ricetti JHZ, de Moura CC. 2014. Discovery of a rare pterosaur bone bed in a Cretaceous desert with insights on ontogeny and behavior of flying reptiles. PLOS ONE, 9(8):e100005.

Maisch MW, Matzke AT, Sun G. 2004. A new dsungaripteroid pterosaur from the Lower Cretaceous of the southern Junggar Basin, north-west China. Cretaceous Research, 25:625-634.

Martill DM, Etches S. 2012. A new monofenestratan pterosaur from the Kimmeridge Clay Formation (Kimmeridgian, Upper Jurassic) of Dorset, England. Acta Palaeontol. Pol., 58:285-294.

Martill DM, Green M, Smith RE, Jacobs ML, Winch J. 2020a. First tapejarid pterosaur from the Wessex Formation (Wealden Group: Lower Cretaceous, Barremian) of the United Kingdom. Cretaceous Research, 113:104487.

Martill DM, Ibrahim N. 2015. An unusual modification of the jaws in cf. *Alanqa*, a mid-Cretaceous azhdarchid pterosaur from the Kem Kem beds of Morocco. Cretaceous Research, 53:59–67.

Martill DM, Smith R, Unwin DM, Kao A, McPhee J, Ibrahim N. 2020b. A new tapejarid (Pterosauria, Azhdarchoidea) from the mid-Cretaceous Kem Kem beds of Takmout, southern Morocco. Cretaceous Research, 112:104424.

Martin-Silverstone E, Glasier JRN, Acorn JH, Mohr S, Currie PJ. 2017. Redescription of *Dawndraco kanzai* Kellner, 2010 and reassignment of the type specimen to *Pteranodon sternbergi* Harksen, 1966. Vertebrate Anatomy Morphology Palaeontology, 3:47–59.

Middleton KM. 2001. The morphological basis of hallucal orientation in extant birds. J. Morphol, 250:51-60.

Meng J, Hu Y, Wang Y, Wang X, Li C. 2006. A Mesozoic gliding mammal from northeastern China. Nature, 444:889-893.

Meng QJ, Ji Q, Zhang YG, Liu D, Grossnickle DM, Luo ZX. 2015. Mammalian evolution. An arboreal docodont from the Jurassic and mammaliaform ecological diversification. Science, 347:764-768.

Mongiardino Koch N, Soto IM, Ramírez MJ. 2015. Overcoming problems with the use of ratios as continuous characters for phylogenetic analyses. Zoologica Scripta, 44(5):463–474.

Naish D, Perron R. 2016. Structure and function of the cassowary's casque and its implications for cassowary history, biology and evolution. Historical Biology, 28(4):507–518.

Naish D, Simpson M, Dyke G. 2013. A new small-bodied azhdarchoid pterosaur from the Lower Cretaceous of England and its implications for pterosaur anatomy, diversity and phylogeny. PLOS ONE, 8(3):e58451.

Naish D, Witton MP. 2017. Neck biomechanics indicate that giant Transylvanian azhdarchid pterosaurs were short-necked arch predators. PeerJ, 5(2):e2908.

Naish D, Witton MP, Martin-Silverstone E. 2021. Powered flight in hatchling pterosaurs: evidence from wing form and bone strength. Scientific Reports, 11(1):1-15.

Napier JR. 1961. Prehensility and opposability in the hands of primates. Symp. Zool. Soc. Lond., 5:115–132.

Napier JR. 1980. Hands, First American Edition (Pantheon Books).

Napier JR, Napier PH. 1967. A Handbook of Living Primates: Morphology, Ecology

and Behaviour of Nonhuman Primates (Academic Press).

Odes EJ, Randolph-Quinney PS, Steyn M, Throckmorton Z, Smilg JS, Zipfel B, Augustine TN, de Beer F, Hoffman JW, Franklin RD, Berger LR. 2016. Earliest hominin cancer: 1.7-million-year-old osteosarcoma from Swartkrans Cave, South Africa. South African Journal of Science, 112(7-8):1-5.

Ősi A. 2011. Feeding-related characters in basal pterosaurs: implications for jaw mechanism, dental function and diet. Lethaia, 44(2):136–152.

Ősi A, Buffetaut E, Prondvai E. 2011. New pterosaurian remains from the Late Cretaceous (Santonian) of Hungary (Iharkút, Csehbánya Formation). Cretaceous Research, 32(4):456–463.

Ősi A, Weishampel DB, Jianu CM. 2005. First evidence of azhdarchid pterosaurus from the Late Cretaceous of Hungary. Acta Palaeontologica Polonica, 50(4):777–787.

Padian K. 1983. Osteology and functional morphology of *Dimorphodon macronyx* (Buckland) (Pterosauria: Rhamphorhynchoidea) based on new material in the Yale Peabody Museum. Postilla, 189:1–44.

Padian K. 1986. A taxonomic note on two pterodactyloid families. Journal of Vertebrate Paleontology, 6:289.

Padian K. 1989. The origin of dinosaurs and the beginning of the age of dinosaurs. Short Courses Paleontol., 2:7–21.

Padian K. 2008a. The Toarcian (Early Jurassic) pterosaur *Dorygnathus* Wagner, 1860. Palaeontology, 80:1–64.

Padian K. 2008b. The Early Jurassic pterosaur *Campylognathoides* Strand, 1928. Palaeontology, 80:65–107.

Pan Y, Sha J, Zhou Z, Fürsich FT. 2013. The Jehol Biota: Definition and distribution of exceptionally preserved relicts of a continental Early Cretaceous ecosystem. Cretaceous Research, 44:30–38.

Petrovic ID, Migliacci J, Ganly I, Patel S, Xu B, Ghossein R, Huryn J, Shah J. 2018. Ameloblastomas of the mandible and maxilla. Ear Nose Throat J., 97(7):E26-E32.

Pêgas RV, Costa FR, Kellner AWA. 2018. New information on the osteology and a taxonomic revision of the genus *Thalassodromeus* (Pterodactyloidea, Tapejaridae, Thalassodrominae). Journal of Vertebrate Paleontology, 38(2):e1443273.

Pêgas RV, Holgado B, David LDO, Baiano MA, Costa FR. 2021. On the pterosaur *Aerotitan sudamericanus* (Neuquén Basin, Upper Cretaceous of Argentina), with comments on azhdarchoid phylogeny and jaw anatomy. Cretaceous Research, 129:e104998.

Pêgas RV, Holgado B, Leal MEC. 2019. On *Targaryendraco wiedenrothi* gen. nov. (Pterodactyloidea, Pteranodontoidea, Lanceodontia) and recognition of a new cosmopolitan lineage of Cretaceous toothed pterodactyloids. Historical Biology, 2019:1–15.

Pêgas RV, Leal MEC, Kellner AWA. 2016. A basal tapejarine (Pterosauria; Pterodactyloidea; Tapejaridae) from the Crato Formation, Early Cretaceous of Brazil. PLOS ONE, 11(9):e0162692.

Pêgas RV, Zhou X, Jin X, Wang K, Ma W. 2023. A taxonomic revision of the *Sinopterus* complex (Pterosauria, Tapejaridae) from the Early Cretaceous Jehol Biota, with the new genus *Huaxiadraco*. PeerJ, 11:e14829.

Pinheiro FL, Fortier DC, Schultz CL, Andrade JAF, Bantim RA. 2011. New information on the pterosaur *Tupandactylus imperator*, with comments on the relationships of Tapejaridae. Acta Palaeontologica Polonica, 56(3):567–580.

Pinheiro FL, Rodrigues T. 2017. *Anhanguera* taxonomy revisited: is our understanding of Santana Group pterosaur diversity biased by poor biological and stratigraphic control?. PeerJ, 5:e3285.

Rehemtulla A. 2010. Dinosaurs and ancient civilizations: reflections on the treatment of cancer. Neoplasia, 12(12):957-968.

Renesto S, Binelli G. 2006. *Vallesaurus cenensis* Wild, 1991, a drepanosaurid (Reptilia Diapsida) from the late Triassic of northern Italy. Rivista Italiana di Paleontologia e Stratigrafia, 112(1):77–94.

Riabinin AN. 1948. Remarks on a flying reptile from the Jurassic of Kara-Tau. Akademii Nauk, Paleontological Institute, Trudy, 15:86–93.

Rothschild BM, Witzke BJ, Hershkovitz I. 1999. Metastatic cancer in the Jurassic. Lancet, 354(9176):398.

Schoener TW. 1968. The Anolis lizards of Bimini: resource partitioning in a complex fauna. Ecology, 49:704-726.

Shen C, Pêgas RV, Gao C, Kundrát M, Zhang L, Wei X, Zhou X. 2021. A new

specimen of *Sinopterus dongi* (Pterosauria, Tapejaridae) from the Jiufotang Formation (Early Cretaceous, China). PeerJ, 9:e12360.

Sigrist T. 2004. Aves do Brasil: uma visão artística. Vinhedo: Avis Brasilis.

Su YS, Gao JH, Li SG, Bu CP, Zhu CQ. 2008. The Basin growth characteristic and hydrocarbon assesment of the Mesozoic in Songnan-Liaoxi Area (in Chinese with English abstract). Geosciences, 22(4):505–519.

Sullivan C, Wang Y, Hone DWE, Wang YQ, Xu X, Zhang FC. 2014. The vertebrates of the Jurassic Daohugou Biota of northeastern China. Journal of Vertebrate Paleontology, 34(2):243–280.

Sustaita D, Pouydebat E, Manzano A, Abdala V, Hertel F, Herrel A. 2013. Getting a grip on tetrapod grasping: form, function, and evolution. Biol. Rev. Camb. Philos. Soc., 88:380-405.

Thiele K. 1993. The Holy Grail of the perfect character: the cladistic treatment of morphometric data. Cladistics, 9(3):275–304.

Tjepkema J, Bell CM, Soukup JW. 2020. Presentation, diagnostic imaging, and clinical outcome of conventional ameloblastoma in dogs. Journal of Veterinary Dentistry, 37(1):6-13.

Unwin DM. 1992. The phylogeny of the Pterosauria. Journal of Vertebrate Paleontology, 12(3):57A.

Unwin DM. 1995. Preliminary results of a phylogenetic analysis of the Pterosauria (Diapsida: Archosauria)'. In: Sixth Symposium on Mesozoic Terrestrial Ecosystems and Biota, Beijing: China Ocean Press, 69–72.

Unwin DM. 2003. On the phylogeny and evolutionary history of pterosaurs. Geological Society, London, Special Publications, 217(1):139–190.

Unwin DM, Bakhurina NN. 1994. *Sordes pilosus* and the nature of the pterosaur flight apparatus. Nature, 371(6492):62–64

Unwin DM, Lü J, Bakhurina NN. 2000. On the systematic and stratigraphic significance of pterosaurs from the Lower Cretaceous Yixian Formation (Jehol Group) of Liaoning. China Fossil Record, 3(1):181–206.

Van Valkenburgh B. 1985. Locomotor diversity within past and present guilds of large predatory mammals. Paleobiology, 11:406–428.

Vidovic SU. 2018. Transformation of quotient values for their use as continuous cladistic characters. bioRxiv

Vidovic SU, Martill DM. 2014. *Pterodactylus scolopaciceps* Meyer, 1860 (Pterosauria, Pterodactyloidea) from the Upper Jurassic of Bavaria, Germany: the problem of cryptic pterosaur taxa in early ontogeny. PLOS ONE, 9(10):e110646.

Vidovic SU, Martill DM. 2017. The taxonomy and phylogeny of *Diopecephalus kochi* (Wagner, 1837) and '*Germanodactylus rhamphastinus*' (Wagner, 1851). Geological Society, London, Special Publications, 455(1):125–147.

Vila Nova BC, Sayão JM, Langer MC, Kellner AWA. 2015. Comments on the cervical vertebrae of the Tapejaridae (Pterosauria, Pterodactyloidea) with description of new specimens. Historical Biology, 27(6):771–781.

Viscardi P, Dyke GJ, Wilkinson M, Rayner JMV. 1999. Missing data and the phylogeny of the Pterosauria. Journal of Vertebrate Paleontology 19:82A.

Vullo R, Marugán-Lobónm J, Kellner AWA, Buscalioni A, Fuente M, Moratalla JJ. 2012. A new crested pterosaur from the Early Cretaceous of Spain: the first European tapejarid (Pterodactyloidea: Azhdarchoidea). PLOS ONE, 7:e38900.

Wang L, Hu D, Zhang L, Zheng S, He H, Deng C, Wang X, Zhou Z, Zhu R. 2013. SIMS U-Pb zircon age of Jurassic sediments in Linglongta, Jianchang, western Liaoning: constraint on the age of oldest feathered dinosaurs. Chin. Sci. Bull., 58:1346–1353.

Wang X, Kellner AWA, Cheng X, Jiang S, Wang Q, Sayao JM, Rodrigues T, Costa FR, Li N, Meng X, Zhou Z. 2015. Eggshell and histology provide insight on the life history of a pterosaur with two functional ovaries. An. Acad. Bras. Cienc. 87:1599–1609.

Wang X, Kellner AW, Jiang S, Cheng X. 2012. New toothed flying reptile from Asia: close similarities between early Cretaceous pterosaur faunas from China and Brazil. Naturwissenschaften, 99(4):249–257.

Wang X, Kellner AW, Jiang S, Cheng X, Meng X, Rodrigues T. 2010. New long-tailed pterosaurs (Wukongopteridae) from western Liaoning, China. Anais da Academia Brasileira de Ciências, 82(4):1045–1062.

Wang X, Kellner AW, Jiang S, Cheng X, Wang Q, Ma Y, Paidoula Y, Rodrigues T, Chen H, Sayão J, Li N, Zhang J, Bantim RAM, Meng X, Zhang X, Qiu R, Zhou Z. 2017. Egg accumulation with 3D embryos provides insight into the life history of a pterosaur. Science, 358(6367):1197-1201.

Wang X, Kellner AW, Jiang S, Wang Q, Ma Y, Paidoula Y, Cheng X, Rodrigues T, Meng X, Zhang J, Li N, Zhou Z. 2014. Sexually Dimorphic Tridimensionally Preserved Pterosaurs and Their Eggs from China. Current Biology, 24:1-8.

Wang X, Kellner AW, Jiang S, Meng X. 2009. An unusual long-tailed pterosaur with elongated neck from western Liaoning of China. Anais da Academia Brasileira de Ciências, 81(4):793–812.

Wang X, Kellner AW, Zhou Z, De Almeida Campos D. 2005. Pterosaur diversity and faunal turnover in Cretaceous terrestrial ecosystems in China. Nature, 437(7060):875–879.

Wang X, Kellner AW, Zhou Z, De Almeida Campos D. 2008. Discovery of a rare arboreal forest-dwelling flying reptile (Pterosauria, Pterodactyloidea) from China. Proc. Natl. Acad. Sci. USA, 105:1983-1987.

Wang X, Zhou Z. 2003a. A new pterosaur (Pterodactyloidea, Tapejaridae) from the Early Cretaceous Jiufotang Formation of western Liaoning, China and its implications for biostratigraphy. Chinese Science Bulletin, 48(1):16-23.

Wang X, Zhou Z. 2003b. Two new pterodactyloid pterosaurs from the Early Cretaceous Jiufotang Formation of Western Liaoning, China. Vertebrata PalAsiatica, 41(1):34-41.

Wang X, Zhou Z. 2004. Pterosaur embryo from the Early Cretaceous. Nature, 429: 621.

Wang X, Zhou Z. 2006. Pterosaur assemblages of the Jehol Biota and their implication for the Early Cretaceous pterosaur radiation. Geological Journal, 41(3–4):405–418.

Wang X, Zhou Z, Zhang F, Xu X. 2002. A nearly completely articulated rhamphorhynchoid pterosaur with exceptionally well-preserved wing membranes and hairs from Inner Mongolia, northeast China. Chinese Science Bulletin, 47(3):226–230.

Wang Y, Saiki K, Zhang W, Zheng S. 2006. Biodiversity and palaeoclimate of the Middle Jurassic floras from the Tiaojishan Formation in western Liaoning, China. Prog. Nat. Sci., 16:222-230.

Warton DI, Wright IJ, Falster DS, Westoby M. 2006. Bivariate line-fitting methods for allometry. Biological Reviews, 81(2):259-291.

Wei X, Pêgas RV, Shen C, Guo Y, Ma W, Sun D, Zhou X. 2021. *Sinomacrops bondei*, a new anurognathid pterosaur from the Jurassic of China and comments on the group. PeerJ, 9:e11161.

Weishampel DB, Dodson P, Osmolska H et al. 2004. The Dinosauria. University of California Press.

Wellnhofer P. 1970. Die Pterodactyloidea (Pterosauria) der OberjuraPlattenkalke Süddeutschlands. Bayerische Akademie der Wissenschaften, Mathematisch-Wissenschaftlichen Klasse, Abhandlungen, 141:1–133.

Wellnhofer P. 1975. Die Rhamphorhynchoidea (Pterosauria) der Oberjura-Plattenkalke Suddeutschlands. Palaeontogr: A, 148:1–33.

Wellnhofer P. 1978. Pterosauria. Handbuch der Palaeoherpetologie, Teil 19. Stuttgart: Gustav Fischer.

Wellnhofer P. 1991. The illustrated encyclopaedia of pterosaurs. London: Salamander Books.

Wellnhofer P, Kellner AWA. 1991. The skull of *Tapejara wellnhoferi* Kellner (Reptilia, Pterosauria) from the Lower Cretaceous Santana Formation of the Araripe Basin, Northeastern Brazil. Mitteilungen der Bayerischen Staatssammlung für Paläontologie und Historische Geologie, 31:89–106.

Witton MP. 2008. A new approach to determining pterosaur body mass and its implications for pterosaur flight. Zitteliana Reihe B: Abhandlungen der Bayerischen Staatssammlung fur Palaontologie und Geologie, B28(28):143–158.

Witton MP. 2009. A new species of *Tupuxuara* (Thalassodromidae, Azhdarchoidea) from the Lower Cretaceous Santana Formation of Brazil, with a note on the nomenclature of Thalassodromidae. Cretaceous Research, 30(5):1293–1300.

Witton MP. 2012. New insights into the skull of *Istiodactylus latidens* (Ornithocheiroidea, Pterodactyloidea). PLOS ONE, 7(3):e33170.

Witton MP. 2013. Pterosaurs: natural history, evolution, anatomy. Princeton: Princeton University Press.

Witton MP. 2015. Were early pterosaurs inept terrestrial locomotors?. PeerJ, 3:e1018.

Wu WH, Zhou CF, Andres B. 2017. The toothless pterosaur *Jidapterus edentus* (Pterodactyloidea: Azhdarchoidea) from the Early Cretaceous Jehol Biota and its paleoecological implications. PLOS ONE, 12(9):e0185486.

Wu ZJ, Gao FL, Pan YQ, Wang X. 2018. Division and correlation of the Jiufotang Formation and their rare fossil-bearing beds in western Liaoning, China (in Chinese with English abstract). Geoscience, 32(4):758-765.

Xi D, Wan X, Li G, Li G. 2019. Cretaceous integrative stratigraphy and timescale of China. Science China Earth Sciences, 62: 256–286.

Xu X, Zhao Q, Norell M, Sullivan C, Hone D, Erickson G, Wang X, Han F, Guo Y. 2009. A new feathered maniraptoran dinosaur fossil that fills a morphological gap in avian origin. Chinese Sci. Bull. 54: 430-435.

Xu X, Zheng X, Sullivan C, Wang X, Xing L, Wang Y, Zhang X, O'Connor JK, Zhang F, Pan Y. 2015. A bizarre Jurassic maniraptoran theropod with preserved evidence of membranous wings. Nature, 521:70–73.

Xu X, Zhou Z, Sullivan C, Wang Y, Ren D. 2016. An updated review of the Middle-Late Jurassic Yanliao Biota: chronology, taphonomy, paleontology and paleoecology. Acta Geol. Sin.-Engl., 90:2229-2243.

Yang ZX, Benton MJ, Hone DW, Xu X, McNamara ME, Jiang B. 2022. Allometric analysis sheds light on the systematics and ontogeny of anurognathid pterosaurs. Journal of Vertebrate Paleontology, 41(5):e2028796.

Yang ZX, Jiang BY, McNamara ME, Kearns SL, Pittman M, Kaye TG, Orr PJ, Xu X, Michael J. Benton MJ. 2018. Pterosaur integumentary structures with complex feather-like branching. Nature Ecology & Evolution, 3: 24-30.

Ye L. 1920. Geological studies of Xishan, Beijing. Special Papers in Geology, 1:192.

Young CC. 1935. On Two Skeletons of Dicynodontia from Sinkiang. ACTA GEOLOGICA SINICA, 14(4): 485-518.

Young CC. 1964. On a new pterosaurian from Sinkiang, China. Vertebrate Palasiatica 8:221–225.

Zhang H, Yang W, Zhou Y, Li D, Dai H, Tan C, Yu H. 2020. Geochemical characteristics and geological significance of the dinosaur fossils burial clasticrocks in the member 1 of Shaximiao Formation in the Yunyang area, Chongqing. Journal of Mineralogy and Petrology, 10:26-35.

Zhang H, Wang MX, Liu XM. 2008. The upper age limit of Tiaojishan Formation (western Liaoning and northern Hebei area) volcanic rocks by LA-ICP-MS. Chinese Science Bulletin, 15:1815–1824.

Zhang L, Yang Y, Zhang L, Guo S, Wang W, Zheng S. 2007. Precious fossil-bearing beds of the lower Cretaceous Jiufotang Formation in Western Liaoning Province, China. Acta Geologica Sinica-English Edition, 81(3):357–364.

Zhang XJ, Jiang SX, Cheng X, Wang XL. 2019. New material of *Sinopterus* (Pterosauria, Tapejaridae) from the Early Cretaceous Jehol Biota of China. Anais da Academia Brasileira de Ciências, 91:e20180756

Zhang YQ, Chen HY. 2015. Study on the characteristics of Tiaojishan Formation (Middle Jurassic) laminar volcanic structure of Chengde Basin. Hebei Geology, 4:8–10.

Zheng X, Bi S, Wang X, Meng J. 2013. A new arboreal haramiyid shows the diversity of crown mammals in the Jurassic Period. Nature, 500:199–202.

Zheng X, You H, Xu X, Dong Z. 2009. An Early Cretaceous heterodontosaurid dinosaur with filamentous integumentary structures. Nature, 458: 333-336.

Zhou CF, Gao K, Yi H, Xue J, Li Q, Fox RC. 2017. Earliest filter-feeding pterosaur from the Jurassic of China and ecological evolution of Pterodactyloidea. R. Soc. open sci: 4160672.

Zhou CF, Niu T, Yu D. 2022. New data on the postcranial skeleton of the tapejarid *Sinopterus* from the Early Cretaceous Jehol Biota. Historical Biology, 1–8.

Zhou CF, Yu D, Zhu Z, Andres B. 2022. A new wing skeleton of the Jehol tapejarid *Sinopterus* and its implications for ontogeny and paleoecology of the Tapejaridae. Scientific Reports, 12(1):1–10.

Zhou XY, Pêgas RV, Leal MEC, Bonde N. 2019. *Nurhachius luei*, a new istiodactylid pterosaur (Pterosauria, Pterodactyloidea) from the Early Cretaceous Jiufotang Formation of Chaoyang City, Liaoning Province (China) and comments on the Istiodactylidae. PeerJ, 7:e7688

Zhou XY, Pêgas RV, Ma W, Han G, Jin X, Leal ME, Bonde N, Kobayashi Y, Lautenschlager S, Wei X, Shen C, Ji S. 2021. A new darwinopteran pterosaur reveals arborealism and an opposed thumb. Current Biology, 31(11):2429–2436.

Zhou Z. 2006. Evolutional radiation of the Jehol Biota: Chronological and ecological perspectives. Geol J, 41:377–393.

Zhou Z. 2014. The Jehol Biota, an Early Cretaceous terrestrial Lagerstätte: new discoveries and implications. Nat Sci Rev, 1:543–559.

Zhou Z, Barrett PM, Hilton J. 2003. An exceptionally preserved Lower Cretaceous ecosystem. Nature, 421(6925):807–814.

Zhou Z, Wang Y. 2010. Vertebrate diversity of the Jehol Biota as compared with other lagerstätten. Science China Earth Sciences, 53(12):1894–1907.

APPENDICEDS

Supplementary File 1: A nexus format file for the software Mesquite, containing the data matrix

https://dfzljdn9uc3pi.cloudfront.net/2021/11161/1/Wei_et_al_2021_Sinomacrops_bondei.nex

Supplemental File 2 : TNT file for *Sinomacrops bondei*

xread

378 56

Macrocnemus_bassanii

100?01101??--?0???--0????0?00?00??01?1000-000?0-110??-----?000020??0???0
0100000-0--0-00?-?-000??0?????00?000?0????0?00???0???????????0-00?01011?00-?
00?0-?000?-????01-00??10000000000001-?000-0100000000000000?0000??000000?
0?001??0???0?000-000000???????00000?????0000200 20??00????11?1211000110
1---??1???--?????00001??0-00--?00-0?????????????????1-??????????01010?0?00???
00?????

Erythrosuchus_africanus

???1?1?????00??21-?????11?00?1??0???1????????0??1???????????1??2?10??1??
???????1?????1?000????12?01010??10?0?????????????????????21?0????????????0-
0?????????????1?031-??00????????????0?????01?????????????????2????0?????00?0??
0?11???0010?0-0??0???211??11?????????????0?????2?????0????01112[0
1]????11?1?????1?????????????????-??--???-???1000201?????00111?0010010101???
0?0?0??010?????[1 2]?

Euparkeria_capensis ???0?1?????00??2[1
2]-??????11?00?1??11??0????????0??1???????????0??2?10??1?????????1?????1?000?
???12?01010??10?0??101??1????1?10??????11?0????????????0-0??1?????????1?03[0
1]???00????????????0?????0?????????????????2????0?????0000?001???1??01000-0
000??0211??11????????????0?????3?????0??0?1111211???11?0?????1?????????????
????-??--???-???100120??????00011?[0 1]010000101???0?0?0??01[0 1]??10?22

Herrerasaurus_ischigualastensis

200?01100110100???--000??0?00?00??00?0-00-510?00100??-----0110020??0???
0010010010--0-00?0?00001?0?????00?0000010000?00???0??00000????0-00101010?
00-?00?0--000--0???0?-0???100000000000000000100100000000000000?0000??10?
00000000???0???0?000-000000???????00000?????000000002000000010?11??2110
00??0?00-??????-0?????00001??0-00--000-0??????????????????????????????0?000?
0?00???20?????

Scleromochlus_taylori

?0?1??1?0??00?021?--0??110010?001101?0-00-??00?0000??--?--0??????10000?
00-00?0010--0-0?01?????10??101?0?1?0????10001????10010000014?10-00???????0?
?1??10-?000--0?012210?011000??0?0???0???????0????????0????00200??0?????0??
0??01???10001000-000??01??1???????00???????0??20010????0?1??11?1[2
3]1???01?0??????1???-0??1???0??????-00--?00-0????0100?????0001???11000?1????
01????01?10??1????

Lagerpeton_chanarensis
??
???1????????????????
????????????????????????????1???1?
001000-0?????????????????????????0???
??????????-??--???-???111120??????00010000100110 01???1?0?1?1110??1??40
Preondactylus_buffarinii
20???110101100002---0??1??110?000?01?1000-010?0??10??---??031011010??1?
??000????0--0-01?????00?0?01??????1?0??????0??????0????????1[2
4]?10-0010101??00-1?010--0?0--?0???[0
1]-0?0002000000000?0011111001111?000?000000200000?1?0????0??0???0????001
1010???????1???010010??????011100021??000?0??1?0021?011100??????0010120??
?0011110?00210?0110?1???????????????00???????0?101?001?001011[1 3]01????[0
1 2]2
Austriadactylus_cristatus
20??0110101100002---0001111101000?01?1000-01020-011100100-0310?101?0?
1?0000020010--0-??010000010001?1?001100?0???1??????10????????4?10-01?010?
1?00-100?0--0?0--00?120-0??00200000000000001111100111110?00?000000[0
2]000?0?1000???0?00??????0000110100?00??????1????????1?????110000?????0????
1???[2
3]1?0?11?0????????????????100010?????2?1?0110?1????????????????????????????1?
?????0??????????????
Austriadraco_dallavecchiai
????????1????0????--0???????0?00??0????0??????????????????????????????????
??????????????1??0?0??1001?02010?01-?0??
0--0???-0???4210???0200000001001?--?1??0?1??0?00??????0?000???0?????????????
???????11010?0?0????????1001000???1?1?11001???????????0?02??0?1????????????
??????????????????1????????????0100??????00001-?0101?0????0?10???????????????
?
Seazzadactylus_venieri
20??11??101??00??---000?????0?00??0????0??1????-??0??---???310101????????
???????0--0-???1?0000?????????????????????0??????0???????????1001?02011?01-?0
0?0--010--????4210???02000000010011--110-011000000?????00?000??????0??????
0???0?????????????0?0????????1????1??????1112???????????????????01111?1?????
01001???0100111?01?0211??11??12???????00201?????????????????1[0
1]1?????????????????
MCSNB_8950
??
???
??0????????????0???
???11010?????????????001011???1110110011??00??????0?021?0201????????011?[0
1]??????0?0[0
1]0??10211??110?1????????????0??????????????0???001??01?10??10???02
Peteinosaurus_zambellii

??????????????????????????????????????0????????????????????????????????????
??[2
4]?10-0?1???1???0-10????-0???-0?0????0??00200000000000?--?1??0?1??0000?000
000?000???1??????????????[0
1]???0?0111100???????????11010??????01?1000?1??00??0?????????011??1?????????
?1??00??01100??00210?0110?12??????????0???000[0 2]??1????101?0010?0??1?[1
3]010?????
Eudimorphodon_ranzii
20??0110101100001---000?12110000?01?1000-10100-020??---?-0310030100?
1?0010020010--0-0100000011020?11001210?0????0?000[0 2]10???????[0
1]4?11001100011?00-10010--010--0100421000002000000010111--1111011000000?
000000[0
1]000?001?0010???000??1?000?0?????0100101010?02111011110?1?111100110000000
00010021?0211111????000021100010011O?11??2[1
2]??0?????210?????00201??????0??????1?0?01????????????????
Arcticodactylus_cromptonellus
??0????010?100????--????????0000??0????0???0?????????????0310001?0?????
??00?????????????0???0?????????????0?????????????????????1??0110?0??????1
00???-??0-????????0??00200000O?0011--110-0?100?000??????02000???0????0????
???????????1???0?00?1?11????10010??????1111200?1??00?000?10???0?011?1?1????
?0001??00?10?110???00211??110?????????????????????????????1000001?????1????
0?????
Carniadactylus_rosenfeldi
20??111011111000??---000???2?10?00??0??1000-?01?1-0?0??-----0310?21??0?????
?0020010--0-0100?00001?0?????00?200?0?0010?????????????????1000?00011?01-
100?0--010?-01014210??002000000010011--110-0110000000-??000?000?0??00010?
0?00??????????11010???010?010101???0??00[0
2]?1101100??0???00?00?0?0?1?0111?????0??001?10000??01100001021[0
1]?0210212?????????????????00????????1?0???10?01010101010?02
Caviramus_schesaplanensis
??????????????????--??
??????????????0????????????????????0?????????????????????2101100201111?00-111??
--0?0--01?04200????100002?01011?--????0?1??100?0?????0?000?0??????????????0?
??
??
Raeticodactylus_filisurensis 20?01110111110001---000?02110000?0101000-101[1
2]1-021211100-0310021100O1?00100200?0--0-0100?00001?020?1?001200?0?0????
0?1210???????12101100201111?00-11100--011--01?04200?0001000020010111--110
-0110010000000000[0
1]000????0??10?0??0?????????????????????????????????????1111100010000?00?
111020?02?00???????????10?????0?101???0?11?0110??1?????????????????????????
00000?1???1?????1??????
Dimorphodon_macronyx
22??0000101100002---2100?30001000?01?0-00-51000-020??-----121113211102?

0010021010--0-11010000011000?110??1000????10?0???10???????14110-011000011?
00110000--0120-11?030-0?0002130100000001--110-01110010?000000[0
2]00000?1??011?0??0?011???000111100100101l??1021010??????111100001000000
0011?0131?0111?1???0??00?[1
3]12000??0110001002l0?0110??2000100?012000100011010101l0?00010001?1110
1000?02
Caelestiventus_hanseni
22??000?101??00???--210?????0?00??0??0-00-5???0-??0??--???1211132??1???
00100????0--0-1??????1?????????????0???????0?0????0???????????0-01?00011?001?
00?0--0120-1???30-0???021301000?0001--?10-01110010?000000?000?????????????
??
??????????????????????????0??
Campylognathoides_liasicus
20000110101100012---0000131101000?01?1000-10100-020??-----13100310000[
0
1]?0010030010--0-10011000010001?11001200?0???10?0002100??????22?10-01002
011?00?10010--010--110030-010002100000000001--000-01100000000000000[0
2]00000?10?010?0?001?1110?000111100100101000112101011101211111001100000?
00110012l?0[1 2]1111???0?000101200010011000l101[1
2]111202101O??10?00?00??????1??????11000[0 1]10?01011[0 1]010?2?32
Campylognathoides_zitteli
20??0110101110012---0000131?01001001?1000-20100-020??-----1310031000?1?
0010030010--0?10011000010?01?11001200???0?????0??10????????2[0
4]?10-01001011?00-10010--010-?100030-0?000210???0000001--000-?110000000000
0000[0
2]000?0??000??????0?01110?000111100100101000112l0?01????2111110011O?????
0?111012??0?11111????0001312O?0110110001101??1122021010?110????0???????1?
?????110?001??01011[0 1]01002?32
Sordes_pilosus
20??1110101110010---000111110100O?01?1000-20110-020??-----1310???01000?
00100?0010--0-110110000120l1?1?001200?0?01111?00?10?1?????12010-0100100?
100?100010?011--1?0?30-0?0022200000000001--000-01000?0100000100000000110
0011?0?001?0110?000?11100100121l??10210104O???2111120021000O??01110031
1121110l??0?000131??0100001200100?10?0110?1200??10103210100l??1011?1?10
100011?1102?211212102
Scaphognathus_crassirostris
20221110111110002---000112110100100l?1000-21111-020??-----131004011001?
0010040010--0-11010000011001?1100l200?0???10?0???10???????12000-01001001
100?10001??011--110030-011021202000000001--000-020000010000010000000O?1
0001000?00111110100001110010010l?????2101020?2211111501110000O??001?013
11111110???0?000?012001000110001002101012021?10?11?103?11??????1??????10
100011211020211212202
Jianchangnathus_robustus
202?1?1011111?0??---0?0??2?10?00??01?1000-211?1-020??-----13100?0??0???

0010040010--0-1101?00001?0?????00?200?0???????????0???????????0-0100100?0
0??00?10001?--1???3?-0?1021202000000001--000-020000010000010000000????000
1???150?010?0???1?????????0?11?0?
?????0??????????0?1?0??002?01?1??212????????????????????????????????01?1??
?1212102

Fenghuangopterus_lii

??22????????1???2?????????1?010?0??1???00-?1?????????????????????1???????
????????????1???0????11??0??1??1??0????????????1????????1411??01??1???????1?
?01??0??--?0?0?0-0?0021202000000001--000?0200000??000?1000000?0??000??????
0111??0??0???????0??101010?1????0??121??11150?21?0000?10?01???1?0111?0????
??00?[0 1]?2?????0?1?0????2??????????00??1??03?10?10?0[0
1]1?1?00010??012??00???????1????

Dorygnathus_banthensis

20001111111110022---0001111101000?0101000-20111-020??-----1010040010001?
0010040010--0-11010000010100?11001200?0001?000000100001110141110020010 0
1100?1000230111--10113210100222020000011001--000-02100000010000001[0
2]00000010001000000011[0 1][0
1]10000011110010010111???02101000?12111115010100000010111003 1?1210100??0
000010030001001100010021010 1[1 2]021100011 0?2020010100211010101000011[0
1]001020101201102

Klobiodon_rochei

????????????????????????????????0???????0????????????????????????????????
??100200?001?00-?00?
?3?111--???????0???22200000011001--?0??021??0?0?0?????1?000????????????????
??
??
??

Bellubrunnus_rothgaengeri

??1?????????????????0?0?????0????????1?00-????????????????????????????????
??
1??111--???????010?22200000101001--000-020000000000?10010?00?????10??????0
1????????01111001 0?????????21?1020???1111110201?0000?1?110?031?1211100????
?011????01?011?0??10221212??2??1?????????10?1????1??111?101??111???02?10
1112?02

Rhamphorhynchus_muensteri

10111111110010022---0000111101000?01111012501110020??----?10100400000
0?0010050000--0-1101000001[0 1]1[0
1]1?11001220001011010 0???0010111012110-02001001110?1000120111--11103[0
1]-011022200000121001--000-020000000000000101000000010110 0?00101[0
1]11000011110020010 11??1021010100[0 1 2]2111115020100000010010 10[2
3]111210110000000113121001101 1?001101212122021120011 0103[0
1]10111002100011110100111111020101100012

Rhamphorhynchus_etchesi

??
??

??????????????????????0??
?????????200????????21010????????115020??000001?010?031?1?11110?????0??????
0011?11????101?12122021 1??
Nesodactylus_hesperius
??????????????????????????????0??
??????????????????????????????????1?0??
??????????????0??0?0?1?0??0??????
???01111??200????????21???2????2???11020??00???1?110?031??????1????????????
??0??01?????101?1212??2????????????0????????????????????????????????
Parapsicephalus_purdoni ?21[0 1]1111?11110022---200111100?00??010???????1[0
1]1-020??-----10100?0?0-01?0010040000--0-11?0000000?12??1100110000?1110?00
0?1???01110??01?0222????????????????????
???????????100??
??
??????????????????????????????
Cacibupteryx_caribensis
?0101111111110021---200111000100??011????????01-0?0??-----10100??10?01?
--10040000--0-???00000?11111?0100?100?010010?000?1?01??11?????????????????
??????????????????????0??0222?00??????01--0?????????????????????100?????????????
??00?????????
??????????????????????????????0??
Qinglongopterus_guoi
??1????1???1???????????0??1?10?????0??1?01????????2?????????????????????0
-10?????????????????000?????????0???200???00?0????????????????????????????????
??1??11???1???3?-0????22200001111001--000-02000????0?????1??0?????0010???0
0?????????0?1110010??????????21?????????111110201??00??1?1?0??3??121??0?????
?010303?????0?1?0???0221102?02????????????10??????1??????10??011??1?02???1
111??2
Harpactognathus_gentryii
?012??111??11????-???????????111??2101?110?????-??1??0?10010100???0?0??
0-?0????????????????????????????????????0?001[0
1]?0????????????????????????0??????0??????????????????0?0?2220000??2??01--0???0?00
0????0???10??101??
??
????????????????????????????
Angustinaripterus_longicephalus
101?1111110110021---0101110101111??01?1?111201?1-021??0?10013100??1100
0?0-10040010--??110000000111[1 2]1?1100121 0?0????0?????10????????[2
4]010-0?001000?00?10001????1--11?132-0?0021200001111001--000-0200000??0?0?
1010?00??
??
????????????????????
Sericipterus_wucaiwanensis
?0121?1111?11?0??---???1????0111??01?1011120???-??1??0?10013100 4??1??1?

0-100????0--0-11?0???0?1?1?????0??200??10???10????0?????????????????0??????0???
????????1--1?1?3??0?0?22200001111001--00??02000????0?0?001??00?0??0?01000??
???0?????????????1001211??1121??0?????????110?1?00000?10110031 1????100???
??????????????????????????????22??210?????????????????0????????????????????????????
???
Dimorphodon_weintraubi
????????????????0??????????????????0??
??
??0????????????????????????????
??????????????????????????????????1?????????????????????021?????????????1????
???11?????1?0???21?????????????????00??????????????????00?0?0??2????1?????
Batrachognathus_volans
??22?---00?--01??0000?1?????1?000?1?00?00-?100011??????--??--?????--1-?1??
????0?????????1???01?0????????1?01?????1100001001??0??1201?????130?10???1
00?0--100--1???2?-0100122020000?0001--000-010000??0?000?000000?0???1???????
????????0?0?11100??0??1?????????????????2003002???020?00?11?111??[1
2]01?????????????????????????001?????????????????????????????00?????????????0?21?
0????211?1????
Sinomacrops_bondei
222??---0??--011?000011?????1?00??11?0-00-?10??11?0-?--------?????--?-?1????
????0--0-???1?1?01???????????10???????1??????0?????????????????????????????0?
-?????????????0???102020000?000???000-010?????0?00?????000?????????????0?????
??0??????0?2?0?????????1?????????120030021??02??????1?1?1?120110??????0????
??????0?0?0???11102?2???0?????????????????????????????10???12??0?02??????????
Dendrorhynchoides_curvidentatus
??22????0??-?????????????????2?000?1?00-00-?1????1??????--????????1??1?????
??????????????????0?????????????01??10011???00??11??0??1201?????1????????1??
00--??0-???0????0?00122020000?000???000-0100????0?00?0??0000?????1????0??0?
?0??010??0???1?2?0101????121?????????11012001 1??000??0?111031?0201101????
0001305??111010200101110202213 1?0???1?????????????1??????1?1??011?0102?21
1110?02
Luopterus_mutoudengensis
??2?????0??-?????????????????2?00??1??0-00-?1????1??????--????????????????
??1??????????????????????????????????
0--????????????0???122020000?000???000-0100????0????????000?????1???????????
??????101011?2?0?????????????????????1101200????00????????????[0
1]20??0??????????0??????0?120??011112?2213??????????????????????????????????1
1?0?0????10?????
Jeholopterus_ningchengensis
??22?---0??--01??000???11?0?2100??1?00-00-?100?11??????--???-?????--1-?1???
????0????????????0?????????????01??????1?0?00??01??0??1????????1?0??????????
0--?0????????2?-0100122020000?0001--000-0100????0???00???000?0?1?1????0?001?
0010?0?10???112?01110101 12???0??????1101100 11??00???0?101031?0201101?????
0013050????00020??01110202213 1?0???10?000002?01??101??0?101?00111010212

11012?02
Anurognathus_ammoni
2222?---0-?-?00?100?0-111?0?2100??1100-00-?101011?0??-------?????1?-1??????
0?0010--0-???11?001?0?[1
2]?011001101??1???1?0-0010??0?01012010-0?013001?0??10000--000--1?0?2?-0?00
12202000000001--000-0100000000000000000010?1?2??????001??110?0110000111?
01011????21?????????1101100110?00001?0111031?0201101 0????00130500100000
200101110202211 1?0??11???????2?1???10?????1010001110102120101 2?02
Vesperopterylus_lamadongensis
??2?????0??-??????????1?????2??0??1??0-00-?????????????-???????????1?????
??????????????????0????????????01??????1?0??????????????????????????????
0-?????????????0???122020000?0001--000-010??0?00?00000??000?????2???????0??
?????0?10000111?0????????21?????????1101100?1??00????????????020??0?????????
????????0012???011102?2211??????????????????????????????001110?02??????2??
?
Pterorhynchus_wellnhoferi
?01??---???--11??1?0???????1??00??01?1000-0????00?1??01010----????--?-???0
0???0?0-?0-110???00??????????0??20?0?001???????0???????????0-0000?????0?????
?10?0?0--1???0?-0???2?200?01000001--000-2000????0?000000?0001???1???0????0?
??????0?0?????0????????????????????????????400????00????0?????????1????????????
??????????????????????0??
Kunpengopterus_sinensis
001?1---1??--11??1100-0??3?10?00??01?1000-121?100?1??012?0-----???--?-?00
0?1600?0--0-1101?1000????????10?310?1????0?0????0??31011????0-??001001?00-?
00?10?010--1???0?-01??22200001000001--000-200000001000000?0000???11??0?
0?00???1???0?0111100?00????????21?102?????1111400?10000??101??????011??0?
0????????24????000120??002101?1102????????????2?????????????????????111?1?12?
??11?????
Wukongopterus_lii
001?0---1??--11??1113?0?????01000?01?1000-021?100?1??000?0----????--0-?0
0001600??????1101?1000????????00?210?1????0??????0???????12110-0000100 1?0
0-100010?010--10?10[0
2]10?0?22200001000001--000-200000001?000000000010??11?10?0?00?1111?10001
11100000121 1??1121010?????11111400?1??000??0011[0
1]??110211?01?????0113?4??10000120000300??11011?01?????????????????1??????
101??11??11120301202112
Darwinopterus_modularis
00101---1??--11011113-01131101000?01???00-0211100?10101010-----??1--0-10
000160010--0-1101010000001?01100121 0?1???1??101[0
1]10???????10110-00001001?00-10001?00?0--10?00210100222000010000 01--000-2
0000000100000000000010?11?110?0?000111101000111100000101 1??11210?020111?
1111400210?000?101110001?0?111010?0?00113?40?111001200100300101101 1?010
110?100000000?01?10110101?0111111120311202002
Cuspicephalus_scarfii

00??1---1??--11??1113?0??3?10?00??01???00-021?100?1??01010----????--?-?00?
???00?0--0-???1?1000????????00?210?1??????1????0?????????????0??10?1??0-?0
0??????0-????????0???2?2?????????????????????????????0000?0?000?????????????
??
??
Changchengopterus_pani
????????1??
??
??0??1???0?0??00?1?
1?1000110?00?001?11??1?????????????111120021??0?0???1110131?0211101?????01
11240??110022000??310?012?1?2011111?0[0
1]000?00??100?011101?111??11?20311100002
Germanodactylus_cristatus
?01?1-?-1??--??011????11311?1000?01?1?00-00?3??0?10101000-??????1--?-1
00010?1010?-0-110011?0?00-111112013 20?1???????12[0
2]0????????10110-0000????10??1??0????10-?10?13210?1021230000000001--000?1
100?????????????000??1??1?0?????01001??0??????????1??1010101????0??????????
???1?????0??0?110021????01?1????00111???01???1??000?????????????????????22?
00?????????????011???1?0?1?1111??12?4[0 1]
Pterodactylus_antiquus
001?1---10?--01211100-01031101000?01?0-00-0112100?0??---------???1--?-100
01061010--0-11000100000-1?01111132 0?2????0?011[0
2]10???????14110-00001001?00?1000200000--10?13210100212000000000001--000?
2100000000000000000000112000?0??0?011010110000111001?11???1210102001
211121500110000?101?00?31?012111100???00132400 1??00220110031020220 21?
011111120[0 2]0020111??0111111?100211011020112-12?31
Pteranodon_sternbergi 010[0 1]1--?10?--01201102-0113[1
2]101110?01?1100-422[1
2]100?0??----------??1--?-?01200?110125111110011 1001-[1
2]0011000230 11??10??0?111011?????23110-200010010 00?1000301000--10?000-11?
?----------?----------?---101???10111101011101 11?10000112100200000???
12?1?0021112151021011011 0?01111300??31110??11100??3?0?1???0??0010?32120
22?3010001120030111000021100100111112 1?0?11?0112-0??40
Anhanguera_piscator
01011--?1----01221102-01121101010?0100-10-0010100?10130101-----??1--?-00
100161111001011100111000-000110002301101100??????1??1????12110-00001001?
0001000 2?000211101100-0?0021202001011101--000?021000000111001000101010110?
1011111??111101111000011211020011?121121201222112151021101010011111130?
022012111111?????? 0111110200010031??0220?01??01?01??????101011?111111100
121101112 0??2-???40
Painten_protopterodactyloid
?????-??????-??021?????10321?1??0????1???????1?????????????????????1?-?-1??
0?????1?????1???00???00?11111??1??0??????????[0
1]?1????????1211?????????????0-1??0?????????1?100???00????0?????????????????

?????????????0????0?????00?0?00?10?10100001O?10???101?????????????????????????
2?????0??0?11?131????11?1?????0013????100?0??001???????????10011110100201
2001??1?1111110l???1?1?0?2031??01?12
;

cnames
{0
Skull,_height,_exclusive_of_cranial_crests_(modified_from_Witton_2012,_Dalla_Vecchia_2019) under_25%_jaw_length over_25% over_30%;
{1
Skull,_dorsal_margin_above_naris_+_antorbital_fenestra_(or_naof),_excluding_cranial_crest_(modified_from_Andres_et_al._2014,_Vidovic_&_Martill_2017_char._79) nearly_straight concave_ convex;
{2 Skull,_entire_margin,_lateral_shape_in_dorsal_view concave/sigmoidal straight convex;
{3
Skull,_in_dorsal_view,_the_pre-orbital_lateral_margin_is_(Vidovic_&_Martill,_2017) straight concave convex;
{4 Skull,_ventral_margin_at_the_articulation_with_mandible_(Dalla_Vecchia_2019) Straight_ Curved_down_caudally;
{5 External_naris,_size_relative_to_skull_openings_(Lü_et_al.,_2009) form_the_largest_skull_opening smaller_than_the_orbit_or_antorbital_opening;
{6 External_naris,_dorsoventrally_compressed absent present;
{7 External_naris,_dorsal_and_ventral_margins,_orientation_(Andres_et_al._2014) acute_angle subparallel_;
{8
External_naris_(or_nasoantorbital_fenestra),_position_relative_to_the_premaxilla_ main_part_dorsal_to_the_ventral_margin_of_the_premaxilla
main_part_displaced_posterior_to_the_premaxilla;
{9 Antorbital_fenestra,_position_(Dalla_Vecchia_2019) lies_level_with_the_naris lies_partially_or_totally_lower_than_the_naris;
{10 Antorbital_fenestra,_shape_(Dalla_Vecchia_2019) length_more_than_twice_the_height_ length_twice_the_height_or_less;
{11
Antorbital_fenestra,_dorsal_and_ventral_margins,_orientation_(Andres_et_al._2014) subparallel acute_angle;
{12 Antorbital_fenestra_ventral_margin_relative_to_external_naris_ventral_margin level ventral;
{13
Antorbital_fenestra_plus_external_naris_(or_nasoantorbital_fenestra),_extension_(Dalla_Vecchia_2019) under_50%_skull_length 50%_skull_length_or_more;
{14 Antorbital_fenestra_and_external_naris,_configuration_ separated confluent,_forming_a_nasoantorbital_fenestra;
{15 (Naso)antorbital_fenestra,_posterior_margin,_shape_(Vidovic_&_Martill,_2017)

straight convex concave;
{16 (Naso)antorbital_fenestra,_posterior_margin,_orientation posterodorsally_reclined perpendicular anterodorsally_reclined;
{17 Nasoantorbital_fenestra,_height_(modified_from_Lü_et_al.,_2009) height_similar_to_or_greater_than_anteroposterior_length elongate;
{18 Nasoantorbital_fenestra,_anterior_end__(Dalla_Vecchia_2019) bordered_by_the_premaxilla_ bordered_by_the_maxilla;
{19 Nasoantorbital_fenestra,_posterodorsal_margin,_shape concave angled;
{20 Orbit,_shape_ subcircular quadrangular_(broad_base) piriform_(dorsoventrally_elongated)_;
{21 Orbit,_size_relative_to_antorbital_fenestra Larger_than_antorbital_fenestra_ Smaller_than_antorbital_fenestra;
{22 Orbit,_length_relative_to_skull_(Dalla_Vecchia_2019) under_half_skull_length about_or_over_half_skull_length;
{23 Orbit,_supraorbital_process_intrudes_into_the_orbit_(Vidovic_&_Martill,_2017) present absent;
{24 Superior_temporal_fenestra,_ventral_margin_(Vidovic_&_Martill,_2017) below_the_middle_of_the_orbit above;
{25
Inferior_temporal_fenestra,_shape_(modified_from_Wang_et_al._2012,_Andres_et_al._2014) trapezoidal,_broad piriform,_with_dorsal_portion_wider_than_ventral__piriform,_with_ventral_portion_wider_than_dorsal_ elliptical;
{26 Inferior_temporal_fenestra,_position_(Vidovic_&_Martill,_2017) behind_the_orbit under_the_orbit,_but_more under_the_orbit,_but_no_more_posterior_than_the_orbit under_the_orbit_and;
{27 Inferior_temporal_fenestra,_orientation_(Andres_et_al._2014) subvertical inclined;
{28 Jaws,_broadness_in_occlusal_view_(modified_from_Kellner_2003,_char._2) narrowing_to_a_point
broader_than_long_with_arching_jaws,_describing_a_semi-ellipse
broader_than_long_with_arching_jaws,_describing_a_semi-circle;
{29
Jaws,_lateral_margin,_nutrient_foramina_positioned_in_a_row_(Andres_et_al.,_2014) present absent;
{30 Jaws,_anterior_occlusal_margin,_shape_(modified_from_Andres_et_al._2014) rounded_edges sharp_or_ridge_(forming_tomial_edge);
{31 Jaws,_posterior_occlusal_margins,_shape_(modified_from_Andres_et_al._2014) rounded sharp_of_ridged;
{32 Jaws,_upper_and_lower_jaws's_occlusal_surface_(Vidovic_&_Martill,_2017) fit_together_ are_opposed,_not_fitting;
{33 Jaws,_opposition,_orientation_of_jaws_axis_(Vidovic_&_Martill,_2017) diverging_anteriorly posterior_to_occluding_jaw_tips;
{34 Rostrum,_shape_(modified_from_Andres_et_al._2014) laterally_attenuated_ anteroposteriorly_shortened_ dorsoventrally_depressed_ laterally_flattened_;

{35 Rostrum,_dorsal_taper_(lateral_view)_(modified_from_Andres_et_al._2014) subparallel attenuated;
{36 Rostrum,_cross-section_of_rostrum_at_external_nares_(Vidovic_&_Martill,_2017) convex_sides concave_sides straight_sides_;
{37 Rostrum,_tip,_shape blunt pointed_tip;
{38 Rostrum,_pointed_tip,_anteroposterior_taper_in_lateral_view broad_(over_20°) slender_(under_20°);
{39 Rostrum,_anterior_lateral_expansion_forming_a_rosette absent present;
{40 Rostrum,_rostral_process_(modified_from_Andres_et_al._2014) absent present;
{41 Rostrum,_rostral_process,_shape_(cross-section)_(modified_from_Andres_et_al.2014) triangular elliptical;
{42 Rostrum,_occlusal_line_shape_(modified_from_Vidovic_&_Martill_2017,_77) straight mainly_straight,_downturned_tip mainly_straight,_upturned_tip downturned upturned sigmoidal;
{43 Rostrum,_prenarial,_dorsal_outline_(modified_from_Vidovic_&_Martill_2017,_78) straight convex concave/sigmoidal;
{44 Rostrum,_length_(pm-naof)_relative_to_the_skull_length_(pm-sq) reduced,_under_20%_ elongated,_between_20_and_50% extremely_elongated_(more_than_half_of_skull_length);
{45 Premaxilla,_posterior_extension_(Vidovic_&_Martill,_2017) does_not_extend_to_the_orbit extends_to_the_orbit,_but_no_further_than extends_to_the_posterior_portion_of_the_orbit extends_past_the_orbit;
{46 Premaxilla,_posteroventral_(maxillary)_process_bordering_ventrally_the_external_naris_(Dalla_Vecchia_2019) present_ absent;
{47 Premaxilla,_posterodorsal_margin_of_nasoantorbital_fenestra_(including_nasal),_width_ wide thin;
{48 Premaxillary_process_separating_the_external_nares_anteriorly_(anterior_narial_bar),_thickness_ wide narrow_;
{49 Premaxilla,_maxillary_process,_position_(Andres_et_al._2014) contacts_nasal_ reaches_posterior_half_of_external_naris_ anterior_to_middle_of_external_naris_;
{50 Premaxilla,_prenarial_premaxillary_bony_crest absent present;
{51 Premaxillary_sagittal_crest,_anterior_margin,_orientation_(Andres_et_al._2014) inclined_caudally approximately_verticle inclined_rostrally;
{52 Premaxillary_sagittal_crest,_anterior_margin,_position_relative_to_rostrum_tip_(modified_from_Andres_et_al._2014) level_with_the_rostrum_tip posterior_to_the_rostral_tip,_but_close close_to_narial_margin;
{53 Premaxillary_crest,_prenarial,_shape low anteriorly_tall posteriorly_tall

semicircular;
{54 Premaxillary_crest,_prenarial,_posterior_extension restricted_to_prenarial_region extending_onto_orbitotemporal_region beyond_occipital_region;
{55 Premaxillary_bony_crest,_texture_(Andres_et_al._2014) striated smooth branching_system_of_broad_grooves;
{56 Premaxillary_crest,_prenarial,_concentric_striae_(Holgado_et_al._2019) absent present;
{57 Premaxillary_crest,_thickness_(Andres_et_al._2014) single_plate two_plates_separated_by_trabeculae;
{58 Maxilla,_antorbital_fossa_(modified_from_Andres_et_al._2014) present absent;
{59 Maxilla,_dorsal=ascending_process,_shape_in_lateral_view_(modified_from_Dalla_Vecchia_2019) short,_broad_and_triangular____ long,_broad_and_arched_backward long,_very_thin_and_straight_ long,_thin_and_slightly_arched_backward_;
{60 Maxilla,_nasal_process_inclined_backwards_(modified_from_Unwin_2003) absent present;
{61 Maxilla,_nasal_process,_backward_inclination_(Dalla_Vecchia_2019) more_than_125_° 125°_or_less;
{62 Maxilla,_dorsoventrally_elongated_foramen_in_the_lateral_side_of_the_basal_part_of_the_dorsal_(Dalla_Vecchia_2019) absent present;
{63 Maxilla,_premaxillary_process,_shape_in_lateral_view__(Dalla_Vecchia_2019) triangular,_tapering_and_pointed,_shorter_and_deeper_than_the_jugal_process_ triangular,_tapering_and_pointed,_low_and_long_like_the_jugal_process_ trapezoidal_and_deep_ trapezoidal_and_low_ harpoon-shaped;
{64 Maxilla,_jugal_process,_shape_in_lateral_view__(Dalla_Vecchia_2019) triangular,_tapering_regularly_to_a_point_ subtrapezoidal,_tapering_to_a_point_only_distally,_proximal_part_with_parallel_dorsal_and_ventral_margins_ rectangular;
{65 Maxilla,_caudal_ramus_expands_ventrally_(Wang_et_al._2012) present absent;
{66 Maxilla,_dorsal_process_(Andres_et_al.,_2014) broad slender_(thinner_than_the_dorsal_process_of_the_jugal);
{67 Maxilla-nasal_contact broad narrow;
{68 Maxilla_and_internal_naris,_contact_ absent_ present_;
{69 Nasal,_contacts_antorbital_fenestra_(Vidovic_&_Martill,_2017) present absent;
{70 Nasal_bar,_broad_with_a_thin_distal_projection_(Vidovic_&_Martill,_2017) present absent;
{71 Nasal_descending_process present absent;
{72 Nasal_descending_process,_position_ placed_laterally placed_medially;
{73 Nasal_descending_process,_length_ long_(almost_reaching_the__ventral_margin_of_the_skull) short knob-like_(extremely_reduced);
{74 Nasal_descending_process,_orientation_(modified_from_Andres_et_al._2014) inclined_anteriorly subvertical inclined_posteriorly;

{75 Nasal_descending_process,_lateral_foramen_ absent_ present_;
{76 Lacrimal,_shape_in_lateral_view__(Dalla_Vecchia_2019) crescent-shaped 'massive_vertical_bar ' 'atched-shaped_with_slender_jugal_process' 'straight_slender_bar ' 'C-shaped,_arched_over_the_antorbital_fenestra' 'short_and_quadrangular' 'massive,_triangular_to_T-shaped';
{77 Lacrimal,_foramination absent_ present,_small present,_enlarged;
{78 Lacrimal,_orbital_process_ absent_ present_;
{79 Frontal,_extension,_anterior_to_the_lacrimal-jugal_bar_(Lü_et_al.,_2009) present absent;
{80 Frontal,_ossified_crest absent present;
{81 Frontal,_ossified_crest,_position_ confined_to_posterior_end_of_skull starting_above_orbit starting_on__posterior_half_of_nasoantorbital_fenestra;
{82 Frontal,_ossified_crest,_shape_(Andres_et_al._2014) low,_blunt short._spike-like,_dorsally_deflected spike-like,_directed_posteriorly narrow,_broad,_directed_posteriorly low,_broad_base,_fans-shaped high,_broad_base,_crown-shaped high,_broad_base,_casqued-shaped high,_broad,_directed_posteriorly,_at_least_doubling_shight_of_skull_above_orbit absent;
{83 Parietal,_ossified_crest absent present;
{84 Parietal,_ossified_crest,_shape_ blunt_ constituting_the_base_of_the_posterior_portion_of_the_cranial_crest expanded,_with_rounded_margin;
{85 Jugal,_antorbital_fossa_(modified_from_Andres_et_al._2014) present absent;
{86 Jugal,_maxillary_process absent present;
{87 Jugal,_maxillary_process,_extension_(Andres_et_al.,_2014) posterior_to_nasoantorbital_fenestra_(or_narial)_anterior_margin same_level_or_anterior;
{88 Jugal,_lacrimal_process_base,_width_ broad narrow;
{89 Jugal,_ascending_process_base_width_(Andres_et_al.,_2014) broad narrow;
{90 Jugal,_lacrimal_process,_inclination_ inclined_anteriorly subvertical inclined_posteriorly;
{91 Jugal,_presence_of_pronounced_ridge_on_the_lateral_side absent present;
{92 Jugal,_lacrimal_and_postorbital_processes,_shape_(Andres_et_al._2014) separated_by_distinct_angle infilled_by_concave_flange;
{93 Jugal,_rostrally_expanded_to_overlap_most_of_the_maxilla_laterally_(Dalla_Vecchia_2019) absent present;
{94 Jugal,_posterior_process_(Vidovic_&_Martill,_2017) (tri-radiate)_lacks_the_posterior_process possesses_the_posterior_process_(tetra-radiate);
{95 Jugal,_ventral_margin_(Andres_et_al.,_2014) straight concave convex;
{96 Jugal,_posterior_process,_orientation posterior ventral;
{97 Jugal/lacrimal_contact_(Vidovic_&_Martill,_2017) in_the_ventral_half_of_the_orbit approximately_in_the_middle_of_the_orbit

in_the_dorsal_half_of_the_orbit;
{98
Jugal,_maxillary_process,_extends_under_the_(naso)antorbital_fenestra_(Vidovic_&_Martill,_2017) by_more_than_half_the_length_of less_than_half_the_length_of_the_vacuity;
{99
Jugal,_if_tri-radiate,_ventral_apex_of_the_jugal,_position_(Vidovic_&_Martill,_2017) _anterior_to_the_quadratojugal_ posterior_to_the_anterior_margin_of_the_quadratojugal;
{100
Jugal,_postorbital_process,_orbital_process_invading_orbit_(Andres_et_al.,_2014) present absent;
{101
Quadratojugal,_robust_(wider_than_quadrate)_and_the_quadrate_is_distinct_from_(Vidovic_&_Martill,_2014) present absent;
{102 Squamosal,_shape_(modified_from_Andres_et_al._2014) unexpanded rounded expanded;
{103 Squamosal,_position_(Andres_et_al._2014) above_base_of_lacrimal_process_of_jugal
below_or_level_with_base_of_lacrimal_process_of_jugal;
{104 Squamosal,_otic_process_large_and_conspicuous_(Vidovic_&_Martill,_2017) present absent;
{105 Quadrate,_inclination_relative_to_ventral_margin_of_skull_ anteriorly subvertical inclined_about_120 ° _posteriorlyned_about_120 ° _backwards_ inclined_about_150° _posteriorly;
{106 Quadrate,_cranio-mandibular_articulation,_position_relative_to_orbit_ _posterior_to_orbit below_posterior_half_of_orbit below_center_of_orbit below_anterior_half_of_orbit anterior_to_orbit;
{107 Quadrate,_shape_(Andres_et_al.,_2014) broad thin_and_cylindrical;
{108 Helical_jaw_joint absent_ present_;
{109 Occiput,_orientation_(Andres_et_al._2014) posterior posteroventral ventral;
{110 Supraoccipital_pneumatic_foraminae_(Andres_et_al.,_2014) present absent;
{111 Basioccipital,_length_relative_to_width_(Andres_et_al._2014) shorter_than_wide longer_than_wide;
{112 Basisphenoid,_body_length_(Wang_et_al._2012) shorter_than_wide at_least_longer_than_wide;
{113 Basipterygoid_processes_(modified_from_Andres_et_al._2014) relatively_short elongated;
{114 Palatal_elements,_shape_ broad thin_bars;
{115 Palate,_incisive_foramen_(Vidovic_&_Martill,_2017) present absent;
{116 Palate,_occlusal_surface smooth discrete_palatal_ridge,_tapering_anteriorly_ strong_palatal_ridge,_tapering_anteriorly
strong_palatal_ridge,_confined_to_the_posterior_portion_of_the_palate;
{117 Palate,_posterior_palatal_plates_of_the_maxilla,_surface flat convex;

{118
Palate_in_the_cross-section_of_the_rostrum_at_the_external_nares_(Vidovic_&_Martill,_2017) straight_ concave convex_;
{119 Palate_surface_shape_at_rostral_tip_(Vidovic_&_Martill,_2017) straight concave convex;
{120
Palate,_the_posterior_palate_descends_below_the_ventral_jugal_margin_(Vidovic_&_Martill,_2017) present absent;
{121 Palatal_tip,_dorsal_deflection_forming_deltoid_facet absent present,_with_first_alveoli_pair_not_surpassing_second_one present,_with_first_alveoli_pair_surpassing_second_one;
{122 Pterygoid,_lateral_process_(Vidovic_&_Martill,_2017) present absent;
{123 Pterygoids,_medial_contact_(Vidovic_&_Martill,_2017) separate contact;
{124 Postpalatine_fenestra,_shape quadrangular/subtriangular oval egg-shaped elongated_egg-shaped_ kite-shaped,_rounded_margin elliptical reduced,_slit-like;
{125 Secondary_subtemporal_fenestra absent present;
{126 Interpterygoid_fenestra,_size smaller_than_subtemporal_fenestra larger_than_subtemporal_fenestra_ extremely_reduced;
{127 Interpterygoid_fenestra,_shape compressed_laterally broad,_longer_than_wide compressed_anteroposteriorly,_wider_than_long round;
{128 Pterygoid_fenestra absent_ present;
{129 Lower_jaw_(Vidovic_&_Martill,_2017) extends_beyond_the_rostrum is_in_line_with_the_rostrum doesn't_extend_to_the_extent_of_the_rostrum;
{130
The_dorsal_and_the_ventral_margins_of_lower_jaw,_beneath_the_antorbital_fenestra_(Vidovic_&_Martill,_2017) bowed,_diverging_ bowed,_converging equidistant/parallel converging diverging;
{131
The_angle_between_the_ventral_mandibular_symphysis_and_the_dorsal_jaw_tip_is_45-90_(Vidovic_&_Martill,_2017) present absent;
{132
Mandible_mid-depth_relative_to_length_(Andres_et_al._2014,_Vidovic_&_Martill_2017_ch._255) _at_most_one-ninth_the_length more_than_one-ninth_the_length;
{133
Mandible,_anterior_end,_dorsal_margin_shape_(modified_from_Andres_et_al._2014) level eminence;
{134
Mandible,_anterior_dorsal_eminence,_height_(modified_from_Andres_et_al._2014) low high;
{135 Mandible,_anterior_half,_main_axis,_orientation straight downturned upturned;
{136 Mandible,_anterior_tip,_orientation continuous_with_main_axis downturned_relative_to_main_axis upturned_relative_to_main_axis hooked;
{137 Mandible,_lateral_surface,_foramination_(modified_from_Andres_et_al._2014) absent_or_incipient a_row_close_to_occlusal_border large_foramina;

{138 Mandible,_lateral_surface,_surface_(modified_from_Andres_et_al._2014) smooth pitted;
{139 Mandibular_rami,_dorsal_margin_anterior_to_the_glenoid_fossa,_shape_(Dalla_Vecchia_2019) dorsally_pointed more_or_less_convex_without_points_or_depressions_ with_two_low_dorsal_peaks_separated_by_a_depression_ totally_straight concave;
{140 Mandible,_elongation_(Dalla_Vecchia_2019) ratio_mandibular_length/height_at_mid-ramus_higher_than_9 ratio_mandibular_length/height_at_mid-ramus_lower_than_9;
{141 Mandible,_surangular_eminence_(modified_from_Unwin,_2003) absent present;
{142 Mandible,_external_mandibular_fenestra__(Dalla_Vecchia_2019) present_ absent;
{143 Mandibular_rami,_elevation_relative_to_symphysis_(modified_from_Lü_et_al.,_2009) level_with_symphysis elevated_well_above_level_of_symphysis;
{144 Mandibular_rami,_orientation_(Andres_et_al._2014) straight_to_upturned downcurved;
{145 Mandibular_ramus,_lateral_surface,_arched_ridge_bounded_dorsally_and_ventrally_ by_narrow_grooves_(Dalla_Vecchia_2019) absent_ present;
{146 Dentary,_mandibular_bony_crest,_extent limited_to_the_rostral_part_of_the_dentary_ continuing_posteriorly_as_a_low_flange_up_to_the_end_of_the_dentary;
{147 Dentary,_extension_relative_to_mandible_(Vidovic_&_Martill_2017) <50%_length_of_lower_jaw _>50%;
{148 Dentary,_large_oval_foramina_every_2_alveoli_(Dalla_Vecchia_2019) absent_ present;
{149 Dentary,_cup-shaped_structures_(Dalla_Vecchia_2019) absent_ present;
{150 Dentary_symphysis_fused present absent;
{151 Dentary_symphysis,_extension_(modified_from_Kellner_2003) short,_limited_to_the_tip short,_extended_posteriorly_less_than_33%_of_mandible_length 33%-55%_the_mandible_length >_55%;
{152 Dentary_symphysis,_occlusal_surface,_anterior_end,_shape approximately_flat_or_slightly_concave fossa convex keeled;
{153 Dentary_symphysis,_posteroventral_cavity absent present;
{154 Dentary,_tip,_well_projected_anteriorly absent_ present_;
{155 Dentary,_tip,_odontoid_process absent present;
{156 Dentary,_ventral_surface_(modified_from_Andres_et_al._2014) smooth keeled crested;
{157 Dentary_ossified_sagittal_crest,_anterior_extension_(modified_from_Andres_et_al._2014) posterior_to_mandibular_tip at_mandibular_tip;

{158 Dentary_ossified_sagittal_crest,_shape_ shallow blade-like deep,_broad_in_lateral_view elongated_ridge absent;
{159 Dentary,_posterior_extension_(modified_from_Andres_et_al._2014) does_not_extend_inbetween_angular_and_surangular extends_between_angular_and_surangular;
{160 Articular,_articular_facet_(Vidovic_&_Martill,_2017) forms_a_right_angle_with_the_retroarticular_process_ forms_an_oblique_angle_with_the_retroarticular_process_;
{161 Glenoid_fossa,_condyle_orientation_(modified_from_Andres_et_al._2014) parasagittal oblique;
{162 Retroarticular_process,_elongation_(Vidovic_&_Martill,_2017) short elongate;
{163 Retroarticular_process,_shape_(modified_from_Andres_et_al._2014) triangular subcircular elongate blunt posteriorly_expanded;
{164 Retroarticular_process,_orientation_(Vidovic_&_Martill,_2017) in_line_with_jaw ascending descending;
{165 Retroarticular_process,_if_descending_(modified_from_Dalla_Vecchia_2019) inclined_about_35° less_than_35°;
{166 Dentition present absent;
{167 Dentition,_pterygoidal_teeth present absent;
{168 Dentition,_premaxilla,_distribution even_along_the_premaxilla premaxillary_tip_edentulous;
{169 Dentition,_position_relative_to_nasoantorbital_fenestra_(modified_from_Vidovic_&_Martill_2017,_66) present_under_nasoantorbital_fenestra absent_under_nasoantorbital_fenestra;
{170 Dentition,_tooth_spacing_along_jaws_(modified_from_Andres_et_al._2014) mesial_teeth_spaced_wider_apart even_along_jaws distal_teeth_spaced_wider_apart;
{171 Dentition,_mesial_teeth,_spacing_relative_to_successive_teeth_(modified_from_Andres_et_al._2014) nearly_touching at_most_diameter_of_teeth more_than_diameter_of_teeth;
{172 Dentition,_distal_teeth,_spacing_relative_to_successive_teeth_(modified_from_Andres_et_al._2014) nearly_touching at_most_diameter_of_teeth more_than_diameter_of_teeth;
{173 Dentition,_crowns,_outline_in_labial/lingual_view_(modified_from_Vidovic_&_Martill_2017,_48) triangular_(continuous_taper_towards_a_point) needle-like_(mostly_subparallel,_tapering_to_a_point_at_the_tip) subrectangular_(subparallel_converging_to_a_blunt_tip) lanceolate_(expanded_above_cervical_region,_then_tapering_to_a_point);
{174 Dentition,_crowns,_cross-section_(modified_from_Vidovic_&_Martill_2017,_52) elliptical,_slightly_compressed elliptical,_strongly_compressed subcircular;

{175 Dentition,_crown,_apex_number_(modified_from_Dalla_Vecchia,_2019) single bifid;
{176 Dentition,_crowns,_apex_shape_(modified_from_Vidovic_&_Martill_2017,_47) tapered blunt bulbous;
{177
Dentition,_crowns,_main_axis_orientation_(modified_from_Andres_et_al._2014,_Vidovic_&_Martill_2017,_49) posteriorly_recurved lingually_recurved sigmoidal;
{178 Dentition,_crowns,_lateral_orientation_(modified_from_Andres_et_al._2014) subvertical inclined_laterally;
{179 Dentition,_crowns,_anteroposterior_inclination upright mesial_crowns_procumbent all_crowns_procumbent;
{180 Dentition,_crowns,_curvature_degree_(modified_from_Andres_et_al._2014) displacement_less_than_tooth_diameter displacement_at_least_tooth_diameter;
{181 Dentition,_crown,_texture_(modified_from_Andres_et_al._2014) smooth striated;
{182 Dentition,_crowns,_cusps_(modified_from_Dalla_Vecchia,_2019) unicuspid multicuspid;
{183 Dentition,_crown,_serration present absent;
{184
Dentition,_serrated_crowns,_number_of_denticles_(modified_from_Andres_et_al._2014) at_least_50 under_50;
{185
Dentition,_serrated_crowns,_denticle_shape_(modified_from_Dalla_Vecchia,_2019) square_or_chisel-like triangular;
{186
Dentition,_variation_in_crown_shape_along_the_upper_jaw_(Dalla_Vecchia,_2019) isodont_ heterodont;
{187
Dentition,_variation_in_crown_shape_along_the_lower_jaw_(Dalla_Vecchia,_2019) isodont_ heterodont;
{188
Dentition,_maxillary_teeth_much_enlarged_below_the_dorsal_process_(Dalla_Vecchia,_2019) absent_ present;
{189
Dentition,_enlarged_maxillary_teeth_below_the_dorsal_process,_number_(modified_from_Vidovic_&_Martill_2017,_68) one two;
{190 Dentition,_peg-like_(cone-shaped)_crowns_(Kellner_2003) absent_ present,_15_or_less_on_each_side_of_the_upper_jaws
present,_more_than_15_on_each_side_of_the_upper_jaws;
{191 Dentition,_anterior_crowns,_height_relative_to_basal_width under_twice_as_wide over_twice_as_wide,_under_4x_as_wide over_4x_as_wide over_10x_as_wide;
{192
Dentition,_crown_elongation,_transition_along_jaws_(modified_from_Andres_et_al.

_2014) continuous_transition_along_tooth_row disparity_between_mesial_and_distal_teeth;
{193
Dentition,_distal_lower_crowns,_size_relative_to_distal_upper_crowns_(modified_from_Dalla_Vecchia_2019) comparable,_at_least_to_part_of_maxillary_crowns_ much_smaller much_larger;
{194
Dentition,_distal_mandibular_crowns,_shape_relative_to_distal_maxillary_crowns_(modified_from_Dalla_Vecchia_2019) similar_ different;
{195 Dentition,_mandibular_teeth,_constricted_collum__(Dalla_Vecchia_2019) absent_ present;
{196
Dentition,_diastema_with_a_concave_outline_between_the_first_two_dentary_teeth_and_those_following_posteriorly_(Dalla_Vecchia_2019) absent_ present;
{197 Dentition,_number_of_mandibular_teeth_(Dalla_Vecchia_2019) more_than_6_tooth_pairs_ six_pairs_or_less;
{198
Dentition,_first_pair_of_premaxillary_teeth,_relatively_small_and_closely_spaced absent present;
{199 Dentition,_anterior,_marked_variation_in_crown_base_width absent present;
{200
Dentition,_upper_jaw,_5th_pair_of_teeth_medially_displaced_(modified_from_Jacobs_et_al._2019,_Holgado_&_Pêgas_2020) absent present;
{201
Dentition,_upper_jaw,_3rd_pair_of_teeth,_size_relative_to_4th_pair_(modified_from_Pêgas_et_al._2019,_Holgado_&_Pêgas_2020) subequal_or_smaller_than larger,_under_twice_the_size twice_the_size,_or_more;
{202
Dentition,_spacing,_first_pair_separated_by_a_thin_sheet_of_bone_(less_than_half_the_alveolous_width)_(modified_Vidovic_&_Martill_2017,_61_and_Pêgas_et_al._2019) absent present;
{203
Dentition,_spacing,_first_three_pairs_more_closely_spaced_than_subsequent_teeth absent present;
{204
Dentition,_upper_jaw,_variation_in_the_size_of_the_anterior_teeth_with_the_5th_and_6th_smaller_than_the_4th absent_ present_;
{205
Dentition,_crown_orientation_relative_to_jaw_margin,_lateral_view__(modified_from_Vidovic_&_Martill_2017,_72,_73) subperpendicular anteriorly_inclined dramatic_change_in_direction,_with_anterior_teeth_anteriorly_inclined;
{206
Dentition,_crowns,_occlusion_between_upper_and_lower_jaws_(modified_from_Vidovic_&_Martill_2017,_76) mesiodistal_interlock crown-on-crown,_apical_occlusion

crown-on-crown,_mesiodistal_oclusion labiolingual_occlusion;
{207
Alveoli,_position_relative_to_occlusal_plane_(modified_from_Holgado_et_al._2019) level raised_(dorsoventrall),_forming_an_elevated_alveolar_row;
{208 Alveoli,_prominently_scalloped_(Pêgas_et_al._2019) absent present;
{209 Alveoli_borders,_thickness laminar slightly_intumesced strongly_intumesced;
{210 Atlas_and_axis_(Howse_1986) unfused_ fused_;
{211 Distinct_cervical_zygapophyses_(Vidovic_&_Martill_2017) present absent;
{212 Postzygapophysis_of_axis_(Vidovic_&_Martill_2017) extended_posterior_from_the_centrum approximately_in_line_with_the_centrum anterior_of_the_centrum;
{213 Third_cervical_vertebra,_centrum_length_(Baron_2020) subequal_to_the_axis_centrum longer_than_the_axis_centrum_;
{214 Mid-cervicals,_neural_spines,_height_(modified_from_Howse_1986) tall low extremely_reduced;
{215 Mid-cervical_vertebrae,_ribs_(Howse_1986,_Dalla_Vecchia_2019) long,_with_filiform_shafts_extending_caudally_up_to_the_successive_cervical_centrum_ reduced,_without_filiform_shaft absent;
{216 Mid-cervical_vertebrae,_postexapophyses_(Howse_1986) absent_ present_;
{217
Mid-cervical_vertebra_neural_arch_lateral_surface_pneumatic_foramen_(Andres_et_al._2014) absent present;
{218
Mid-cervical_vertebra_centrum_lateral_surface_pneumatic_foramen_(Andres_et_al._2014) absent present;
{219
Mid-cervical_vertebra_lateral_to_neural_canal_pneumatic_foramina_(Andres_et_al._2014) absent present;
{220
Mid-cervical_vertebrae_neural_spines_lateral_outline_shape_(Andres_et_al._2014) blade_ triangular ridge fan;
{221 Mid-cervicals,_arch,_accessory_pneumatic_foramen absent present;
{222 Cervical_9,_shape_(Andres_et_al._2014) dorsalized cervicalized;
{223 Notarium absent_ present_;
{224 First_dorsal_rib_more_robust_than_other_ribs_(Vidovic_&_Martill,_2017) present absent;
{225 Lateral_processes_on_the_dorsals_(Vidovic_&_Martill,_2017) approximately_twice_as_long_as_the_neural_spine approximately_equal_in_length_to_the_neural_spine_;
{226 Lateral_processes_on_the_dorsals_are_(Vidovic_&_Martill,_2017) oblique_to_the_vertebral_centrum perpendicular_to_the_vertebral_centrum_;
{227 Sacral_vertebrae,_number_(Dalla_Vecchia_2019) three_or_less_ more_than_three;
{228 Neural_spines_of_sacral_vertebrae_(Vidovic_&_Martill,_2017)

fused_(supraneural_plate)_ unfused;
{229 Sacral_ribs_(Naish_et_al._2013) separate fused_for_part_of_their_length,_forming_fenestrated_sacral_shield;
{230 Proximal_caudal_vertebrae_have_distinct_lateral_processes_(Vidovic_&_Martill,_2017) present absent;
{231 Proximal_caudal_vertebrae_centrum,_centrum_shape_(Wang_et_al.,_2012) single douplex;
{232 Neural_spines_and_hypapophyses_of_caudals_(Vidovic_&_Martill,_2017) slender_and_rod-like_ robust;
{233 Caudal_vertebrae,_number_(from_Kellner,_2003) over_15 15_or_less;
{234 Caudal_vertebrae,_elongation__(Dalla_Vecchia_2019) short,_longest_caudal_centrum_less_than_twice_a_mid-dorsal_centrum elongate,_longest_caudal_centrum_over_twice_a_mid-dorsal_centrum;
{235 Caudal_vertebrae,_zygapophyses_forming_rod-like_ossified_processes_(modified_from_Andres_et_al._2014) absent present;
{236 Caudal_vertebrae,_rod-like_processes_of_zygapophyses,_extension_(modified_from_Andres_et_al._2014) relatively_short_(extending_only_a_little_beyond_the_centrum) elongate_(forming_a_stiff_sheath_over_the_caudal_series);
{237 Caudal_vertebrae,_hemapophyses_sending_filiform_processes_below_the_adjacent_centra__(Dalla_Vecchia_2019) absent_ present;
{238 Caudal_series,_length_respect_to_the_dorsal_series__(Dalla_Vecchia_2019) longer_ shorter;
{239 Caudal_vertebrae,_quantity_ more_than_15_ 15_or_less_;
{240 Coracoid,_relative_dorsoventral_length_(Dalla_Vecchia_2019) less_than_two-thirds_length_of_scapula from_at_least_two-thirds_up_to_similar_length_to_scapula longer_than_scapula_;
{241 Scapula,_proximal_end_ elongated_ sub-oval_;
{242 Scapula,_shape_ elongated_ stout,_with_constructed_shaft_;
{243 Scapula,_orientation_relative_to_vertebral_column_(Vidovic_&_Martill,_2017) perpendicular_to_the_vertebral_column adjacent_to_the_vertebral_column;
{244 Glenoid_fossa_is_located_mainly_on_the_(Vidovic_&_Martill,_2017) scapula coracoid scapulocoracoid;
{245 The_cross-section_of_the_scapula_is_(Vidovic_&_Martill,_2017) rounded spatulate;
{246 Supracoracoideus_crest_(Vidovic_&_Martill,_2017) present absent;
{247 Supracoracoideus_crest_(Vidovic_&_Martill,_2017) prominent not_prominent;
{248 Supracoracoideus_crest_(Vidovic_&_Martill,_2017) proximal_to_the_glenoid distal;
{249 Post-glenoid_strut_(Vidovic_&_Martill,_2017) present absent;

{250 Distal_end_of_the_coracoid_(Vidovic_&_Martill,_2017) has_distinct_condyles _rounded_and_blunt;
{251 Coracoid,_shape_(Dalla_Vecchia_2019) subcircular_or_crescentic_ with_(dorsoventrally)_elongated_and_broad_shaft,_flattened_at_midshaft_ with_strut-like_shaft,_slender_and_cylindrical_at_midshaft;
{252 Coracoid,_relative_dorsoventral_length__(Dalla_Vecchia_2019) less_than_2/3_length_of_scapula_ 2/3_or_more_length_of_scapula;
{253 Coracoid,_proximal_end,_shape flattened oval;
{254 Coracoid,_sternal_articulation_ no_developed_articulation articulation_surface_straight_or_slightly_concave articulation_surface_strongly_concave;
{255 Coracoid,_sternal_articulation,_posterior_expansion_ absent present;
{256 Sternal_plate,_shape_(Dalla_Vecchia_2019) triangular_ quadrangular_ semicircular_or_triangular_inverted_(apex_opposite_to_cristospine)_ small_and_narrow;
{257 Sternal_plate,_lateral_process_on_each_side_of_its_posterior_end_(Dalla_Vecchia_2019) absent_ present;
{258 Sternum_is_approximately_one_and_a_half_times_the_length_of_its_width_(Vidovic_&_Martill,_2017) present absent;
{259 Posterolateral_periphery_of_the_sternal_plate_is_(Vidovic_&_Martill,_2017) square triangular semicircular;
{260 Anterolateral_periphery_of_the_sternum_plate_is_(Vidovic_&_Martill,_2017) square convex,_tapering_anteriorly concave,_tapering_anteriorly;
{261 Cristospine,_shape absent_ shallow_and_elongated_ deep_and_short;
{262 Forelimb_(h+u+mcIV+phalanges_of_digit_IV),_relative_length_(Dalla_Vecchia_2019) less_than_2.5_times_the_length_of_hind_limbs_(fe+ti+mtIII)_ 2.5_times_the_length_of_hind_limbs_or_more;
{263 Humerus,_proportional_length_relative_to_the_femur_(hu/fe)_(modified_from_Kellner_2003,_char._55) hu/fe_=_0.85_or_lower 1.6_>_hu/fe_>___0.85 1.60_or_over;
{264 Humerus,_proportional_length_relative_to_the_metacarpal_IV_(hu/mcIV)_ hu/mcIV_>_2.50_ 1.50_<_hu/mcIV_<_2.50_ 0.40_<_hu/mcIV_<_1.50 hu/mcIV_<_0.40;
{265 Deltopectoral_crest,_projection_(Dalla_Vecchia_2019) scarcely_developed_(less_wide_than_humeral_shaft)_ well-developed_and_projecting;
{266 Deltopectoral_crest,_shape_of_main_shaft_(modified_from_Kellner_2003,_Unwin_2003,_Andres_et_al._2014,_Dalla_Vecchia_2019) Trapezoidal,_narrow Trapezoidal,_broad Subtriangular Subrectangular Hooked Tongue-shaped_(laterally_longer_than_proximodistally_broad);

{267
Deltopectoral_crest,_distal_tip,_orientation_(modified_from_Kellner_2003,_Unwin_2003,_Andres_et_al._2014,_Dalla_Vecchia_2019) continuous_with_main_shaft warped;
{268
Deltopectoral_crest,_distal_end,_shape_(modified_from_Kellner_2003,_Unwin_2003,_Andres_et_al._2014) unexpanded slightly_expanded hatchet-shaped;
{269 Deltopectoral_crest,_size_relative_to_humeral_head_(Vidovic_&_Martill,_2017) longer_than_the_humeral_head_is_wide subequal_to_humeral_head not_as_long_as_the_humeral_head_is_wide extremely_reduced_;
{270
Humerus_plus_ulna,_proportional_lengths_relative_to_the_femur_plus_tibia_(hu+ul/fe+ti)_
humerus_plus_ulna_about_0.80%_or_less_of_femur_plus_tibia_length_(hu+ul/fe+ti_<_0.80)_
humerus_plus_ulna_larger_than_0.80%_of_femur_plus_tibia_length_(hu+ul/fe+ti_>_0.80)_;
{271
Humerus,_proximal_end,_small_foramen_on_dorsal_surface_distal_to_proximal_articulation absent present;
{272
Humerus,_proximal_end,_foramen_on_ventral_surface_close_to_proximal_margin_absent_ present_;
{273 Humerus,_ulnar_crest,_development reduced well-developed;
{274 Humerus,_ulnar_crest,_shape triangular trapezoidal rounded;
{275 Humerus,_distal_surface,_shape oval_or_D-shaped_ subtriangular_;
{276 Humerus,_between_distal_condyles,_pneumatic_foramen_(Andres_et_al._2014) absent present;
{277 Humerus,_shaft,_cross-section_(Andres_et_al._2014) subcircular tapered;
{278 Humerus,_distal_surface,_pneumatic_foramen_(Andres_et_al._2014 absent present;
{279
Humerus,_entepicondyle,_anteroposterior_width_(modified_from_Andres_et_al._2014) entepicondyle_wider_than_ectepicondyle ectepicondyle_at_most_entepicondyle_width;
{280 Brachial_crest_on_the_humeral_diaphysis_(Vidovic_&_Martill,_2017) prominent not_prominent;
{281
In_palmar_view_the_humeral_diaphysis,_from_the_head_to_the_condyle_(Vidovic_&_Martill,_2017) bent straight;
{282
In_cranial_view_the_humeral_diaphysis,_from_the_head_to_the_condyle_(Vidovic_&_Martill,_2017) bent straight;
{283

Humeral_head_flares_out_from_the_diaphysis_giving_an_S-shape_or_T-shape_to_the_(Vidovic_&_Martill,_2017) present absent;
{284 Humeral_head,_size_relative_to_condylar_end_(Vidovic_&_Martill,_2017) more_than_twice_the_width_of_the_condyle approximately_twice less_than_twice_the_width_of_the_condyle approximate_the_same;
{285 Humerus,_epicondyles,_shape_(Vidovic_&_Martill,_2017) angular rounded;
{286
Round_fossa_in_the_anconal_surface_of_the_humerus_(Vidovic_&_Martill,_2017) present absent;
{287 Ulna,_length_relative_to_humerus_(Dalla_Vecchia_2019) less_than_1.5_times_length_of_humerus 1.5_times_length_of_humerus_or_more;
{288 Ulna,ulna/tibia_ratio__(Dalla_Vecchia_2019) <0.9 0.9-1.2 >1.2;
{289 Ulna,_length_relative_to_metacarpal_IV ul/mcIV_>_3.60 3.60_>_ul/mcIV_>_2.00 2.00_>_ul/mcIV_>_1.00 1.00_>_ul/mcIV;
{290 The_articulations_of_the_ulna_are_(Vidovic_&_Martill,_2017) much_wider_than_the_diaphysis not_much_wider;
{291 Hooked_olecranon_process_of_the_ulna_(Vidovic_&_Martill,_2017) present absent;
{292 Ulna_and_radius,_diameter_at_midshaft_(Kellner_2003) subequal_ diameter_of_radius_about_half_that_of_ulna
diameter_of_radius_less_than_half_that_of_ulna;
{293 Hooked_proximal_tubercle_of_radius_(Vidovic_&_Martill,_2017) present absent;
{294 Proximal_syncarpal,_large_posterodistal_process absent present;
{295 Proximal_syncarpal,_shape_(proximal_view)_(Unwin_2003) quadrangular_or_irregular pentagonal;
{296 Distal_syncarpals,_shape_(distal_view)_(Unwin_2003) irregular form_rectangular_unit_ form_triangular_unit;
{297
Distal_syncarpal,_ventral_articular_facet_for_metacarpal_IV,_size_relative_to_dorsal_facet_(Andres_et_al.,_2014) ventral_facet_smaller subequal_in_size;
{298 Distal_syncarpal_cross-section_shape__(Andres_et_al.,_2014) rectangular triangular;
{299 Pteroid_(Vidovic_&_Martill,_2017) present absent;
{300 Pteroid,_width_relative_to_radius_(Vidovic_&_Martill,_2017) at_least_approximately_half_the_width_of_the_radius much_thinner_than_radius;
{301 Pteroid,_shape_of_epiphysis_(Vidovic_&_Martill,_2017) Pteroid_with_a_broad_epiphysis_ simple_rod;
{302 Pteroid,_orientation_(Vidovic_&_Martill,_2017) straight proximally_bent,_distally_straight distally_bent,_proximally_straight bowed;
{303 Pteroid,_elongation_(Dalla_Vecchia_2019) 1/6_ulnar_length_or_less 1/6_-_2/5_ulnar_length more_than_2/5_ulnar_length more_than_half_ulnar_length;
{304 Pteroid,_shape_(Andres_et_al_2014) anged_at_midsection stout_hook straight_and_tapered_with_expanded_proximal_end straight_with_expanded_ends

curved_slender_rod curved_and_subparallel-sided;
{305 Lateral_carpal,_shape_(Vidovic_&_Martill,_2017) robust slender,_much_like_the_pteroid;
{306 Metacarpal,_distal_end_between_condyles,_shape flat medial_ridge_;
{307 Metacarpal_IV,_diaphyseal_crest/carina_(crista_metacarpi)_(Vidovic_&_Martill,_2017) present absent_(smooth,;
{308 Roller_joint_of_wing-metacarpal_(Vidovic_&_Martill,_2017) approximately_round ellipse;
{309 Roller_joint_of_the_wing_metacarpal_(Vidovic_&_Martill,_2017) _flush_with_the_anterior_margin_of_the_diaphysis rounded_on_the_anterior_margin;
{310 Metacarpus,_metacarpals_articulating_with_carpus_(Dalla_Vecchia_2019) all_only_some_or_one;
{311 Metacarpal_IV,_posterior_crest_(Vidovic_&_Martill_2017) absent_ present;
{312 Metacarpus,_metacarpal_IV-humerus_ratio_(Dalla_Vecchia_2019) less_than_35% more_than_35%_but_less_than_80% more_than_80%;
{313 Metacarpus,_relative_length_of_elements_I-III_(Dalla_Vecchia_2019) metacarpal_I_<_metacarpal_II_<_metacarpal_III_ metacarpal_I_<_metacarpal_II_=_metacarpal_III_ All_the_same_length;
{314 Unguals_on_manus_(Vidovic_&_Martill,_2017) larger_than_on_pes smaller,_or_equal_to_those_on_pes;
{315 Digit_three_phalanx_one_morphology_(Vidovic_&_Martill,_2017) straight_and_similar_to_all_other_phalanges has_a_kink_in_its_proximal_portion_;
{316 Digit_three_phalanx_one_is_more_robust_than_the_other_long_bones_in_the_manus_(Vidovic_&_Martill,_2017) present absent;
{317 Manus_digits,_digit_IV,_relative_length__(Dalla_Vecchia_2019) Equal_or_less_than_65%_total_forelimb_length_ more_than_65%_total_forelimb_length;
{318 Manual_digit_IV_first_phalanx,_extension_relative_to_whole_finger_(Dalla_Vecchia_2019) less_than_35%_wing_finger_length_ 35%_wing_finger_length_or_more;
{319 Manual_digit_IV_first_phalanx,_proportional_length_relative_to_metacarpal_IV_(ph1d4/mcIV)_ both_small_and_reduced_ ph1d4/mcIV>4.0 4.0>ph1d4/mcIV>2.0 '2.0>_ph1d4/mcIV>1.0' 'ph1d4/mcIV<_1.0';
{320 Manual_digit_IV_first_phalanx,_proportional_length_relative_to_tibiotarsus_(ph1d4/ti)_ ph1d4_reduced_ ph1d4_elongated_and_less_than_twice_the_length_of_ti_(ph1d4/ti_smaller_than_2.00) ph1d4_elongated_about_or_longer_than_twice_the_length_of_ti_(ph1d4/ti_subequal/larger_than_2.00);

{321
Manual_digit_IV_second_phalanx,_length_relative_to_ulna_(Dalla_Vecchia_2019) shorter_than_ulna_ as_long_as_ulna_or_longer;
{322
Manual_digit_IV_second_phalanx,_proportional_length_relative_to_first_phalanx_(ph2d4/ph1d4)_ both_short_or_absent_ elongated_with_second_phalanx_about_the_same_size_or_longer_than_first_(ph2d4/ph1d4_larger_than_1.00)_
elongated_with_second_phalanx_up_to_30%_shorter_than_first_(ph2d4/ph1d4_between_0.70_-_1.00)
elongated_with_second_phalanx_more_than_30%_shorter_than_first_(ph2d4/ph1d4_smaller_than_0.70);
{323
Manual_digit_IV_second/third_phalanx,_cross-section,_shape_(Andres_et_al._2014) round_to_subtriangular concave_posteriorly oval ventral_ridge;
{324
Manual_digit_IV_third_phalanx,_proportional_length_relative_to_first_phalanx_(ph3d4/ph1d4)_ both_short_or_absent_ ph3d4_about_the_same_length_or_larger_than_ph1d4_ ph3d4_shorter_than_ph1d4;
{325
Manual_digit_IV_third_phalanx,_proportional_length_relative_to_the_second_phalanx_(ph3d4/ph2d4)_ both_short_or_absent_ ph3d4_about_the_same_size_or_longer_than_ph2d4_ ph3d4_shorter_than_ph2d4;
{326
Manual_digit_IV_phalanx_four,_extension_relative_to_whole_digit_(Dalla_Vecchia_2019) more_than_30%_the_length_of_the_wing_phalanx_3_ extremely_reduced;
{327
Manual_digit_IV_phalanx_four,_length_relative_to_the_first_phalanx_of_manual_digit_IV_(ph4d4/ph1d4) both_short_or_absent
both_elongated,_with_the_forth_phalanx_longer_than_the_first_(ph4/d4>1.00)
both_elongated,_with_the_forth_phalanx_the_same_length_or_shorter,_but_longer_than_35%_the_lenght_of_the_first
both_elongated,_with_the_forth_phalanx_less_than_35%_the_lenght_of_the_first;
{328 Manual_digit_IV_phalanx_four_strongly_bowed_(Vidovic_&_Martill,_2017) present absent;
{329
Manual_digit_IV_phalanx_four,_extensor-tendon_process,_shape_(Vidovic_&_Martill,_2017) rounded saddle-shaped,_with_deep_proximal_groove approximately_square;
{330 Pre-acetabular_process_is_(Vidovic_&_Martill,_2017) _spinous_(narrow_to_a_point)_ parallel-sided_(broad)_ semi-circular_and_broad_;
{331 Preacetabular_process_(Vidovic_&_Martill,_2017) straight dorsally_curving;
{332 Postacetabular_process_of_ilium_(Naish_et_al.,_2013) with_subhorizontal_dorsal_surface with_convex_dorsal_surface_;

{333 The_length_of_the_postacetabular_process_of_ilium_(Naish_et_al.,_2013) unexpanded,_or_less_than_length_of_acetabulum
expanded,_as_long_or_longer_than_the_acetabulum_;
{334 Postacetabular_process_of_the_ilium_(Vidovic_&_Martill,_2017) approximately_equal_in_size_to_the_preacetabular_process
smaller_in_size_than_the_preacetabular_process longer_than_the_preacetabular;
{335 Postacetabular_process_(Vidovic_&_Martill,_2017) caudally_directed,_only has_a_cranial,_dorsal_projection has_a_cranial_hooked_process_;
{336
Postacetabular_process_fused_to_supra-neural_plate_(Vidovic_&_Martill,_2017) present absent;
{337 Prepubic_boot_projects_(Vidovic_&_Martill,_2017) more_anterodorsally_than_posteroventrally
more_posteroventrally_than_anterodorsally equally_in_all_directions;
{338 Prepubic_boot_is__(Vidovic_&_Martill,_2017) rounded/rocker_shaped_ angular,_square angular,_triangular spatulate;
{339 Prepubis_is_(Vidovic_&_Martill,_2017) equal_in_width_to_the_ischium _wider_than_the_ischium not_as_wide_as_the_ischium_;
{340 Prepubis_(Vidovic_&_Martill,_2017) _spade-like bifurcating;
{341 Diaphysis_of_prepubis_(Naish_et_al.,_2013) well_differentiated_from_distal_expansion
short_(equal_to_or_less_than_twice_the_length_of_its_width)_and_poorly_differenti ated_from_distal_expansion;
{342 Pubis_(Vidovic_&_Martill,_2017) as_long_or_longer_than_the_preacetabular_process
_more_than_half_the_length_of_the_preacetabular_process
less_than_half_the_length_of_the_preacetabular_process;
{343 Pubis,_anterior_margin_(Naish_et_al.,_2013) with_straight_anterior_margin_ anterior_margin_concave;
{344 Posterior_margin_of_the_ischium_(Vidovic_&_Martill,_2017) angular rounded;
{345 Pubis_and_ischium_are_(Vidovic_&_Martill,_2017) _completely_fused only_partially_in_contact_and_fused;
{346 Obturator_foramen_(Vidovic_&_Martill,_2017) present absent;
{347 Obturator_foramen_(Vidovic_&_Martill,_2017) anterior_of_the_acetabulum central_to_the_acetabulum posterior_of_the_acetabulum;
{348 In_dorsal_view_the_pelvis_is_(Vidovic_&_Martill,_2017) almost_as_wide_as_it_is_long longer_than_it_is_wide_;
{349 Angle_between_the_ilium_and_the_pubis_is_(Vidovic_&_Martill,_2017) approximately_at_a_right_angle oblique;
{350 The_sciatic_notch_is_(Vidovic_&_Martill,_2017) approximately_equal_in_depth_to_the_acetabulum larger_than_the_acetabulum;
{351 Ischiopubic_plate_(Naish_et_al.,_2013) with_pubis_unexpanded_and_rod-like both_elements_expanded_(pubis_is_approximately_equal_to_or_greater_than_half_t he_width_of_the_ischium)_;

{352 Ischiopubic_plate,_depth_(Naish_et_al.,_2013) depth_less_than_or_equal_to_twice_approximate_length_of_acetabulum depth_more_than_twice_length_of_acetabulum;
{353 Ischium_ventral_margin_shape_(Andres_et_al.,_2014) straight convex;
{354 Acetabulum_(Naish_et_al.,_2013) circular_or_sub-circular_oval,_longest_axis_horizontal;
{355 Femur,_shaft,_orientation_(Lü_et_al.,_2009) strongly_bowed slight_curvature_;
{356 Femoral_neck_shape__(Andres_et_al.,_2014) indistinct constricted;
{357 Distal_end_of_femur_with_complex_condylar_morphology_(Lü_et_al.,_2009) present absent;
{358 Femur,_foramen_on_proximal_portion_of_the_femur_(Andres_et_al._2014) absent present;
{359 Femur,_angle_of_caput_femoris_to_shaft__(Dalla_Vecchia_2019) 145 °_or_less_ more_than_145°;
{360 Femur,_length_relative_to_metacarpal_IV_length_(fe/mcIV)_femur_at_least_twice_the_metacarpal_IV_length_(fe_?_mcIV_>_2.00) femur_longer_but_less_than_twice_the_length_of_metacarpal_IV_(1.00_<_fe/mcIV_<_2.00)_
femur_about_the_same_length_or_shorter_than_metacarpal_IV_(fe/mcIV_<_1.00);
{361 Tibia,_length_relative_to_femur_(ti/fe) ti/fe_<_1.19 over_1.19,_under_1.29 over_1.29,_under_1.46 over_1.46,_under_1.6 over_1.6;
{362 Fibula,_relative_length__(Dalla_Vecchia_2019) similar_length_as_tibia_shorter_than_tibia,_not_reaching_the_tarsus;
{363 Proximal_tarsals_(Vidovic_&_Martill,_2017) larger_than_the_distal_tarsals_smaller_than_the_distal_tarsals are_equal_in_size_to_the_distal_tarsals;
{364 Metatarsals,_arrangement__(Dalla_Vecchia_2019) tightly_bound_in_a_single_unit,_parallel_and_contacting_each_other_for_at_least_the_proximal_half_of_the_elements_
spreading_and_contacting_each_other_for_less_than_the_proximal_half_of_the_elements;
{365 Metatarsal_I_(Vidovic_&_Martill,_2017) significantly_more_robust_than_other_pedal_metatarsals approximately_the_same_size_as_other_metatarsals;
{366 Metatarsal_III,_proportional_length_relative_to_tibia_length_(Kellner_2003) more_than_30%_of_tibia_length_ less_than_30%_of_tibia_length_;
{367 Metatarsals,_relative_length_of_metatarsal_IV__(Dalla_Vecchia_2019) longer_than_metatarsals_I-III_ subequal_in_length_to_metatarsals_II-III shorter_than_metatarsals_I-III;
{368 Proximal_width_of_metatarsal_V_(Vidovic_&_Martill,_2017) much_wider_that_the_distal_end approximately_equal_in_size_to_the_distal_end;
{369 Phalanges_of_pedal_digit_IV_(Vidovic_&_Martill,_2017) all_approximately_equal_in_length_
unequal_in,_length,_the_proximal_phalanx_is_larger_than_all_those_succeeding_it unequal_in_length,_the_distal_phalanx_is_larger_than_all_those_preceding_it

unequal_in_length,_the_distal_and_proximal_phalanges_are_longer_than_those_between_them;
{370 Pedal_digit_IV_phalanx_II_and_III_(Vidovic_&_Martill,_2017) longer_than_they_are_wide_ _as_wide,_or_wider_than_they_are_long;
{371 Pedal_digit_V,_number_of_phalanges_(Kellner_2003) with_four_phalanges_ with_2_phalanges_ with_1_or_no_phalanx_(extremely_reduced);
{372 Pedal_digit_V,_phalanx_2,_shape_(Dalla_Vecchia_2019) straight_or_slightly_arched_ curved/bent_(exterior_angle_over_140 °) extremely_bent_(exterior_angle_under_140°);
{373 Longest_pedal_digit_(Vidovic_&_Martill,_2017) as_long_or_longer_than_metatarsals_ shorter;
{374 Terminal_phalanx_of_pes_digit_V_(Vidovic_&_Martill,_2017) approximately_equal_in_size_to_preceding_phalanx longer_than_preceding_phalanx _shorter_than_preceding_phalanx_;
{375
If_terminal_phalanx_of_pes_digit_V_is_not_straight,_it_curves/kinks_(Vidovic_&_Martill,_2017) proximally medially distally;
{376 Pedal_digit_V_(Vidovic_&_Martill,_2017) approximately,_as_long_as_pedal_digit_IV
longer_than_metatarsal,IV,_but_not_as_long_as_the_digit_
approximately_the_length_of_metatarsal_IV
approximately_half_the_length_of_metatarsal_IV restricted_to_tarsal_region_;
{377
Number_of_phalanges_in_pedal_digit_V_is_equal_to_(Vidovic_&_Martill,_2017)
zero one two;
;ccode + 0 44 105 151 191 263 264 269 284 288 289 292 303 312 319 320 322 361 *; proc /; comments 1 {17 8 1;

Supplemental File 3: Table S1 (Morphometric dataset)

Taxa	ti/fe	Gap-weighting score	Categorization	Sources for metric data	Supp. Refs.
Anurognathus ammoni	1.41	1.095541401	1	Bennett 2007	See main text
Vesperopteryl us lamadongensi s	1.37	1.044585987	1	Lü et al. 2018	See main text
Jeholopterus nigchengensis	1.23	0.866242038	1	Wang et al. 2002	See main text
Dendrorhynch oides curvidentatus	1.37	1.044585987	1	Ji & Ji 1998	See main text
Luopterus mutoudengen sis	1.29	0.942675159	1	Hone & Lü 2012	See main text
IVPP V16728	1.40	1.082802548	1	Jiang et al. 2014	See main text
NJU-57003	1.47	1.171974522	1	Yang et al. 2019	See main text
Sinomacrops bondei	2.12	2	2	This work	-
Batrachognath us volans	1.75	1.52866242	2	Riabinin 1948	See main text

Macrocnemus bassanii	1.10	0.700636943		1	Jaquier et al. 2017, p. 5	Jaquier, V. P., Fraser, N. C., Furrer, H., & Scheyer, T. M. (2017). Osteology of a new specimen of Macrocnemus aff. M. fuyuanensis (Archosauromorpha, Protorosauria) from the Middle Triassic of Europe: potential implications for species recognition and paleogeography of tanystropheid protorosaurs. *Frontiers in Earth Science*, *5*, 91.
Erythrosuchus africanus	0.55		0	0	Ezcurra et al. 2013	Ezcurra, M. D., Butler, R. J., & Gower, D. J. (2013). 'Proterosuchia': the origin and early history of Archosauriformes. *Geological Society, London, Special Publications*, *379*(1), 9-33.

Euparkeria capensis	0.84	0.369426752	0	Ewer 1965, Demuth et al 2020	Ewer, R. F. (1965). The anatomy of the thecodont reptile Euparkeria capensis Broom. *Philosophical Transactions of the Royal Society of London. Series B, Biological Sciences*, *248*(751), 379-435.; Demuth, O. E., Rayfield, E. J., & Hutchinson, J. R. (2020). 3D hindlimb joint mobility of the stem-archosaur Euparkeria capensis with implications for postural evolution within Archosauria. Scientific reports, 10(1), 1-14.
Ornithosuchus woodwardi	0.84	0.369426752	0	Walker 1964	Walker, A. D. (1964). Triassic reptiles from the Elgin area: Ornithosuchus and the origin of carnosaurs. *Philosophical Transactions of the Royal Society of London. Series B, Biological Sciences*, *248*(744), 53-134.

Postosuchus kirkpatricki	0.75	0.25477707	0	Weinbaum 2002	Weinbaum, J. C. (2002). *Osteology and relationships of Postosuchus kirkpatricki (Archosauria: Crurotarsi)* (Doctoral dissertation, Texas Tech University).
Herrerasaurus ischigualastensis	0.92	0.47133758	0	Novas 1994	Novas, F. E. (1994). New information on the systematics and postcranial skeleton of Herrerasaurus ischigualastensis (Theropoda: Herrerasauridae) from the Ischigualasto Formation (Upper Triassic) of Argentina. *Journal of Vertebrate Paleontology*, *13*(4), 400-423.
Scleromochlus taylori	1.04	0.624203822	1	Bennett 2020	Bennett, S. C. (2020). Reassessment of the Triassic archosauriform Scleromochlus taylori: neither runner nor biped, but hopper. *PeerJ*, *8*, e8418.

Lagerpeton chanarensis	1.19	0.815286624	1	Sereno & Arcucci 1994	Sereno, P. C., & Arcucci, A. B. (1994). Dinosaurian precursors from the Middle Triassic of Argentina: Lagerpeton chanarensis. *Journal of Vertebrate Paleontology*, *13*(4), 385-399.
Marasuchus lilloensis	1.30	0.955414013	1	Bonaparte 1975	Bonaparte, J. F., & JF, B. (1975). NUEVOS MATERIALES DE LAGOSUCHUS TALAMPAYENSIS ROMER.(THECODONTIA-PSEUDOSUCHIA) Y SU SIGNIFICADO EN EL ORIGEN DE LOS SAURISCHIA. CHANARENSE INFERIOR, TRIASICO MEDIO DE ARGENTINA.
Preondactylus buffarinii	1.35	1.01910828	1	Dalla Vecchia 2019	See main text
Peteinosaurus zambellii	1.30	0.955414013	1	Dalla Vecchia 2019	See main text
Dimorphodon macronyx	1.42	1.108280255	1	Unwin 2003, Dalla Vecchia 2009	See main text

Arcticodactylus cromptonellus	1.04	0.624203822	1	Jenkins et al 2001, Dalla Vecchia 2019	Jenkins, F. A., Shubin, N. H., Gatesy, S. M., & Padian, K. E. V. I. N. (2001). A diminutive pterosaur (Pterosauria: Eudimorphodontidae) from the Greenlandic Triassic. *Bulletin of the Museum of Comparative Zoology*, *156*(1), 151-170.
Austriadraco dallavecchiai	1.52	1.23566879	1	Wellnhofer 2003, Dalla Vecchia 2019	Wellnhofer, P. (2003). A Late Triassic pterosaur from the Northern Calcareous Alps (Tyrol, Austria). *Geological Society, London, Special Publications*, *217*(1), 5-22.
Seazzadactylus venieri	1.22	0.853503185	1	Dalla Vecchia 2019	See main text
Carniadactylus rosenfeldi	1.46	1.159235669	1	Dalla Vecchia 2019	See main text
MCSNB 8950	1.27	0.917197452	1	Dalla Vecchia 2019	See main text
Raeticodactylus filisurensis	1.50	1.210191083	1	Dalla Vecchia 2019	See main text
Campylognathoides liasicus	1.25	0.891719745	1	Padian 2008	See main text
Campylognathoides zitteli	1.31	0.968152866	1	Padian 2008	See main text
Sordes pilosus	1.38	1.057324841	1	Unwin et al 2000	See main text

Scaphognathus crassirostris	1.12	0.72611465	1	Wellnhofer 1975a, Bennett 2014	See main text
Dorygnathus banthensis	1.34	1.006369427	1	Padian 2008	See main text
Rhamphorhynchus muensteri	1.38	1.057324841	1	Lü et al. 2012a	Lü, J., Unwin, D. M., Zhao, B., Gao, C., & Shen, C. (2012). A new rhamphorhynchid (Pterosauria: Rhamphorhynchidae) from the Middle/Upper Jurassic of Qinglong, Hebei Province, China. *Zootaxa*, *3158*(1), 1-19.
Qinglongopterus guoi	1.25	0.891719745	1	Lü et al. 2012a	Lü, J., Unwin, D. M., Zhao, B., Gao, C., & Shen, C. (2012). A new rhamphorhynchid (Pterosauria: Rhamphorhynchidae) from the Middle/Upper Jurassic of Qinglong, Hebei Province, China. *Zootaxa*, *3158*(1), 1-19.
Bellubrunnus rothgaengeri	1.20	0.828025478	1	Hone et al. 2012	See main text

Fenghuangopterus lii	1.75	1.52866242	2	Lü et al. 2010a	Lü, J., Pu, H., Xu, L., Wei, X., ChanG, H., & Kundrát, M. (2015). A new rhamphorhynchid pterosaur (Pterosauria) from the Jurassic deposits of Liaoning Province, China. *Zootaxa*, *3911*(1), 119-129.
Kunpengopterus sinensis	1.35	1.01910828	1	Wang et al. 2010	See main text
Kunpengopterus sp.	1.52	1.23566879	1	Zhou et al. In press	-
Wukongopterus lii	1.55	1.27388535	1	Wang et al. 2009	See main text
Darwinopterus modularis	1.33	0.993630573	1	Lü et al. 2010b	See main text
Changchengopterus pani	1.19	0.815286624	1	Lü et al. 2009a	See main text
Germanodactylus cristatus	1.53	1.248407643	1	Wellnhofer 1970	Wellnhofer, P. 1970. Die Pterodactyloidea (Pterosauria) der OberjuraPlattenkalke Su¨ ddeutschlands. Bayerische Akademie der Wissenschaften, Mathematisch-Wissenschaftlichen Klasse, Abhandlungen 141: 1–133.

Altmuehlopterus rhamphastinus	1.51	1.222929936	1	Wellnhofer 1970, Vidovic & Martill 2017	Wellnhofer, P. 1970. Die Pterodactyloidea (Pterosauria) der OberjuraPlattenkalke Su¨ ddeutschlands. Bayerische Akademie der Wissenschaften, Mathematisch-Wissenschaftlichen Klasse, Abhandlungen 141: 1–133.
Cycnorhamphus suevicus	1.31	0.968152866	1	Bennett 2013	Bennett, S. C. (2013). The morphology and taxonomy of the pterosaur Cycnorhamphus. *Neues Jahrbuch für Geologie und Paläontologie-Abhandlungen*, *267*(1), 23-41.
Pterodactylus antiquus	1.38	1.057324841	1	Wellnhofer 1970	Wellnhofer, P. 1970. Die Pterodactyloidea (Pterosauria) der OberjuraPlattenkalke Su¨ ddeutschlands. Bayerische Akademie der Wissenschaften, Mathematisch-Wissenschaftlichen Klasse, Abhandlungen 141: 1–133.

Aerodactylus scolopaciceps	1.33	0.993630573	1	Vidovic & Martill 2014	Vidovic, S. U., & Martill, D. M. (2014). Pterodactylus scolopaciceps Meyer, 1860 (Pterosauria, Pterodactyloidea) from the Upper Jurassic of Bavaria, Germany: the problem of cryptic pterosaur taxa in early ontogeny. *PloS one*, *9*(10), e110646.
Ardeadactylus longicollum	1.45	1.146496815	1	Pers. Obs.	-
Ctenochasma elegans	1.56	1.286624204	1	Bennett 2007b	Bennett, S. C. (2007). A review of the pterosaur Ctenochasma: taxonomy and ontogeny. *Neues Jahrbuch für Geologie und Paläontologie-Abhandlungen*, *245*(1), 23-31.
Pterodaustro guinazui	1.50	1.210191083	1	Wellnhofer 1978	Wellnhofer, P. 1978. Pterosauria. Handbuch der Palaeoherpetologie, Teil 19. Stuttgart: Gustav Fischer Verlag.

Pteranodon longiceps	1.31	0.968152866	1	Miller 1971	Miller, H. W. (1971). A skull of Pteranodon (Longicepia) longiceps Marsh associated with wing and body bones. Transactions of the Kansas Academy of Science (1903), 20-33.
Pteranodon sternbergi	1.43	1.121019108	1	Martin-Silverstone et al. 2017	Martin-Silverstone, E. (2016). Redescription of Dawndraco kanzai Kellner, 2010 and reassignment of the type specimen to Pteranodon sternbergi Harksen, 1966. *Vertebrate Anatomy Morphology Palaeontology*, *3*.
Tethydraco regalis	1.09	0.687898089	1	Longrich et al. 2018	Longrich, N. R., Martill, D. M., & Andres, B. (2018). Late Maastrichtian pterosaurs from North Africa and mass extinction of Pterosauria at the Cretaceous-Paleogene boundary. *PLoS biology*, *16*(3), e2001663.

Nyctosaurus gracilis	1.56	1.286624204	1	Frey et al. 2012	Frey, E., Buchy, M. C., Stinnesbeck, W., Gonzalez, A. G., & Di Stefano, A. (2006). Muzquizopteryx coahuilensis ng, n. sp., a nyctosaurid pterosaur with soft tissue preservation from the Coniacian (Late Cretaceous) of northeast Mexico (Coahuila). *Oryctos*, *6*, 19-40.
Muzquizopteryx coahuilensis	1.39	1.070063694	1	Frey et al. 2012	Frey, E., Buchy, M. C., Stinnesbeck, W., Gonzalez, A. G., & Di Stefano, A. (2006). Muzquizopteryx coahuilensis ng, n. sp., a nyctosaurid pterosaur with soft tissue preservation from the Coniacian (Late Cretaceous) of northeast Mexico (Coahuila). *Oryctos*, *6*, 19-40.

Mimodactylus libanensis	1.45	1.146496815	1	Kellner et al. 2019	Kellner, A. W., Caldwell, M. W., Holgado, B., Dalla Vecchia, F. M., Nohra, R., Sayão, J. M., & Currie, P. J. (2019). First complete pterosaur from the Afro-Arabian continent: insight into pterodactyloid diversity. *Scientific reports*, *9*(1), 1-9.
Nurhachius ignaciobritoi	1.23	0.866242038	1	Wang et al. 2005	Wang, X., Kellner, A. W., Zhou, Z., & de Almeida Campos, D. (2005). Pterosaur diversity and faunal turnover in Cretaceous terrestrial ecosystems in China. *Nature*, *437*(7060), 875-879.
Zhenyuanopterus longirostris	0.95	0.50955414	1	Lü 2010	Lü, J. (2010). A new boreopterid pterodactyloid pterosaur from the Early Cretaceous Yixian Formation of Liaoning Province, northeastern China. *Acta Geologica Sinica-English Edition*, *84*(2), 241-246.

Boreopterus cuiae	1.00	0.573248408	1	Lü & Ji 2005	Lü & Ji. (2005). A new ornithocheirid from the Early Cretaceous of Liaoning Province, China. *Acta Geologica Sinica-English Edition*, *79*(2), 157-163.
Anhanguera spielbergi	1.24	0.878980892	1	Veldmeijer et al. 2006	Veldmeijer, A. J., Meijer, H. J. M., & Signore, M. (2006). Coloborhynchus from the Lower Cretaceous Santana Formation, Brazil (Pterosauria, Pterodactyloidea, Anhangueridae); an update. *PalArch's Journal of Vertebrate Palaeontology*, *3*(2), 15-29.
Noripterus complicidens	1.85	1.656050955	2	Hone et al. 2017	Hone, D. W. E., Jiang, S., & Xu, X. (2017). A taxonomic revision of Noripterus complicidens and Asian members of the Dsungaripteridae. *Geological Society, London, Special Publications*, *455*(1), 149-157.

Noripterus parvus	1.70	1.464968153	1	Lü et al. 2009b	Lü, J. (2009). A new non-pterodactyloid pterosaur from Qinglong County, Hebei Province of China. *Acta Geologica Sinica-English Edition*, *83*(2), 189-199.
Tupuxuara leonardii	1.34	1.006369427	1	Pers. Obs.	-
Tapejara wellnhoferi	1.39	1.070063694	1	Eck et al. 2011	Eck, K., Elgin, R. A., & Frey, E. (2011). On the osteology of Tapejara wellnhoferi Kellner 1989 and the first occurrence of a multiple specimen assemblage from the Santana Formation, Araripe Basin, NE-Brazil. *Swiss Journal of Palaeontology*, *130*(2), 277.
Sinopterus dongi	1.44	1.133757962	1	Wang & Zhou 2003	Wang, X., & Zhou, Z. (2003). A new pterosaur (Pterodactyloidea, Tapejaridae) from the Early Cretaceous Jiufotang Formation of western Liaoning, China and its implications for biostratigraphy. *Chinese Science Bulletin*, *48*(1), 16-23.

Huaxiapterus corollatus	1.68	1.439490446	1	Wu et al. 2017	Wu, W. H., Zhou, C. F., & Andres, B. (2017). The toothless pterosaur Jidapterus edentus (Pterodactyloidea: Azhdarchoidea) from the Early Cretaceous Jehol Biota and its paleoecological implications. *Plos one*, *12*(9), e0185486.
Eopteranodon lii	1.46	1.159235669	1	Wu et al. 2017	Wu, W. H., Zhou, C. F., & Andres, B. (2017). The toothless pterosaur Jidapterus edentus (Pterodactyloidea: Azhdarchoidea) from the Early Cretaceous Jehol Biota and its paleoecological implications. *Plos one*, *12*(9), e0185486.
Chaoyangopterus zhangi	1.53	1.248407643	1	Wu et al. 2017	Wu, W. H., Zhou, C. F., & Andres, B. (2017). The toothless pterosaur Jidapterus edentus (Pterodactyloidea: Azhdarchoidea) from the Early Cretaceous Jehol Biota and its paleoecological implications. *Plos one*, *12*(9), e0185486.

Shenzhoupterus chaoyangensis	1.36	1.031847134	1	Wu et al. 2017	Wu, W. H., Zhou, C. F., & Andres, B. (2017). The toothless pterosaur Jidapterus edentus (Pterodactyloidea: Azhdarchoidea) from the Early Cretaceous Jehol Biota and its paleoecological implications. *Plos one*, *12*(9), e0185486.
Jidapterus edentus	1.46	1.159235669	1	Wu et al. 2017	Wu, W. H., Zhou, C. F., & Andres, B. (2017). The toothless pterosaur Jidapterus edentus (Pterodactyloidea: Azhdarchoidea) from the Early Cretaceous Jehol Biota and its paleoecological implications. *Plos one*, *12*(9), e0185486.
Zhejiangopterus linhaiensis	1.19	0.815286624	1	Wu et al. 2017	Wu, W. H., Zhou, C. F., & Andres, B. (2017). The toothless pterosaur Jidapterus edentus (Pterodactyloidea: Azhdarchoidea) from the Early Cretaceous Jehol Biota and its paleoecological implications. *Plos one*, *12*(9), e0185486.

Aurorazhdarcho micronyx	1.47	1.171974522	1	Frey et al. 2011	Frey, E., Meyer, C. A., & Tischlinger, H. (2011). The oldest azhdarchoid pterosaur from the Late Jurassic Solnhofen Limestone (early Tithonian) of southern Germany. *Swiss Journal of Geosciences*, *104*(1), 35-55.
Gladocephaloideus jingangshanensis	1.56	1.286624204	1	Lü et al. 2016	Lü, J., Kundrát, M., & Shen, C. (2016). New material of the pterosaur Gladocephaloideus Lü et al., 2012 from the Early Cretaceous of Liaoning Province, China, with comments on its systematic position. *Plos one*, *11*(6), e0154888.
Painten Pro-pterodactyloid	1.17	0.789808917	1	Tischlinger & Frey 2014	Tischlinger, H., & Frey, E. (2014). Ein neuer Pterosaurier mit Mosaikmerkmalen basaler und pterodactyloider Pterosauria aus dem Ober-Kimmeridgium von Painten (Oberpfalz, Deutschland). *Archaeopteryx*, *31*, 1-14.
Diopecephalus kochi	1.33	0.993630573	1	Vidovic & Martill 2017	See main text

Supplemental File 4.

Sheet 1: Skeletal measurements - Tapejaridae

Specimen	Rostrum def.°	Naof height/length	Orbit°	Q°	cvlV	cvV	Hu	Ul	Pteroid	Metacarpal IV	Metacarpal I	ph1d4	ph2d4	ph3d4	ph4d4	fe	ti	mtI	mtII
Tapejara wellnhoferi SMNK PAL 1137	26	1.35	60	145	25.8	25.8	69.4	101.5	?	107	107	144	113.8	?	36.2	82.5	114.7	28.3	30.3
Caiuajara dobruskii scaled composite	34.5	1.38	60	147.3	?	?	91	124.65	?	126.3	?	170	164.9	162.35	49.9	91.3	111.88	?	?
Tupandactylus navigans GP/2E 9266	23	2.1	60	145	49.9	46.7	131	188.1	97	181.7	82.1	304	196.1	129.9	39.3	163.1	248.8	35.8	47.2
Sinopterus dongi holotype	14	3	90	160	?	?	58	87.5	38	95	93	121	88	63	38	74	104	24.5	21
Huaxiapterus jii holotype	14	3	?	?	?	?	79	117	60	132	119	163	127	91	45	100	141	?	34
D3072	?	?	?	?	22.5	19	55.1	82.6	32	90.8	88.5	107.7	85.6	67.8	45	?	97.7	24.9	23.6

Sinopterus lingyuanensis holotype	12	3.2	90	160	20	16	47	58	31	58	?	84	66	50	?	52.5	78.8	20.5	22
Huaxiapterus atavismus holotype	14	3	?	?	15.5	13	42	62	24.3	66	?	85	65	45	29	?	68	18	21
IVPP V 23388	14	3	90	?	30.8	23.85	79.77	116.32	?	127.49	107.92	158.87	122.59	?	?	97.86	149.59	33.58	35.36
D2525	?	?	?	?	?	?	?	110	157	75	181	59.73	215	156	106	43	135	185	36	37
Huaxiapterus benxiensis holotype	20	2.39	68	147	24	26	82	118	59	132	53	174	134	94	32	115	154	?	?
Huaxiapterus corollatus holotype	21	2.24	?	?	?	?	?	75	105	49	130	44	152	108	69	29	87	147	?	?
Eopteranodon lii D2526	?	?	?	?	25	23	68	93	54	106	106	137	103	75	62	80	117	23	27
Eopteranodon lii holotype	15	2.1	?	?	26	24	63	94	52	99.5	?	131	99	?	?	75	?	?	?
D4019	13.5	?	?	162	26	25	64	99	?	123	101	?	?	?	45	84	115	?	?

BPMC 103	20	2.5	65	?	?	?	79	125	?	129	42	167	118	73	35	?	149	32	33
							10									13			
BPMC 104	20	2.3	?	?	?	?	0	162	?	182	60	226	170	112	50	2	210	44	46
BPMC 105	20	2.2	65	?	?	?	69	106	?	114	?	129	96	63	26	78	99	?	?
							11									14			
BPMC 107	15	?	?	?	?	?	1	171	62	167	166	219	182	118	65	2	211	47	46

Sheet 2: Log-transformed values. Dataset for SMA analyses (Sinopterinae only).

Specimen	Rostrum deflection°	Naof height/length	Orbit°	Q°	cvIV	cvV	Hu	Ul	Pteroid	Metacarpal IV	Metacarpal I	ph1d4	ph2d4	ph3d4	ph4d4	fe	ti	mtI	mtII
Sinopterus		0.477	1.95																
dongi	1.14	1212	4242	2.20			1.76	1.94	1.57	1.97	1.96	2.08	1.94	1.79	1.50	1.86	2.01	1.38	1.32
holoty	6128	55	509	4119			3427	2008	9783	7723	8482	2785	4482	9340	5149	9231	7033	9166	2219
pe	036			983	?	?	994	053	597	605	949	37	672	549	978	72	339	084	295
Huaxiapterus		0.477																	
jii	1.14	1212	?				1.89	2.06	1.77	2.12	2.07	2.21	2.10	1.95	1.65		2.14		1.53
holoty	6128	55					7627	8185	8151	0573	5546	2187	3803	9041	3212		9219		1478
pe	036			?	?	?	091	862	25	931	961	604	721	392	514	2	113	?	917
					1.35	1.27	1.74	1.91	1.50	1.95	1.94	2.03	1.93	1.83	1.65		1.98	1.39	1.37
		?	?		2182	8753	1151	6980	5149	8085	6943	2215	2473	1229	3212		9894	6199	2912
D3072	?			?	518	601	599	047	978	849	271	703	765	694	514	?	564	347	003

Sinopterus lingyuanensis holotype	1.07919246	0.505149978	1.95424509	2.204119983	1.301029996	1.204119983	1.672097858	1.763427994	1.491361694	1.763427994	?	1.924279286	1.819543936	1.698970004	?	1.720159303	1.896526217	1.311753861	1.342422681
*Huaxiapterus atavismus*holotype	1.14612803603	0.47712125555	?	?	1.190331698	1.113943352	1.623249029	1.792391689	1.385606274	1.819543936	?	1.929418926	1.812913357	1.653212514	1.462397998	?	1.832508913	1.255272505	1.322219295
IVPP V 23388	1.14612803603	0.47712125555	1.95424509	?	1.488550717	1.377488383	1.901839592	2.065654394	?	2.105476121	2.033101937	2.201041896	2.088455045	?	?	1.990605211	2.174902562	1.526080692	1.548512256
D2525	?	?	?	?	?	?	2.041392685	2.195899652	1.875061263	2.257678575	1.776192515	2.332438046	2.193124598	2.025305865	1.633468456	2.130333768	2.267171728	1.556302501	1.568201724
*Huaxiapterus benxiensis*holotype	1.30102999696	0.37839797201	1.83250891327	2.167317335	1.380211242	1.414973348	1.913813852	2.071882007	1.770852012	2.120573931	1.724275487	2.240549248	2.127104798	1.973127854	1.505149978	2.060697084	2.187520721	?	?
*Huaxiapterus corollatus*holotype	1.32221929547	0.35024801818	?	?	?	?	1.875061263	2.021189299	1.690196080	2.113943352	1.643452676	2.181843588	2.033423755	1.838491091	1.462397998	1.932539253	2.167317335	?	?

ype																			
Eopter																			
anodo					1.39	1.36	1.83	1.96	1.73	2.02	2.02	2.13	2.01	1.87	1.79	1.90	2.06	1.36	1.43
n lii					7940	1727	2508	8482	2393	5305	5305	6720	2837	5061	2391	3089	8185	1727	1363
D2526	?	?	?	?	009	836	913	949	76	865	865	567	225	263	689	987	862	836	764
Eopter																			
anodo																			
n lii	1.17	0.322			1.41	1.38	1.79	1.97	1.71	1.99		2.11	1.99			1.87			
holoty	6091	2192			4973	0211	9340	3127	6003	7823		7271	5635			5061			
pe	259	95	?	?	348	242	549	854	344	081	?	296	195	?	?	263	?	?	?
	1.13			2.20	1.41	1.39	1.80	1.99		2.08	2.00				1.65	1.92	2.06		
	0333			9515	4973	7940	6179	5635		9905	4321				3212	4279	0697		
D4019	768	?	?	015	348	009	974	195	?	111	374	?	?	?	514	286	84	?	?
	1.30	0.397	1.81				1.89	2.09		2.11	1.62	2.22	2.07	1.86	1.54		2.17	1.50	1.51
BPMC	1029	9400	2913				7627	6910		0589	3249	2716	1882	3322	4068		3186	5149	8513
103	996	09	357	?	?	?	091	013	?	71	29	471	007	86	044	?	268	978	94
	1.30	0.361						2.20		2.26	1.77	2.35	2.23	2.04	1.69	2.12	2.32	1.64	1.66
BPMC	1029	7278						9515		0071	8151	4108	0448	9218	8970	0573	2219	3452	2757
104	996	36	?	?	?	?	2	015	?	388	25	439	921	023	004	931	295	676	832
	1.30	0.342	1.81				1.83	2.02		2.05		2.11	1.98	1.79	1.41	1.89	1.99		
BPMC	1029	4226	2913				8849	5305		6904		0589	2271	9340	4973	2094	5635		
105	996	81	357	?	?	?	091	865	?	851	?	71	233	549	348	603	195	?	?
BPMC	1.17						2.04	2.23	1.79	2.22	2.22	2.34	2.26	2.07	1.81	2.15	2.32	1.67	1.66
107	6091	?	?	?	?	?	5322	2996	2391	2716	0108	0444	0071	1882	2913	2288	4282	2097	2757

259				979	11	689	471	088	115	388	007	357	344	455	858	832	

Sheet 3. Log-transformed values. Dataset for clustering analyses (Tapejaridae).

Specimen	Rostrum def.	Naof h/l	Orbit	Q°	CIV/CV	ul/hu	pt/hu	mcIV/hu	mcI/hu	ph1d4/hu	ph2d4/hu	ph3d4/hu	ph4d4/hu	mtI/hu	mtII/hu
Tapejara wellnhoferi SMNK PAL 1137	1.3979 40009	0.1303 33768	1.7781 5125	2.1613 68002	0	0.1651 06572	?	0.1880 24307	0.1880 24307	0.3170 03022	0.2147 82791	?	-0.2826 509	-0.3895 73035	-0.3599 16842
Caiuajara dobruskii scaled composite	1.5378 19095	0.1398 79086	1.7781 5125	2.1682 02747	?	0.1366 50891	?	0.1423 61958	?	0.2714 07529	0.2581 79263	0.2514 10901	-0.2609 40847	?	?
Tupandactylus navigans GP/2E 9266	1.3979 40009	0.3222 19295	1.7781 5125	2.1613 68002	0.0287 83665	0.1571 175	-0.1304 99562	0.1420 83632	-0.2029 28139	0.3656 02288	0.1752 06298	-0.0036 62145	-0.5228 78745	-0.5633 88269	-0.4433 29296
Sinopterus dongi holotype	1.1461 28036	0.4771 21255	1.9542 42509	2.2041 19983	0.0413 92685	0.1785 8006	-0.1836 44397	0.2142 95612	0.2050 54955	0.3193 57377	0.1810 54678	0.0359 12556	-0.2582 78015	-0.3742 61909	-0.4412 08698
Huaxiapterus jii holotype	1.1461 28036	0.4771 21255	?	?	?	0.1705 5877	-0.1194 75841	0.2229 4684	0.1779 1987	0.3145 60513	0.2061 7663	0.0614 14301	-0.2444 14578	?	-0.3661 48174
D3072	?	?	?	?	0.0734 28917	0.1758 28448	-0.2360 01621	0.2169 3425	0.2057 91672	0.2910 64104	0.1913 22166	0.0900 78095	-0.0879 39085	-0.3449 52252	-0.3682 39596

Sinopterus lingyuanensis holotype	1.0791 81246	0.5051 49978	1.9590 41392	2.2041 19983	0.0969 10013	0.0913 30136	-0.1807 36164	0.0913 30136	?	0.2521 81428	0.1474 46078	0.0268 72146	?	-0.3603 43997	-0.3296 75177
Huaxiapterus atavismus holotype	1.1461 28036	0.4771 21255	?	?	0.0763 88346	0.1691 42399	-0.2376 43016	0.1962 94645	?	0.3061 69635	0.1896 64066	0.0299 63223	-0.1608 51293	-0.3679 76785	-0.3010 29996
IVPP V 23388	1.1461 28036	0.4771 21255	1.9542 42509	?	0.1110 62333	0.1638 14802	?	0.2036 36529	0.1312 62344	0.2992 02303	0.1866 15453	?	?	-0.3757 589	-0.3533 27336
D2525	?	?	?	?	?	0.1545 06967	-0.1663 31422	0.2162 8589	-0.2652 0017	0.2910 45775	0.1517 31913	-0.0160 8682	-0.4079 24229	-0.4850 90185	-0.4731 90962
Huaxiapterus benxiensis holotype	1.3010 29996	0.3783 97901	1.8325 08913	2.1673 17335	-0.0347 62106	0.1580 68155	-0.1429 61841	0.2067 60079	-0.1895 37983	0.3267 35396	0.2132 90946	0.0593 14001	-0.4086 63875	?	?
Huaxiapterus corollatus holotype	1.3222 19295	0.3502 48018	?	?	?	0.1461 28036	-0.1848 65184	0.2388 82089	-0.2316 08587	0.3067 82325	0.1583 62492	-0.0362 12173	-0.4126 63265	?	?
Eopteranodon lii D2526	?	?	?	?	0.0362 12173	0.1359 74036	-0.1001 15153	0.1927 96952	0.1927 96952	0.3042 11654	0.1803 28312	0.0425 52351	-0.0401 17223	-0.4707 81077	-0.4011 45148
Eopteranodon lii holotype	1.1760 91259	0.3222 19295	?	?	0.0347 62106	0.1737 87304	-0.0833 37206	0.1984 82531	?	0.3179 30746	0.1962 94645	?	?	?	?

D4019	1.1303	?	?	2.2095	0.0170	0.1894	?	0.2837	0.1981	?	?	?	-0.1529	?	?
	33768			15015	33339	55221		25137	414				6746		
BPMC 103	1.3010	0.3979	1.8129	?	?	0.1992	?	0.2129	-0.2743	0.3250	0.1742	-0.0343	-0.3535	-0.3924	-0.3791
	29996	40009	13357			82922		62619	77801	8938	54916	04231	59047	77113	13151
BPMC 104	1.3010	0.3617	?	?	?	0.2095	?	0.2600	-0.2218	0.3541	0.2304	0.0492	-0.3010	-0.3565	-0.3372
	29996	27836				15015		71388	4875	08439	48921	18023	29996	47324	42168
BPMC 105	1.3010	0.3424	1.8129	?	?	0.1864	?	0.2180	?	0.2717	0.1434	-0.0395	-0.4238	?	?
	29996	22681	13357			56775		55761		40619	22142	08541	75743		
BPMC 107	1.1760	?	?	?	?	0.1876	-0.2529	0.1773	0.1747	0.2951	0.2147	0.0265	-0.2324	-0.3732	-0.3825
	91259					73132	31289	93493	85109	21136	48409	59028	09622	25121	65148

Raw values

Specimen	**Rostrum def.**	**Naof h/l**	**Orbit°**	**Q°**	**CIV/CV**	**ul/hu**	**pt/hu**	**mcIV/hu**	**mcI/hu**	**ph1d4/hu**	**ph2d4/hu**	**ph3d4/hu**	**ph4d4/hu**	**mtI/hu**	**mtII/hu**
Tapejara wellnhoferi SMNK		1.35	60		1	1.4625 36023	?	1.5417 86744	1.5417 86744	2.0749 27954	1.6397 69452	?	0.5216 13833	0.40778 098	0.43659 9424
PAL 1137	26			145											
Caiuajara dobruskii scaled		1.38	60		?	1.3697 8022	?	1.3879 12088	?	1.8681 31868	1.8120 87912	1.7840 65934	0.5483 51648	?	?
composite	34.5			147.3											
Tupandactylus navigans		2.1	60		1.0685 22484	1.4358 77863	0.7404 58015	1.3870 22901	0.6267 17557	2.3206 10687	1.4969 46565	0.9916 03053	0.3	0.27328 2443	0.36030 5344
	23			145											

GP/2E 9266														
Sinopterus dongi holotype	14	3	90	160	?	1.5086 2069	0.6551 72414	1.6379 31034	1.6034 48276	2.0862 06897	1.5172 41379	1.0862 06897	0.6551 72414	0.42241 3793	0.36206 8966
Huaxiapterus jii holotype	14	3	?	?	?	1.4810 12658	0.7594 93671	1.6708 86076	1.5063 29114	2.0632 91139	1.6075 94937	1.1518 98734	0.5696 20253	?	0.43037 9747
D3072	?	?	?	?	1.1842 10526	1.4990 92559	0.5807 6225	1.6479 12886	1.6061 70599	1.9546 27949	1.5535 3902	1.2304 90018	0.8166 96915	0.45190 5626	0.42831 216
Sinopterus lingyuanensis holotype	12	3.2	91	160	1.25	1.2340 42553	0.6595 74468	1.2340 42553	?	1.7872 34043	1.4042 55319	1.0638 29787	?	0.43617 0213	0.46808 5106
Huaxiapterus atavismus holotype	14	3	?	?	1.1923 07692	1.4761 90476	0.5785 71429	1.5714 28571	?	2.0238 09524	1.5476 19048	1.0714 28571	0.6904 7619	0.42857 1429	0.5
IVPP V 23388	14	3	90	?	1.2914 04612	1.4581 92303	?	1.5982 19882	1.3528 89557	1.9916 00852	1.5367 93281	?	?	0.42096 0261	0.44327 4414
D2525	?	?	?	?	?	1.4272 72727	0.6818 18182	1.6454 54545	0.543	1.9545 45455	1.4181 81818	0.9636 36364	0.3909 09091	0.32727 2727	0.33636 3636
Huaxiapterus benxiensis	20	2.39	68	147	0.9230 76923	1.4390 2439	0.7195 12195	1.6097 56098	0.6463 41463	2.1219 5122	1.6341 46341	1.1463 41463	0.3902 43902	?	?

holotype															
Huaxiapte					?	1.4	0.6533	1.7333	0.5866	2.0266	1.44	0.92	0.3866	?	?
rus							33333	33333	66667	66667			66667		
corollatus															
holotype	21	2.24	?	?											
Eopterano					1.0869	1.3676	0.7941	1.5588	1.5588	2.0147	1.5147	1.1029	0.9117	0.33823	0.39705
don lii					56522	47059	17647	23529	23529	05882	05882	41176	64706	5294	8824
D2526	?	?	?	?											
Eopterano					1.0833	1.4920	0.8253	1.5793	?	2.0793	1.5714	?	?	?	?
don lii					33333	63492	96825	65079		65079	28571				
holotype	15	2.1	?	?											
D4019					1.04	1.5468	?	1.9218	1.5781	?	?	?	0.7031	?	?
	13.5	?	?	162		75		75	25				25		
BPMC 103					?	1.5822	?	1.6329	0.5316	2.1139	1.4936	0.9240	0.4430	0.40506	0.41772
	20	2.5	65	?		78481		11392	4557	24051	70886	50633	37975	3291	1519
BPMC 104	20	2.3	?	?	?	1.62	?	1.82	0.6	2.26	1.7	1.12	0.5	0.44	0.46
BPMC 105					?	1.5362	?	1.6521	?	1.8695	1.3913	0.9130	0.3768	?	?
	20	2.2	65	?		31884		73913		65217	04348	43478	11594		
BPMC 107					?	1.5405	0.5585	1.5045	1.4954	1.9729	1.6396	1.0630	0.5855	0.42342	0.41441
	15	?	?	?		40541	58559	04505	95495	72973	3964	63063	85586	3423	4414

Sheet 4:

Variable 1 - Rostrum deflection		**Variable 2 -Naof height/length**		**Variable 3 - Orbit ventral angle**		**Variable 4 - Quadrate inclination**		**Variable 5 - cIV/cV**	
Morphotype I	Morphotype II	Morphotype I	Morphotype II	Morphotype I	Morphotype II	Morphotype I	Morphotype II	Morphotype I	Morphotype II
1.146128036	1.301029996	0.477121255	0.378397901	1.954242509	1.832508913	2.204119983	2.167317335	0.041392685	-0.034762106
1.146128036	1.322219295	0.477121255	0.350248018	1.959041392	1.812913357	2.204119983		0.073428917	
1.079181246	1.301029996	0.505149978	0.397940009	1.954242509	1.832508913	2.209515015		0.096910013	
1.146128036	1.301029996	0.477121255	0.361727836					0.076388346	
1.146128036	1.301029996	0.477121255	0.342422681					0.111062333	
1.130333768	1.176091259							0.017033339	
Results: H = 8,308, Hc = 8,932, p = 0,002802		Results: H = 6,818, Hc = 7,258, p = 0,007058		Results: H = 3,857, Hc = 4,091, p = 0,04311		Results: N/A		Results: N/A	

Variable 6 - Ul/hu		**Variable 7 - pt/hu**		**Variable 8 - mcIV/hu**		**Variable 9 - mcI/hu**		**Variable 10 - ph1d4/hu**	
Morphotype I+O30A11:A11:O30	Morphotype II	Morphotype I	Morphotype II	Morphotype I	Morphotype II	Morphotype I	Morphotype II	Morphotype I	Morphotype II

0.17858006	0.154506967	-0.183644397	-0.166331422	0.214295612	0.21628589	0.205054955	-0.26520017	0.319357377	0.291045775
0.17055877	0.158068155	-0.119475841	-0.142961841	0.22294684	0.206760079	0.17791987	-0.189537983	0.314560513	0.326735396
0.175828448	0.146128036	-0.236001621	-0.184865184	0.21693425	0.238882089	0.205791672	-0.231608587	0.291064104	0.306782325
0.091330136	0.199282922	-0.180736164		0.091330136	0.212962619	0.131262344	-0.274377801	0.252181428	0.32508938
0.169142399	0.209515015	-0.237643016		0.196294645	0.260071388	0.1981414	-0.22184875	0.306169635	0.354108439
0.163814802	0.186456775	-0.252931289		0.203636529	0.218055761	0.174785109		0.299202303	0.271740619
0.189455221				0.283725137				0.295121136	
0.187673132				0.177393493					

Results: H = 0,01667, Hc = 0,01667, p = 0,8973		Results: H = 1,067, Hc = 1,067, p = 0,3017		Results: H = 1,35, Hc = 1,35, p = 0,2453		Results: H = 7,5, Hc = 7,5, p = 0,00617		Results: H = 1, Hc = 1, p = 0,3173	
Variable 11 - ph2d4/hu		**Variable 12 - ph3d4/hu**		**Variable 13 - ph4d4/hu**		**Variable 14 - mtI/hu**		**Variable 15 - mtII/hu**	
Morphotype I	Morphotype II	Morphotype I	Morphotype II	Morphotype I	Morphotype II	Morphotype I	Morphotype II	Morphotype I	Morphotype II
0.181054678	0.151731913	0.035912556	-0.01608682	-0.258278015	-0.407924229	-0.374261909	-0.485090185	-0.441208698	-0.473190962

0.20617663	0.213290946	0.061414301	0.059314001	-0.24441457	-0.40866387	-0.34495225	-0.39247711	-0.36614817	-0.37911315
				8	5	2	3	4	1
0.191322166	0.158362492	0.090078095	-0.03621217	-0.08793908	-0.41266326	-0.36034399	-0.35654732	-0.36823959	-0.33724216
			3	5	5	7	4	6	8
0.147446078	0.174254916	0.026872146	-0.03430423	-0.16085129	-0.35355904	-0.36797678		-0.32967517	
			1	3	7	5		7	
0.189664066	0.230448921	0.029963223	0.049218023	-0.15296746	-0.30102999	-0.3757589		-0.30102999	
					6			6	
0.186615453	0.143422142	0.026559028	-0.03950854	-0.23240962	-0.42387574	-0.37322512		-0.35332733	
			1	2	3	1		6	
0.214748409								-0.38256514	
								8	

Results: H = 0,5102, Hc = 0,5102, p = 0,4751	Results: H = 2,564, Hc = 2,564, p = 0,1093	Results: H = 8,308, Hc = 8,308, p = 0,003948	Results: H = 1,067, Hc = 1,067, p = 0,3017	Results: H = 0,6364, Hc = 0,6364, p = 0,425

Sheet 5: Rostrum deflection angle in tapejarid specimens.

Species	Specimen	Rostrum deflection angle
Tapejara wellnhoferi	MN 6595-V	26°
	AMNH 2440	25°
	SMNK PAL 1137	25°
	SAO 12891	28°
Tupandactylus imperator	MCT 1622-R	25°
	CPCA 3590	21°

Tupandactylus navigans	holotype	25°
	paratype	23°
	GP/2E 9266	23°
Caiuajara dobruskii	CP.V 1449 (holotype)	37°
	CP.V 1005	37°
	CP.V 1447	34°
	CP.V 1001	32°
Eopteranodon lii	holotype	15°
Jiufotang Morphotype I	*S. dongi* holotype	14°
	H. jii holotype	14°
	S. lingyuanensis holotype	12°
	H. atavismus holotype	14°
	IVPP V 23388	14°
	D4019	13,5°
	BPMC 106	15°
Jiufotang Morphotype II	*H. benxiensis* holotype	20°
	H. corollatus holotype	21°
	BPMC 103	20°
	BPMC 104	20°
	BPMC 105	20°

Sheet 6:

Specimen	Humerus length	Wingspan	Dorsal centra and neural arches, fusion	Scapulacoracoid, fusion	Humeral epiphyses, fusion	Syncarpals, fusion	Extensor tendon process, fusion	Synsacrum, fusion	Pelvic bones, fusion	Fibula, fusion	Tarsal elements, fusion
BPV-077 (holotype of *Sinopterus gui*)	35.5 mm	~800 mm	?	?	?	?	?	?	No	No	?
XHPM 1009 (holotype of *H. atavismus*)	42 mm	~850 mm	?	?	?	No	No	?	?	?	No
JPM-2014-005 (holotype of *S. lingyuanensis*)	47 mm	~850 mm	?	?	No	No	No	?	No	No	No
D3072	55 mm	1135 mm	No	No	No	No	No	?	?	?	No
BPMC 106	~55 mm	?	No	?	No	No	?	?	?	?	?
IVPP V 13363 (holotype of *S. dongi*)	58 mm	1200 mm	No	No	No	No	No	?	?	No	No
D4019	64 mm	?	?	No	No	No	No	?	?	?	No

BPMC 105	69 mm	1288 mm	?	?	No	No	No	No	?	?	No
GMN-03-11-001 (holotype of *H. jii*)	79 mm	1602 mm	Partially	No	No	No	No	?	?	?	No
BPMC 103	79 mm	1546 mm	?	?	No	No	No	?	?	?	No
ZMNH M813 (holotype of *H. corollatus*)	75 mm	1560 mm	?	No	?	Yes	No	?	?	?	Yes
IVPP V 23388	79 mm	~1600 mm	Yes	No	No	No	Partially	Partially	Partially	Yes	Partially
BXGM V0011 (holotype of *Huaxiapterus benxiensis*)	82 mm	1600 mm	?	?	Yes	Yes	Yes	?	?	Yes	Yes
BPMC 104	100 mm	2124 mm	Yes	Yes	Yes	?	No	?	Partially	Yes	Partially
D2525	110 mm	2000 mm	Yes	Yes	Yes	Yes	Yes	?	Yes	Yes	Yes
BPMC 107	111 mm	2180 mm	?	Yes	Yes	Yes	Yes	?	Partially	Yes	Yes

Scatter plot (humerus length/wingspan)

Specimen	Hu (mm)	Wingspan (mm)
BPV-077 (holotype of *Sinopterus gui*)	35.5	800
XHPM 1009 (holotype of *H. atavismus*)	42	850
JPM-2014-005 (holotype of *S. lingyuanensis*)	47	850
D3072	55	1135
IVPP V 13363 (holotype of *S. dongi*)	58	1200
BPMC 105	69	1288
GMN-03-11-001 (holotype of *H. jii*)	79	1602
BPMC 103	79	1546
ZMNH M813 (holotype of *H. corollatus*)	75	1560
IVPP V 23388	79	1600
BXGM V0011 (holotype of *Huaxiapterus benxiensis*)	82	1600
BPMC 104	100	2124
D2525	110	2000
BPMC 107	111	2180

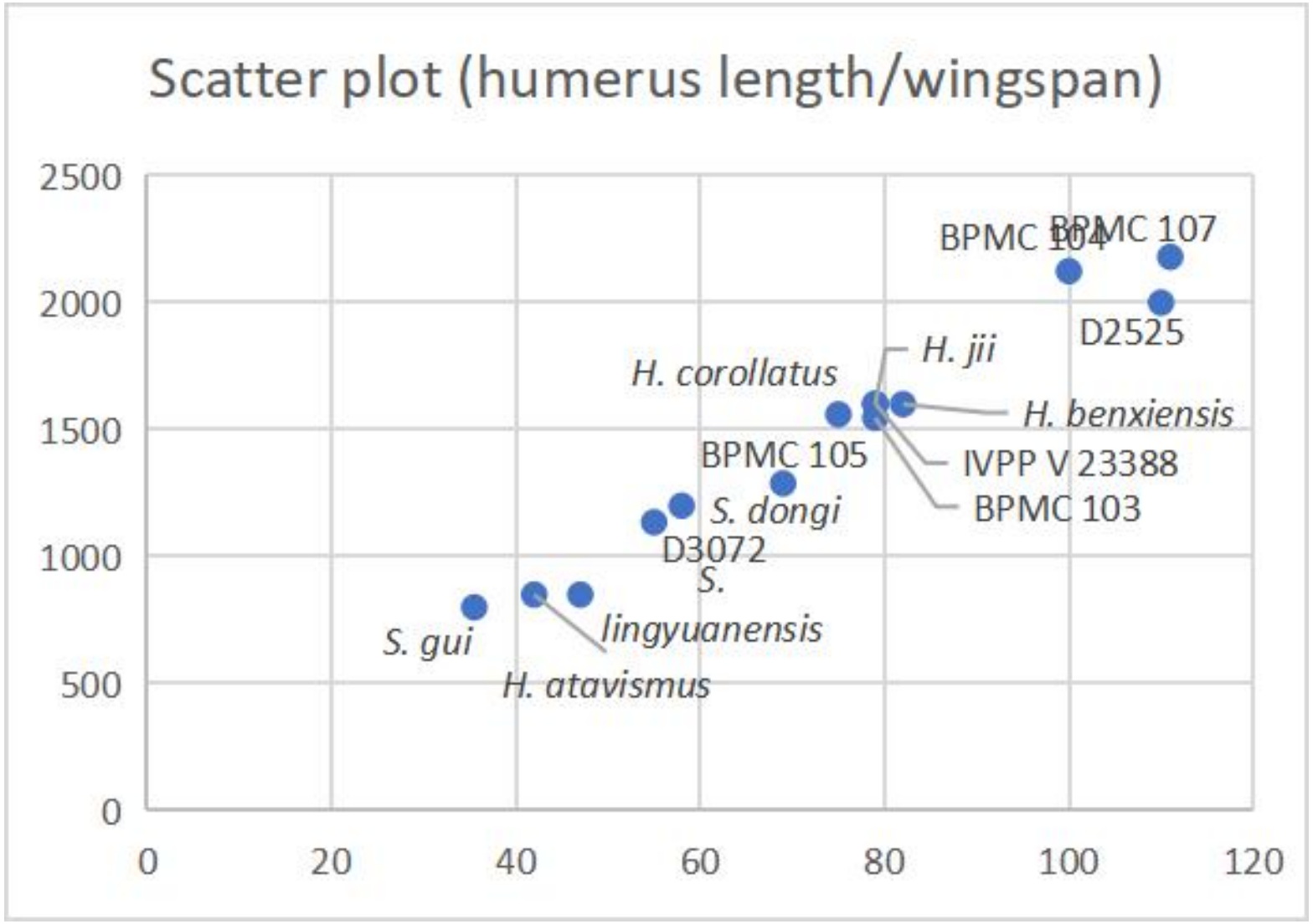
Scatter plot (humerus length/wingspan)
2500
2000
1500
1000
500
0
0
20
40
60
80
100
120
BPMC 104
BPMC 107
D2525
H. jii
H. corollatus
H. benxiensis
BPMC 105
IVPP V 23388
S. dongi
BPMC 103
D3072
S. lingyuanensis
S. gui
H. atavismus

Supplemental File 5: A nexus-format file for Mesquite, containing the phylogenetic data matrix.

https://dfzljdn9uc3pi.cloudfront.net/2023/14829/1/SI_02_Mesquite_file_Huaxiadraco.nex

Supplemental File 6: TNT file for the phylogenetic analysis.

xread

230 101

Ornithosuchus_woodwardi

000000?2000001000000000000-??0100-00?00-?000------0----0100---0000000000000--0-00000--0??0?0-----00000?0000--?0000000--0000--0-010000000????000000000000010000?0000000000-???000-000?0?000001000000000000000000?00000000000000000000000000

Herrerasaurus_ischigualastensis

000010?0000000000000000000-??0100-00-00-?000------0----0100---0000000000000--0-00000--0??0?0-----0000000000--?0000000--0000--0-000000000????000000000000100000000000000000-???000-000?0?000001000000000000000000?00000000000000000000000020

Scleromochlus_taylori

000010?0000000000000000?00???2?00-00-?0-?000------0----0100---00001?0?20??0--0-00?????????0-----000??0?00?--???????????0000--0??????000???????0??00?00?000??00?00???00??-????????0?????0000???0?00??01?00??00??????00???00?000?0000?0??

Anurognathus_ammoni

000000?1000000000001001000-??2100-00-00-?010------0----0110---0001100010??0--0-00000--0????0-----010000000?--???000-0--0000--0?1?0??0000????000000010100100000000??0???-?????0-?00????010000?0?????010110?100?000?000??10011202?00011

Rhamphorhynchus_muensteri

110010?000001100111000000??0011000-00-?000------0----0100---0000000021000--0-000000-0??0?0-----100000121002?0000000--0100--0-000030001????000000010000100000000000000000-???000-000?000001000000100101111002002000011 00?100122022210012

Darwinopterus_linglongtaensis

101100?0000011??????00?00-??001??00-00-?00?2000000----00-10101000100021?00--0-00?00--?????0-----??0?0?1??000??????0???00?0--0?100?00000????000000012000000?0000???101?-?????0-?00?0?0001?00?00?00?011110?101100?0110??100311?1111?022

Darwinopterus_robustodens

101100??00?011??????00?00-??001??00-00-?00?2000000----00-1010?000100021?00--0-00?00--?????0-----??0?0?1???00??????0???00?0--0?100?00000????000000012000000?0000???1???-?????0-?00?0?0001?00?00????01111??101100?0110??100311?1111?02?

Kunpengopterus_sinensis

101110?00000?11310110000?-??0011????00--000------0----00-1000100010021??0--0-00?0????????0-----?0???0?121??????????00--0010--??1?0?00000000?000000012000000?00000001010-?????0-?00?0??0010?000?100?011110010110??0110??100211?1121?022

Pterodactylus_antiquus

101000?0000011??????00000-??0010?00-00-?000------0----00-1001000010003 1?00--0-10?0???0????0-----??0?0?120000??????00--0000--0?000?30000????000000012000100000000021100????00-?00?000010000000100101211005001 00?02100?100312022220020

Pteranodon_longiceps

101000?2000011131231000002??1021002--0-?000------0----00-112?0000110023101231100100--0????0-----100001131?20?000001---0000--?0001004----------111110 1-???0000000?000110101101200101211014000111031112202322022321020

Pteranodon_sternbergi

101000?2000011?????000002??10210?2--0--000------0----00-?????0101100231012511 00?0????????0-----??0???131?20??????1---0000--??001?04----------1111101-?? ???0??00?000110101101 2?0101211014000111?31???20232 2?2232?020

Tethydraco_regalis

??-?-???01???0140001110?????????????????????

Nyctosaurus_gracilis

101010?000001101001?000002??1021000--0-?000------0----00-?????000110021100--12 00?0???0????0-----100001131?00?000000---0000--100000040----------11?1101 -?????00?00?000110000?00100100311013102 0?003111221232202 2?200??

Muzquizopteryx_coahuilensis

?01010??000011???????0???????0???????????0???????0----00-?????0001?0021?00--12 00??????????0-----?????????????????????????0????000?34----------???1101-?? ??????0??0??1???0?1??????01?11??31020????11??21???????????1??

Ikrandraco_avatar

101000?00000110????100?00???0011?00-00--000--00--0---?00-11001?0100031 1?0--0-00?0???1???-0?-?-?10000120?00???00?00??001212??100?00000--??000??0012010100010 0?01111101-???????????0?0????0????????012????40001???221?2201??20????0???

Lonchodraco_giganteus

1?????????????????????000????????1?00-?0--0?1??0000?----?????????????????????????????1???-0?-?-???????1?00?????????0?0?012?0?????????00--0??000000120101000100 10???????????????????????????????????0??????????????????????????????????

Haopterus_gracilis_

1010?????????????????00000???0?11?00-00--000-?0?--?---?00-?????0?????????????????????????-0?-?-??????1121??????????0???010--0?1?0??2000--??000000011010100010000???11??-?????????????????111?1??2??2???04??0????2?1?????3??2?22????20

Hongshanopterus_lacustris

??????????????03011000?00?????11?00-?0--0????0?--?---?0?????????????????1??????00??0--1??0-0?-?-?100??1???????0???0?????????????????2000--???000000100200001 0?001?111101-???

Nurhachius_ignaciobritoi

101100?20?1031??????0000????0111?00-00--000--00--0---?00-1?10?011210032000--0?0000???3???-1?-?-??00?0?121?00??????00000010--??100??3000--??00000001002000111000011111101-???????????0??1???0111020020121 1?040001???221?2??1312?22?2?1??

Nurhachius_luei

101100?20010310?????000?????0111????0??-000--0---0---?00-?????0?12?0?32?00--??0 0?0???3???010-???????0?1210????0???00100010--??1?0?03000000?00000001002000111 00

00?11?101?????????0??0?0??
Liaoxipterus_brachyognathus
????????????????????01????????0??
??????????????????????110?????0????0??00??????????23?00????00000?0100200001 0?0????
??
Istiodactylus_latidens
101100?0111111?????00100???0100-00-00--000--00--0---?00-1110?01121 1033 0?0--0-
001????????-0?-?-??000011100 00?????00??0010--??100?23000--??000000010021000010000
00?111?01-???????????0?01???0111020020 1?1?1040001 1?1?2112?????????????
Istiodactylus_sinensis
101100?0111111?????00?0????0100-00-00--000--00--0---?00-?????0112 1033 0?0--0-0
0?0???3???-0?-?-???0?0?11?000?????00??0010--??100?23000--??000000010021000010000
1??11??-????????0??0?01????1?1?????0121???4000????221????1312?22???1??
Zhenyuanopterus_longirostris
101000?2001011?????00?0????002?-?0-00-?0014?00000---?00-1?00?0?101??22??0--1
000?0????????00-???????0?13??00?????0???0000--??100?0001 2000?000?00010100 2100?0
000?111101-?????0??00?0?01100?1?1?????01211??40001???22????0?312?2222?120
Boreopterus_giganticus
101010?2001011?????00?0????002?-?0-00-?000------0---??0-??????110??032?????????
??????????00-?????0?0?1???00??????0???0000--??100?2001 2000?000?00010100 2100??000?
??????????????0????????????????????????00?????????????????????
Boreopterus_cuiae
1010???200??????????00?0????002?-?0-00-?000------0---?0??????????0??032??????????
?????????00-?????0???13??00??????0??0000??-??100?2001 2000?000?000?0100 2100?0000??
????????????????0????????????????????0?0????????????????????
Ornithocheirus_simus
10????????????????????00??2?????0?00-00--0??????????0????????????????????????
??0--???0000-?0??0?0000?1?000010000?1??010?0???
??
Targaryendraco_wiedenrothi
????????????????????01??
??????????????????????0000?0??0??1110010--0????000??????11?00?010000?1000100????
??
Aussiedraco_molnari
????????????????????01??
??????????????????????1?00??????0??111?000--???????0???????11?00?0??????????100??????
??
Barbosania_gracilirostris
1010?0??0?0?????????001?0???0020??0-00--000------0---?00-1????0??????21??0----00?
0????????1000?0??0???120000-?????0??10000--??000?0001 1000?111000010000210001000?
????????????????????0??1???01?1???0?0121???40001???22???201???????2????
Camposipterus_nasutus
1????????????????????01????????0?00-10--0?0------????????????????????????????

100100001000000?????????????????????????????????????0???0000?101100?????????1000????
??

Cimoliopterus_cuvieri

1?????????????????????01????????0?00-10--0?1?20000?0000?????????????????????????????
??100100001000000?????????????????????????????????????0???0000?1?1100?????????1000??
??

Cimoliopterus_dunni

1?????????????????????01????????0?00-10-?0?1?20000????0?????????????????????????????
??1001000?1??0?0?????????????????????????????????????0??????0?1?1100?????????1000???
??

Aetodactylus_halli

??????????????????????01?0?????????????????0------?????????????????????????????????
??????????????????????120000?0??0??1000?0--0??0?0?0???????01011?000000?1???100?????
??

Hamipterus_tianshanensis_

101000?20000?101101100000???0020?00-0101001210011000000-?????00101002 11?
0--0-00100--10000100000100011120000?0000000200010--1-0001?001100000110000100002
100010001111101-?????00?0??000????01?????0?01???104000100?22?12?0????0????0???

Iberodactylus_andreui

??????????????????????00????????0?00-01010?1?10011?0000?????????????????????????
???0--100001000 00?????????????????????????????????????0???000??1?000010000?1??010?0?
??

Tropeognathus_mesembrinus

101000?200001101001100000????010-00-0100001020000010000 0-?????01001002110
1001000100--201001000001000111 10000?000000000000201000001?001?000001?0000100
00110001000?111101-???000000??00?1???0?11???0201??????0?0?10??211?????????????????
?

Siroccopteryx_moroccensis

??????????????????????00????????0?00-01000?1??0000?1000?????????????????????????
???0--2?100110000?????????????????????????????????????0??00000?110000100001?0001000?
??

Ferrodraco_lentoni

1?????????????????????000???????0?0??0100001020000010000?????????????????????????
????0--1?000100000??????1?00?????????0000002?1???????0??000000110000100001100011
100???

Mythunga_camara

101?????????????????????0???
????????????????????????1?????????????????????????????0?????????????010000?100?110??????
??

Aerodraco_sedgwickii

??????????????????????0?????????0?0??01210????0000??00?????????????????????????
???1001?000110000???0111?110000?????????1000?
??

Coloborhynchus_clavirostris
????????????????????00????????0?00-01210????0000?1000????????????????????????
???0--1?000110000????????????????????????????????????0???1111?110000??00??????1000??
??
Uktenadactylus_wadleighi
????????????????????00????????0?00-01210????0000?0110????????????????????????
???0--1?001110001????????????????????????????????????0???1111?110000??00??????1000??
??
Uktenadactylus_rodriguesae
????????????????????0?????????0?0??012?0???????0????0????????????????????????
????????1110001??1???0??0???????????00?????
??
Nicorhynchus_capito
????????????????????0?????????0????012?0??????00?0110????????????????????????
?????1??1011111??1111???0??0???????????100?????
??
Nicorhynchus_fluviferox
????????????????????0?????????0????012?0??????00?11?0????????????????????????
????????1011111O??1??1???0??0????????????0?????
??
Anhanguera_spielbergi
101010?2000011010011000??1020?00-01?10010200000?00100-1100101011002110
1001000100--1100010000010001?1???000???????????00?2?10???010001?0010?11001010000
21??010001111101-???000000??000?1??02111210?01???104000110l?21?2??1????????????
Anhanguera_blittersdorffi
101010?2000011010011000??1020?00-0101001020000000100-?????01011002110
1001000100--1100010000010001l???0???0?000?????00201?0?00?0001?001??11001010000
210001000?????????????????????0??
Anhanguera_piscator
101010?2000011?1????00000???1020-00-0101001020000000100-1100101011002110
1001000100--????0100000100??1120000??????0???0002010??00?000110010011001010000
2100010001111101-???0000000?000?10102111210201211104000110122112??1???0???201
20
Liaoningopterus_gui
101?0??2000011???????0?0????????0-00-010?00102000?000???????????0110?211?????
????????1????100000??0?????0?00??????0?????02010?????001100??01100101000021000
1000111?1??
Cearadactylus_atrox
10100???0010?101????0?000???10?0-00-0101001020000????1?????00??1011?0211????
??????0--1100010000010001?120000?000000020000?--00000?000110010011001010000210
0010?0??
Maaradactylus_kellneri
101?0??2001011???????0000????0?0?00-0101001020000?1001?0?1?????0110?211?1??

??????0--11000100000??0?????0?????????????????2010??????00110010?11001010000210001
10?0??
Ludodactylus_sibbicki
101000?0000011?????00?00???1020-00-0???00???00000????00-110010100100211011
61100?00--1?0??100000??00?1120?00??00?00??1000201??000?00011?0?001100101000021
0001001???
Guidraco_venator
10?000?0000011??????00?0????1020-00-0???00???00000????00-?????0?00100211?116
1100?0????????100?0??00?1?120?00??????0???000?--??000?00011?0??0110010100002100
01001?1111??-????????0????0??
Caulkicephalus_trimicrodon
10?????0??0???????????00?0???1??0?00-01?10?10200000?01?????????????????????1161
1????0--11?00100000?0????????????????????????????????????00???010?110010???0??????10??
??
Dsungaripterus_weii
101000?0101111041021000000?20011002-00-?1011100000????10-?---00001000211012
21101110--1????0?-?-?10000112102O?0000000--0000--1-000?0110-????--0--0110000-00000
0001111100-???000000??000110??000???1201210??5011?00?31001??1312022?20120
Noripterus_parvus
101000?0101111?????000000?20011000-00-?1011100000????10-?---0000100021?012
21101?10--?????0?-?-??0000?121000?0000?00--0000--?-00??0110-????--0--0110000-00000
000?11??0?????00??00??000???????????1?0???????011??00??0?1???????????????
Keresdrakon_vilsoni
1010??0?????????????00000100??21100-00--00????000?----00-?????????????????????
??1000???-0--?-???01??12100??0101010--000400??000??4----------?111100-1
1?000000?0000???????00201?01???0150112?????????????????????
Tupuxuara_longicristatus
??????1?????????????0000100??????0-??????1340000?----?????????????????????????
??1003?---????????02????????????????????????????4----------????????????
??
Tupuxuara_leonardii
1011001200203 1?5102100000100011 1100-00-?0013400000????00-?????001100022101
2711011110030---0--?-?10021113 1000?000?00---0000--10000004----------111
1100-1100000000000 1???20000201?012100150112010310 01?01313????2????
Kariridraco_dianae
10110?02002031?5?????0000??0011???????????1?????????????0-???????1110022???????
???????3????????????0021?1??0?????????????0??0--??000??4----------1111100-
11000000???000???
Thalassodromeus_sethi
10110002002031?6102100000300011 1200-00-?0013400000????00-111000011 10?2210
12711011110030---0--?-?1003011?1102?000?00---0000--10000004----------???
??
Thalassodromeus_oberlii

??????????????????????????030??
??????????????????????????102?000?00---0000--1-?0???4----------?????????????
??
Caupedactylus_ybaka
10110002002031?5102100010100211110l0-0---013400000----00-?????1012100321012
71101111000----??????1011011?1010-000100---00021011?0???4----------?????
????????00???????????20000201?01???0150012?10??????????????????
Aymberedactylus_cearensis
??????????????????????0001010????1??1??
????????????-?-???????1210100000100---00021?11?00024----------???????????
??
Tupandactylus_imperator
10110002002031??????10???2??21112?10-0-?0013310000???00-??????012??122?012
21101??????????0?-?-???????121?100????0?-??100212??100?04----------?????
???????????0??0????????????????????????01????????????????????????
Tupandactylus_navigans
101100020020311 51??110?102??21112110-0---013410000----00-1111110121012200120
1101111000----0-----1011?11210100000???---100212??100?04----------???????
????????00?0001?????????????1??????011???????????2????????????
Caiuajara_dobruski
10110002002031??????1001021021112110-0-?00133100?????00-???????11101220?12
21101111100--??0?-?-???1??11210100000200---10021210110?04----------?111
100-?????00?0??000??0?200002?1?0121?1150l120?031??120?????????????
Europejara_olcadesorum
???????2???031???????0??????????1?1?-????????????????0?????????????0220?12???0?
????????????-?-?1????112??10000??00---100212??100??4----------???????????
??
Tapejara_wellnhoferi
10110002002031 02????1001021021112110-0-?0013300000????00-?????101110122001
221101111100--??0?-?-?101101121010000020 0---10021210110004----------?1
11100-110000000000000??0?20000201?012101150112000310012013l?????21120
Afrotapejara_zouhri
??????????????????????00??210???11011-0--??1????????????????????????????????????
?1010----0-----??
??
Bakonydraco_galaczi
??????????????????????001021????11011?0--????????????????????????????????????
??1010--??????????????????0100000110???1??2???0100104----------??????????
??
Wightia_declivirostris
??????????????????????00??210???10011?0--??1????????????????????????????????????
??1100--??
??

Eopteranodon_lii

101??002??2?????????10??0???2011??10?0-?0013300??1????00-1101????????42???1???
??????????????-?-???????1?1?101??????-??1002????20??24----------??????????
???0??01?????????????????0121???5011????2??????13?2?22?2????

Sinopterus_dongi

10110001002031??????100102??20111?10-0-?0013300001????00-1101?1011?0042?111
11101?1????????0--?-???1???1210101?0???0---1002101?200124----------?111
100-?????0??01????1???20000202?01211?150012???310??20131?2232?120

Huaxiadraco_corollatus

10110002002O?1??????1001021?21111?10-0-?0013301001????00-??????????0?32?1111
110????????????0?-?-???????121?101000?10-??100210???2???24----------?1111
00-????????00000?????2000??????1211??5011?2???3????202313?2232?120

M_4895

??
??121
10011??0??0??0000???

Shenzhoupterus_chaoyangensis

10100102002031??????00?0????10211?0-00-?010----------00-?????0??2????2?0124110
1??????????0?-?-???0?0?121?00??????0-??0000--??000?040----------?1021??0?
???????00????????10?0???2??1200??5011????310?????312?2232?1??

Lacusovagus_magnificens

101?????????????????0001??0???1??0-?0--010----------??????????????????????????
??40----------??????????????
??

Chaoyangopterus_zhangi

101??10?0????????????00?0110?10211?0-00-?01???00--?????00-?????????????????1?????
???????????0?-?-???0???1?1020??0????-??0000--??000??40----------?1021100??
???0??00?0?0????1000???2??1200???0?1????310??201313?22?2?1?0

Jidapterus_edentus_

101???0?????????????0000011001?21100-00-?01???00--?????00-?????????0?0??????????
???????????0?-?-???????131020???0??1---0000--1?000?040----------?1?21100??
???0??00?0?0????1??0???2??1200??5011?0?0310????1313122321120

Xericeps_curvirostris

??????????????????????????0102??????0-??
??????????????????????????12??0?110???????0?????0????????????????????????????????
??

Leptostomia_begaaensis

??????????????????????????0102??????0-??
??????????????????????????10??0?1101??????0?????0????????????????????????????????
??

Alanqa_saharica

??????????????????????????0102??????0-??
??????????????????????????00??0?1101??????3?????0????????????????????????????????

??
Argentinadraco_barrealensis
????????????????????????010??
????????????????????????0???001?01??????3???0?01????????????????????????????????
??
Montanazhdarcho_minor
????????????????????00??102??
????????????????????1??0???0?0??1?--???0????????????????????????????????????2?
10????????????????????????????????????0???1??????????????????
Aralazhdarcho_bostobensis
??
??1031
220?001?0?0???000????????????????????1?????????????????1????????
Phosphatodraco_mauritanicus
??
??1031
22010110000001000??
Wellnhopterus_brevirostris
101???0?????????????000001000?111?0-00--0?1???000?????0????????????????????????
????????????????????121000??????0-??0000--???01??40----------?1031220?
0???000001[0 1]?0??
Eurazhdarcho_langendorfensis
??
??1031
220111000000001000?????????????????????????????????????1????????
Zhejiangopterus_linhaiensis
101000020020?1??????00?0????0021100-00--000--00--0????00-0---00001000?2?00--0-
01???????????0?-?-???0?0?1?1?00?0????1-??0000--??001?040--????--0--0010000-------001??
31221?????0??0000??1?0?1000???22?1200??510?????310??202413????2????
Azhdarcho_lancicollis
????????????????????00?????????1?0??????0????0?--??????0-?????????????1?????????
?????????0?-?-?????????????0???0?-????0??????????40--??????0??0010000-------00110312
211100000012?00001?????????????????0151???0?????????????1????????
Cryodrakon_boreas
??
??031
221110000011000000?????????????11???0151012000??????0????1????????
Quetzalcoatlus_northropi
??
??0?1
22?01???011??100?????????????10???0151012011?1?????????????????
Quetzalcoatlus_lawsoni
101000020020????????000001000021100-00--0014?00--?????00-0---000010?0?210????

?????0--0????0?-?-?10011?131000?000001---0000--10001?040--????--0--0010000-------0011
03122201?001111000011?0?1000020221020?015101200131001??2413122?21?20
Quetzalcoatlus_FSAC-OB_14
??
??1031
22?01000111??0001???
Hatzegopteryx_thambema
??
??????????????????1???????????1???10?1
22?01001001??0000?????????????????1??????101?????????????????????????
Albadraco_tharmisensis
??????????????????????00??100????1??
??1000----????????????????000-0??1??---???0--???????40----------??0?122?01?
01001??0000???
Arambourgiania_philadelphiae
??
??1031
222010000?11?0111???
Mistralazhdarcho_maggii
??????????????????????0?0??
??????????????????????????001?1?010???????????0?0????????????????????????????????????03
1222010?0???1?0111?????????????11??????101?????????????????????????
Aerotitan_sudamericanus
??????????????????????0???00??
??????????????????????????001?1?01?????????????????0????????????????????????????????????
??
;

cnames
{0 External_naris_(or_nasoantorbital_fenestra),_position_relative_to_the_premaxilla_
main_part_dorsal_to_the_ventral_margin_of_the_premaxilla
main_part_displaced_posterior_to_the_premaxilla;
{1 External_naris,_dorsoventrally_compressed absent present;
{2 External_naris_and_antorbital_fenestra,_configuration_ separated
confluent,_forming_a_nasoantorbital_fenestra;
{3
External_naris_and_antorbital_fenestra_(or_nasoantorbital_fenestra),_ventral_margin_length
_relative_the_skull_length shorter_than_40%_of_the_skull_length_
longer_than_40%_of_the_skull_length;
{4 Antorbital_(or_nasoantorbital)_fenestra,_posterior_margin,_shape_ straight_ concave_;
{5 Nasoantorbital_(or_antorbital)_fenestra_extending_dorsal_to_the_orbit_ absent present;
{6 Nasoantorbital_fenestra,_anteriormost_region,_elevation_(new) elevated
ventrally_displaced;

{7 Orbit,_shape_ subcircular subquadrangular_(broad_base)
piriform_(dorsoventrally_elongated)_;
{8 Orbit,_comparatively_small absent_ present_;
{9 Ventral_margin_of_the_orbit closed open;
{10 Orbit,_position
middle_of_the_skull,_with_the_ventral_margin_of_the_orbit_below_the_middle_of_the_ant
orbital_(or_nasoantorbital)_fenestra_and_the_dorsal_margin_of_the_orbit_above_the_dorsal
_margin_of_the_antorbital_(or_nasoantorbital)_fenestra
high_in_the_skull,_with_the_dorsal_margin_of_the_orbit_surpassing_the_level_of_the_naso
antorbital_fenestra
low_in_the_skull,_with_the_entire_orbit_lower_than_the_dorsal_margin_of_the_antorbital_(
or_nasoantorbital)_fenestra;
{11 Suborbital_opening absent_ present_;
{12 Lower_temporal_fenestra,_shape
comparatively_broad,_with_extensive_subhorizontal_ventral_margin
piriform,_with_dorsal_portion_wider_than_ventral__
piriform,_with_ventral_portion_wider_than_dorsal_ reduced_(slit-like);
{13 Lower_temporal_fenestra,_position_relative_to_orbit posterior_to_orbit
reaches_under_posterior_margin_of_orbit;
{14 Choanae,_separation separated_by_vomer confluent;
{15 Postpalatine_fenestra,_shape quadrangular/subtriangular oval egg-shaped
elongated_egg-shaped_ kite-shaped,_rounded_margin elliptical reduced,_slit-like;
{16 Secondary_subtemporal_fenestra absent present;
{17 Interpterygoid_fenestra,_size smaller_than_subtemporal_fenestra
larger_than_subtemporal_fenestra_ extremely_reduced;
{18 Interpterygoid_fenestra,_shape compressed_laterally broad,_longer_than_wide
compressed_anteroposteriorly,_wider_than_long round;
{19 Pterygoid_fenestra absent_ present;
{20 Jaws,_marked_gap_during_occlusion absent_ present;
{21 Jaws,_shape laterally_compressed_ comparatively_broad_;
{22 Jaws,_anterior_half,_margins_in_occlusal_view continuous_taper subparallel;
{23
Jaws,_lateral_expansion_level_with_anterior_margin_of_the_nasoantorbital_(or_naris_+_ant
orbital)_fenestra absent present;
{24 Jaws,_lateral_flaring_of_the_jawline absent present;
{25 Jaws,_pointed_tip,_occlusal_surface_(new) convex
gently_sulcate,_with_low_tomial_edges sulcate,_with_tall,_protruding_tomial_edges keel;
{26 Jaws,_pointed_tip,_tomial_edges slender thick;
{27 Jaws,_pointed_tip,_cross-section,_(modified_from_Vidovic_&_Martill,_2017)
straight_lateral_sides concave_lateral_sides bowed_out_lateral_margins;
{28 Skull,_main_part_of_dorsal_margin,_curvature_excluding_cranial_crest nearly_straight
concave_ convex;
{29 Skull,_height,_exclusive_of_cranial_crests under_25%_jaw_length over;

{30 Length_of_the_rostrum_(pm-naof)_relative_to_the_skull_length_(pm-sq)
reduced,_under_20%_ elongated,_between_20_and_50%
extremely_elongated_(more_than_half_of_skull_length);
{31 Rostrum,_anterior_end,_shape blunt pointed sharp_tip;
{32 Rostrum,_pointed_tip,_anteroposterior_taper_in_lateral_view up_to_11° 12°_-_25°
over_25°;
{33 Rostrum,_distinct_fossa_on_occlusal_surface absent present;
{34 Rostrum,_prenarial,_main_axis,_orientation straight downturned upturned;
{35 Rostrum,_prenarial,_downward_deflection_of_main_axis,_location;
{36 Rostrum,_anterior_end,_small_blunt_anterior_projection_above_first_teeth_pair absent
present;
{37 Premaxilla,_anterior_expansion absent present;
{38 Premaxilla,_anterior_expansion,_lateral_margins rounded straight,_subparallel;
{39 Premaxilla,_anterior_expansion,_width_relative_to_post-rosette_width Under_130%
Between_130%_and_140% Over_140%;
{40 Premaxillae,_anterior_end_rodlike absent present;
{41 Premaxilla,_posterodorsal_margin_of_nasoantorbital_fenestra_(including_nasal),_width_
wide thin;
{42 Premaxillary_sagittal_crest absent present;
{43 Premaxillary_sagittal_crest_position confined_to_the_anterior_portion_of_the_skull_
starting_anterior_to_the_anterior_margin_of_the_nasoantorbital_fenestra,_extending_beyond
_occipital_region
starting_at_about_the_anterior_margin_of_the_nasoantorbital_fenestra,_reaching_the_skull_r
oof_above_the_orbit_but_not_extending_over_the_occipital_region
starting_close_or_at_the_anterior_portion_of_the_skull_and_extended_over_the_occipital_re
gion starting_at_the_posterior_half_of_the_nasoantorbital_fenestra
starting_at_the_middle_part_of_the_nasoantorbital_fenestra_and_extended_over_the_occipit
al_region absent;
{44 Premaxillary_sagittal_crest,_shape striated,_low_with_a_nearly_straight_dorsal_margin
striated,_high_with_a_nearly_straight_dorsal_margin round_dorsal_margin,_bladeshaped
smooth,_expanded_anteriorly_and_forming_a_low_rod-like_extension_posteriorly
smooth,_starting_low_anteriorly_and_very_expanded_posteriorly
striated,_low,_convex_dorsal_margin;
{45 Premaxillary_crest,_elongated_dorsal_premaxillary_spike-like_projection_ absent_
present_;
{46 Premaxillary_crest,_distinct_expansion_on_the_anterior_part_ absent present;
{47 Premaxillary_crest,_concentric_striae_on_the_anterior_region absent present;
{48 Premaxillary_crest,_anterior_expansion_of_the_anterior_margin absent present;
{49 Premaxilla,_posterior_dorsal_process,_curved_upward absent present;
{50 Premaxillary_blade-like_crest,_position posterior_to_rostral_tip at_rostral_tip;
{51
_Premaxillary_blade-likecrest,_dorsal_margin_of_rostrum_connecting_to_crest_(REESCRE
VER) round/keeled broad,_flat/grooved;

{52 Premaxillary_blade-like_crest,_anterior_margin_of_crest_strongly_concave absent present;
{53 Premaxillary_blade-like_crest,_anterior_base_thickness thick,_tapering_dorsally slender,_constricted_base;
{54 Maxilla,_posterior_ventral_expansion_ absent_ present_;
{55 Maxilla-nasal_contact absent present;
{56 Maxilla-nasal_contact,_broadness broad narrow;
{57 Nasal_descending_process absent present;
{58 Nasal_descending_process,_position_ placed_laterally placed_medially absent;
{59 Nasal_descending_process,_length_
long_(almost_reaching_the__ventral_margin_of_the_skull) short
knob-like_(extremely_reduced);
{60 Nasal_descending_process,_orientation_ inclined_anteriorly subvertical absent;
{61 Nasal_descending_process,_lateral_foramen_ absent_ present_;
{62 Lacrimal,_extensive_fenestration absent_ present_;
{63 Lacrimal,_orbital_process_ absent_ present_;
{64 Jugal,_lacrimal_process_base,_width_ broad narrow;
{65 Jugal,_lacrimal_process,_inclination_ inclined_anteriorly subvertical
inclined_posteriorly;
{66 Jugal,_presence_of_pronounced_ridge_on_the_lateral_side absent present;
{67 Jugal,_posterior_process,_orbital_process absent present;
{68
Jugal,_tetraradiate_(with_a_posterior_process_skirting_most_of_the_posterior_margin_of_the_lower_temporal_fenestra) absent present;
{69 Quadrate,_inclination_relative_to_ventral_margin_of_skull_ anteriorly subvertical
inclined_about_120°_posteriorlyned_about_120°_backwards_
inclined_about_150°_posteriorly about_160°;
{70 Cranio-mandibular_articulation,_position_relative_to_orbit_
_posterior_to_posterior_margin_of_orbit under_center_of_orbit_
under_anterior_margin_of_the_orbit anterior_to_anterior_margin_of_orbit;
{71 Helical_jaw_joint absent_ present_;
{72 Frontal,_anterior_portion_rugose absent present;
{73 Frontal,_ossified_crest absent present;
{74 Frontal,_ossified_crest,_position_ confined_to_posterior_end_of_skull
starting_above_orbit starting_on__posterior_half_of_nasoantorbital_fenestra;
{75 Frontal,_ossified_crest,_shape low,_blunt short._spike-like,_dorsally_deflected
spike-like,_directed_posteriorly narrow,_broad,_directed_posteriorly
low,_broad_base,_fans-shaped high,_broad_base,_crown-shaped
high,_broad_base,_casqued-shaped
high,_broad,_directed_posteriorly,_at_least_doubling_shight_of_skull_above_orbit absent;
{76 Parietal,_ossified_crest absent present;
{77 Parietal,_ossified_crest,_shape_ blunt_
constituting_the_base_of_the_posterior_portion_of_the_cranial_crest

expanded,_with_rounded_margin;
{78 Posterior_region_of_the_skull_rounded_with_the_squamosal_displaced_ventrally
absent_ present_;
{79 Supraoccipital does_not_extend_backwards_ extends_backwards_;
{80 Supraoccipital,_foramen_ absent_ present_;
{81 Paroccipital_processes,_expanded_distal_ends_ absent_ present_;
{82 Palate,_neurovascular_foraminae,_rows absent present;
{83 Palate,_neurovascular_foramina,_spacing continuous_spacing cluttered;
{84 Palate,_neurovascular_foramina,_shape slit-like pit-like;
{85 Palate,_occlusal_surface smooth discrete_palatal_ridge,_tapering_anteriorly_
strong_palatal_ridge,_tapering_anteriorly
strong_palatal_ridge,_confined_to_the_posterior_portion_of_the_palate;
{86 Palate,_palatal_ridge,_reducing_posteriorly absent present;
{87 Palate,_palatal_ridge,_position anterior_to_fifth_tooth_position
posterior_to_fifth_tooth_position;
{88 Palate,_depression_posterior_to_second_tooth absent present;
{89 Palate,_bulbous_projection_between_the_second_alveolar_pair absent present;
{90 Palatal_tip,_dorsal_deflection absent
present,_with_first_alveoli_pair_not_surpassing_second_one
present,_with_first_alveoli_pair_surpassing_second_one;
{91 Palatal_tip,_dorsal_deflection,_angle_relative_to_remaining_palatal_plane under_90°
90°;
{92 Deltoid_facet,_height_relative_to_width height_subequal_to_or_lower_than_width
higher_than_wide;
{93 Deltoid_facet,_dorsolateral_edges smooth anterior_ridges;
{94 Deltoid_facet,_anteroventral_depression_reaching_ventral_palatal_surface absent
present;
{95 Deltoid_facet,_round_depression_above_first_pair_of_alveoli absent present;
{96 Maxilla_and_internal_naris,_contact_ absent_ present_;
{97 Palatal_elements,_shape_ broad thin_bars;
{98
Palate,_lateral_expansion_close_to_the_anterior_margin_of_the_nasoantorbital_(or_naris_+_
antorbital)_fenestra absent present;
{99 Palate,_posterior_palatal_plates_of_the_maxilla,_surface flat slightly_convex
strongly_convex concave;
{100 Pterygoids,_position_relative_to_palatal_plane elevated depressed;
{101 Basisphenoid_body,_length_ shorter_than_wide longer_than_wide;
{102 Mandibular_rostral_end,_opposing_dentaries_ unfused fused;
{103 Mandibular_rostral_end,_extension_of_the_contact_surface_of_opposing_dentaries_
short,_limited_to_the_tip short,_extended_posteriorly_less_than_30%_of_mandible_length
long,_up_to_55%_the_mandible_length long,_extended_over_55%_of_mandible_length;
{104 Mandibular_rostral_end,_shape rounded pointed sharp_tip;
{105

Dentary_symphysis,_lateral_sides_extend_beyond_tomial/alveolar_edges_in_cross-section_(Thomas_et_al._2022);
{106 Dentary_symphysis,_main_axis,_orientation straight downturned upturned;
{107 Dentary_symphysis,_anterior_tip,_orientation continuous_with_main_axis downturned_relative_to_main_axis upturned_relative_to_main_axis;
{108 Dentary_symphysis,_dorsal_eminence,_position;
{109 Dentary_symphysis,_occlusal_surface,_anterior_median_ridge absent present;
{110 Dentary_symphysis,_occlusal_surface,_posterior_median_ridge absent present;
{111 Dentary_symphysis,_occlusal_surface,_paired_ridges_bordered_by_paired_sulcus absent present;
{112 Dentary_symphysis,_occlusal_surface,_foramination absent_or_poor paired_row_of_foramina numerous_foramina;
{113 Dentary_symphysis,_occlusal_surface,_midway_transverse_ridge absent present;
{114 Dentary_symphysis,_slenderness,_length_over_10_times_median_depth absent present;
{115 Dentary_symphysis,_laterolateral_compression_relative_to_alveolar_diameter over_3_times_alveolar_diameter subequal_to_3_times_alveolar_diameter;
{116 Dentary_symphysis,_occlusal_groove,_anterior_extension posterior_to_second_tooth_pair reaching_first_tooth_pair,_but_not_the_rostral_tip reaching_rostral_tip;
{117 Dentary_symphysis,_rims_of_occlusal_groove,_lateral_view,_dorsal_heigth level_with_alveolar_borders conspicuously_raised_above_alveolar_level;
{118
Dentary,_dorsal_margin,_distinct_posterior_eminence_close_to_the_separation_of_mandibular_rami absent present;
{119 Dentary,_tip,_projected_anteriorly absent_ present_;
{120 Dentary,_tip,_odontoid_process absent present;
{121 Dentary_symphysis,_ventral_margin smooth keeled crested_anteriorly crested_posteriorly;
{122 Dentary_ossified_sagittal_crest,_position_ confined_to_the_anterior_third_of_the_lower_jaw extinding_close_to_the_middle_portion_of_the_lower_jaw;
{123 Dentary_ossified_sagittal_crest,_shape_ shallow blade-like deep,_broad_in_lateral_view elongated_ridge absent;
{124 Dentary,_posteroventral_fossa absent present;
{125 Dentary,_posteroventral_fossa,_surface concave flat;
{126 Mandibular_rami,_dorsal_margin convex straight concave;
{127 Mandibular_rami,_deepness;
{128 Mandibular_rami,_orientation_relative_to_mandibular_symphysis_(Thomas) straight bowed;
{129 Mandible,_glenoid_fossa,_U-shaped absent present;
{130 Retroarticular_process,_shape_(Andres_et_al._2014) triangular_ subcircular elongate blunt rectangular;
{131 Teeth,_position_and_presence present,_evenly_distributed_along_the_jaws_

teeth_absent_from_the_anterior_portion_of_the_jaws_
confined_to_the_anterior_half_of_the_jaws confined_to_the_anterior_third_of_the_jaws
jaws_toothless;
{132 Maxillary_teeth,_largest_positioned_posteriorly_ absent_ present_;
{133 Teeth,_shape_variation isodont heterodont;
{134
Teeth,_anterior_positions_(first_through_fourth),_crown_height_over_four_times_diameter
absent present;
{135 Teeth,_upper_jaw,_second_pair,_position_in_horizontal_plane medial_to_third_pair
aligned_with_third_pair;
{136 Teeth,_upper_jaw,_3rd_pair_of_teeth_double_size_than_4th_pair absent present;
{137 Teeth,_upper_jaw,_5th_pair_of_teeth_medially_displaced absent present;
{138 Teeth,_upper_jaw,_first_pair_of_slender_elongated_teeth,_cross-section subcircular
elliptical;
{139 Teeth,_lower_jaw,_first_pair_of_teeth_enlarged_(subequal_to/larger_than_second_pair)
absent present;
{140 Teeth,_both_jaws,_third_tooth_larger_than_fourth absent present;
{141 Teeth,_anterior,_marked_variation_in_width absent present;
{142
Teeth,_spacing,_first_pair_separated_by_a_thin_sheet_of_bone_(less_than_half_the_alveolo
us_width) absent_ present;
{143 Teeth,_spacing,_first_three_pairs_more_closely_spaced_than_subsequent_teeth absent
present;
{144
Teeth,_upper_jaw,_variation_in_the_size_of_the_anterior_teeth_with_the_5th_and_6th_smal
ler_than_the_4th absent_ present_;
{145 Teeth,_base_broad_and_oval absent_ present_;
{146 Teeth,_serrated present absent;
{147 _Teeth,_peg-like_(cone-shaped) absent_
present,_15_or_less_on_each_side_of_the_upper_jaws
present,_more_than_15_on_each_side_of_the_upper_jaws;
{148 Teeth,_small_needle-shaped absent present;
{149 Teeth,_lateral_compression absent present,_moderate present,_strong;
{150 Teeth,_sharp_carinae absent present;
{151 Teeth,_anterior_positions,_relative_elongation under_twice_as_wide
over_twice_as_wide,_under_4x_as_wide over_4x_as_wide;
{152 Teeth,_striated absent_ present;
{153 Teeth,_crowns,_with_labial_and_lingual_depressions absent present;
{154 Teeth,_labial/lingual_view,_mesiodistal_constriction_between_crown_and_root absent
present;
{155 Teeth,_cingulum absent present;
{156 Alveoli,_prominently_scalloped absent present;
{157 Alveoli_borders,_strongly_raised absent present;

{158 Alveoli,_lateral_platform absent present;
{159 Alveoli,_toothline,_curvature_between_upper_alveoli_4_and_8 absent present;
{160 Atlas_and_axis unfused_ fused_;
{161 Cervical_vertebrae,_postexapophyses_ absent_ present_;
{162 Mid-cervicals,_centrum,_lateral_foramen_ absent_ present_;
{163 Mid-cervical_vertebrae,_length short,_sub-equal_in_length_
longer_than_wide,_with_length_less_than_3_times_width
elongated,_with_length_more_than_3_times_width extremely_elongate;
{164 Mid-cervicals,_ribs present_ absent_;
{165 Mid-cervicals,_arch,_neural_spines,_height_ tall low extremely_reduced_or_absent;
{166 Mid-cervicals,_arch,_neural_spines,_shape_ blade-shaped spike-shaped_ ridge;
{167 Mid-cervicals,_elongate_vertebrae,_maximum_cervical_V_elongation
under_7_times_width between_7_and_12 over_12;
{168 Mid-cervicals,_arch,_accessory_pneumatic_foramen_(dorsal_to_neural_canal) absent
present;
{169 Mid-cervicals,_arch,_adjacent_pneumatic_foramina_(lateral_to_neural_canal) absent
present;
{170 Mid-cervicals,_neural_canal,_position_relative_to_prezygapophyses
level/slightly_dorsal ventral;
{171 Mid-cervicals,_prezygapophyseal_peduncles,_medial_margin_in_dorsal_view
concave/straight convex;
{172 Mid-cervicals,_prezygapophyses,_lateral_extension
approximately_level_with_postzygapophyses
extending_further_laterally_relative_to_postzygapohyses;
{173 Mid-cervicals,_centrum,_posterior_lateral_constriction absent present;
{174 Mid-cervicals,_centrum,_deep_ventral_fossa_anterior_to_postexapophyses absent
present;
{175 Mid-cervicals,_centrum,_ventral_surface,_sagittal_keel_connecting_to_hypapophysis
fades_posteriorly,_smooth_ventral_surface
extends_posteriorly,_forming_a_mostly_acuminated_ventral_surface;
{176
Mid-cervicals,_heterometry_(dramatic_length_discrepancy_along_the_series,_CV_V_is_150
%_the_length_of_CIII_or_more) absent present;
{177 Mid-cervicals,_fourth_longer_than_the_fifth absent present;
{178 Mid-cervicals,_lateral_margin_in_dorsoventral_view concave
straight,_with_subparallel_sides;
{179 Mid-cervicals,_cross-section,_width/height_proportion_(excluding_neural_spine)
wider_than_high_(dorsoventrally_depressed) subcircular;
{180 Mid-cervicals,_cotyle,_depth_relative_to_width wider_than_deep
about_as_wide_as_deep;
{181 Mid-cervicals,_transverse_ridge,_dorsal_reflection;
{182 Notarium absent_ present_;
{183 Caudal_vertebrae,_quantity_ more_than_15_ 15_or_less_;

{184 Caudal_vertebrae,_zygapophyses_forming_rod-like_ossified_processes_ absent present;
{185 Proximal_caudal_vertebrae_centrum,_centrum_shape_ single douplex;
{186 Pectoral_girdle,_position_of_the_glenoid_fossa top-decker middle-decker bottom-decker;
{187 Scapula,_length_relative_to_coracoid_length subequal_or_longer_than_coracoid_ scapula_shorter_than_coracoid_(1_>_sca/cor_>_0.80)_ substantially_shorter_than_coracoid_(sca/cor_<_0.80);
{188 Scapula,_proximal_end_ elongated_ sub-oval_;
{189 Scapula,_shape_ elongated_ stout,_with_constructed_shaft_;
{190 Coracoid,_proximal_end,_shape flattened oval;
{191 Coracoid,_sternal_articulation_ no_developed_articulation articulation_surface_straight_or_slightly_concave articulation_surface_strongly_concave;
{192 Coracoid,_sternal_articulation,_posterior_expansion_ absent present;
{193 Coracoid,_ventral_surface smooth tubercle flange;
{194 Cristospine,_shape absent_ shallow_and_elongated_ deep_and_short;
{195 Humerus,_proximal_end,_cross-section crescent horseshoe;
{196 Humerus,_mid-shaft,_shape constricted unconstricted;
{197 Humerus,_proportional_length_relative_to_the_metacarpal_IV_(hu/mcIV)_ hu/mcIV_>_2.50_ 1.50_<_hu/mcIV_<_2.50_ 0.40_<_hu/mcIV_<_1.50 hu/mcIV_<_0.40;
{198 Humerus,_proportional_length_relative_to_the_femur_(hu/fe)_ hu/fe_<0.80_ 1.4_>_hu/fe>___0.80_ hu/fe_>_1.40;
{199 Humerus_plus_ulna,_proportional_lengths_relative_to_the_femur_plus_tibia_(hu+ul/fe+ti)_ humerus_plus_ulna_about_0.80%_or_less_of_femur_plus_tibia_length_(hu+ul/fe+ti_<_0.80)_ humerus_plus_ulna_larger_than_0.80%_of_femur_plus_tibia_length_(hu+ul/fe+ti_>_0.80)_;
{200 Humerus,_proximal_end,_small_foramen_on_dorsal_surface_distal_to_proximal_articulation absent present;
{201 Humerus,_proximal_end,_foramen_on_ventral_surface_close_to_proximal_margin_ absent_ present_;
{202 Humerus,_deltopectoral_crest,_shape_ reduced,_positioned_close_to_the_humerus_shaft enlarged,_proximally_placed,_with_almost_straight_proximal_margin_ enlarged,_hatchet_shaped,_proximally_placed enlarged,_hatched_shaped,_positioned_further_down_the_humerus_shaft enlarged,_warped long,_proximally_placed,_curving_ventrally enlarged,_square_outline;
{203 Humerus,_deltopectoral_crest,_position proximally_placed distally_displaced;
{204 Humerus,_deltopectoral_crest,_orientation;
{205 Humerus,_deltopectoral_crest,_medial_and_lateral_margins,_orientation converge_distally subparallel diverge_distally;
{206 Humerus,_ulnar_crest reduced_ directed_posteriorly_ massive,_with_a_developed_proximal_ridge;

{207 Humerus,_distal_articulation,_shape oval_or_D-shaped_ subtriangular_;
{208 Humerus,_between_distal_condyles,_pneumatic_foramen absent present;
{209 Humerus,_distal_surface,_pneumatic_foramen absent present;
{210 Ulna,_proportional_length_relative_to_metacarpal_IV_(ul/mcIV)_
ulna_3.6_times_longer_than_metacarpal_IV_(ul/mcIV_>_3.6)_
length_of_ulna_between_3.6_and_two_times_the_length_of_metacarpal_IV_(3.6_>ul/mcIV
>2)_ ulna_between_double_and_the_same_length_of_metacarpal_IV_(2>ul/mcIV>1)
ulna_the_same_size_or_smaller_than_metacarpal_IV_(ul/mcIV_<_1);
{211 Ulna_and_radius,_diameter_at_midshaft_ subequal_
diameter_of_radius_about_half_that_of_ulna
diameter_of_radius_less_than_half_that_of_ulna;
{212 Proximal_syncarpal,_large_posterodistal_process absent present;
{213 Proximal_syncarpal,_shape_(proximal_view) quadrangular_or_irregular pentagonal;
{214 Distal_syncarpals,_shape_(distal_view)_ irregular form_rectangular_unit_
form_triangular_unit;
{215 Pteroid absent_ shorter_than_half_the_length_of_the_ulna_
longer_that_half_the_length_of_the_ulna;
{216 Pteroid,_proximal_articulation,_expanded_in_right_angle_with_shaft absent present;
{217 Metacarpals_I_-_III,_relation_with_carpus_ articulating_with_carpus_
metacarpal_I_articulates_with_carpus,_metacarpals_II_and_III_reduced_
not_articulating_with_carpus;
{218
Manual_digit_IV_first_phalanx,_proportional_length_relative_to_metacarpal_IV_(ph1d4/mc
IV)_ both_small_and_reduced_ ph1d4/mcIV>4.0 4.0>ph1d4/mcIV>2.0
'2.0>_ph1d4/mcIV>1.0' 'ph1d4/mcIV<_1.0';
{219
Manual_digit_IV_first_phalanx,_proportional_length_relative_to_tibiotarsus_(ph1d4/ti)_
ph1d4_reduced_
ph1d4_elongated_and_less_than_twice_the_length_of_ti_(ph1d4/ti_smaller_than_2.00)
ph1d4_elongated_about_or_longer_than_twice_the_length_of_ti_(ph1d4/ti_subequal/larger_t
han_2.00);
{220
Manual_digit_IV_second_phalanx,_proportional_length_relative_to_first_phalanx_(ph2d4/p
h1d4)_ both_short_or_absent_
elongated_with_second_phalanx_about_the_same_size_or_longer_than_first_(ph2d4/ph1d4_
larger_than_1.00)_
elongated_with_second_phalanx_up_to_30%_shorter_than_first_(ph2d4/ph1d4_between_0.7
0_-_1.00)
elongated_with_second_phalanx_more_than_30%_shorter_than_first_(ph2d4/ph1d4_smaller
_than_0.70);
{221 Manual_digit_IV_second_phalanx,_longitudinal_ridge absent present;
{222
Manual_digit_IV_third_phalanx,_proportional_length_relative_to_first_phalanx_(ph3d4/ph1

d4)_ both_short_or_absent_ ph3d4_about_the_same_length_or_larger_than_ph1d4_ ph3d4_shorter_than_ph1d4;
{223 Manual_digit_IV_third_phalanx,_proportional_length_relative_to_the_second_phalanx_(ph3d4/ph2d4)_ both_short_or_absent_ ph3d4_about_the_same_size_or_longer_than_ph2d4_ ph3d4_shorter_than_ph2d4;
{224 Proportional_length_of_the_forth_phalanx_of_manual_digit_IV_relative_to_the_first_phalanx_of_manual_digit_IV_(ph4d4/ph1d4) both_short_or_absent
both_elongated,_with_the_forth_phalanx_longer_than_the_first_(ph4/d4>1.00)
both_elongated,_with_the_forth_phalanx_the_same_length_or_shorter,_but_longer_than_35%_the_lenght_of_the_first
both_elongated,_with_the_forth_phalanx_less_than_35%_the_lenght_of_the_first;
{225 Femur,_length_relative_to_metacarpal_IV_length_(fe/mcIV)_ femur_at_least_twice_the_metacarpal_IV_length_(fe_?_mcIV_>_2.00)
femur_longer_but_less_than_twice_the_length_of_metacarpal_IV_(1.00_<_fe/mcIV_<_2.00)_ femur_about_the_same_length_or_shorter_than_metacarpal_IV_(fe/mcIV_<_1.00);
{226 Femur,_foramen_on_proximal_portion_of_the_femur absent present;
{227 Metatarsal_III,_proportional_length_relative_to_tibia_length_ more_than_30%_of_tibia_length_ less_than_30%_of_tibia_length_;
{228 Pedal_digit_V,_number_of_phalanges_ with_four_phalanges_ with_2_phalanges_ with_1_or_no_phalanx_(extremely_reduced);
{229 Pes,_second_phalanx_of_digit_V,_shape_ reduced_or_absent_ elongated,_straight_ elongated,_curved elongated,_very_curved_(boomerang_shape);
;

proc /;
comments 7
{16 1 Although not easy to separate, the naof indicates this;
{16 124 could not see one. alternatively could score ?;
{16 190 partially broken, but oval, not tapejarid condition;
{16 191 has to be; not strongly concave;
{16 193 cannot be sure if in the holotype the exposed margin is anterior or posterior;
{16 194 does not appear to be elongated, but shorter and somewhat deep, particularly anterior to the articulation surfaces for the coracoid;
{16 211 Esta muito perto de 2. Compressão;
;